

# **Generation and Application of Antibodies for Detection of Prostate Cancer Biomarker**

**Julia Zapatero Rodríguez M.Sc.**

**Thesis Submitted for the Award of Ph.D.**

Based on research carried out in The Applied Biochemistry  
Group, School of Biotechnology, Dublin City University,  
Dublin 9, Ireland.

Supervisor: Prof. Richard O'Kennedy

January 2017

## **DECLARATION**

I hereby certify that this material, which I now submit for assessment on the programme of study leading to the award of Ph.D. is entirely my own work, that I have exercised reasonable care to ensure that the work is original, and does not to the best of my knowledge breach any law of copyright, and has not been taken from the work of others save and to the extent that such work has been cited and acknowledged within the text of my work.

Signed:

(Candidate) ID No.:

Date:

*“One never notices what has been done; one can only see what remains to be done”.*

*— Marie Curie*

## Acknowledgments

Firstly, I would like to thank my supervisor, Richard O’Kennedy, for his giving me the opportunity to work with his group and for his guidance throughout, as well as for his enthusiasm and expertise in the field.

Thanks to all the members of the Applied Biochemistry Group, for their scientific and technical advice and, more importantly, for all the good moments we spent together, in and outside DCU. I would like to especially acknowledge Dr. Shikha Sharma for opening my mind to new research areas and for being a valuable friend. Shikha, you cannot imagine how much I have missed our coffee breaks, lunches together and conference trips since you left. I will always consider you my travel companion (we made it to seven countries in two years—not too bad!) and I know we will see each other again. Also, I would like to make a special mention of Jessie and Rory, for keeping me entertained during the long hours in the lab and becoming friends beyond work, and of Sarah, for staying in contact and working with me even from the UK.

To all my PROSENSE fellows, who made our meetings so enjoyable and informative, I cannot imagine a better group than this. In you I have met such wonderful friends and colleagues. Pedro, you made PROSENSE possible and to you I owe the great experience of being part of it. Susana, thanks for being such a great host in Pontypool, showing us around and opening your home to us. Pawan, Kate, Stefan and Ioulia, it was a pleasure to work with you and share some laughs along the way. Thank you to the party animals (you know who you are) that were never too tired to go out after the workshops. I will always keep good memories of our meetings and hope that someday our paths cross again.

—

*También me gustaría agradecer a mis padres por su apoyo y por animarme siempre a dar lo mejor de mí misma. Por recibirme en España siempre con los brazos abiertos y por nuestras habituales conversaciones por Skype. No hay palabras para expresar*

*todo lo que habéis hecho por mí. Espero que estéis orgullosos de tener otra 'doctora' en la familia, aunque no sea médico.*

*A mi querido hermano Miguel, mis tías Julia e Irene, siempre tentándome a ir a la playa, mis tíos Luis y Javier, y mi tía Lola. Me siento agradecida de tener una familia maravillosa que se preocupa por mi. A Rebeca, mi amiga canaria en Dublín, gracias por esas tardes en el NuBar, las fiestas de Halloween y nuestros viajes a Cork.*

*Gracias a mis amigas de siempre, por demostrarme que, a pesar de la distancia, siempre puedo contar con ellas. Teresa, Virginia, Elena y Lucía, nuestros reencuentros siempre fueron el punto fuerte de las Navidades. Marta, Paloma, Esther y Raquel, siempre me hicisteis sentir en casa cada vez que volvía a Valladolid. Planear ese viaje a Islandia con Teresa me dio el empujoncito que necesitaba para acabar la tesis y fue la mejor manera de celebrar mi 'thesis submission'.*

—

Finally, I would like to dedicate this work to my other half, Richard, for being there day after day during the good and the hard moments. Thank you for making me laugh every day and for believing in me. You made me happy throughout this time and kept me optimistic during the writing process. I don't know how this would have been possible without you.

## Table of contents

Declaration.....	ii
Acknowledgements.....	iv
Table of Contents.....	vii
List of Abbreviations.....	xi
Units.....	xiv
List of Figures .....	xix
List of Tables.....	xviii
List of Publications .....	xix
Abstract.....	xii
<b>Chapter 1: Introduction.....</b>	<b>1</b>
<b>1.1 PROSENSE - THE MARIE CURIE INITIAL TRAINING NETWORK.....</b>	<b>2</b>
<b>1.2 THESIS SUMMARY .....</b>	<b>3</b>
<b>1.3 INTRODUCTION TO PROSTATE CANCER.....</b>	<b>3</b>
<b>1.4 BIOMARKERS FOR PROSTATE CANCER DIAGNOSIS: LIMITATIONS OF SERUM PSA AND THE SEARCH FOR NEW BIOMARKERS.....</b>	<b>6</b>
1.4.1 Candidate protein biomarkers for prostate cancer .....	7
1.4.2 Next generation diagnostic tools for Prostate Cancer .....	9
<b>1.5 ANTIBODIES AND RECOMBINANT ANTIBODY TECHNOLOGY .....</b>	<b>14</b>
1.5.1 Introduction to the immune system .....	14
1.5.2 Antibody overview .....	15
1.5.3 Generation of avian recombinant antibodies by phage display .....	16
1.5.3.1 Recombinant antibody fragments .....	16
1.5.3.2 Phage display.....	18
1.5.3.3 Panning of phage display libraries.....	19
1.5.4 Clinical applications of recombinant antibody fragments .....	20
<b>1.6 BIOSENSORS IN CANCER DIAGNOSIS .....</b>	<b>21</b>
1.6.1 Overview to biosensors .....	21
1.6.2 Biosensors for cancer detection .....	24
1.6.2.1 Amperometric biosensors .....	25
1.6.2.2 Impedimetric biosensors .....	26
<b>1.7 MICROFLUIDICS PLATFORMS FOR BIOANALYSIS.....</b>	<b>27</b>
1.7.1 Microfluidic-integrated biosensors for diagnostics .....	29
1.7.2 Microfluidics for multiplexing.....	31

<b>1.8 AIMS.....</b>	<b>32</b>
----------------------	-----------

<b>Chapter 2: Materials and Methods.....</b>	<b>34</b>
--	-----------

<b>2.1 MATERIALS AND EQUIPMENT .....</b>	<b>35</b>
--	-----------

2.1.1 Equipment.....	35
2.1.2 Reagents .....	36
2.1.3 Bacterial strains .....	37
2.1.4 Antibodies.....	37
2.1.5 Antigens .....	38
2.1.6 Commercial kits .....	38
2.1.7 Culture Media formulations.....	38
2.1.8 Buffer formulations.....	39
2.1.8.1 <i>General buffers</i> .....	39
2.1.8.2 <i>Buffers for sodium dodecyl sulfate-polyacrylamide gel electrophoresis</i> .....	39
2.1.8.3 <i>Buffers for Immobilized metal ion affinity chromatography (IMAC) purification</i> .....	40
2.1.8.4 <i>Buffers for magnetic beads bioconjugation</i> .....	40
2.1.8.5 <i>Other solution formulations</i> .....	41

<b>2.2 METHODS .....</b>	<b>41</b>
--------------------------	-----------

2.2.1 General molecular biological techniques.....	41
2.2.1.1 <i>Agarose gel electrophoresis</i> .....	41
2.2.1.2 <i>Extraction of DNA from agarose gels using NucleoSpin® Gel and PCR Clean-Up (MN)</i> .....	41
2.2.1.3 <i>Ethanol precipitation of DNA</i> .....	42
2.2.1.4 <i>Sodium dodecyl sulphate polyacrylamide gel electrophoresis (SDS-PAGE)</i> .....	42
2.2.1.5 <i>Western Blotting</i> .....	43
2.2.2 Animal immunisation for recombinant antibody production .....	44
2.2.2.1 <i>Chicken immunization with the ERBB2 extracellular domain</i> .....	44
2.2.2.2 <i>Serum antibody titre determination by indirect ELISA</i> .....	44
2.2.3 Generation of an immune chicken scFv library.....	45
2.2.3.1 <i>Extraction and isolation of total RNA from immunised chicken spleen</i> .....	45
2.2.3.2 <i>First-strand cDNA synthesis from total RNA</i> .....	46
2.2.3.3 <i>PCR Primers for the construction of a chicken scFv library</i> .....	47
2.2.3.4 <i>Amplification of chicken antibody variable heavy and light chain genes</i> .....	48
2.2.3.5 <i>Optimisation of MgCl<sub>2</sub> and primer concentration for amplification of DNA</i> .....	49
2.2.3.6 <i>Splice by overlap extension (SOE) PCR using Platinum Taq polymerase</i> .....	49
2.2.3.7 <i>Plasmid DNA purification and preparation of an E. coli glycerol stock expressing pComb3XSS</i> .....	51
2.2.3.8 <i>Restriction-digestion of the scFv insert and pComb3XSS vector</i> .....	51
2.2.3.9 <i>Ligation of SOE-product into pComb vector</i> .....	52
2.2.4 Antibody phage display and library panning.....	53
2.2.4.1 <i>Transformation of E. coli XL1-Blue electrocompetent cells with scFv-containing plasmid and rescue of scFv-displaying phage</i> .....	53
2.2.4.2 <i>Enrichment of phage library via panning against immobilised HER2</i> .....	54

2.2.4.3 Polyclonal phage ELISA .....	55
2.2.5 Analysis of scFv-expressing single clones.....	56
2.2.5.1 Soluble expression of antibody fragments.....	56
2.2.5.2 Soluble Monoclonal scFv ELISA .....	57
2.2.5.3 Competitive scFv ELISA for the detection of free HER2 .....	57
2.2.5.4 Sequence analysis of the anti-HER2-specific clones.....	58
2.2.6 Expression, purification and characterisation of anti-HER2 scFv A4.....	59
2.2.6.1 Optimisation of expression conditions for A4 scFv .....	59
2.2.6.2 Immobilised metal affinity chromatography (IMAC) purification.....	60
2.2.6.3 Optimisation of assay parameters for HER2 detection in a competitive format.....	61
2.2.6.4 Competitive ELISA for the detection of HER2 using A4 scFv .....	61
2.2.6.5 Fluorescence-based competitive ELISA for the detection of HER2 .....	62
2.2.7 Isolation and characterisation of polyclonal antibodies to HER2 .....	62
2.2.7.1 IgY purification from eggs of an immunised chicken .....	62
2.2.7.2 Competitive ELISA for anti-HER2 polyclonal antibody characterisation .....	63
2.2.8 Development of a novel centrifugal microfluidic platform for multiplex biomarker detection .....	63
2.2.8.1 Centrifugal disc fabrication.....	63
2.2.8.2 Centrifugal disc testing .....	64
2.2.8.3 Conventional benchtop sandwich ELISA for the detection of fPSA .....	65
2.2.8.4 Conventional competitive ELISA for the detection of HER2 extracellular domain (ECD).....	66
2.2.8.5 Lab-on-a-Disc ELISA protocols .....	66
2.2.9 Evaluation of anti-PSA recombinant antibodies by optical and electrochemical magneto-immunoassay .....	67
2.2.9.1 Tosyl-modified magnetic particles bioconjugation .....	67
2.2.9.2 Antibody titration for determination of bioconjugation efficiency.....	68
2.2.9.3 Colorimetric magneto ELISA .....	69
2.2.9.4 Amperometric magneto-immunoassay .....	70
2.2.10 Immunosensor fabrication and characterization for HER2 detection .....	71
2.2.10.1 Fabrication of the immunosensor and electrochemical procedure .....	71
2.2.10.2 Impedance measurement procedure .....	73

## **Chapter 3: Anti-HER2 scFv antibody: Production, Characterisation and Use for the Development of an Impedimetric Biosensor.....74**

<b>3.1 INTRODUCTION .....</b>	<b>75</b>
3.1.1 The <i>HER2</i> oncogene .....	75
3.1.2 HER family signaling pathways.....	76
3.1.3 HER2 overexpression in cancer.....	78
<b>3.2 AIMS OF THIS CHAPTER.....</b>	<b>79</b>

<b>3.3 RESULTS</b> .....	<b>79</b>
3.3.1 Immunisation of chicken with HER2 ECD and serum antibody titre determinations .....	79
3.3.2 Purification of anti-HER2 polyclonal IgY from chicken eggs.....	80
3.3.3 Generation of avian anti-HER2 scFv library .....	82
3.3.3.1 <i>RNA isolation from immunised chicken spleen lymphocytes and cDNA synthesis</i> .....	82
3.3.3.2 <i>PCR amplification of chicken variable heavy (<math>V_H</math>) and light (<math>V_L</math>) chains</i> .....	83
3.3.3.2.1 <i>Optimisation of <math>MgCl_2</math> concentration for PCR amplification</i> .....	84
3.3.3.2.2 <i>Optimisation of primer concentration for <math>V_H</math> PCR amplification</i> .....	85
3.3.3.2.3 <i>Amplification of <math>V_H</math> and <math>V_L</math> with optimised PCR conditions</i> .....	85
3.3.3.3 <i>Splice by Overlap Extension (SOE) PCR to anneal variable heavy and variable light chain genes</i> .....	86
3.3.3.4 <i>Restriction-digestion and ligation of the SOE PCR product and the pComb3XSS vector</i> .....	87
3.3.4 Antibody library screening.....	90
3.3.4.1 <i>Enrichment of phage library via panning</i> .....	90
3.3.4.2 <i>Soluble expression and monoclonal analysis of single clones by ELISA</i> .....	91
3.3.4.3 <i>Analysis of putative anti-HER2 clones by competitive ELISA</i> .....	93
3.3.4.4 <i>Sequence analysis of selected clones</i> .....	94
3.3.4.5 <i>Dose-response competitive studies of anti-HER2 clones</i> .....	95
3.3.5 Purification and characterisation of anti-HER2 scFv A4.....	97
3.3.5.1 <i>Purification of A4 scFv by immobilised metal affinity chromatography (IMAC)</i> .....	97
3.3.5.2 <i>Development of a competitive ELISA assay using scFv A4 for the detection of HER2</i> .....	99
3.3.5.2.1 <i>Optimisation of assay conditions</i> .....	100
3.3.5.2.2 <i>Evaluation of competitive assay in serum</i> .....	102
3.3.5.3 <i>Fluorescence-based competitive assay</i> .....	103
3.3.6 Impedimetric biosensor for HER2 detection.....	104
3.3.6.1 <i>Determination of optimum time duration, temperature and pH for immune-complexation</i> .....	107
3.3.6.2 <i>HER2 measurements using an impedimetric immunosensor</i> .....	111
<b>3.4 DISCUSSION</b> .....	<b>113</b>

## **Chapter 4: ‘Lab-on-a-Disc’ for Multiplexed Detection of PSA and HER2 from Whole Blood** .....

<b>4.1 INTRODUCTION</b> .....	<b>121</b>
4.1.1 Centrifugal microfluidics .....	122
4.1.2 Dissolvable-film tabs.....	123
4.1.3 Design of the microfluidic ‘flow cell’.....	127
<b>4.2 AIM OF THIS CHAPTER</b> .....	<b>129</b>



## List of Abbreviations:

<b>Ab</b>	Antibody
<b>Ag</b>	Antigen
<b>AP</b>	Alkaline phosphatase
<b>APC</b>	Antigen-presenting cell
<b>AR</b>	Amphiregulin
<b>BPH</b>	Benign prostatic hyperplasia
<b>BSA</b>	Bovine serum albumin
<b>BTC</b>	Betacellulin
<b>CAE</b>	Carcinoembryonic Antigen
<b>cDNA</b>	Complementary deoxyribonucleic acid
<b>cPSA</b>	Complex prostate specific antigen
<b>CD</b>	Compact disc
<b>CDR</b>	Complementarity determining region
<b>C<sub>H</sub></b>	Constant heavy chain
<b>C<sub>L</sub></b>	Constant light chain
<b>DF</b>	Dissolvable film
<b>DNA</b>	Deoxyribonucleic acid
<b>diH<sub>2</sub>O</b>	Distilled water
<b>DMSO</b>	Dimethyl sulfoxide
<b>dNTP</b>	Deoxyribonucleotide triphosphate
<b>DRE</b>	Digital rectal examination
<b>ECD</b>	Extracellular domain
<b>EGF</b>	Epidermal grow factor
<b>EGFR</b>	Epidermal grow factor receptor
<b>EIS</b>	Electrochemical impedance spectroscopy
<b>ELISA</b>	Enzyme-linked immunosorbent assay
<b>EN-2</b>	Engrailed-2
<b>Fab</b>	Antibody binding fragment
<b>FDA</b>	U.S. Food and Drug Administration
<b>FISH</b>	Fluorescence <i>in situ</i> hybridization

<b>fPSA</b>	Free prostate specific antigen
<b>Fv</b>	Fragment variable (of an antibody)
<b>GOx</b>	Glucose oxidase
<b>GST</b>	Glutathione S-transferase
<b>HA</b>	Haemagglutinin
<b>HB-EGF</b>	Heparin-binding EGF-like growth factor
<b>HER2</b>	Receptor tyrosine-protein kinase erbB-2
<b>His</b>	Histidine
<b>hk2</b>	Human kallikrein related peptidase 2
<b>HQ</b>	Hydroquinone
<b>HRP</b>	Horse radish peroxidase
<b>HRPC</b>	Hormone-refractory prostate cancer
<b>Ig</b>	Immunoglobulin
<b>IHC</b>	Immunohistochemistry
<b>IMAC</b>	Immobilised metal affinity chromatography
<b>IPTG</b>	Isopropyl- $\beta$ -D-galactopyranoside
<b>LB</b>	Luria Broth
<b>LOD</b>	Limit of detection
<b>mAb</b>	Monoclonal antibody
<b>MgCl<sub>2</sub></b>	Magnesium Chloride
<b>MG H<sub>2</sub>O</b>	Molecular grade water
<b>MiPS</b>	Mi-Prostate Score
<b>MPs</b>	Magnetic particles
<b>MRI</b>	Magnetic resonance imaging
<b>mRNA</b>	Messenger ribonucleic acid
<b>MW</b>	Molecular weight
<b>NPV</b>	Negative predictive value
<b>NRG</b>	Neuroregulin
<b>O/N</b>	Overnight
<b>pAb</b>	Polyclonal antibody
<b>PBS</b>	Phosphate buffer saline
<b>PBS-T</b>	Phosphate buffer saline with 0.05% (v/v) Tween-20
<b>PCa</b>	Prostate cancer
<b>PCR</b>	Polymerase chain reaction

<b>pH</b>	Negative logarithm of the molarity of hydrogen ion
<b>phi</b>	Prostate Health Index
<b>PMMA</b>	Poly methyl-methacrylate
<b>PRKC-<math>\zeta</math></b>	Protein kinase C- zeta
<b>PIN</b>	Prostatic intraepithelial neoplasia
<b>POC</b>	Point-of-care
<b>PSA</b>	Prostate specific antigen
<b>P-SA</b>	Pressure sensitive adhesive
<b>PSMA</b>	Prostate specific membrane antigen
<b>Rct</b>	Charge-transfer resistance
<b>RIA</b>	Radioimmunoassay
<b>RT</b>	Room temperature
<b>'RT'</b>	Reverse transcriptase
<b>SAM</b>	Self assembled-monolayer
<b>scAb</b>	Single chain antibody
<b>scFv</b>	Single chain variable fragment
<b>SB</b>	Super Broth
<b>SDS-PAGE</b>	Sodium dodecyl sulphate polyacrylamide gel electrophoresis
<b>SOC</b>	Super optimal catabolite
<b>SOE</b>	Splice by overlap extension
<b>SPE</b>	Screen-printed electrode
<b>T2-ERG</b>	Transmembrane protease, serine 2:ETS-related gene fusion
<b>TAAAs</b>	Tumour-associated antigens
<b>TEMED</b>	Tetramethylethylenediamine
<b>TGF</b>	Transforming growth factor-alpha
<b>TMB</b>	3,3',5,5'-Tetramethylbenzidine
<b>Topo2A</b>	DNA topoisomerase II-alpha
<b>U</b>	Unit
<b>UV</b>	Ultra violet
<b><i>v-erb</i></b>	Avian erythroblastic leukemia viral oncogene homolog 2
<b>V<sub>H</sub></b>	Variable heavy chain
<b>V<sub>L</sub></b>	Variable light
<b>Z'</b>	Real component of impedance
<b>Z''</b>	Imaginary component of impedance

## Units:

<b>%</b>	Percent
<b>Ω</b>	Ohm
<b>bp</b>	Base pairs
<b>cfu</b>	Colony-forming units
<b>cm</b>	Centimetres
<b>g</b>	Grams
<b>kb</b>	Kilobase
<b>kDa</b>	Kilodaltons
<b>kg</b>	Kilogram
<b>L</b>	Litre
<b>m</b>	Metre
<b>M</b>	Molar
<b>mg</b>	Milligram
<b>mL</b>	Millilitres
<b>nM</b>	Nanomolar
<b>°C</b>	Degrees Celcius
<b>OD</b>	Optical density
<b>R<sup>2</sup></b>	Coefficient of determination
<b>rpm</b>	Revolutions per minute
<b>V</b>	Volt
<b>v/v</b>	Volume per unit volume
<b>w/v</b>	Weight per unit volume
<b>μg</b>	Microgram
<b>μL</b>	Microlitre
<b>μM</b>	Micromoles
<b>ω</b>	Angular frequency
<b>x g</b>	Times gravity

## List of Figures:

<b>Figure 1.1</b>	Commercial tests for the management of prostate cancer.....	11
<b>Figure 1.2</b>	Production of autoantibodies by plasma cells in response to tumour associated antigens (TAAs).....	13
<b>Figure 1.3</b>	Basic structure of an IgG molecule.....	16
<b>Figure 1.4</b>	Schematic structure of the IgY molecule and scFv, scAb and Fab antibody fragment.....	17
<b>Figure 1.5</b>	Panning for selection of antibody fragments from phage-display libraries.....	19
<b>Figure 1.6</b>	Schematic representation of a biosensor operating mechanism.....	23
<b>Figure 2.1</b>	Exploded assembly drawing of the multi-layered, centrifugal microfluidic disc.....	64
<b>Figure 2.2</b>	Centrifugal testing set up for spinning of the disc and observation of the fluids behaviour.....	65
<b>Figure 2.3</b>	Schematic display of the steps involved in the bioconjugation of scAb E1 to tosyl-activated magnetic particles.....	69
<b>Figure 2.4</b>	Schematic representation of the immunomagnetic separation and amperometric detection of free PSA ('two-step' protocol).....	71
<b>Figure 2.5</b>	Schematic representation of the immunosensor fabrication.....	72
<b>Figure 3.1</b>	Representation of HER ligands and receptors.....	76
<b>Figure 3.2</b>	Overview of HER family signalling pathways.....	77
<b>Figure 3.3</b>	The antibody titre of an avian antiserum response to HER2 after boost 3.....	80
<b>Figure 3.4</b>	Western blot analysis of the IgY purified from the eggs.....	81
<b>Figure 3.5</b>	Competitive analysis for the detection of HER2 using IgY purified from eggs.....	82
<b>Figure 3.6</b>	cDNA synthesis by reverse transcription of mRNA from chicken spleen using the Superscript III first-strand synthesis system for RT-PCR.....	83
<b>Figure 3.7</b>	PCR optimisation for variable light and variable heavy gene amplifications using MgCl <sub>2</sub> concentrations from 1–4 mM.....	84
<b>Figure 3.8</b>	PCR optimisation of variable heavy gene amplifications using primer concentrations within the range of 0.4–1 μM.....	85
<b>Figure 3.9</b>	Optimised PCR amplifications of variable heavy and variable light genes using the cDNA from a HER2 ECD-immunised chicken.....	86
<b>Figure 3.10</b>	SOE-PCR of V <sub>H</sub> and V <sub>λ</sub> fragments for the construction of a scFv library.....	87

<b>Figure 3.11</b>	pComb3XSS vector map.....	88
<b>Figure 3.12</b>	Digestion of the pComb3XSS vector and SOE product.....	89
<b>Figure 3.13</b>	Polyclonal phage ELISA following four rounds of panning.....	91
<b>Figure 3.14</b>	Soluble monoclonal ELISA screening for anti-HER2-specific scFv from 96 randomly selected clones from round 3 and 4 of panning.....	92
<b>Figure 3.15</b>	Competitive analysis of clones lysates.....	93
<b>Figure 3.16</b>	Sequence alignment of the deduced CDR V <sub>L</sub> and V <sub>H</sub> regions.....	94
<b>Figure 3.17</b>	Antibody titre of HER2-specific clones, screened against HER2.....	95
<b>Figure 3.18</b>	Western blotting analysis of cell lysates.....	96
<b>Figure 3.19</b>	Competitive analysis of HER2-specific clones H4, G1, H2 and A4	97
<b>Figure 3.20</b>	Antibody titre for the selection of optimal IPTG concentration and expression temperature for scFv A4.....	98
<b>Figure 3.21</b>	SDS-PAGE analysis of the fractions obtained during the IMAC purification of A4 scFv.....	99
<b>Figure 3.22</b>	Indirect competitive inhibition ELISA format.....	100
<b>Figure 3.23</b>	Selection of optimal coating buffer for use in a competitive ELISA for the detection of HER2.....	101
<b>Figure 3.24</b>	Selection of optimal HER2 coating concentration (1–4 µg/mL) and scFv dilution for use in a competitive ELISA for the detection of HER2.....	101
<b>Figure 3.25</b>	Competitive analysis of anti-HER2 scFv A4 using optimised conditions.....	102
<b>Figure 3.26</b>	Competitive analysis of anti-HER2 scFv A4 to detect HER2 in 10 mM PBS buffer and in human serum.....	103
<b>Figure 3.27</b>	Fluorescence-based competitive ELISA for HER2 detection.....	104
<b>Figure 3.28</b>	Example of Nyquist diagram for EIS data representation.....	105
<b>Figure 3.29</b>	Representation of the gold nanoparticle-based immunosensor for the detection of HER2.....	106
<b>Figure 3.30</b>	Optimisation of immune-complexation time.....	108
<b>Figure 3.31</b>	Optimisation of immune-complexation temperature.....	109
<b>Figure 3.32</b>	Optimisation of immune-complexation pH.....	110
<b>Figure 3.33</b>	EIS analysis of immunosensor in 5 mM [Fe(CN) <sub>6</sub> ] <sup>3-</sup> / <sup>4-</sup> redox probe with increasing concentrations of HER2 (0.1–500 ng/mL) spiked in PBS buffer or serum.....	112
<b>Figure 3.34</b>	EIS analysis of immunosensor in 5 mM [Fe(CN) <sub>6</sub> ] <sup>3-</sup> / <sup>4-</sup> redox probe at low HER2 concentrations (0.001–0.1 ng/mL).....	113
<b>Figure 4.1</b>	Inertial forces acting in centrifugal microfluidics.....	122

<b>Figure 4.2</b>	Actuation of centrifugo-pneumatic dissolvable film (DF) valves.....	125
<b>Figure 4.3</b>	Radially and circularly patterned release chambers with DF tabs (positional multiplexing).....	126
<b>Figure 4.4</b>	Dependence of release frequency on the radial position (R) of the trigger lip and the radius of the pneumatic compression chamber.....	126
<b>Figure 4.5</b>	Lab-on-a-Disc for multiplexed detection of prostate cancer biomarkers from whole blood.....	128
<b>Figure 4.6</b>	Optimisation of sandwich ELISA incubation times for the detection of fPSA.....	130
<b>Figure 4.7</b>	Functionalisation of disc PMMA surface.....	131
<b>Figure 4.8</b>	fPSA and HER2 calibration curves using conventional ELISA.....	134
<b>Figure 4.9</b>	fPSA and HER2 calibration curves using LoD platform.....	135
<b>Figure 4.10</b>	Investigation of interference of anti-HER2 scFv in the serum sample with PSA detection.....	136
<b>Figure 5.1</b>	Selected strategy for the detection of free PSA.....	146
<b>Figure 5.2</b>	Optimisation of assay conditions by magneto-ELISA.....	148
<b>Figure 5.3</b>	Magneto-ELISA immunosensing of fPSA.....	149
<b>Figure 5.4</b>	Cyclic voltammogram derived using a 6-mm working electrode carbon screen-printed electrode (BE2150327D2/001).....	150
<b>Figure 5.5</b>	Amperometric response obtained for 0.1 and 0.2 mg/mL of bioconjugated MPs on the SPE using two different fPSA concentrations (5 and 10 ng/mL).....	151
<b>Figure 5.6</b>	Amperometric response obtained using a one-step protocol versus the two-step protocol.....	152
<b>Figure 5.7</b>	Amperometric magneto-immunosensor standard curve with a linear range from 0 to 10 ng/mL fPSA .....	153
<b>Figure 5.8</b>	Interference analysis.....	153

## List of Tables:

<b>Table 1.1</b>	Prostate cancer staging factors in clinical practice.....	35
<b>Table 1.2</b>	Prostate cancer can be grouped in four stages combining the TNM system, the Gleason Score and the PSA levels.....	6
<b>Table 1.3</b>	Selected prostate cancer protein biomarkers.....	8
<b>Table 1.4</b>	New FDA-approved tests for Prostate Cancer diagnosis.....	12
<b>Table 1.5</b>	Example of monoclonal antibody fragments with FDA approval for diagnostic and therapeutic clinic use.....	21
<b>Table 1.6</b>	List of FDA-approved microfluidic-based tests.....	30
<b>Table 3.1</b>	Panning conditions used for each round of selection for the anti-HER2 scFv library.....	90
<b>Table 3.2</b>	List of FDA cleared or approved companion diagnostic ( <i>in vitro</i> and imaging tools).....	114
<b>Table 4.1</b>	Spin frequency protocol for each laboratory unit operation (LUO) in the LoaD ELISA.....	133

## Publications, posters and presentations

### Publications:

Sharma, S., Zapatero-Rodríguez, J., and O'Kennedy, R. (2014). Prostate Cancer—Towards a Greater Understanding and Better Diagnosis. *Institute of Biology of Ireland Newsletter*, Autumn 2014.

Sharma, S. \*, Zapatero-Rodríguez, J.\*, Estrela, P., and O'Kennedy, R. (2015). Point-of-Care Diagnostics in Low Resource Settings: Present Status and Future Role of Microfluidics. *Biosensors*, 5(3), 577-601.

Gilgunn, S.; Millán Martín, S.; Wormald, M. R.; Zapatero-Rodríguez, J.; Conroy, P. J.; O'Kennedy, R. J.; Rudd, P. M. and Saldova, R. (2016). Comprehensive N-glycan Profiling of Avian Immunoglobulin Y. *PLOS one* 11.7: e0159859.

Sharma, S., Zapatero-Rodríguez, J., and O'Kennedy, R. Prostate Cancer Diagnostics: Current Challenges and the Need for Future Diagnostic Tools (2016). *Biotechnology Advances*, DOI: 10.1016/j.biotechadv.2016.11.009.

### Publications submitted:

Zapatero-Rodríguez, J., Liébana, S., Gilgunn, S., Sharma, S., and O'Kennedy. Single-Chain Antibody Based Magneto-Immunoassay for the Detection of Free Prostate Specific Antigen (fPSA). Submitted to *BioNanoScience* on November 2016.

### Publications in preparation:

Mishra, R. \*, Zapatero-Rodríguez, J.\*, Sharma, S. \*, Kelly, D., McAuley, D., Gilgunn, S., O'Kennedy, R., and Ducreé, J. Automation of Multiple-Analyte Prostate Cancer Biomarker Immunoassays from Whole Blood Based on Purely Rotational Flow Control.

Tzouvadaki, I., Zapatero-Rodríguez, J., Naus, S., O'Kennedy, R., and Carrara, S. Full Chain and Single-Chain Antibody Fragment (scAb)-Based Memristive Biosensors.

Sharma, S., Saxena, R., Zapatero-Rodríguez, J., Srivastava, S., and O'Kennedy, R. A Disposable Gold Nanoparticles based Impedimetric HER2 Immunosensor using Single-Chain Antibody Fragments.

***\*These authors contributed equally to this work.***

## Poster Presentations:

Zapatero-Rodríguez, J., O'Reilly, J.A, and O'Kennedy, R. Generation and application of antibodies to prostate cancer biomarkers. PROSENSE workshop on 'The production and application of antibodies and their use in biosensors and arrays', 2-4 July 2013, Dublin City University.

Zapatero-Rodríguez, J., O'Reilly, J.A, and O'Kennedy, R. Generation of recombinant antibodies to biomarkers of prostate cancer. PROSENSE workshop on 'Application of lectins in various formats of analysis for glycoprofiling', 24 January 2014, Institute of Chemistry, Slovak Academy of Science, Bratislava.

Zapatero-Rodríguez, J., O'Reilly, J.A, and O'Kennedy, R. Generating avian recombinant antibodies to Her2 for prostate cancer detection. School of Biotechnology 6th Annual Research day, 7 February 2014, Dublin City University.

Zapatero-Rodríguez, J., O'Reilly, J.A, and O'Kennedy, R. Generation of a chicken anti-HER2 extracellular domain scFv antibody library for prostate cancer diagnosis. PROSENSE Summer School on 'Clinical perspectives and commercial forces on biosensor devices', 15-19 September 2014, University of Bath, UK.

Zapatero-Rodríguez, J., O'Reilly, J.A, and O'Kennedy, R. Generation of avian recombinant antibodies to Her2 for prostate cancer diagnosis. 22<sup>nd</sup> Meeting of the EAU Section of Urological Research (ESUR), 9-11 October 2014, Glasgow, UK.

Zapatero-Rodríguez, J., Gilgunn, S., Sharma, S., and O'Kennedy, R. Application of generated antibodies to prostate cancer biomarkers in a CD-like device for the diagnosis of the disease. PROSENSE workshop on 'Biosensor construction', 14-16 January 2015, University of Cardiff, Wales, UK.

Zapatero-Rodríguez, J., Gilgunn, S., Sharma, S., and O'Kennedy, R. Application of generated antibodies to prostate cancer biomarkers into a CD-like device for the diagnosis of the disease. School of Biotechnology Research day, 30 January, 2015, Dublin City University.

Zapatero-Rodríguez, J., Gilgunn, S., Sharma, S., and O'Kennedy, R. Recombinant antibody-based immunoassays for prostate cancer diagnosis. PROSENSE workshop on 'Microfluidics and biosensors for point-of-care devices', 16 July 2015, Técnico-University of Lisbon, Portugal.

Zapatero-Rodríguez, J., Mishra, R., Sharma, S., Kelly, D., Gilgunn, S., Ducrée, J. and O'Kennedy, R. 'Lab-on-a-disc' for prostate cancer biomarkers detection. PROSENSE Winter School on 'New nano-bio-sensing tools for theragnostics', 1-5 February 2016, École Polytechnique Fédérale de Lausanne (EPFL), Switzerland.

Zapatero-Rodríguez, J., Mishra, R., Sharma, S., Kelly, D., McAuley, D., Gilgunn, S., Ducreé, J. and O’Kennedy, R. ‘Lab-on-a-disc’ (LoaD) for multiplex cancer biomarkers detection. PROSENSE Conference on ‘Prostate Cancer Diagnosis’, 12-13 September 2016, University of Bath, UK.

## **Oral Presentations:**

Zapatero-Rodríguez, J. PROSENSE workshop on ‘The production and application of antibodies and their use in biosensors and arrays’, 2-4 July 2013, Dublin City University.

Zapatero-Rodríguez, J. PROSENSE workshop on ‘Application of lectins in various formats of analysis for glycoprofiling’, 24 January 2014, Institute of Chemistry at Slovak Academy of Science, Bratislava.

Zapatero-Rodríguez, J. PROSENSE Summer School on ‘Clinical perspectives and commercial forces on biosensor devices’ 15-19 September 2014, University of Bath, UK.

Zapatero-Rodríguez, J. PROSENSE workshop on ‘Biosensor construction’, 14-16 January 2015, University of Cardiff, Wales, UK.

Zapatero-Rodríguez, J. PROSENSE workshop on ‘Microfluidics and biosensors for point-of-care devices’, 16 July 2015, Instituto Superior Técnico - University of Lisbon, Portugal.

Zapatero-Rodríguez, J. PROSENSE Winter school on ‘New nano-bio-sensing tools for theragnostics’, 1-5 February 2016, École Polytechnique Fédérale de Lausanne (EPFL), Switzerland.

Zapatero-Rodríguez, J. PROSENSE Spring school on ‘Label-free techniques for electronic sensing of biomolecules’ 27 April- 2 May 2016, University of Applied Sciences Kaiserslautern, Zweibrücken, Germany.

## **Video Presentation:**

Zapatero-Rodríguez, J. Engineered antibodies– a better diagnosis of prostate cancer is possible. ‘Tell-it-straight’ competition, 29 April 2015, DCU, Ireland.

# Generation and Application of Antibodies for Detection of Prostate Cancer Biomarker

## Abstract

**Julia Zapatero-Rodríguez.**

Prostate cancer is one of the main health problems in men—over 3,300 new cases are diagnosed each year in Ireland alone. Serum Prostate Specific Antigen (PSA) is the main biomarker used to aid in the early detection of prostate cancer. However, its use has resulted in a high rate of overdiagnosis and overtreatment. Finding alternative, more sensitive and specific biomarkers/biomarker panels is now a priority. HER2 is a promising candidate biomarker for this panel, as it is related with cancer progression and survival.

This research describes the construction of an avian-derived HER2-specific scFv library, from which highly specific antibodies were isolated and characterised. After extensive optimization of assay conditions, a competitive ELISA for HER2 detection was developed, but the sensitivity required to detect HER2 within the clinical-relevant range could not be achieved. To circumvent this, fluorescence-based HER2 detection was investigated, but did not result in an improved sensitivity. Thus, an electrochemical impedance spectroscopy (EIS)-based immunosensor was designed for highly sensitive detection of HER2. Nanomaterial-based electrochemical detection exhibited great sensitivity for HER2 from serum samples, with a LOD of 0.01 ng/mL.

'In-house'-generated anti-HER2 and anti-fPSA scFv antibodies were also incorporated in a centrifugal microfluidic 'lab-on-a-disc' platform for the simultaneous detection of a panel of prostate cancer biomarkers. ELISA-based detection of HER2 and fPSA was demonstrated on a compact, automated and robust CD-like device that employs purely rotational fluidic flow control for the entire assay protocol, from plasma separation to signal production. This work provides an insight about the potential of microfluidic technologies for multi-marker assay-based detection.

Finally, the application of a magneto-immunoassay for the detection of fPSA was explored in collaboration with The Gwent Group Ltd. Anti-fPSA scAb antibodies were immobilised on magnetic beads for the capture and easy separation of this antigen from the sample. A 'proof-of-concept' amperometric magneto-immunosensor for the detection of fPSA within the clinical-relevant ranges (0.5–10 ng/mL) was developed.

# **Chapter 1**

## **Introduction**

## **1.1 PROSENSE - THE MARIE CURIE INITIAL TRAINING NETWORK**

In order to increase the understanding of the clinical relevance of prostate cancer biomarkers and improve the sensitivity, robustness and speed of biosensing technologies for the simultaneous screening of such biomarkers, the European Commission funded a new initiative in October 2012, the Marie Curie Skłodowska Innovative Training Network (ITN) “Cancer Diagnosis: Parallel Sensing of Prostate Cancer Biomarkers” (PROSENSE). This was an interdisciplinary network with the aim of developing improved devices for prostate cancer diagnosis, prognosis and treatment. PROSENSE is an amalgamation of various scientific disciplines involving university groups, R&D sections of small and medium enterprises, research institutes, hospitals and the R&D section of a large enterprise in the biomedical field. The project is coordinated by Dr. Pedro Estrela from the Department of Electronic & Electrical Engineering, University of Bath. The multidisciplinary group includes teams from the UK (University of Bath, Cardiff University), Portugal (INESC-Microsistemas e Nanotecnologias), Ireland (School of Biotechnology, Dublin City University), Germany (University of Applied Sciences Kaiserslautern), Slovakia (Institute of Chemistry, Slovak Academy of Sciences), Switzerland (Integrated Systems Laboratory, École Polytechnique Fédérale De Lausanne). PROSENSE involves two SMEs (Applied Enzyme Technology Ltd., UK and Xeptagen Ltd., Italy) and one big company (Euroimmun, Germany). The associated members are the University Hospital of Wales, Bristol Urological Institute, Royal United Hospital Bath, Avacta Life Sciences (UK), and the University of the West of England (Faculty of Health and Life Sciences and Institute of Bio-Sensing Technology).

The focus area in my project (Early-stage researcher 3 [ESR3]: Generation and applications of antibodies to biomarkers of prostate cancer) includes the development and study of potential prostate cancer biomarkers and generation of highly-specific recombinant antibodies to these biomarkers. As part of PROSENSE ITN requirements, I visited other host organisations for secondments or training workshops and I established collaborations with multiple fellows within the network.

## 1.2 THESIS SUMMARY

The clinical utility of current prostate specific antigen (PSA) tests for prostate cancer diagnosis is severely limited. It is commonly agreed that, due to the complexity of prostate cancer, a single biomarker may be insufficient for early diagnosis.

This thesis describes the generation, characterisation and application of recombinant antibodies to prostate cancer biomarkers for improved diagnosis of prostate cancer. In this study, the construction of a single-chain antibody fragment (scFv) library to HER2, a potential prostate cancer biomarker, is described. The applications of recombinant antibodies to PSA (scAb) and HER2 (scFv) in impedimetric and amperometric biosensors and in a microfluidic 'lab-on-a-disc' device are also investigated. General approaches for recombinant antibody generation are described in detail and different examples for their use in biosensors are demonstrated.

## 1.3 INTRODUCTION TO PROSTATE CANCER

The prostate is a small exocrine gland in the reproductive system in men that secretes prostatic fluid, which accounts for 30 % of the semen fluid (which also contains seminal fluid and spermatozoa) (Lilja *et al.*, 1989). The prostate is located beneath the bladder and surrounds the urethra, the duct that connects the bladder to the urinary meatus and conducts urine and semen outside the body (Rizzo, 2015).

Prostate cancer (PCa) is the most commonly diagnosed cancer in men in Europe and the third most frequent cancer in the entire European population (Ferlay *et al.* 2013). More than 90 % of prostate cancers are acinar adenocarcinomas, where the tumour arises from the secretory prostatic acinar cells. Prostate cancer can be detected at early stages by digital rectal examination (DRE) or PSA test (Heidenreich *et al.*, 2011), although controversy has arisen related to the low specificity of this biomarker. During the DRE a doctor inserts a gloved finger into the rectum to feel

the prostate surface for swelling, harder areas or lumps that can indicate the presence of a tumour. PSA blood test measures the levels of this protein in blood. PSA levels under 4 ng/mL are considered 'normal', levels between 4 and 10 ng/mL are considered 'intermediate' (within the diagnostic 'grey zone', in which cancer is present in 25 % of patients) and PSA levels over 10 ng/mL are considered 'high' (in which 50 % of the patients will have advanced disease) (Catalona *et al.*, 1994; Ezenwa *et al.*, 2012). DRE and PSA test are only indicators of cancer risk and if abnormal results are obtained in these tests, a biopsy is often recommended to examine prostate tissue samples for cancer cells. If cancer cells are present, the pathologist will assign a Gleason score—on a scale of 2 to 10—based on the appearance of cancer cells compared to normal cells, to help evaluate the prognosis of patients with prostate cancer (Table 1.1).

Staging of prostate cancer provides information about the extent of the cancer to help medical personnel predict prognosis and decide how it should be treated. The most widely used staging system is the American Joint Committee on Cancer (AJCC) TNM (tumour, lymph node, metastasis) system (Table 1.1). Overall staging can be achieved by combining the TNM status, with the Gleason score and PSA level (Table 1.1) as described in Table 1.2 (Harisinghani *et al.*, 2003).

The majority of prostate cancers are slow growing and organ-confined, and the relative 5-year survival rate (based on patients diagnosed more than 5 years ago) is 98.8 %, according with the SEER (surveillance, epidemiology, and end results) program 2005-2011 (Howlader *et al.*, 2015). This is the reason why active surveillance (regular monitoring of the disease) is a viable treatment option for men with low-risk, low-stage prostate cancer. Other treatment options include prostatectomy (surgery to remove the prostate gland), androgen-deprivation therapy (to stop the release of testosterone, which promotes the growth of prostate cells), radiotherapy or chemotherapy (Heidenreich *et al.*, 2011).

**Table 1.1** Prostate cancer staging factors in clinical practice. Taken from Sharma *et al.*, 2016.

Staging strategy	Factor to be considered	Classification	Description
<b>TNM staging</b>	Extent of primary tumour (T)	TX	Primary tumour not assessed.
		T1 (a–c)	Clinically insignificant (it cannot be felt during DRE or seen on scans (e.g. TRUS)).
		T2 (a–c)	Tumour confined to the prostate gland.
		T3 (a–b)	Tumour spreads outside the prostate (may invade seminal vesicles).
		T4	Extra-prostatic growth of the tumour into tissues other than seminal vesicles.
	Spread of the tumour to regional lymph nodes (N)	NX	Nearby lymph nodes not assessed.
		N0	Tumour has not spread to regional lymph nodes.
		N1	Tumour has spread to regional lymph nodes.
	Distant metastasis (M)	PM1c	More than one site of metastasis present.
		MX	Distant metastasis not assessed
		M0	Absence of distant metastasis.
		M1 (a–c)	Presence of distant metastasis.
	<b>Histopathologic grading</b>	Microscopic appearance of cancer cells– Gleason Score (G)	G 2–4: lowly aggressive G 5–6: mildly aggressive G 7: moderately aggressive G 8–10: highly aggressive
<b>PSA levels</b>	PSA at diagnosis	<4 ng/mL	‘Normal’ PSA serum concentration
		4–10 ng/mL	Diagnostic ‘grey zone’. % fPSA test recommended.
		>10ng/mL	High probability of prostate cancer. Biopsy recommended.

DRE–Digital rectal examination; fPSA–free Prostate Specific Antigen; TRUS–transrectal ultrasound.

**Table 1.2** Prostate cancer can be grouped in four stages combining the TNM system, the Gleason Score and the PSA levels. Taken from Sharma *et al.*, 2016.

Stage	T	N	M	Gleason score	PSA (ng/mL)
I	T1	N0	M0	≤6	≤10
	T2a	N0	M0	≤6	≤10
IIa	T1	N0	M0	=7	<20
	T1	N0	M0	≤6	10–20
	T2 (a/b)	N0	M0	≤7	<20
IIb	T2c	N0	M0	Any	Any
	T1/T2	N0	M0	Any	≥20
	T1/T2	N0	M0	≥8	Any
III	T3	N0	M0	Any	Any
IV	T4	N0	M0	Any	Any
	Any	N1	M0	Any	Any
	Any	Any	M1	Any	Any

T–Tumour; N–Node ; M–Metastasis.

#### 1.4 BIOMARKERS FOR PROSTATE CANCER DIAGNOSIS: LIMITATIONS OF SERUM PSA AND THE SEARCH FOR NEW BIOMARKERS

The use of biomarkers for the diagnosis of prostate cancer has led to earlier detection of the disease. PSA, a member of the kallikrein-related peptidase family, (kallikrein-3), synthesized by the prostate tissue, was the gold-standard biomarker for the detection of prostate cancer for nearly two decades. However, PSA screening has led to a high rate of over-diagnosis resulting in men with indolent disease undergoing unnecessary treatment (Etzioni *et al.*, 2002) which is frequently accompanied by patient anxiety and side-effects such as erectile dysfunction or urinary incontinence (Mirza *et al.* 2011).

Additionally, PSA is not specific to prostate cancer. It may also be present in increased amounts in prostate conditions such as benign prostatic hyperplasia (BPH), prostatic intraepithelial neoplasia (PIN), prostatitis and prostatic infarction. In these conditions, a significant increase in serum PSA is observed relative to the normal low levels found in healthy individuals and, consequently, patients with high serum PSA levels do not necessarily suffer from prostate cancer. Furthermore, PSA levels

increase with age and vary among ethnic groups (Lilja *et al.*, 2008). In addition, this biomarker has minimal predictive ability to differentiate prostate cancer from BPH and to determine the Gleason score and cancer stage (Fan *et al.*, 2011). Attempts to increase the specificity and sensitivity of PSA assays by using different PSA isoforms (e.g. pro-PSA, free PSA and complex PSA) and altered PSA glycosylation patterns (discussed in Section 1.4.2) have considerably improved the accuracy of PSA testing. However, this has not solved the problem of distinguishing between significant and insignificant disease (Gilgunn *et al.*, 2013). In 2012, the U.S. Preventive Services Task Force (USPSTF) published a recommendation against the use of PSA for screening of prostate cancer, considering that the benefits (early detection, which can avoid 0-1 deaths cancer deaths per 1000 men screened) do not outweigh the harms (negative psychological effects, unnecessary biopsies or overtreatment) (Moyer *et al.*, 2012). Therefore, new diagnostic tools are required. For clinical diagnosis, non-invasive techniques using either serum or urine markers would be most suitable. These biological matrices should be focussed on to identify new, more sensitive and specific biomarkers. According with the FDA (U.S. Food and Drug Administration), an ideal biomarker should be specific, sensitive, quantifiable, predictive and robust. A biomarker should also bridge pre-clinical and clinical trials and be easily accesible by non-invasive methods (Karley *et al.*, 2011). Unfortunately, to date, no ideal biomarker for prostate cancer has been discovered.

#### **1.4.1 Candidate protein biomarkers for prostate cancer**

A wide variety of potential prostate cancer biomarkers have been discovered thanks to advances in proteomic and genomic technologies. Different types of biomarkers have been proposed, including genetic and protein markers, circulating miRNAs, autoantibodies (Figure 1.1), microparticles (exosomes and prostasomes) and circulating tumour cells (CTCs). Among all of these, protein biomarkers have been widely researched because they are abundant and easily accessible in body fluids. Table 1.3 summarizes some proposed biomarkers from the literature that could potentially be used in conjunction with PSA for diagnosis and monitoring of PCa.

**Table 1.3.** Selected prostate cancer protein biomarkers.

Biomarker	Source	Sensitivity & Specificity (*)	Correlation with: G.S./ Bad prognosis		Distinguish BPH from PCa	Reference
<b>PSA</b>	S	Sensitivity: 24 % Specificity: 93 % (PSA level < 4 ng/ml)	N	N	N	Lilja <i>et al.</i> (2008)
<b>Hk2</b>	S	Specificity: 13.7 % (0.029 ng/ml cut-off) Sensitivity: 9 % (0.245 ng/ml cut-off)	N	Y (if combined with % fPSA)	Y (if combined with % fPSA)	Raaijmakers <i>et al.</i> (2007)
<b>PSMA</b>	S	Sensitivity: 65.9 % Specificity: 94.5 %	UN	Y	Y	Mhawech-Fauceglia <i>et al.</i> (2007)
<b>EN-2</b>	U	Sensitivity: 66 % Specificity: 88.2 % (42.5 ng/ml cut-off)	UN	Y	Y	Morgan <i>et al.</i> (2011)
<b>PRKC-ζ</b>	S	PRKC-ζ-PrC specific for PCa	Y	Y	Y (PKC-ζ-a and PKC-ζ-PrC)	Yao <i>et al.</i> (2012)
<b>Her-2/neu</b>	S	Low specificity (undefined)	N	Y	N	Ricciardelli <i>et al.</i> (2008)
<b>Topo2A</b>	S	Low specificity (undefined)	Y	Y	Y	Willman <i>et al.</i> (2000)
<b>Mcm5</b>	U	Sensitivity: 82 % Specificity: 73-93 %	Y	N	Y	Dudderidge <i>et al.</i> (2010)
<b>ANXA3</b>	U	Sensitivity: 50 % Specificity: 90 % (AUROC of 0.755)	Y	Y	Y	Schostak <i>et al.</i> (2009)
<b>MSP</b>	P/ SF	Unknown	N	Y	Y	Bjartell <i>et al.</i> (2009)
<b>Cav-1</b>	S	High sensitivity and specificity (undefined)	Y	Y	Y	Corn <i>et al.</i> (2010)
<b>AMACR</b>	U/S	Sensitivity: 70 % Specificity: 71 % (10.7 ng/ml cut-off)	N	N	Y	Ouyang <i>et al.</i> (2009)

(\*) In some cases, sensitivity and specificity as reported by individual studies. PSA–Prostate specific antigen; Hk2–Human kallikrein related peptidase 2; PSMA–Prostate Specific Membrane Antigen; EN-2–Engrailed-2; PRKC-ζ–Protein kinase C- zeta; Her-2/neu–Receptor tyrosine-protein kinase erbB-2; Topo2A–DNA topoisomerase II-alpha; Mcm5–Minichromosome maintenance protein 5; ANXA3–Annexin A3; MSP–β-microseminoprotein; Cav-1–Caveolin 1; AMACR–alpha-methylacyl-CoA racemase; EPCA–Early prostate cancer antigen; S–serum; U–Urine; P–plasma; SF–Seminal Fluid; N–No; Y–Yes; UN–Unknown; G.S.–Gleason Score; BPH–Benign prostatic hyperplasia.

Further investigation of the complementarity and clinical use of these biomarkers is needed in order to assemble a panel of biomarkers with the necessary performance characteristics suitable for clinical implementation.

#### **1.4.2 Next generation diagnostic tools for Prostate Cancer**

In recent years, efforts have been made to validate biomarker panels with associated use of appropriate statistical models to predict high-risk prostate cancer in order to avoid unnecessary biopsies (Figure 1.1). For example, the 4Kscore<sup>®</sup> test (OPKO Lab, Nashville, TN) involves measurements of the plasma levels of a panel of four kallikrein protein biomarkers (free PSA, intact PSA, total PSA and hk2) in conjunction with collection of other clinical information (age, DRE and prior biopsy results). Furthermore, an algorithm is used to predict risk (in terms of probability) of high-grade (Gleason score 7 or higher) cancer on biopsy (Punnen *et al.*, 2015). This test allows for individual risk prediction to aid decisions on whether or not to perform a prostate biopsy. Similarly, the biopsy-based ProMark (Metamark Genetics) prognosis test uses an eight-protein signature (DEL2L1, CUL2, SMAD4, PDSS2, HSPA, FUS, pS6 and YBOX1) for risk stratification in prostate cancer. Cutting-edge automated immunofluorescence imaging technology allows the *in situ* measurement of multiple biomarkers in the 'region of interest' (where these biomarkers are known to be altered as a result of prostate cancer) on tissue sections (Grönberg *et al.*, 2015). Prostarix (Metabolon Inc.) is a liquid chromatography-mass spectroscopy-based test that evaluates four metabolites (sarcosine, alanine, glutamate and glycine) in post-DRE urine. The test allows for risk stratification and aid in the decision of biopsy in patients within the diagnostic 'grey zone' (PSA values 2.5–10 ng/mL and suspicious DRE) and also of re-biopsy in men with prior negative biopsy (Sartori *et al.*, 2014). OurView Prognostic Panel (OPPP, from OURLab) examines prostate cancer-related clinical (PSA, age, clinical stage and biopsy report), morphological (Gleason grade) and biomolecular (PTEN, Ki67 and DNA ploidy) factors in biopsy samples. OPPP scores under 50 are characteristic of less aggressive tumours (Murphy *et al.*, 2015). Stockholm 3 (STHLM3) is a recent study that incorporates a combination of plasma

protein biomarkers (PSA, intact PSA, free PSA, hk2, MSMB and MIC1), single nucleotide polymorphisms (232 SNP), clinical variables and prostate examination in a multiple logistic regression model for the identification of clinically significant cancers. The STHLM3 model has shown utility in the detection of high-grade cancer in men with low PSA levels (1–3 ng/mL) and has the potential of reducing prostate biopsies by one third, compared with PSA screening (Grönberg *et al.*, 2015).

Genomic and transcriptome-based markers are also gaining prominence. The Oncotype DX Prostate Cancer Assay (Genomic Health, Inc.), a RT-PCR assay that measures a 17-gene ‘signature’ in prostate needle biopsies, provides information about the aggressiveness of recently diagnosed early-stage prostate cancer. The 17-gene panel includes genes involved in four tumorigenesis-related pathways: the androgen pathway (AZGP1, KLK2, SRD5A2, and FAM13C), cellular organization (FLNC, GSN, TPM2, GSTM2), stromal response (BGN, COL1A1, and SFRP4) and proliferation (TPX2), and five reference genes. Using this assay, the Genomic Prostate Score (GPS) algorithm can be calculated to identify patients that can benefit from active surveillance (Knezevic *et al.*, 2013). Also, for measuring prostate cancer aggressiveness, the Prolaris test analyses the activity of cell cycle progression (CCP) genes in prostate cancer biopsy samples. The CCP score is calculated from the expression levels of 31 genes to predict cancer death outcome in men with clinically localised disease. The evidence suggests that the CCP score can be a valuable tool to decide treatment options and has the potential of reducing the number of surgery interventions (Sommariva *et al.*, 2016). The Prostate Core Mitomic Test (MDNA Life Sciences) uses a different approach to find cancer in prostate needle core samples from negative biopsies: based on mitochondrial DNA (mtDNA) deletions, it is able to identify malignant cells in appearing potential normal tissue (Parr *et al.*, 2013; Kaisary *et al.*, 2016), which could reduce the sampling error of prostate biopsies. Cancer-specific epigenetic status of prostate cancer gene biomarkers can also help to detect prostate cancer. The Confirm MDx assay (MdxHealth) uses epigenetic multiplex PCR to detect aberrant methylation in promoter regions of GSTP1, ACT and RASSF1 genes in biopsy specimens. This test has shown a sensitivity of 68 %, specificity of 64 %, and a NPV of 90 % to confirm the absence of cancer in men with

suspicion of cancer but initial negative biopsy (Stewart *et al.*, 2013). This proves the utility of Confirm MDx assay to detect occult prostate cancer and reduce the rate of repeated biopsies (Wojno *et al.*, 2014; Shindel, 2016). Prosta Vysion (Bostwick Laboratories) is a panel of genetic biomarkers involved in prostate carcinogenesis: gene fusion/translocation analysis of the ERG protein and the loss of PTEN tumour suppressor gene. The Prosta Vysion Score provides information about the aggressiveness and prognosis of prostate cancer (Bostwick Laboratories, 2011).

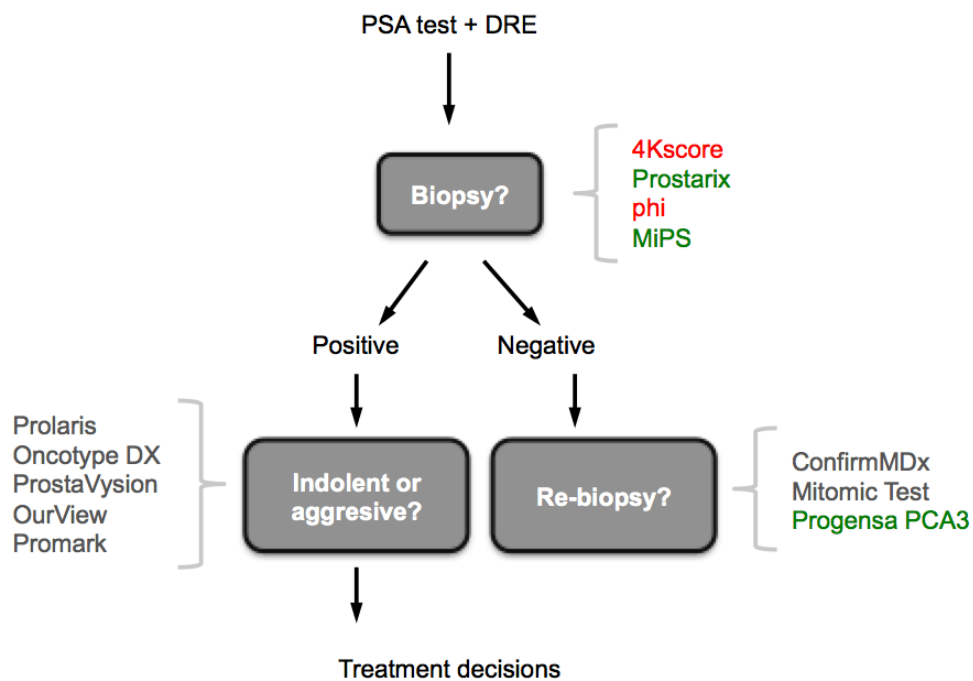


**Figure 1.1.** Commercial tests for the management of prostate cancer, classified according to the clinical application: diagnostic tests to aid with biopsy recommendations and prognosis tests to allow risk stratification following a positive biopsy result. Red: blood sample; Green: urine sample; Grey: tissue sample. Adapted from Murphy *et al.* (2015).

In addition to this, a few diagnostic approaches based on a combination of multiple genomic and/or protein biomarkers have already received FDA approval (Table 1.4). The ProgenSA PCA3 assay is RT-PCR-based test uses PCA3 transcripts normalised by PSA mRNA in post-DRE urine samples and it may allow clinicians to decide whether or not to repeat a biopsy in men with a previous negative result (Capoluongo *et al.*, 2014). The Prostate Health Index (phi) is a multiple biomarker immunoassay test based on an algorithm that combines serum total PSA, free PSA and [-2] proPSA. According to Loeb and Catalona (2013), PHI outperforms conventional PSA and free-

PSA tests and has clinical utility for biopsy decisions, risk stratification and treatment decision-making (Loeb *et al.*, 2013). The Mi-Prostate Score (MiPS, from University of Michigan Health System) risk model combines the analysis of T2-ERG gene fusion, PCA3, and serum PSA for individualised prostate cancer risk assessment (Tomlins *et al.*, 2015).

**Table 1.4.** New FDA-approved tests for Prostate Cancer diagnosis.

Test and FDA approval year	Biomarker and type of sample	Potential use in PCa diagnosis	Advantages	Reference
<b>Progenza® PCA3 Assay, 2012</b>	PCA3 and PSA RNA in post-DRE urine samples	Determine whether to re-biopsy previously biopsy-negative patients for prostate cancer or not.	Negative predictive value of 90 %	Capoluongo <i>et al.</i> (2014)
<b>The Prostate Health Index (phi), 2012</b>	Serum PSA, fPSA and p2PSA	Identify biopsy candidates in men older than 50 with PSA levels between 4–10 ng/mL and with no suspicion of cancer.	Predicts clinically significant PCa reducing over-detection of indolent PCa. Associated with Gleason Score.	Sartori <i>et al.</i> (2014); Loeb <i>et al.</i> (2014)
<b>Mi-Prostate Score (MiPS), 2013</b>	Urine T2:ERG gene fusion and a snippet from PCA3 gene combined with PSA levels	Decide after PSA testing whether or not to monitor PSA levels or perform a prostate biopsy.	Can predict risk of aggressive PCa. T2:ERG fusion is ultra-specific for PCa	Young <i>et al.</i> (2012), Tomlins <i>et al.</i> (2015)

PCA3–Prostate cancer antigen 3; PSA–Prostate specific antigen; fPSA–free PSA; p2PSA–[-2] proPSA; T2:ERG–Transmembrane protease, serine 2:ETS-related gene fusion.

Another approach to detect prostate cancer at early stages is taking advantage of the body’s immune system. Autoantibodies (see Figure 1.2) against a number of tumour-associated antigens (TAAs) have been found in the serum of prostate cancer patients (Cho-Chung, 2006; Massoner *et al.*, 2012; Ummanni *et al.*, 2015). Due to their presence following any perturbation in the cellular microenvironment (e.g. protein mutation, degradation, overexpression or release from damaged tissue), they represent ideal candidates for early detection of cancer. An autoantibody signature in prostate cancer patients is also useful for the identification of new

biomarkers. In a recent study, Schipper and co-workers identified a group of 18 potential biomarkers through iterative biopanning (using a T7 phage-peptide display library derived from prostate cancer tissue) against biopsy and serum samples from healthy and prostate cancer patients (Schipper *et al.*, 2015). From these, a logistic regression model based on 8 biomarkers was developed. The score from this algorithm can be used to identify the risk of prostate cancer, particularly for patients in the 'gray zone' (Schipper *et al.*, 2015). In addition to this, glycoprofiling of biomarkers could also be helpful for the early detection of prostate cancer (Belicky and Tkac, 2015). Aberrant glycosylation patterns are typical of tumour cells and altered glycan structures in PSA have been reported in prostate cancer (Gilgunn *et al.*, 2013). A recent publication by Tkac's group described the development of a lectin-based impedimetric biosensor for PSA quantification (down to 4 aM) and glycoprofiling on the same interface. *Sambucus nigra* (SNA) lectin (a sugar-binding protein) was used for 'in-situ' glycoprofiling of PSA glycan, while simultaneously detecting PSA concentrations down to aM levels (Pihíková *et al.*, 2016).  $\alpha$ -2,6-linked sialic acid is lower in serum PSA from prostate cancer patients in comparison with BPH, while  $\alpha$ 2,3-linked sialic acid is more abundant in PSA from cancer patients (Meany *et al.*, 2008). This could have a clinical value to differentiate BPH from prostate cancer at the time of diagnosis.

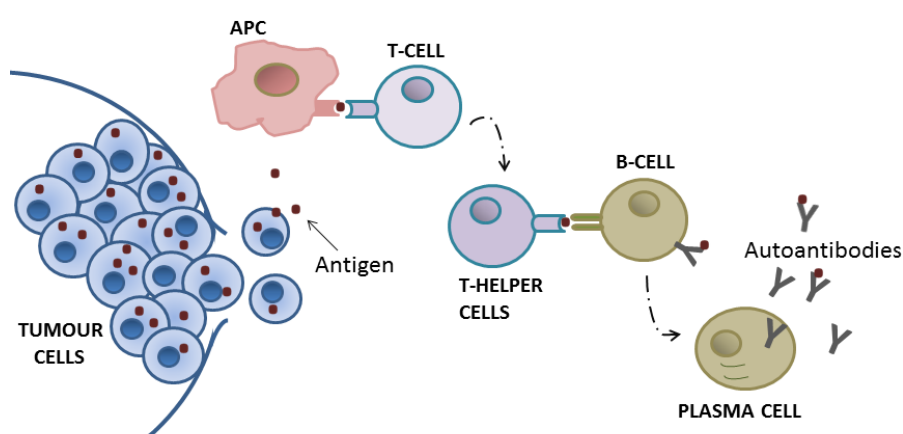


**Figure 1.2.** Production of autoantibodies by plasma cells in response to tumour associated antigens (TAAs). Antigen-presenting cells (APCs) take up TAAs from tumour cells and present them to T-cells. This results in the activation of the T-helper cells which interact with B-cells stimulating their maturation into plasma cells that produce autoantibodies specific to the initially presented TAA.

Though PSA-based testing is still the standard practice to identify patients that may be at risk for prostate cancer, and it is clearly evident from the level of recent research and development that clinicians, scientist and industries have a strong commitment towards developing new tools for better management of prostate cancer. The simultaneous detection of a panel of novel biomarkers in a multiplex platform may help to answer critical clinical questions and generate novel and highly specific and sensitive devices in the future. A panel of biomarkers has already successfully been used for early diagnosis of bowel cancer by DCU scientists from the Applied Biochemistry Group (founded by Prof. Richard O'Kenendy), in collaboration with the Irish biotech firm Randox (unpublished data).

## **1.5 ANTIBODIES AND RECOMBINANT ANTIBODY TECHNOLOGY**

### **1.5.1 Introduction to the immune system**

The immune system is a protection system designed to detect and eliminate foreign particles and infectious organisms that enter the body. This defence mechanism can be divided in two categories: innate and adaptive immunity. Innate immunity refers to non-specific mechanisms that act as the first line of defence against foreign molecules (antigen) and include physical (e.g. the skin or mucous membranes) and chemical (e.g. gastric juice) barriers, as well as cellular (phagocytosis and cell lysis) and chemical responses (inflammation, fever, etc.). The adaptive system differs from the innate system in the way it is acquired after the antigen is first processed and recognised and it is able to create an 'immune memory' to tailor an enhanced, specific response against the antigen previously encountered (Alberts *et al.*, 2002). Adaptive immunity is mediated by different types of lymphocytes (B cells and T cells) that carry out two types of responses: antibody responses and cell-mediated responses. Once B-cells are activated, they differentiate into plasma cells, which produce antibodies that are released into the blood for neutralisation of viruses and toxins and marking out pathogens for destruction by phagocytic cells. In cell-mediated immune responses, activated T-cells respond directly against antigens that

are displayed on the surface of a host cell, inducing apoptosis in the infected cell (Alberts *et al.*, 2002).

### 1.5.2 Antibody overview

Antibodies are soluble glycoproteins called immunoglobulins (Ig) secreted by plasma cells in response to the antigen. The basic structure of an immunoglobulin consists of four polypeptide chains—two identical heavy chains (with a molecular weight of 50 kDa) and two identical light chains (25 kDa)—held together by disulphide bonds. Both chains contain constant (C) and variable (V) domains. In mammals, there are five different antibody isotypes, based on the type of heavy chain ( $\alpha$ ,  $\delta$ ,  $\epsilon$ ,  $\gamma$  and  $\mu$ ) that is found in IgA, IgD, IgE, IgG and IgM antibodies, respectively. IgG is the most abundant antibody class found in serum and the most widely used for immune library construction and assay development. The basic structure of the IgG molecule is outlined in Figure 1.3. The heavy (H) chain has a variable ( $V_H$ ) and three constant domains ( $C_{H1}$ ,  $C_{H2}$ ,  $C_{H3}$ ), while the light (L) chain is composed of single variable ( $V_L$ ) and constant ( $C_L$ ) domains (Conroy *et al.*, 2009). The fragment crystallisable (Fc) of the immunoglobulin molecule is composed of the  $C_{H2}$  and  $C_{H3}$  domains and it is responsible of the antibody binding to effector molecules and cells. The antigen-binding region of the molecule consists of two identical fragments termed the fragment antigen-binding (Fab). Each Fab fragment is composed of one constant and one variable domain of each of the heavy and light chains, and each of these variable domains contains three complementarity determining regions (CDRs), that are hyper-variable regions that are crucial for the specific binding to antigens (Janeway *et al.*, 2001). The third heavy-chain CDR (CDRH3) shows the greatest variation in terms of length and sequence, and is considered to be the key determinant of antibody specificity (Xu *et al.*, 2000).

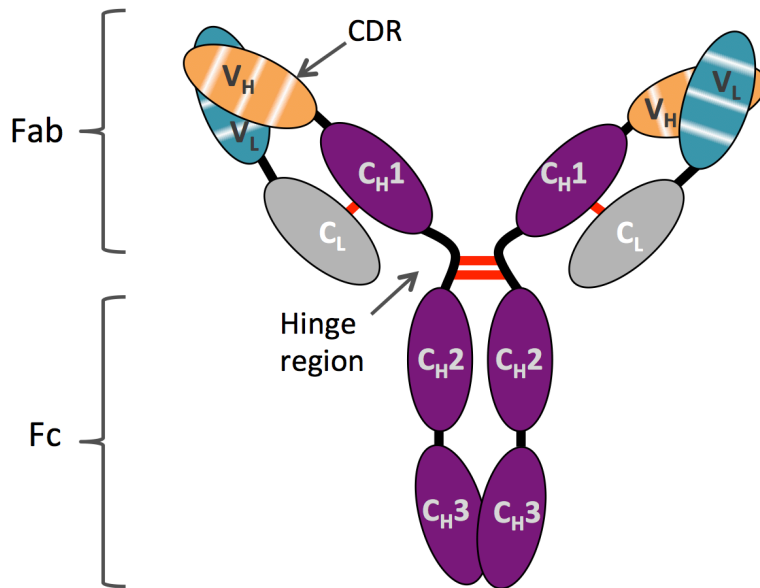


**Figure 1.3.** Basic structure of an IgG molecule. The disulphide bridges are indicated by red lines. The antigen binds in the complementary determining regions (CDRs) of the heavy and light chains. C<sub>L</sub>–Constant light chain; C<sub>H</sub>–Constant heavy chain; V<sub>L</sub>–Variable light chain; V<sub>H</sub>–Variable heavy chain.

### 1.5.3 Generation of avian recombinant antibodies by phage display

#### 1.5.3.1 Recombinant antibody fragments

Understanding of the antibody structure and function and developments in molecular biology in the 1990s made it possible to amplify the heavy and light chain variable domains (V<sub>H</sub> and V<sub>L</sub>) genes of IgY molecules and clone them in eukaryotic expression vectors (Karu *et al.*, 1995). This allowed the soluble expression of antibody fragments from *E. coli*. The smallest of such fragments that retains antigen-binding activity is the scFv fragment, a fusion protein of the V<sub>H</sub> and V<sub>L</sub> chains of the antibody, connected by a serine-glycine linker (Figure 1.4). The scFv format possesses a number of advantages such as simplified antibody library construction and good scFv yields from *E. coli*. Over the past few decades, recombinant antibody technology has allowed the generation of scFv and other antibody fragments from a number of species, including mice, humans, rabbits and chickens (Barbas *et al.*, 2001). Chickens offer certain advantages for the production of immune libraries.

Avian immunoglobulin diversity is generated by a single recombination event and a process known as ‘gene conversion’. Gene conversion uses non-functional pseudogenes located upstream of the functional  $V_H$  or  $V_L$  gene to translocate short sequences into the variable regions and does not affect the N- or C-terminal sequences of the rearranged gene segment, which means that only two primer sets, one for  $V_H$  and other for  $V_L$ , are needed for gene amplification (Narat, 2003). Another advantage of using chickens is the greater phylogenetic distance from humans, compared with other commonly used lab mammalian animals, resulting in a stronger immune response to epitopes that are highly conserved in mammals. In addition to this, polyclonal antibodies (IgY) can be extracted from the eggs of the immunized chicken (Hof *et al.*, 2008). Avian IgY is similar to the IgG in mammals, although it contains an extra constant domain and it is less flexible than the IgG molecule due to the absence of the hinge region (Narat, 2003). Figure 1.4 shows a representation of the IgY molecule and some of its recombinant antibody formats.

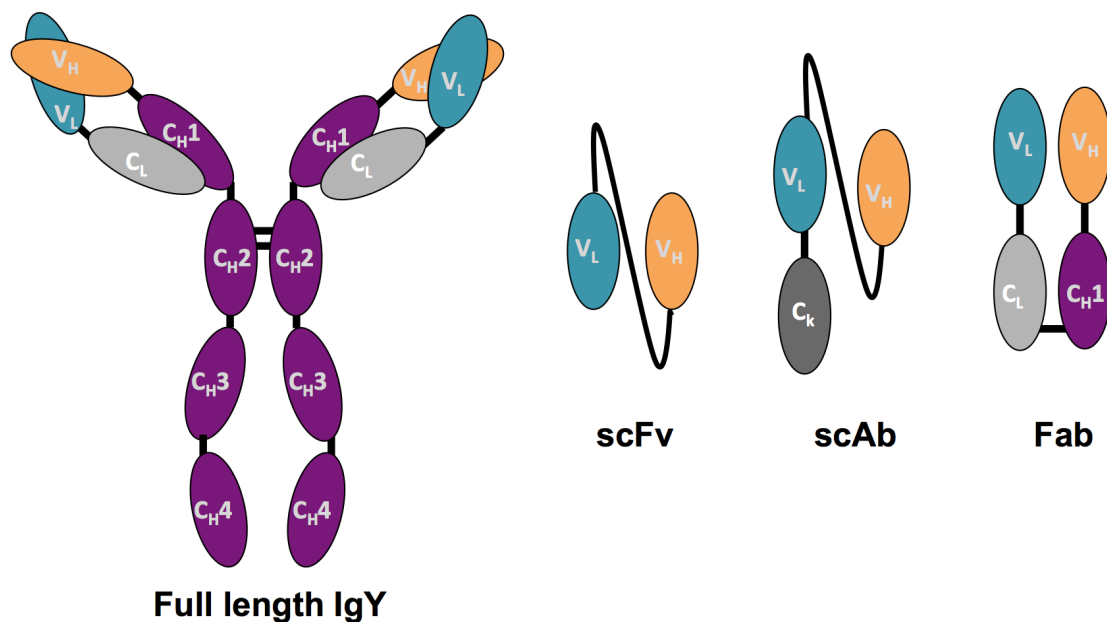


**Figure 1.4.** Schematic structure of the IgY molecule and scFv, scAb and Fab antibody fragments. The scFv consists of the variable heavy ( $V_H$ ) and variable light ( $V_L$ ) domains joined by a flexible protein linker. The scAb (single chain antibody fragment) has an extra fused human kappa light chain constant domain ( $C_k$ ). The Fab fragment is composed of one constant and one variable domain of each of the heavy and light chains.

### **1.5.3.2 Phage display**

Phage display technology was first described by Smith in 1985 (Smith, 1985) and, at present, is the main technique used for *in vitro* screening for identifying ligands that recognise antigens with high affinity. Antigen-specific antibody fragments can be selected from phage-displayed recombinant antibody libraries generated from immune or non-immune libraries. Messenger RNA (mRNA) is isolated from B-cells (typically harvested from the spleen and bone marrow of an immunised animal) and reverse transcribed to complementary DNA (cDNA). The heavy and light chain genes are then amplified by the polymerase chain reaction (PCR) using specific oligonucleotide primers. The amplified heavy and light chains are subsequently annealed together (e.g. by splicing by overlap extension PCR) to construct a complete scFv fragment that is ligated into a phage display vector (e.g. pComb3X) and then transformed into *E. coli* to produce a phage antibody library of approximately  $10^8$  independent *E. coli* transformants. The resulting phage display the antibody as a fusion to a phage coat protein, usually as pIII (Barbas *et al.* 2001; Hammers *et al.* 2014).

Phagemid vectors are filamentous phage-derived vectors containing the origin of replication of a plasmid and a phage-derived origin of replication (also known as the major intergenic region). They also contain an affinity tag to aid in purification and an antibody marker (ampicillin-resistance gene) to confer antibiotic resistance to the host cell upon infection to allow selection and propagation of infected *E. coli* cells. Phagemids usually encode only one type of coat protein and helper phage are required to complete their life-cycle and produce new phage. Helper phage (e.g. VCSM13 or M13K07) provide the phage proteins and enzymes required for replication and package of the phagemid genome. In addition, they bear an independent antibody marker (kanamycin-resistance gene) that favours the selection of cells co-infected with helper phage. Phage particles displaying coat protein-fused antibodies will only be produced when both the phagemid and helper phage have infected the bacterial cell. The helper phage genome has a defective origin of replication so that the resulting phage particles contain predominantly

phagemid DNA (Barbas *et al.* 2001). The physical link between phenotype and genotype in phage display allows the screening of phage encoding target-specific antibodies from large phage pools and also facilitates the determination of the nucleotide sequence of the scFv product by sequencing the corresponding DNA section from the phage genome (Crameri *et al.* 1999).

### 1.5.3.3 Panning of phage display libraries

Screening of phage display libraries can be accomplished by a technique called (bio-) panning (see Figure 1.5). Surface display of the antibodies allows the affinity selection of phage by applying the phage library to an immobilised antigen (on ELISA plates, immunoplates or on cells or microparticle surfaces) and washing away unbound phage. During each round, bound phage are eluted by trypsinisation or low pH and amplified by replication in *E. coli* for another round of selection. Enrichment of the library can be improved by panning under increasing stringency in each round, for example, by increasing the number of washing steps or reducing the amount of coating antigen. Antigen-specific binders predominate after three or four rounds of panning (Barbas *et al.*, 2001).

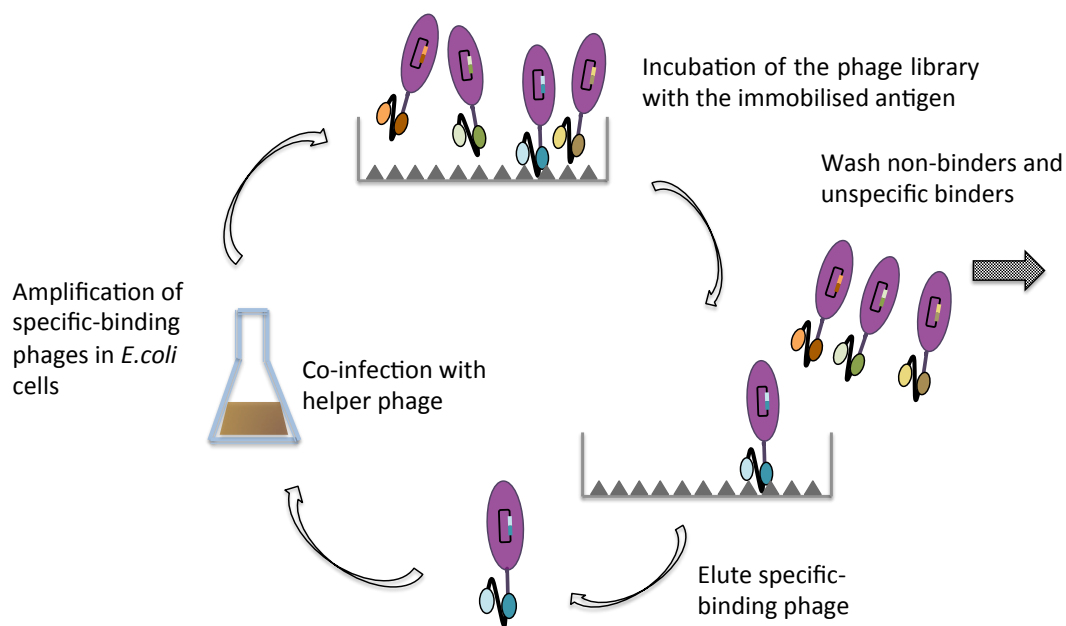


**Figure 1.5.** Panning for selection of antibody fragments from phage-display libraries. A phage library displaying potential scFv of interest is exposed to an immobilised antigen. Unbound phages are washed away and specific-binders are eluted and re-amplified in *E. coli*, in the presence of helper phage. For panning on immobilised antigens, typically 3-6 rounds of panning are necessary.

#### 1.5.4 Clinical applications of recombinant antibody fragments

Although full-size IgG is still the predominant monoclonal antibody format used for clinical applications, many antibody fragments have also been successfully introduced in the clinic, mainly with therapeutic purposes (Table 1.5). Fab fragments have been the most developed in the therapeutic area, receiving FDA approval for a variety of applications over the last two decades. The small size and the lack of the Fc region in these antibodies fragments are responsible for the short serum half-lives and lack of effector functions of these antibodies. These properties can be beneficial when a rapid elimination of the antibodies from blood is desirable, such as in radioimmunotherapy or imaging applications, or for local therapy (Chames *et al.* 2009; Arruebo *et al.* 2011).

ScFv fragments are also becoming very relevant in the biopharmaceutical market and account for 35 % of antibody fragments in clinical trials. Applications for scFv fragments are being explored in the fields of cancer therapy, neurodegenerative diseases, *in vivo* imaging and as vehicles for the delivery of drugs (Monnier *et al.*, 2013). However, some challenges for the *in vivo* use of scFv still need to be overcome—their small size makes them unstable and compromises their ability to concentrate at the target site. Some scFv antibodies are can overcome these limitations, such as Oportuzumab monatox (Viventia Bio Inc.), an anti-epithelial cell adhesion molecule scFv fused to a truncated form of *Pseudomonas* exotoxin A, which is undergoing phase II/III clinical trials for bladder cancer therapeutics. The intravesical administration of this drug maximizes local drug concentration, while limiting its systemic exposure (Kowalski *et al.*, 2012).

**Table 1.5.** Example of monoclonal antibody fragments with FDA approval for diagnostic and therapeutic clinic use. Adapted from Arruebo *et al.* (2011).

Antibody, trade name and company	Type of antibody	Target	Function	FDA approval year
<b>Abciximab (ReoPro)</b> Centocor B.V.	Chimeric Fab	Glycoprotein (GP) IIb/IIIa receptor of human platelets	Platelet aggregation inhibitor	1994, for prevention of cardiac ischemic complications
<b>Certolizumab pegol (Cimzia®)</b> UCB	Humanised Fab'	Tumor necrosis factor $\alpha$ (TNF- $\alpha$ )	Inhibition of systemic inflammation in autoimmune and immune-mediated disorders	2008, for treatment of Crohn's disease; 2009, for treatment of rheumatoid arthritis; 2013, for treatment of psoriatic arthritis and ankylosing spondylitis
<b>Nofetumomab merpentan (Verlurma)</b> Poniard Pharmaceuticals Inc.	MOUSE Fab IgG <sub>2b</sub> -merpentan- <sup>99m</sup> Tc	40 kDa glycoprotein	Nofetumomab is attached to the chelator merpentan, which links it to the radioisotope technetium-99m for radio imaging.	1996, for diagnosis of small cell lung cancer
<b>Lucentis (ranibizumab)</b> Roche	Humanised Fab	Vascular endothelial growth factor A (VEGF-A)	Inhibition of angiogenesis and leakiness of the vessels	2006, for the treatment of Wet Age-Related Macular Degeneration; 2010, for the treatment of macular edema; 2015 for treatment of diabetic retinopathy
<b>ACTEMRA® (tocilizumab)</b> Genentech USA, Inc.	Humanised Fab	Interleukin-6 (IL-6)	Immunosupresor	2010, for treatment of rheumatoid arthritis; 2013 for treatment of juvenile idiopathic arthritis

## 1.6 BIOSENSORS IN CANCER DIAGNOSIS

### 1.6.1 Overview to biosensors

The term 'biosensor' refers to an analytical device that converts a biological response into an electrical signal that can be amplified, displayed and analysed. The operation principle of a biosensor and its main components are shown in Figure 1.6.

Biosensors consist of three components: a bioreceptor or biorecognition element, which recognizes the target analyte; a signal transducer, that converts the biological signal into an electric signal; and a signal processor, which relays and displays the results (Bohunicky *et al.*, 2011).

The specificity of a biosensor depends on the binding capabilities of the bioreceptor molecule, whereas the sensitivity depends on both the recognition element and the transducer used to detect the biological signal. Examples of recognition elements are protein receptors, antibodies, enzymes, nucleic acids, aptamers and phage. Among these, antibodies, DNA, aptamers and phage are also called affinity recognition elements (Arugula *et al.*, 2014). Due to their high affinity, versatility and commercial availability, antibodies have been the most widely used affinity-based recognition elements. Antibodies can be made to be 'fit-for-purpose' in a particular assay. Many immunoassays use labels covalently attached to antibodies, such as horseradish peroxidase (HRP) or alkaline phosphatase (AP), which act as signal-generating molecules.

Analyte binding to the recognition element leads to a change in optical properties, electric charge, mass or heat generation, which can be detected and converted into an electrical signal by a variety of transducers. Transducers can be classified into four major categories: electrochemical (e.g. potentiometric, amperometric, impedimetric), optical (e.g. luminescent, fluorescent, colorimetric), mass-based (e.g. piezoelectric, acoustic wave, magnetoelastic) and calorimetric (heat-based) (Bohunicky *et al.*, 2011).

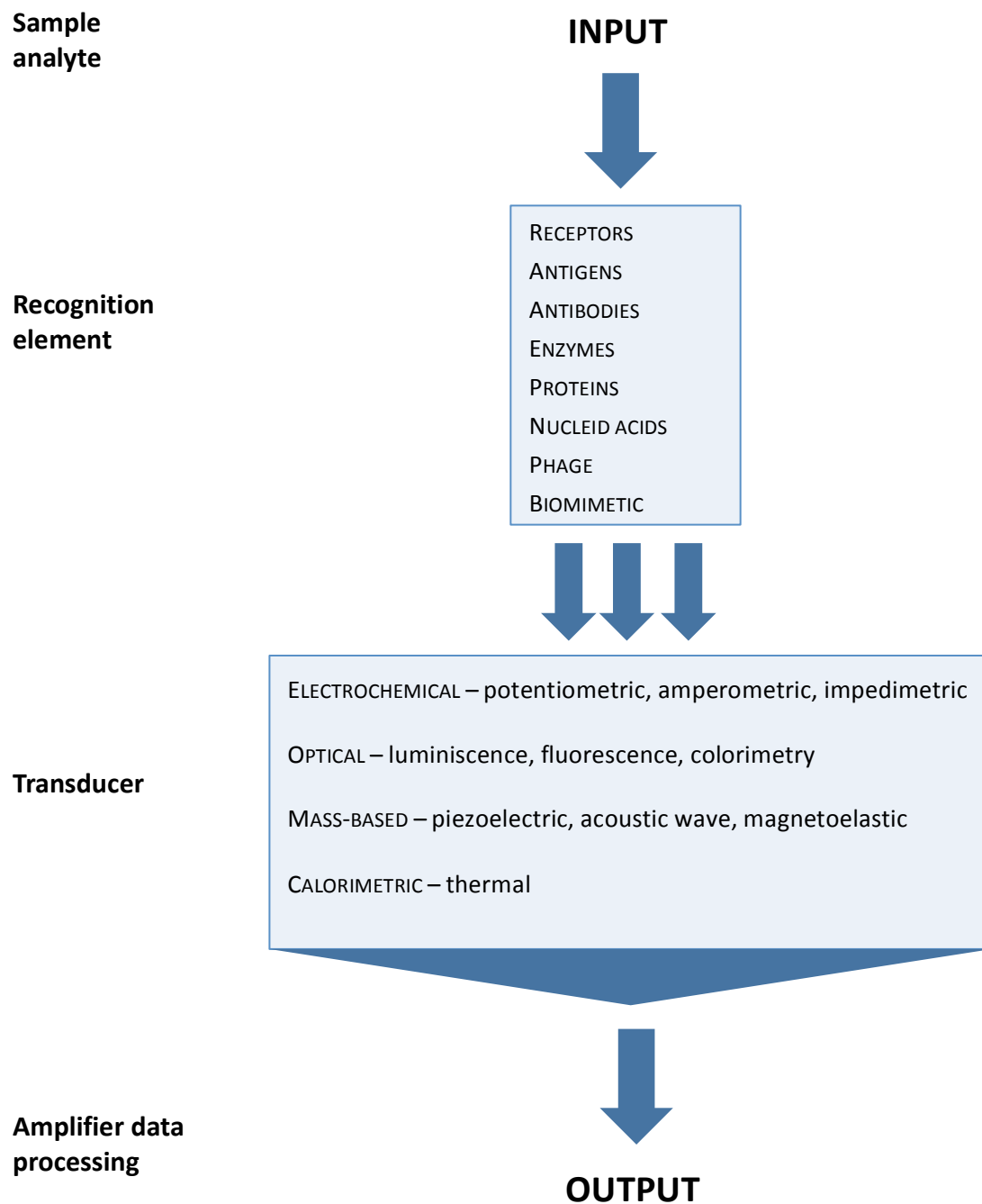


**Figure 1.6.** Schematic representation of a biosensor operating mechanism. A biosensor consists of a biological sensing element (that recognizes the analyte of interest) and a transducer, which translates the biological response into a quantifiable and processable signal. Adapted from Bohunicky *et al.* (2011).

Nanotechnology is having an increasing impact in the field of biosensors. In recent years, the use of nanomaterials (in scale from 1 to 100 nm) for the construction of biosensors has allowed the introduction of new types of transduction mechanisms that provide an improved sensitivity, selectivity or response time (Jena *et al.*, 2008;

Filip *et al.*, 2014; Spain *et al.*, 2015). Carbon nanotubes (Texeira *et al.*, 2014), graphene (Tehrani, 2014), quantum dots (Xia *et al.*, 2015; Jenrette *et al.*, 2015), nanowires and nanoparticles (Texeira *et al.*, 2014; Spain *et al.*, 2015) are some examples of nanomaterials that have been used in biosensors for diagnostics applications.

### **1.6.2 Biosensors for cancer detection**

Biosensors are emerging as practical and useful bioanalytical tools in the diagnostics industry. They have the potential to provide low-cost, fast and accurate detection of target analytes in biological fluids, such as blood, serum or urine. Biosensors are also good candidates for point-of-care (POC) applications, allowing rapid testing near the site of patient care (Okafor *et al.*, 2008; Wilkes and Evans, 2014; Hsieh *et al.*, 2015; ).

In terms of cancer diagnosis, biosensors can detect tumour biomarkers, providing information about the presence of the tumour and its nature (whether benign or aggressive). Given the complexity of cancer, multiplex biosensors that can detect a panel of biomarkers simultaneously are particularly useful (Wei *et al.*, 2010; Lee *et al.*, 2015). Existing clinical methods to detect tumor markers rely strongly on traditional immunological methods, such as immunohistochemistry (IHC) or enzyme-linked immunosorbent assay (ELISA), which can be highly sensitive and specific, but usually require specific and costly lab equipment. Furthermore, in most cases, the samples collected have to be sent to centralized laboratories for analysis by qualified medical staff, which increases the time required to obtain a test result and delays treatment decisions. The introduction of biosensors into the clinic will help to reduce test costs and turnaround times, fulfilling the need of multiplexing and point-of-care early diagnosis.

Electrochemical biosensors have been demonstrated to be promising tools for pharmaceutical and medical analysis, examples of which are the vastly commercially available glucose biosensors (from Life Scan, Roche Diagnostics, Abbott and Bayer).

They offer certain advantages, including low-cost fabrication (Sokolov *et al.*, 2009), the possibility of miniaturisation (Yang and Huang, 2009; Lazerges *et al.*, 2013), minimal power requirements, and suitability for medical implantable devices and point-of-care applications (Stingl *et al.*, 2013; Ghafar-Zahel, 2014; Sun *et al.*, 2014). Electrochemical biosensors are based on the detection of a measurable current (amperometric), potential difference between the working electrode and the reference electrode (potentiometric), impedance change caused by a biorecognition process (impedimetric) or (conductometric). Since the present work involves the use of recombinant antibodies as recognition elements in amperometric and impedimetric biosensors, these will be described in more detail.

#### **1.6.2.1 Amperometric biosensors**

The first biosensors developed (Clark *et al.*, 1956; Updike and Hicks, 1967) were based on electrochemical detection. Amperometric biosensors measure the current resulting from the oxidation or reduction of electroactive materials in a biochemical reaction, when a constant potential is applied between two electrodes (Grieshaber *et al.*, 2008). In amperometry, redox conversion of the electroactive species results in a succession of electron transfers that creates a current flow (typically from nano to micro-amperes) proportional to the analyte concentration that can be measured. (Monošík *et al.*, 2012). Since not all analytes are able to act as redox partners, artificial electrons acceptors (mediators) can be used for direct or indirect transduction (Chaubey *et al.*, 2002; Grieshaber *et al.*, 2008). In amperometry, the current is measured as a function of time, providing information about the rate at which electrochemically active species (analyte or mediator) are being oxidised or reduced on the surface of the electrode (Rousell *et al.*, 2014).

In recent years, several groups have investigated the use of amperometric biosensors for the detection of cancer biomarkers. Sarkar and co-workers developed an immunoassay for PSA detection on amperometric screen-printed electrodes with a LOD of 0.25 ng/mL (Sarkar *et al.*, 2002). An anti-PSA monoclonal antibody was

immobilised on the working electrode and a HRP-labelled antibody to PSA was used as tracer. The HRP conjugated to the antibody catalysed the reaction of iodine ions with the glucose oxidase (GOx)-generated hydrogen peroxide, so the resulting change in current was proportional to the concentration of PSA. Similarly, another group was able to detect very low concentrations of HER2 (26 pg/mL) from human serum and cell lysates with an amperometric magneto-immunosensor based on a sandwich ELISA (Eletxigerra *et al.*, 2015). Carcinoembryonic Antigen (CEA) detection for colon cancer diagnostic below clinically relevant threshold (5 ng/mL) was also achieved by amperometric detection (Laboria *et al.*, 2010). In this case, surface chemistry was used to facilitate the antibody immobilisation in a self-assembled monolayer (SAM).

#### **1.6.2.2 Impedimetric biosensors**

Impedimetric biosensors measures changes in the opposition to electron flow (in terms of resistance and reactance) of a conducting medium, arising from binding events (Bahadir and Sezgintürk, 2014) or from bacterial metabolic redox reactions (Broesel-Oliu *et al.*, 2015). Electrochemical impedance spectroscopy (EIS) measures the current response to the application of an AC potential voltage as a function of the frequency, and represents a powerful tool for 'label-free' detection of biorecognition events, such as antibody-antigen interactions (Kongsunphol *et al.*, 2014), or for the detection and quantification of pathogenic bacteria (Wang *et al.*, 2012; Barreiros dos Santos *et al.*, 2013; McPartlin and O'Kennedy, 2014). EIS examines the electrical properties at the biosensor surface and, therefore, is commonly used for electrode surface characterisation after modification, layer formation or immobilization of biorecognition elements. A main advantage of EIS, compared to amperometry, is that it provides non-electroactive detection of molecules (ErtuğruL and Uygun, 2013). However, this also means that EIS is non-chemically specific and non-specific binding on the electrode surface can also produce an impedimetric change. Therefore, the selection of highly-specific

recognition elements and blocking non-specific binding sites are essential (Riquelme *et al.*, 2016).

Reported literature reflects that EIS can be used for the detection of cancer cells and biomarkers. Seven *et al.* (2013) developed a biosensor for the label-free detection of MCF-7 breast cancer cells (overexpressing HER2 on their surface) using an anti-HER2 antibody covalently grafted on electro-generated polymers (Seven *et al.*, 2013). Detection of HeLa cervical cancer cells was also possible using an impedimetric biosensor based on PEGylated arginine-functionalised magnetic nanoparticles. Functionalisation of the magnetic nanoparticles accelerated the electron transfer for an enhanced detection of cancer cells (LOD = 10 cells/mL) (Chandra *et al.*, 2011). In addition, several groups have shown the utility of impedimetric biosensors for the detection of serum biomarkers (Asav and Sezgintürk, 2014; Johari-Ahar *et al.*, 2015; Spain *et al.*, 2015; Jolly *et al.*, 2016). For example, Jolly and co-workers developed an aptamer-based impedimetric biosensor for PSA detection using thiol-terminated sulfo-betamine surface chemistry to prevent non-specific binding to the sensor surface (Jolly *et al.*, 2016).

## 1.7 MICROFLUIDICS PLATFORMS FOR BIOANALYSIS

Microfluidics is a multidisciplinary field that deals with the design and fabrication of systems in which micrometer-sized chambers and tunnels are used for the manipulation and control of small fluids, ranging for  $10^{-9}$  to  $10^{-18}$  litres (Whitesides, 2006).

Microfluidics technology became popular in the early 1990s, when the application of microchannels for sample separation for the miniaturisation of chemical sensing systems was demonstrated (Manz *et al.*, 1990; Harrison *et al.*, 1992). Nowadays, the focus of microfluidics research is on their integration in biosensors to facilitate miniaturisation, automation, fast turn-around times and multiplexing.

The excitement behind microfluidics systems for biosensing mainly relies on their ability to integrate and miniaturise complex laboratory procedures onto a small single chip, cartridge or disc (Chin *et al.*, 2012). This is the origin of 'lab-on-a-chip' or 'lab-on-a-disc' platforms. In recent years, microfluidic technologies have been successfully implemented in several of the main bioanalytical techniques (Table 1.6), including blood chemistries (Nwankire *et al.*, 2014), immunoassays (Yu *et al.*, 2015), nucleic-acid amplification tests (Mauk *et al.*, 2015), and flow cytometry (Maleki *et al.*, 2012). The integration of multiple preparative and analytical microfluidic technologies in a single device allows the use of unprocessed samples to run an entire assay at a point-of-care (POC) setting. Preconditioning of samples, when needed, is possible thanks to centrifugation, which allows the purification of plasma from blood, or microfluidic technologies such as an on-chip filter trench where blood cells are sedimented and captured (Yager *et al.*, 2006; Lee *et al.*, 2011). As mentioned previously, microfluidic systems facilitate the miniaturisation of assays, thus reducing the surface-to-volume ratios, enhancing aspects of assay kinetics and allowing significant reductions in sample/reagent volumes. In this context of micrometre-sized channels, sample flow is laminar, and fluid mixing needs to be achieved by means other than traditional turbulent diffusion. Controlled fluid flow and mixing is essential for biosensing and in a microfluidic system this can be accomplished by passive methods (e.g., by lamination, use of specific surface chemistries for immobilisation of reagents, minimisation of non-specific binding, generation of hydrophobic/hydrophilic regions, and by use of specific geometries or topographies of channels), by the use of micro-pumps or micro-valves, or by applying an external energy supply (Lee *et al.*, 2011). The ability of sacrificial valves to create vapour barriers makes them ideal for reagent storage. Traditionally, sacrificial valves required external actuators (e.g., laser diodes) in order to be activated. The use of all external actuators except a spindle motor can be excluded by using new valve designs, such as dissolvable-film (DF) valves that dissolve beyond a critical rotational frequency (Nwankire *et al.*, 2011). Thus, centrifugal microfluidic platforms offer precise fluid control and only require a simple motor for powering the system (Hugo *et al.*, 2014). The technology needed to drive the microfluidic discs is as simple as that used in CD players or DVD drivers.

In the view of these advantages, the coupling of microfluidics and biosensing offers new opportunities for future sensors, such as portability, low-cost, reduced assay times and multiplexing ability.

### **1.7.1 Microfluidic-integrated biosensors for diagnostics**

At the moment, more than ninety companies are working on microfluidic-based diagnostics worldwide, as registered in FluidicMEMs database (last updated: February 9, 2016). The ultimate goal for lab-on-a-chip devices is the integration of sample preparation and processing and detection techniques in a self-contained, disposable system. One of the strengths of microfluidics is that they are able to produce sensitive results by detecting the signal produced in a very small area using fluorescence or other more recently implemented but ultrasensitive detection methods. Electrochemical detection, in particular, has been widely explored for improving the sensitivity and also often the specificity of traditional tests, generating quantitative testing due to the use of portable electrochemical analysers in POC platforms. For example, the i-Stat blood gas analyser (Table 1.6) combines self-contained cartridges with microfluidic components and electrochemical detection (including amperometry, voltammetry, and conductance, depending on the testing analyte). Each cartridge contains a sample chamber, a calibration solution, a waste chamber, and a unique combination of sensors, depending on the test. i-Stat analysers are also battery-powered, making its use suitable in remote areas (Sharma *et al.*, 2016).

**Table 1.6:** List of FDA-approved microfluidic-based tests. Adapted from Sharma *et al.* (2015).

Test name and company	Tested analyte	Sample required	Components	Results type and turnaround time
The Piccolo® (Abaxis)	Blood chemistries	10µL of WB/S/P	Disposable test discs and portable analyzer	Quantitative results in 12 min.
Alere Triage® MeterPro (Biosite, Alere)	Blood/urine chemistries including “waived” Lipid and liver panels	225µL WB/P/U	Disposable cartridges, and meter	Qualitative results in 15-20 min.
The epoc® Blood Analysis System (Epcal, Alere)	Blood chemistries	92µL WB	Test cards and wireless card reader with a host mobile computer	Quantitative results in about 30 sec.
Simplexa (Focus Dx, Quest)	Flu A/B & RSV	Nasopharyngeal swabs	PCR platform (3M™ Integrated Cycler) and amplification discs with sample wells	Quantitative results in 1h.
BD MAX™, GBS Assay, IDI-Strep B Assay (HandlyLab, BD)	Group B Streptococcus (GBS)	Vaginal/rectal swab samples	Cepheid Smart Cycler® RT-PCR system, disposable cartridge and computer system	Qualitative results in 1h.
i-STAT Analyser (i-STAT Corp, Abbot)	Blood chemistries; coagulation; cardiac markers	Two drops of WB	Handheld analyser and self-contained cartridges	Quantitative results in less than 15 min.
FilmArray RP (Idaho Technologies)	Panel of respiratory pathogens	Nasopharyngeal swabs	FilmArray instrument and freeze-dried reagents in pouches	Qualitative results. 2 min of hands-on time; about a 1-h turnaround time
Proxima (Sphere Medical)	Blood chemistry	Arterial blood	Disposable multi-parameter microanalyser, silicon chips	Quantitative results in approximately 3 min.
TearLab Osmolarity System (TearLab)	Osmolarity of human tears (diagnosis of Dry Eye Disease)	50nL of tear film	Disposable microchip works in conjunction with a pen that convey data to the osmolarity reader	Quantitative results in seconds

WB – whole blood; S – Serum; P – Plasma; U – Urine.

Much of the research published on microfluidics focuses on individual components of microfluidic platforms, such as those needed for sample pre-treatment (Haeberle *et al.*, 2006; Kim *et al.*, 2009; Wu *et al.*, 2011) or reagent mixing (Leong *et al.*, 2007; Weng *et al.*, 2009; Weng *et al.*, 2011) and those describing integrated microfluidic systems remain in a proof-of-concept state (Hugo *et al.*, 2014; Tai *et al.*, 2014). Some companies have, nevertheless, managed to satisfy all the criteria needed to launch their microfluidic-based platforms on the market. Table 1.6, adapted from Sharma *et al.* (2016) shows a compilation of FDA-approved microfluidics-based technologies for 'on-site' tests.

### **1.7.2 Microfluidics for multiplexing**

Multiplexed assays are crucial in the field of diagnostics. The benefits of using multiplexed assays include improved differential diagnostic of malignant diseases, thanks to the use of biomarker panels (Amonkar *et al.*, 2009; Biella *et al.*, 2013), and cost-effectiveness, saving time and reducing sample volume requirements.

Microfluidics provides suitable platforms for multiplexing, facilitating the automation of fluid handling and allowing flow control for the incorporation of sequential steps. For example, the Optimiser™ technology platform (Siloam biosciences) provides an alternative to conventional 96-well ELISA plates. This technology combines a typical 96-well microtitre layout with a microfluidic channels connected to each well. The wells of the Optimiser™ are used only for sample loading, as the binding events occur in the microfluidic channels. This increases the surface-area-to-volume ratio, increasing the area to capture antibodies while reducing diffusion distances, improving assay kinetics. Traditional washing steps are also eliminated—each microchannel has a volume of only 4.5  $\mu\text{L}$ , so the addition of the next reagent in assay step flushes unbound reagents from the microchannels. Only a final wash with wash buffer is required before the addition of substrate (Kay *et al.*, 2011). Compared to conventional ELISA plates, this platform reduces assay time (13 minutes for a sandwich assay), reduces sample volumes (<2  $\mu\text{L}$  per data point) and improves

sensitivity up to 1,000-fold (as claimed by manufacturers). Luminescence or fluorescence detection can be achieved with a conventional microplate reader.

Other diagnostic companies have developed microfluidic-based systems to perform multiplexed immunoassay blood tests directly at the point-of-care. Some of the disposable cartridges for the already mentioned i-Stat analyser (Table 1.6) allow for multiplex detection of cardiac troponin I (cTnI), B-type natriuretic peptide (BNP) and creatine kinase MB isoenzyme (CK-MB) for the diagnosis and treatment of myocardial infarction (i-STAT System | Abbott Point of Care website). OPKO Diagnostics' platform (Opko website) also uses cartridges where different panels of biomarkers can be measured from blood, such as cardiac cTnI, BNP and D-dimer (cardio panel) or total PSA, free PSA, testosterone and novel markers (PCa panel).

## **1.8 AIMS**

While PSA has been a well-established biomarker in clinical practice, its limitations for prostate cancer diagnosis are well known. A variety of alternative biomarkers, including different PSA isoforms, has been proposed by different research groups, but their use for the detection of prostate cancer is still unclear. The aim of my project is to generate recombinant antibodies against some of these biomarkers and incorporate them in different biosensing platforms to elucidate if the simultaneous testing of these new biomarkers with PSA isoforms can improve current diagnostic approaches.

For this purpose, the specific objectives of this work were:

- The generation of a novel recombinant antibody for the detection of HER2, a potential new biomarker for prostate cancer.
- Purification and characterisation of novel avian recombinant antibody fragments (scFv) by ELISA, SDS-PAGE and Western blotting.

- Incorporation of anti-HER2 scFv antibodies into a highly sensitive impedimetric immunosensor for HER2 detection from serum samples.
- The application of recombinant antibodies to HER2 and free PSA for the development of a centrifugal microfluidic 'lab-on-disc' to enable simultaneous multiplex-analyte detection.
- The integration of 'in-house' generated anti-fPSA scAb antibodies on an amperometric magneto-immunosensor for the sensitive detection of this PSA isoform.

# **Chapter 2**

## **Materials and Methods**

## 2.1 MATERIALS AND EQUIPMENT

### 2.1.1 Equipment

Equipment name	Supplier
Heraeus™ Microcentrifuge D-37520 with #3325 rotor DynaMag™-2 Magnet Px2 Thermal Cycler HBPX2220	Thermo Fisher Scientific Inc., 81 Wyman Street, Waltham, MA 02451, USA.
NanoDrop™ 1000 Spectrophotometer	NanoDrop products, 3411 Silverside Rd., Bancroft Building, Wilmington, DE 19810, USA.
Tecan Sunrise™ Microplate Reader Tecan Safire2™ Microplate Reader Infinite™ 200	Tecan Safire2™ Microplate Reader Group Ltd., Seestrasse 103, CH-8708 Männedorf, Switzerland.
Vibra Cell™ sonicator	Sonics and Materials Inc., 53 Church Hill Road, Newtown, CT 06470-1614, USA.
Gene Pulser Xcell PowerPac™ Basic Mini-PROTEAN Tetra Cell DNA Gel Apparatus Bio-Rad (Wide-Mini- Sub® Cell GT) Gel Doc™ EZ System Trans-Blot® SD Semi-Dry Transfer System	Bio-Rad Laboratories, Inc., 4000 Alfred Nobel Drive, Hercules, CA 94547, USA.
Centrifuge 5810 R with swing-bucket rotor (A-4-62) and fixed- angle rotors (F-45-30-11 and F-34-6-38) Thermomixer C with Thermoblock	Eppendorf House, Gateway 1000 Whittle Way, Arlington Business Park, Stevenage, SG1 2FP, UK.
Spectrafuge™ Mini Laboratory Centrifuge	Labnet International, Inc., 31 Mayfield Avenue, Edison, NJ, 08837, USA.
Roller mixer SRT1	Scienlab, Inc., 14025 Smith Rd., Houston, Texas 77396, USA.
Homogeniser Ultra Turrax	IKA-Werk Ultra-Turrax, Janke & Kunkel-Str. 10. 79219 Staufen, Germany.
Dark Reader® Transilluminator	Clare Chemical Research, Inc., 995 Railroad Ave, Unit E, Dolores, CO 81323, USA.
Explorer E11140 in Digital Scale	OHAUS Corporation, 7 Campus Drive, Suite 310, Parsippany, NJ 07054, USA.
HermLe Z2333 MK-2 refrigerated centrifuge	HermLe Labortechnik GmbH, Siemensstr. 25, D-78564 Wehingen, Germany.
Autoclave (60 L)	Priorclave Ltd., 129-131 Nathan Way, West Thamesmead Business Park, London, SE28 0AB, UK.

Drying oven DC125	Genlab Limited, Tanhouse Lane, Riverview Industrial Estate, Widnes, Cheshire, WA8 0SR, UK.
Sanyo Orbital Incubator	Panasonic Biomedical Sales Europe, BV, 9 The Office Village, North Road, Loughborough, Leicestershire, LE11 1QJ, UK.
Knife-plotter machine (Graphtec CE5000)	Graphtec America Inc., 1762 Armstrong Avenue Irvine, CA 92614-5724, USA.
CO <sub>2</sub> Laser Engraver	Epilog Laser, 16371 Table Mountain Parkway Golden, CO 80403, USA.
Hot Roll Laminator	ChemInstrument, 510 Commercial Drive, Fairfield, OH 45014, USA.
Electrochemical workstation CH604E	CH Instruments, Inc., 3700 Tenneson Hill Drive Austin, TX 7838-5012, USA

### 2.1.2 Reagents

All reagents were purchased from Sigma-Aldrich Ireland Ltd., Vale Road, Arklow, Wicklow, Ireland, unless otherwise specified.

Reagent	Supplier
GoTaq® DNA Polymerase 1kb DNA Ladder	Mybio Ltd., Kilkenny Research & Innovation Centre, Saint Kieran's College, College Road, Kilkenny, Ireland.
Deoxynucleotide (dNTP) Solution Mix	New England Biolabs, 240 County Road, Ipswich, MA 01938-2723, USA.
Primers	Integrated DNA Technologies, BVBA, Interleuvenlaan 12A, B-3001 Leuven, Belgium.
Sfil T4 DNA ligase Antarctic phosphatase	Brennan & Company, 61 Birch Avenue, Stillorgan Industrial Park, Stillorgan, Ireland.
RNA later RNase zap Platinum® Taq DNA Polymerase SOC media Helper phage 3M Sodium Acetate SYBR® Safe DNA gel stain	Bio-Sciences Ltd., 3 Charlemont Terrace, Crofton Road, Dun Laoghaire, Ireland.
Kanamycin Tetracycline Carbenicillin Glycerol	Fisher Scientific Ireland Ltd., Suite 3 Plaza, 212 Blanchardstown, Corporate Park 2, Ballycoolin, Dublin 15, Ireland.

Agarose Agar Dynabeads® M-280 Tosylactivated Pierce™ 1-Step Transfer Buffer	
Tryptone Yeast extract	Cruinn Diagnostics Ltd., Unit 5/6B Hume Centre, Parkwest Industrial Estate, Dublin 12, Ireland.

### 2.1.3 Bacterial strains

Strain	Supplier
XL1-Blue <i>E.coli</i>	Agilent Technologies Ireland, Euro House, Euro Business Park, Little Island, Cork, Ireland.
TOP10F' chemically competent <i>E.coli</i>	Bio-Sciences Ltd., 3 Charlemont Terrace, Crofton Road, Dun Laoghaire, Ireland.

### 2.1.4 Antibodies

Antibody	Source	Supplier
HRP-labelled anti-M13	Mouse	GE Healthcare Life Sciences, Amersham Place, Little Chalfont, Buckinghamshire, HP7 9NA, UK.
Anti-HA high-affinity	Rat	Roche Diagnostics Ltd., Charles Avenue, Burgess Hill, West Sussex, RH159RY, United Kingdom
Anti-chicken IgY-fab-HRP	Donkey	Gallus Immunotech Inc., RR#3, 6570 1st Line West Garafraxa, Fergus, ON N1M 2W4, Canada.
HRP-labelled anti-Prostate Specific Antigen antibody [5A6] (ab24466)	Mouse	Abcam, 330 Cambridge Science Park, Cambridge, CB4 0F, UK.
Anti-Prostate Specific Antigen antibody (ab46976)	Rabbit	

### 2.1.5 Antigens

Antigen	Source	Supplier
Recombinant human ERBB2	Human cells	CD Biosciences, Inc., 45-16 Ramsey Road, Shirley, NY 11967, USA.
Free PSA	Human semen	Lee Biosolutions, Inc., 10850 Metro Ct., Maryland Heights, MO 63043, USA.

### 2.1.6 Commercial kits

Kit	Supplier
RNeasy Mini Kit	Qiagen Ltd., Skelton House, Lloyd Street North, Manchester M15 6SH, United Kingdom.
SuperScript® II First-Strand Synthesis System for RT-PCR	Bio-Sciences Ltd., 3 Charlemont Terrace, Crofton Road, Dun Laoghaire, Ireland.
NucleoSpin® Gel and PCR Clean-Up NucleoSpin® Plasmid NucleoBond® Xtra Midi	Macherey-Nagel GmbH & Co. KG Neumann- Neander-Straße 6-8 52355 Düren
EggPress IgY purification kit	Gallus Immunotech Inc., RR#3, 6570 1st Line West Garafraxa, Fergus, ON N1M 2W4, Canada.

### 2.1.7 Culture Media formulations

Media	Components
Luria- Bertani Broth (LB)	Tryptone 10 g/L Yeast Extract 5 g/L NaCl 10 g/L Agar (if needed) 15 g/L
Super Broth (SB)	MOPS 10 g/L Tryptone 30 g/L Yeast Extract 20 g/L Final pH: 7.0
100X 505	Glycerol 50 mL Glucose 5 g diH <sub>2</sub> O Up to 100 mL
1M MgSO <sub>4</sub>	MgSO <sub>4</sub> 12.37 g diH <sub>2</sub> O 100 mL

## 2.1.8 Buffer formulations

### 2.1.8.1 General buffers

Buffer	Components
1X Phosphate-buffered saline (PBS, 10 mM)	NaCl 8 g Na <sub>2</sub> HPO <sub>4</sub> 1.15 g KH <sub>2</sub> PO <sub>4</sub> 0.24 g diH <sub>2</sub> O Up to 1 L Final pH: 7.3
1X PBS-Tween 20 (PBS-T)	1X PBS 1L Tween 20 0.05 % (v/v) Final pH: 7.3
50 mM Carbonate buffer	Na <sub>2</sub> CO <sub>3</sub> 0.795 NaHCO <sub>3</sub> 1.465 diH <sub>2</sub> O Up to 500 mL Final pH: 9.6
20 mM Tris buffer	Tris Base 2.42 g NaCl 8.77 g diH <sub>2</sub> O Up to 800 mL Final pH: 8.5

### 2.1.8.2 Buffers for sodium dodecyl sulfate-polyacrylamide gel electrophoresis

Buffer	Components for 1 gel (6 mL)
12.5 % Separating Gel	1 M TrisHCl, pH 8.8 1.5 mL 30 % (v/v) Acrylagel 2.5 mL 2 % (v/v) Bis-Acrylagel 1 mL Di H <sub>2</sub> O 934 µL 10 % (w/v) SDS 30 µL 10 % (w/v) APS 30 µL Tetramethylethylenediamine (TEMED) 6 µL
4.5 % Stacking Gel	1 M TrisHCl, pH 8.8 300 µL 30 % (v/v) Acrylagel 375 µL 2 % (v/v) Bis-Acrylagel 150 µL Di H <sub>2</sub> O 1.74 mL 10 % (w/v) SDS 24 µL 10 % (w/v) APS 24 µL Tetramethylethylenediamine (TEMED) 2.5 µL
4X Loading buffer	0.5 M Tris, pH 6.8 2.5 mL Glycerol 2 mL β-mercaptoethanol 0.5 mL 20 % (w/v) SDS 2.5 mL Bromophenol Blue 220 ppm Di H <sub>2</sub> O 2.5 mL
10X Electrophoresis buffer	10 mM Trizma Base 30 g Glycine 144 g 0.1 % (w/v) SDS 10 g Di H <sub>2</sub> O Up to 1 L

### 2.1.8.3 Buffers for Immobilized metal ion affinity chromatography (IMAC) purification

Buffer	Components
10X Phosphate-buffered saline (PBS)	NaCl 80 g Na <sub>2</sub> HPO <sub>4</sub> 11.5 g KH <sub>2</sub> PO <sub>4</sub> 2.4 g diH <sub>2</sub> O Up to 1 L Final pH: 7.3. Autoclave.
1X PBS	10X PBS 100 mL diH <sub>2</sub> O 900 mL Final pH: 7.3. Autoclave.
Sonication buffer	0.5 M NaCl 14.71 g 20 mM Imidazole 0.681 g 1X PBS 500 mL
Running Buffer	0.1 % (v/v) Tween-20 in sonication buffer
Elution buffer 1	100 mM NaAc, pH 4.4
Neutralisation buffer	100 mM NaOH 50 µL 10X PBS 50 µL
Elution buffer 2	250 mM imidazole in 1X PBS, pH 7.5

### 2.1.8.4 Buffers for magnetic beads bioconjugation

Buffer	Components
0.1 M Borate Buffer	Boric acid 0.6183 g diH <sub>2</sub> O Up to 100 mL Final pH: 8.5
3 M Ammonium Sulfate in Borate Buffer	(NH <sub>4</sub> ) <sub>2</sub> SO <sub>4</sub> 12.37 g 0.1 M Borate Buffer Up to 25 mL
10 mM Phosphate Buffer	NaHPO <sub>4</sub> 115mg NaH <sub>2</sub> PO <sub>4</sub> x H <sub>2</sub> O 26.18 mg diH <sub>2</sub> O Up to 100 mL Final pH: 7.4
Phosphate buffer, 0.1 % (w/v) BSA	BSA 25 mg NaCl 220 mg 10 mM Phosphate Buffer 25 mL
Phosphate buffer, 0.5 % (w/v) BSA	BSA 125 mg NaCl 220 mg 10 mM Phosphate Buffer 25 mL

### **2.1.8.5 Other solution formulations**

<b>Buffer</b>	<b>Components</b>	
10 X Blue DNA Loading Dye	Glycerol	5 mL
	EDTA, disodium salt	37.2 mg
	Bromophenol blue	4 mg
	diH <sub>2</sub> O	Up to 10 mL

## **2.2 METHODS**

### **2.2.1 General molecular biological techniques**

#### **2.2.1.1 Agarose gel electrophoresis**

Agarose gels were used for the separation and analysis of DNA. Agarose was dissolved at the required concentration (0.6–2 % [w/v]) in Tris-acetate-EDTA (TAE) buffer by boiling the mixture for 1–3 minutes. Once cooled, 10 µL of SYBR® Safe DNA Gel Stain per 100 mL of agarose gel were added and mixed by gently stirring. The gel was immediately poured into a prepared gel mould. Blue DNA loading dye was added (when needed) to the samples at a 1X concentration prior to loading for tracking migration during electrophoresis. Along with the samples, 1 kb Plus DNA molecular weight ladder (Promega) was loaded in each gel for size quantification. The gel was electrophoresed at 90V for approximately 1 hour until distinct bands were observed. Gels were visualised using a blue light Dark Reader transilluminator and imaged with a Gel Doc™ EZ Imager.

#### **2.2.1.2 Extraction of DNA from agarose gels using NucleoSpin® Gel and PCR Clean-Up (MN)**

The appropriate DNA bands were cut out from the agarose gel using a sterile scalpel under the blue light of a Dark Reader transilluminator. Extraction of DNA from agarose gels was performed using NucleoSpin® Gel and PCR Clean-Up kit, as per the

manufacturer's guidelines. The product was then quantified using the Nanodrop ND-1000 Spectrophotometer and stored at -20°C.

#### ***2.2.1.3 Ethanol precipitation of DNA***

Ethanol-precipitation of DNA was used to change the solvent in which the DNA was suspended and/or to concentrate DNA samples. DNA was ethanol-precipitated by adding 0.1 volumes of 3 M sodium acetate (pH 5.2), mixing, adding 2 volumes of absolute ethanol, mixing, and incubating O/N at -20°C. Following precipitation, DNA was pelleted by centrifugation at 15,994 x g for 30 minutes at 4°C in a HermLe Z2333 MK-2 centrifuge. The supernatant was carefully discarded and the sample was centrifuged as before for a further minute to remove residual liquid from the pellet. The pellet was then rinsed with 1 mL of 70 % (v/v) ethanol and centrifuged at 16,000 x g for 2 minutes. The supernatant was carefully removed and the pellet air-dried and resuspended in ultrapure molecular grade water.

#### ***2.2.1.4 Sodium dodecyl sulphate polyacrylamide gel electrophoresis (SDS-PAGE)***

SDS-PAGE was used for the separation of proteins by electrophoresis for the assessment of protein relative molecular masses, purity and quality. SDS is used to denature the proteins and confers them with a negative charge. SDS-treated proteins have a similar charge-to-mass ratio, resulting in a separation of proteins by relative size during electrophoresis.

The 1-D vertical gel casting apparatus (Mini-PROTEAN Tetra Cell) was set up as per the manufacturer's instructions. Separating and stacking gels were prepared as outlined in Section 2.1.8.2, adding the APS and TEMED just before pouring the gels in the glass plates (held together in the casting stand by clamps), as their addition to the gels initiates polymerisation. Firstly, the separating gel was poured until it reached approximately 2–3 cm from the top of the smaller glass plate. Once the separating gel had polymerised, the stacking gel was poured on top of the separating

gel and a plastic comb was gently placed into the gap between the two glasses to create the wells for sample loading. When the stacking gel was fully polymerised, the gel cassettes were assembled into the running module and placed in the electrophoresis chamber, which was then filled with 1X electrophoresis buffer. Samples were prepared at the required dilution by adding loading buffer to a final 1X concentration and heating for 5 minutes at 95°C. The loading buffer contains  $\beta$ -mercaptoethanol, a thiol-reducing agent that disrupts disulphide bonds to allow complete protein unfolding. The comb was gently removed from the gel and approximately 7  $\mu$ L of pre-stained molecular weight marker (in the first well) and 12  $\mu$ L of sample were added to the wells. The gel was run at 120 V until the tracker dye (bromophenol blue) reached the bottom of the gel. The gels were then removed from the gel cassettes and stained with InstantBlue™ for 10–15 minutes to allow visualisation. The gels were washed twice with diH<sub>2</sub>O and a gel photo was taken using the Gel Doc™ EZ System.

#### **2.2.1.5 Western Blotting**

After running a SDS-PAGE gel, the gel was equilibrated in Pierce™ 1-Step transfer buffer for 10 minutes. Two pieces of blotting filter paper (7 x 8.4 cm) and the nitrocellulose membrane were also soaked in transfer buffer for approximately 15 minutes. The proteins were transferred to the nitrocellulose membrane using a Trans-Blot® SD semi-dry electrophoretic transfer cell (Bio-Rad). The membrane was then placed in a large weight boat and blocked with 5 % (w/v) milk Marvel in PBS, with gently agitation, O/N at 4°C. After blocking, the membrane was washed three times with 10 mL of PBS-T, with gently agitation, for 5 minutes each time. The membrane was then incubated with 10 mL of the appropriate HRP-labelled antibody (at the required dilution, prepared in 1 % [w/v] milk Marvel in PBS) while gently shaking in the dark at RT. After a 2-hour incubation, the membrane was washed as before and developed by the addition of 5 mL of TMB peroxidase substrate for membranes. When the protein bands became visible, the membrane was washed with diH<sub>2</sub>O and a photo was taken using the Gel Doc™ EZ System.

## **2.2.2 Animal immunisation for recombinant antibody production**

### **2.2.2.1 Chicken immunization with the ERBB2 extracellular domain**

A White Leghorn female chicken was initially immunised sub-cutaneously with 1 mL of a mixture of equal parts of HER2 ECD (ERBB2-922H, 30 µg) in PBS (10 mM, pH 7.3) and Freund's complete adjuvant. The first boost (day 21) was performed by administering 15 µg of HER2 mixed in a 1:1 ratio with Freund's incomplete adjuvant in a final volume of 1 mL. Further boosts were administered (on days 42, 64 and 99) with smaller immunogen quantities (12.5 µg, 10 µg and 10 µg, respectively) in the same manner as the first boost. Finally, the chicken was sacrificed by intravenous injection using sodium pentobarbitone (day 106). Spleen and bone marrow were collected and immediately immersed in RNeasy<sup>®</sup> to stabilise and protect the RNA.

### **2.2.2.2 Serum antibody titre determination by indirect ELISA**

Serum antibody titres were determined to measure the chicken immune response to HER2. The chicken was bled one week after each boost and the collected whole blood was left for 2 hours in the tube to ensure complete clotting. The inner surface of the tube was scraped with an applicator stick to dislodge the clotted blood from the sides and transfer it to a clean tube. The sample was then centrifuged at 3,050 x g for 30 minutes in an Eppendorf 5810R centrifuge. The serum was collected in 200 µL aliquots and stored at -20°C. An indirect ELISA format was used for titering the serum of the immunised chicken. To achieve this, Nunc MaxiSorp<sup>™</sup> immunoplates were coated with 100 µL of HER2 at a concentration of 1 µg/mL in PBS (10 mM, pH 7.3) and incubated O/N at 4°C. BSA was also coated onto the ELISA plate to check for non-specific binding of the antiserum. The liquid in the plates was discarded and the plates were blocked with 300 µL/well of 3 % (w/v) BSA in PBS and incubated at 37°C for 1 hour. The blocking reagent was washed with PBS. Five-fold serial dilutions (from 1:5 to 1:390,125 dilutions) of the serum samples in 1 % (w/v) BSA in PBS were added to each well (200 µL/well). An appropriate blank was also added. The plate was incubated at 37°C for 90 minutes and then washed 3 times

with PBS-T and 3 times with PBS. Subsequently, 100  $\mu$ L of a 1:2,000 dilution of HRP-labelled anti-chicken IgY Fab' conjugate in PBS was applied to each well. The plate was incubated at 37°C for 1 hour and washed six times as before. Then, 100  $\mu$ L of tetramethylbenzidine (TMB) substrate solution were added to each well. Once colour was observed, the reaction was stopped with 100  $\mu$ L of 10 % (v/v) HCl per well. The absorbance was read at 450 nm. The results of the titrations were graphed to compare the response in different bleeds.

### **2.2.3 Generation of an immune chicken scFv library**

#### ***2.2.3.1 Extraction and isolation of total RNA from immunised chicken spleen***

Prior to animal sacrifice, all laboratory plastic ware, instruments and equipment that was not 'RNase free' was treated with Presept and RNaseZap® to remove all contaminating RNases enzymes that catalyse the degradation of RNA. All reagents were also 'RNase-free'. All procedures were carried out in a "RNase-free" laminar flow, sterilized with UV light and decontaminated from Rnases with RNaseZap®.

The RNeasy®- stabilised spleen was removed from the reagent and weighted in a 'RNase-free' tube. RNA was purified from half of the spleen using a RNeasy Mini Kit (Qiagen) and the remaining tissue was flash-frozen and stored at -80°C. Spleen tissue was cut into small pieces and homogenised using a sterile (autoclaved, washed in Presept disinfectant solution and rinsed with molecular grade water and RNaseZap® prior to use) homogenizer. Ethanol was then added to the homogenised sample to provide ideal binding conditions before loading the lysate onto the RNeasy silica-membrane spin columns. Silica selectively binds to RNA under certain salt and buffer conditions (Gauch *et al.*, 1998). Contaminants were washed away and RNA was eluted using 30  $\mu$ L of molecular grade water. RNA was quantified using the Nanodrop ND-1000 Spectrophotometer.

### 2.2.3.2 First-strand cDNA synthesis from total RNA

cDNA was synthesized by reverse transcription using Superscript III first-strand synthesis system for RT-PCR (Biosciences). The resulting cDNA was used for constructing the scFv antibody library.

Two master mixes (mixture 1 and 2) were made as described in the tables below. RNA was incubated with the primers in mixture 1. Oligo (dT)s that hybridise to 3' poly (A) tails in the RNA were used as the priming method. Mixture 2 is the cDNA synthesis mix, in which SuperScript™ III Reverse Transcriptase ('RT') is introduced to the reaction.

Mixture 1	1X	20X
RNA	5 µg	100 µg
50 µM Oligo (dT)	1 µL	20 µL
10 mM dNTP mix	1 µL	20 µL
Total	23 µL	460 µL

Mixture 2	1X	Concentration in 460 µL reaction
10X 'RT' Buffer	2 µL	92 µL
25 mM MgCl <sub>2</sub>	4 µL	184 µL
0.1 M DTT	2 µL	92 µL
RNaseOut (40 U/µL)	1 µL	46 µL
SuperScript III 'RT' (200 U/µL)	1 µL	46 µL

First-strand reaction was performed in the thermal cycler under the following conditions:

Stage 1:	65°C	5 minutes
	Pause	
Stage 2:	50°C	50 minutes
	85°C	5 minutes
	Pause	
Stage 3:	37°C	20 minutes
	4°C	hold

Mixture 1 and Mixture 2 were prepared in a 1:1 ratio. For each reaction, 5 µg of total RNA were used. The reaction was scaled up (20X) and the mixture 1 was split into 25 µL-aliquots that were quick ('touch') spin-down in a benchtop microcentrifuge to collect liquid at the bottom of the PCR tubes. Step 1 of the reaction was run. The PCR tubes were left to cool on ice for 1–3 minutes and subsequently an equal volume of Mixture 2 (25 µL) was added to each PCR tube. Step 2 of the reaction was run. PCR tubes were placed on ice for 1–3 minutes and 2 µL of RNase H were added to each tube. Step 3 of the reaction was run. PCR tubes were placed on ice and pooled in a single 2-mL tube afterwards. cDNA was quantified using the NanoDrop spectrophotometer and subsequently stored at -20°C.

### **2.2.3.3 PCR Primers for the construction of a chicken scFv library**

The primers were used for the construction of a chicken scFv library with a long linker, using pComb vector. These primers were previously described by Barbas *et al.* (2001) and were obtained from Integrated DNA Technologies. The light- and heavy-chain sense primers (CSCVHo-FL and CSCVK) have a sequence tail that are recognised by the overlap extension primers for the generation of the full-length product. CSCG-B and CSCVK have a sequence tail that contains an *Sfi*I site for the restriction-

digestion of the overlap product.

Chicken scFv primers		Nucleic acid sequence
<b>V<sub>H</sub> Primers</b>	CSCVHo-FL (sense), Long Linker	5'– GGT CAG TCC TCT AGA TCT TCC GGC GGT GGT GGC AGC TCC GGT GGT GGC GGT TCC GCC GTG ACG TTG GAC GAG – 3'
	CSCG-B (reverse)	5'– CTG GCC GGC CTG GCC ACT AGT GGA GGA GAC GAT GAC TTC GGT CC – 3'
<b>V<sub>λ</sub> Primers</b>	CSCVK (sense)	5' – GTG GCC CAG GCG GCC CTG ACT CAG CCG TCC TCG GTG TC – 3'
	CKJo-B (reverse)	5'– GGA AGA TCT AGA GGA CTG ACC TAG GAC GGT CAG G – 3'
<b>Overlap Extension Primers</b>	CSC-F (sense)	5'– GAG GAG GAG GAG GAG GAG GTG GCC CAG GCG GCC CTG ACT CAG – 3'
	CSC-B (reverse)	5' – GAG GAG GAG GAG GAG GAG GAG CTG GCC GGC CTG GCC ACT AGT GGA GG – 3'

#### **2.2.3.4 Amplification of chicken antibody variable heavy and light chain genes**

Spleen cDNA obtained from reverse transcription was used for the PCR-amplification of the variable heavy and variable light genes.

PCR components were as follows:

cDNA	0.5 µg
dNTP's	0.2 mM
Forward primer	60 pm
Reverse primer	60 pm
MgCl <sub>2</sub>	4 mM
5X buffer	1X
GoTaq Polymerase (5 U/µL)	1 unit
MG H <sub>2</sub> O	Up to 50 µL

PCR was performed with the following cycling conditions :

Stage 1:	94°C	Initial denaturation	2 minutes
Stage 2:	94°C	Denaturation	15 seconds
30 cycles of	56°C	Annealing	30 seconds
	72°C	Extension	90 seconds
Stage 3:	72°C	Final extension	10 minutes
	4°C		hold

#### ***2.2.3.5 Optimisation of MgCl<sub>2</sub> and primer concentration for amplification of DNA***

Magnesium is a required co-factor for Taq Polymerase and thus optimising the MgCl<sub>2</sub> (source of magnesium ion) concentration is critical to the success of the PCR. Varying MgCl<sub>2</sub> concentrations from 1 mM to 4 mM were analysed (using conditions described in Section 2.2.3.4).

Primers determine what region of the DNA is amplified during the PCR. Excessive primers concentration can lead to the annealing of the primers to non-target regions—generating false products in a PCR—or to the formation of primer dimers that amplify independent to the target DNA. On the other hand, if the primer concentration is too low, there will be little or no amplification during the PCR. Forward and reverse primer concentrations were optimised using concentrations from 0.4 to 1 μM (Section 2.2.3.4).

#### ***2.2.3.6 Splice by overlap extension (SOE) PCR using Platinum Taq polymerase***

In the SOE PCR the variable heavy and variable light products are pooled in equal ratios to generate the scFv library. The SOE PCR primers recognise the sequence tails

generated by the primers used for the amplification of the variable chains, allowing the extension of the full-length product.

Platinum® Taq DNA Polymerase High Fidelity was used to generate the SOE product to ensure a high yield and robust amplification. This “hot start” thermostable DNA polymerase (inactive until the initial PCR denaturation step) also allowed for room temperature reaction assembly.

SOE PCR reaction components and conditions using Platinum® Taq DNA Polymerase High Fidelity Polymerase were as follows:

10X High Fidelity PCR Buffer	1X
10 mM dNTP mixture	0.2 mM
50 mM MgSO <sub>4</sub>	2 mM
Forward primer	0.4 μM
Reverse primer	0.4 μM
V <sub>H</sub> product	150 ng
V <sub>λ</sub> product	150 ng
Platinum Taq High Fidelity	1 U
MG water	Up to 50 μL

PCR conditions were as follows:

Stage 1:	94°C	Initial denaturation	2 minutes
Stage 2:	94°C	Denaturation	15 seconds
30 cycles of	55°C	Annealing	15 seconds
	68°C	Extension	90 seconds
Stage 3:	68°C	Final extension	5 minutes
	4°C		hold

### **2.2.3.7 Plasmid DNA purification and preparation of an *E. coli* glycerol stock expressing pComb3XSS**

Initially, a glycerol stock of XL1-Blue *E. coli* cells expressing pComb3XSS was inoculated in a LB agar plate supplemented with 100 µg/mL carbenicillin. Following incubation at 37°C O/N, a single colony was picked from the plate and grown O/N on 5 mL of SB + carbenicillin (100 µg/mL) medium at 37°C and 220 rpm. Five hundred µL of the overnight culture was sub-cultured into 100 mL SB + carbenicillin (100 µg/mL) medium. The subculture was incubated O/N at 37°C and 220 rpm.

The following morning, cells were pelleted by centrifugation in an Eppendorf 5810R for 15 minutes at 4°C and 3220 x g. A NucleoBond® Xtra Midi kit (MN) was used for plasmid purification from the harvested bacterial cells, as per the manufacturer's instructions. The purified plasmid was reconstituted in 300 µL of molecular grade water. The product was subsequently quantified using a Nanodrop ND-1000 Spectrophotometer and stored at -20°C.

### **2.2.3.8 Restriction-digestion of the scFv insert and pComb3XSS vector**

The SOE-PCR products and the pComb3XSS vector were prepared for cloning by performing restriction enzyme digestion with *SfiI* enzyme (20,000 units/mL) from New England Biolabs.

The purified overlap scFv PCR product was *SfiI*-digested by setting up two 100-µL reactions as follows:

Purified scFv product	5 µg
<i>SfiI</i> (36 U per µg of DNA)	180 U
10X NE Buffer	10 µL
Water	Up to 100 µL

Both digestion reactions were incubated at 50°C for 5 hours.

For digestion of the purified pComb3XSS vector, two 100- $\mu$ L reactions were prepared as follows:

pComb3XSS	10 $\mu$ g
Sfil (36 U per $\mu$ g of DNA)	60 U
10X NE Buffer	10 $\mu$ L
Water	Up to 100 $\mu$ L

Both digestion reactions were incubated at 50°C for 5 hours. Then, Antarctic Phosphatase (AP) enzyme (10 units) and Antarctic Phosphatase buffer (10X) were added to each 100- $\mu$ L digestion reaction and this was incubated at 37°C for 30 minutes. After this time, AP was heat-inactivated by incubating the reactions at 65°C for 5 minutes. AP catalyzes the removal of 5' phosphate from the plasmid DNA, preventing self-ligation.

The digested scFv products were purified on a 1.5 % (w/v) agarose gel and the vector and Stuffer fragment were purified on a 0.8 % (w/v) gel using NucleoSpin® Gel and PCR Clean-Up (MN). The purified, digested PCR products, vector and Stuffer fragment were quantified using the Nanodrop ND-1000 Spectrophotometer.

#### **2.2.3.9 Ligation of SOE-product into pComb vector**

The ligation of the purified *Sfil*-digested scFv insert to the pComb vector was performed by setting up the following reaction:

<i>Sfil</i> -digested, AP-treated pComb	1.4 $\mu$ g
<i>Sfil</i> -digested SOE PCR product	0.7 $\mu$ g
T4 DNA Ligase buffer	6 $\mu$ L
T4 DNA Ligase	10 $\mu$ L
Water	Up to 60 $\mu$ L

Two ligation reactions were carried out and incubated O/N at RT. The resulting solution was ethanol-precipitated as described in Section 2.2.1.3.

## 2.2.4 Antibody phage display and library panning

### 2.2.4.1 Transformation of *E. coli* XL1-Blue electrocompetent cells with scFv-containing plasmid and rescue of scFv-displaying phage

The library ligation product was spun at 15,994 x g for 30 minutes at 4°C in a HermLe Z2333 M-K2 microcentrifuge. The supernatant was discarded and the pellet was washed twice with 70 % (v/v) ethanol. The pellet was centrifuged again for 2 minutes and air-dried for 15 minutes to remove any remaining ethanol. The pellet was then resuspended in 15 µL of pre-warmed MG water by brief heating at 37°C and gentle vortexing.

The ligated library and the 2.5 mm electroporation cuvettes were placed on ice for 10 minutes. At the same time the electrocompetent *E. coli* XL1-Blue cells were thawed in ice. Half of the ligation (7.5 µL) was added to each of two tubes containing 150 µL of cells that were incubated in ice for 1 minute. The sample was then electroporated at 2.5 kV, 25 µF and 200 Ω. The cuvette was immediately flushed with 1 mL and then twice with 0.5 mL of pre-warmed (37°C) SOC medium and the resulting suspension was transfer to a 50-mL polypropylene tube. Cells were incubated for one hour at 37°C and 250 rpm. After this time, 10 mL of prewarmed (37°C) SB medium with 3 µL carbenicillin (100 mg/mL) and 30 µL of tetracycline (5 mg/mL) were added. To titre transformed bacteria, 100 µL and 10 µL of a 1:100 dilution of the 15-mL culture were plated on LB agar plates supplemented with 100 µg/mL carbenicillin. The plates were incubated O/N at 37°C and the number of transformants was calculated as follows:

$$\text{N}^{\circ} \text{ of colonies} \times \frac{\text{culture volume}(\mu\text{L})}{\text{plating volume}(\mu\text{L})} \times \frac{\text{total ligation volume}(\mu\text{L})}{\text{ligation vol transformed}(\mu\text{L})} = \text{Total transformants}$$

The previous culture was shaken at 250 rpm for an additional hour at 37°C. Subsequently, 4.5 µL of carbenicillin (100 mg/mL) was added to the culture, which was then incubated as before. M13K07 helper phage (2 mL) was added to the culture, which was transferred to a 500-mL flask prior to addition of 183 mL of

prewarmed SB medium, 92.5  $\mu\text{L}$  of carbenicillin (100 mg/mL) and 370  $\mu\text{L}$  of tetracycline (5 mg/mL). This was grown at 300 rpm for an hour at 37°C. Finally, 140  $\mu\text{L}$  of kanamycin (50 mg/mL) was added and the culture was incubated O/N at 300 rpm and 37°C. Final antibiotic concentrations in the O/N culture were approximately 50  $\mu\text{g}/\text{mL}$  of carbenicillin, 10  $\mu\text{g}/\text{mL}$  of tetracycline and 35  $\mu\text{g}/\text{mL}$  of kanamycin.

The O/N culture was spun down at 1,520 x g for 30 minutes at 4°C and the resulting supernatant was transfer to four clean sterile Oakridge tubes. The phage particles were precipitated by addition of PEG 8000 (to 4 % [w/v]) and sodium chloride (to 3 % [w/v]). The PEG-NaCl solution was dissolved by shaking at 300 rpm for 5 minutes at 37°C. The Oakridge tubes were incubated on ice for 30 minutes and then centrifuged at 10,404 x g for 20 minutes at 4°C. The phage pellet was resuspended in 2 mL of 1 % (w/v) BSA in PBS buffer (10 mM, pH 7.3) and then transferred to 2 mL sterile centrifuge tubes, that were spun at 15,994 x g at 4°C. The phage-containing supernatant was used for panning.

#### **2.2.4.2 Enrichment of phage library via panning against immobilised HER2**

Four rounds of panning were performed with increasingly stringent conditions to enrich for high-affinity HER2-specific clones. The panning conditions employed during the screening process were as follows:

	Pan 1	Pan 2	Pan 3	Pan 4
<b>Coating concentration</b>	50 $\mu\text{g}/\text{mL}$	25 $\mu\text{g}/\text{mL}$	10 $\mu\text{g}/\text{mL}$	5 $\mu\text{g}/\text{mL}$
<b>Number of washes</b>	3X PBS 3X PBS-T	5X PBS 5X PBS-T	10X PBS 10X PBS-T	15X PBS 15X PBS-T
<b>Culture Volume/ # wells</b>	200 mL / 8 wells	100 mL/ 4 wells	100 mL/ 4 wells	100 mL/ 4 wells
<b>Helper phage</b>	2 mL	1 mL	1 mL	1 mL

A Maxisorb ELISA plate was coated O/N at 4°C with 100 µL of 50 µg/mL HER2 dilution. The coating solution was discarded and the wells were blocked with 100 µL of 5 % (w/v) milk Marvel in PBS for 90 minutes at 37°C. The blocking solution was discarded and 100 µL of the freshly prepared phage library were added to the wells that were sealed and incubated for 2 hours at RT. The solution was removed from the ELISA plate and non-binding phage were discarded by washing 3 times with PBS and 3 times with PBS-T. Freshly prepared ice-cold 10 mg/mL trypsin in PBS (100 µL) was added to each well and the plate was sealed and incubated for 30 minutes at 37°C to elute bound phage particles. The trypsin-treated samples (phage output) were pipetted up and down and the eluates were transferred to a 2-mL *E.coli* XL1-Blue culture ( $OD_{600} \approx 1$ ) and incubated static for 30 minutes at 37°C. For output titering, serial dilutions ( $10^{-1}$ – $10^{-4}$ ) in XL1-Blue cells were prepared and incubated static for 30 minutes at 37°C. After the incubation, 100 µL of each dilution were plated out on LB agar containing 100 µg/mL carbenicillin. The remaining culture was added to 50-mL tube with 6 mL of pre-warmed SB medium with 1.6 µL of carbenicillin (100 mg/mL) and 12 µL of tetracycline (5 mg/mL). After incubation at 230 rpm for 1h at 37°C, 2.4 µL of carbenicillin were added to the culture and this was incubated for a further hour at the same conditions. Then, the culture was co-infected with M13KO7 helper phage and transferred to 250 mL- bluffed bottom flask with 91 mL of prewarmed SB medium, 46 µL of carbenicillin (100 mg/mL) and 184 µL of tetracycline (5 mg/mL). The culture was incubated at 300 rpm for an hour at 37°C and 140 µL of kanamycin (50 mg/mL) were added before an O/N incubation at 300 rpm and 37°C.

#### **2.2.4.3 Polyclonal phage ELISA**

To evaluate the success of the panning experiment, phage pools resulting from different rounds of panning were tested by ELISA. A Nunc Maxisorb plate was coated with 100 µL per well of 10 µg/mL HER2 (and control BSA) in PBS (10 mM, pH 7.3) O/N at 4°C. The excess antigen was discarded and the plate was blocked with 250 µL of 5 % (w/v) milk Marvel in PBS for 90 minutes at 37°C. Precipitated phage from each

round of panning (100  $\mu$ L of a 1:3 dilution in 1 % [w/v] milk Marvel in PBS that was incubated for 1 hour at RT) was added to the wells in triplicate. M13 helper phage was also added in triplicate as a negative control. The plate was incubated for 2 hours at 37°C and then washed three times with PBS-T and 3 times with PBS. Bound antibodies were detected following the addition of 200  $\mu$ L of a 1:5,000 dilution of HRP-labelled anti-M13 antibody in 1 % (w/v) milk Marvel in PBS. The plate was incubated for 1 hour at 37°C and washed as before. TMB substrate was added (100  $\mu$ L per well) and incubated for 10 minutes at RT. The reaction was stopped by the addition of 10 % (v/v) HCl and the absorbance was read at 450 nm using Tecan Sunrise™ Microplate Reader.

## **2.2.5 Analysis of scFv-expressing single clones**

### **2.2.5.1 Soluble expression of antibody fragments**

Soluble scFv fragments were produced by infecting 5  $\mu$ L of phagemid from rounds 3 and 4 of panning into two 5mL- overnight cultures of Top10F' *E. coli* in SB with 10  $\mu$ g/mL tetracycline at a mid-logarithmic growth phase. After static incubation for 1 hour at 37°C, each culture was added to a 20-mL tube containing 6 mL of SB with 50  $\mu$ g/mL carbenicillin and 10  $\mu$ g/mL tetracycline and further incubated while shaking at 220 rpm for 1 hour at 37°C. Culture dilutions from  $10^{-1}$  to  $10^{-7}$  were plated on agar plates with 100  $\mu$ g/mL carbenicillin and incubated O/N at 37°C. Single colonies (96 from each round of panning) were inoculated into individual wells containing 200  $\mu$ L of SB with 50  $\mu$ g/mL carbenicillin and 10  $\mu$ g/mL tetracycline (stock plates). After an O/N incubation at 37°C, 15  $\mu$ L of each well of the stock plates were subcultured into 150  $\mu$ L SB in the presence of carbenicillin (50  $\mu$ g/mL) and shaken at 220 rpm and 37°C until OD=0.6-0.8. Meanwhile, master plates of the original clones were prepared by adding 20 % (v/v) glycerol to the stock plates and storing at -80°C. Once the desired optical density was achieved, 1 mM IPTG was added and to each well and the cultures were induced O/N at 220 rpm 30°C. Cells were pelleted by centrifugation of the plates for 10 minutes at 2,750 x g and 4°C using a A-4-62 rotor with MTP buckets in an Eppendorf 5810 centrifuge. Each pellet was resuspended in

300  $\mu$ L of PBS and subjected to 3 cycles of freeze-thawing (the plates were frozen at  $-80^{\circ}\text{C}$  and then thawed at  $37^{\circ}\text{C}$ ) for the extraction of periplasmic scFv. The plates were then centrifuged for 20 minutes as before and the resulting lysates were used to perform an ELISA-based analysis of single clones.

#### ***2.2.5.2 Soluble Monoclonal scFv ELISA***

To assess the specificity of the selected clones, scFv from cell lysates (prepared as described in Section 2.2.5.1) were tested for HER2-binding by ELISA. Two 96-well ELISA plates were coated O/N with 5  $\mu\text{g}/\text{mL}$  HER2 in PBS (10 mM, pH 7.3), and then blocked with 250  $\mu\text{L}$  of 5 % (w/v) milk Marvel in PBS for 90 minutes at  $37^{\circ}\text{C}$ . The plates were washed three times with PBS-T and three times with PBS. ScFv- enriched lysates were added in a 1:2 dilution in 1 % (w/v) milk Marvel in PBS-T to the wells and incubated for 1 hour at  $37^{\circ}\text{C}$ . The plates were washed as before and a HRP-conjugated rat anti-HA monoclonal antibody (1:1,000 dilution in 1 % [w/v] milk Marvel in PBS) was used to detect scFv that were specific to HER2. After 1 hour incubation at  $37^{\circ}\text{C}$ , the plates were washed as before and 100  $\mu\text{L}$  of TMB were added to each well and incubated at RT for 5 minutes, followed by the addition of 50  $\mu\text{L}$  of 10 % (v/v) HCl to stop the reaction. The absorbance was read at 450 nm using a Sunrise™ Tecan Microplate Reader.

#### ***2.2.5.3 Competitive scFv ELISA for the detection of free HER2***

Eight positive clones from the monoclonal scFv ELISA were taken forward for competitive analysis in order to determine if they were specific for free HER2. Competition occurs between free HER2 in solution and adsorbed HER2 in the ELISA plate for binding to the anti-HER2-specific scFv.

Single clones were grown inoculating 10  $\mu\text{L}$  of the glycerol stocks (from the Master plate) into 5 mL of SB with 50  $\mu\text{g}/\text{mL}$  carbenicillin and 10  $\mu\text{g}/\text{mL}$  tetracycline and incubating O/N at 220 rpm and 37°C. The O/N cultures (50  $\mu\text{L}$ ) were subcultured into 10 mL of SB with 100  $\mu\text{g}/\text{mL}$  carbenicillin, 1X 505 and 1mM  $\text{MgSO}_4$  and then incubated at 220 rpm and 37°C until  $\text{OD}_{600}\approx 0.6$ . The remaining O/N culture was used to make 20 % (v/v) glycerol stocks, that were stored at -80°C. Once the culture reached the exponential phase, antibody expression was induced by adding 1 mM IPTG and incubating the culture O/N at 220 rpm and 30°C.

Cell lysates were prepared as previously described in Section 2.2.5.1, with the exception that 50-mL centrifuge tubes were used instead of ELISA plates. The wells of an ELISA plate were coated with 100  $\mu\text{L}$  of 2  $\mu\text{g}/\text{mL}$  HER2 in PBS (10 mM, pH 7.3) O/N at 4°C. The plate was blocked with 250  $\mu\text{L}$  of 5 % (w/v) milk Marvel in PBS for 90 minutes at 37°C. The lysates (50  $\mu\text{L}$ ) were added in a 1:50 dilution (for a final 1:100 dilution) to a half of the plate with 50  $\mu\text{L}$  of PBS (direct ELISA) and to the other half of the plate with 50  $\mu\text{L}$  of a 4  $\mu\text{g}/\text{mL}$  HER2 solution (competitive ELISA), incubating the dilutions for 5 minutes on the bench before adding them to the wells. The plate was washed three times with PBS-T and three times with PBS, followed by the addition of 100  $\mu\text{L}$  of a 1:1,000 dilution of HRP-labelled monoclonal anti-HA antibody in 1 % (w/v) milk Marvel in PBS. After 1 hour incubation at 37°C the plate was washed as before and 100  $\mu\text{L}$  of TMB substrate were added to each well and the plate was covered and incubated for 5 minutes at RT. The reaction was stopped with 10 % (v/v) HCl and the absorbance read at 450 nm using a Sunrise™ Tecan Microplate Reader.

#### ***2.2.5.4 Sequence analysis of the anti-HER2-specific clones***

Plasmid preparations of the selected plasmids from round 4 of panning were prepared and sent for Sanger sequencing. Anti-HER2-specific clones glycerol stocks were used to streak LB agar plates with 100  $\mu\text{g}/\text{mL}$  carbenicillin. Single colonies were grown in 5mL SB with 10  $\mu\text{g}/\text{mL}$  of tetracycline O/N at 37°C. Plasmids were purified

from the O/N cultures using the MN NucleoSpin Plasmid purification kit, as per the manufacturer's instructions. Double-stranded DNA Sanger sequencing was performed by Source Bioscience, Tramore, Ireland, using the following primers:

- Ompseq (forward primer): AAG ACA GCT ATC GCG ATT GCA G
- gBack (reverse primer): GCC CCC TTA TTA GCG TTT GCC ATC

The heavy and light chain CDRs of the antibody were identified (Kabat definition) by examining the sequences. The ExPASy translation tool (<http://web.expasy.org/translate/>) was used to determinate the amino acid sequences and ClustalW2 program (<http://www.ebi.ac.uk/Tools/msa/clustalw2/>) allowed the alignment of the sequences.

## **2.2.6 Expression, purification and characterisation of anti-HER2 scFv A4**

### ***2.2.6.1 Optimisation of expression conditions for A4 scFv***

Expression conditions for A4 clone were optimised. A4 glycerol stock was used for scFv expression as described in Section 2.2.5.3, with the exception that two different post-induction temperatures—37°C and 30°C—and three different IPTG concentrations—0.1 mM, 0.5 mM and 1 mM—were tested. These variables are decisive for the induction of scFv expression.

ScFv-enriched lysates (100 µL) were added in a 1:5 dilution in 1 % (w/v) milk Marvel in PBS-T to an ELISA plate coated with 2 µg/mL HER2. After an hour incubation at 37°C, the plate was washed three times with PBS-T and three times with PBS. ScFv were detected by adding 100 µL of a 1:1,000 dilution of HRP- conjugated anti-HA mAb in 1 % (w/v) milk Marvel in PBS-T. The plate was subsequently incubated for an hour at 37°C and washed as before. HRP product formation was detected as explained in Section 2.2.5.3.

### **2.2.6.2 Immobilised metal affinity chromatography (IMAC) purification**

Prior to scFv purification by IMAC, the expression procedure was scaled-up. A4 scFv glycerol stock was streaked on a LB agar plate containing 100 µg/mL carbenicillin. A single colony was inoculated into 5 mL of SB media with 100 µg/mL carbenicillin and incubated O/N at 220 rpm and 37°C. Four mL of the O/N culture were sub-cultured in 996 mL of SB media containing 100 µg/mL carbenicillin, 1X 505 media supplement and 1mM MgSO<sub>4</sub>. The culture was incubated at 220 rpm and 37°C until an approximate OD<sub>600</sub> = 0.6 was reached. Expression was then induced by addition of 1 mM IPTG and the culture was incubated O/N at 220 rpm and 30°C.

The following morning, the culture was transferred to four 250-mL sorvall tubes and centrifuged at 3,220 x g for 30 minutes. The pellets were resuspended in 10 mL of sonicator buffer from tube to tube and transferred to a clean 50-mL tube. Resuspended pellets were subjected to three cycles of freeze-thawing to burst the *E. coli* cells and release periplasmic proteins. To ensure complete cell lysis, the sample was sonicated on ice 4 seconds on, 2 seconds off, at 40 % amplitude, for 2 minutes. The sonicated sample was then dispensed in 2-mL Eppendorf tubes and centrifuged at 15,994 x g for 30 minutes at 4°C in a HermLe Z2333 M-K2 microcentrifuge. Meanwhile, 2 mL of Ni<sup>+</sup>-NTA resin (Qiagen) were equilibrated with 40 mL of running buffer. After centrifugation, the lysates were collected, pooled and filtered through a 0.2-µm filter to remove any residual cell debris. The filtered lysates were added to a 50-mL tube containing the equilibrated resin and incubated in a roller for 1 hour at 4°C. The lysate/resin mixture was transferred to a 20-mL column. The flow-through was collected and stored at 4°C. The column was washed twice with 30 mL of running buffer to remove any loosely bound non-specific proteins. Bound scFv was eluted with 8 mL of 100 mM NaOH, pH 4.4 and collected in a tube containing 4 mL of neutralisation buffer (2 mL of 100 mM NaOH and 2 mL of 10X PBS). A second elution step using a high concentration of imidazole (1X PBS, 250 mM Imidazole, pH 7.5) was performed to elute remaining bound proteins. The eluted scFv was then buffer exchanged against sterile PBS (10 mM, pH 7.3) using a 10 kDa

'cut-off' Vivaspin™ column (AGB, VS0611). After buffer exchange, scFv concentration was quantified using the Nanodrop ND-1000 Spectrophotometer.

### ***2.2.6.3 Optimisation of assay parameters for HER2 detection in a competitive format***

The assay conditions for the development of a competitive ELISA for the detection of HER2 using the IMAC-purified scFv were optimised by checkerboard ELISA (Murphy and O'Kennedy, forthcoming).

The optimal coating buffer was selected by testing three different buffers at different pHs: 10 mM PBS, pH 7.3; 20 mM Tris buffer, pH 8.5; and 50 mM carbonate buffer, pH 9.6. The ELISA plate was coated with 1 µg/mL of HER2 prepared in each of the buffers O/N at 4°C. The immunoplate was blocked with 300 µL of 5 % (w/v) milk Marvel in PBS for 90 minutes at 37°C and then washed three times with PBS-T and three times with PBS. Anti-HER2 A4 scFv dilutions (1:100–10,000,000) were added to the wells and incubated for 1 hour at 37°C. The plate was washed as before and 100 µL of a 1:1,000 dilution of HRP-labelled anti-HA antibody were added. After an hour incubation at 37°C, the plate was washed as before and HRP was detected as previously described in Section 2.2.5.3.

Once the optimal coating buffer was chosen, checkerboard ELISA was used for the determination of optimal HER2 coating concentration and optimal scFv A4 dilution for use in a competitive assay. A Nunc Maxisorb™ plate was coated with varying HER2 concentrations (1 µg/mL, 2 µg/mL and 4 µg/mL) in carbonate buffer (50 mM, pH 9.6). The direct ELISA was performed as explained in Section 2.2.5.3.

### ***2.2.6.4 Competitive ELISA for the detection of HER2 using A4 scFv***

A Nunc MaxiSorp™ clear plate was coated with 100 µL of 1 µg/mL HER2 in 50 mM PBS, pH 9.6 O/N at 4°C. The plate was blocked with 300 µL of 5 % (w/v) milk Marvel

in 1X PBS for 90 minutes at 37°C. Meanwhile, 50 µL of different HER2 concentrations were incubated with the same volume of a 1:5,000 dilution of the chicken anti-HER2 A4 scFv (for final HER2 concentrations from 5-10,035 ng/mL and a final 1:10,000 scFv dilution) for 10 minutes at 37°C. The plate was washed three times with PBS-T and three times with PBS and the mixture was added to the wells and incubated for 1 hour at 37°C. The plate was washed as before and 100 µL of a 1:1,000 dilution of HRP-labelled anti-HA antibody was added. After an hour incubation at 37°C, the plate was washed as before and HRP was detected as previously described in Section 2.2.5.3.

#### ***2.2.6.5 Fluorescence-based competitive ELISA for the detection of HER2***

The competitive assay was performed as previously described in Section 2.2.6.4 with the following exceptions. The immunoplate used to perform the assay was a black Nunc MaxiSorp plate, designed to quench autofluorescence. HRP was detected by the addition of Ampliflu Red peroxidase substrate. The Ampliflu Red working solution (50 µM Ampliflu Red, 200 µM H<sub>2</sub>O<sub>2</sub> in 10 mM PBS) was prepared using a 10 mM Ampliflu™ Red stock in DMSO and a 20 mM H<sub>2</sub>O<sub>2</sub> stock in diH<sub>2</sub>O, and added (100 µL) to the wells following the washing step after incubation with the secondary antibody. On contact with the HRP-labelled anti-HA antibody, Ampliflu Red converts into highly fluorescent resorufin. After a 30-minute incubation, imaging was done on a Tecan Safire2™ Microplate Reader Infinite™ 200 at 544/590 nm excitation/emission wavelengths.

#### **2.2.7 Isolation and characterisation of polyclonal antibodies to HER2**

##### ***2.2.7.1 IgY purification from eggs of an immunised chicken***

Polyclonal antibodies (IgY) were purified from three eggs of the immunized chicken. The egg yolks were separated from the albumen using an egg separator and IgY was purified using the IgY EggsPress Purification Kit, as per the manufacturer's instructions. The IgY pellet was resuspended in the original yolk volume with PBS (10

mM, pH 7.3) and the concentration was quantified using the Nanodrop ND-1000 Spectrophotometer. The yield of the preparation was calculated by multiplying the concentration by the final volume of IgY. The IgY solution was then filter-sterilized, aliquoted in 1-mL volumes and stored at -20°C.

#### ***2.2.7.2 Competitive ELISA for anti-HER2 polyclonal antibody characterisation***

A Nunc MaxiSorp™ plate was coated with 100 µL of 2 µg/mL HER2 in PBS (10 mM, pH 7.3) O/N at 4°C. The plate was blocked with 300 µL of 5 % (w/v) milk Marvel in 1X PBS for 90 minutes at 37°C. Meanwhile, different HER2 concentrations from 30 to 1,200 ng/mL (50 µL) were incubated with the same volume of a 1:1,000 dilution of the chicken anti-HER2 pAb for 10 minutes at 37°C (for final Her 2 concentrations from 15 to 600 ng/mL and a final antibody dilution of 1:2,000). The plate was washed three times with PBS-T and three times with PBS and the mixture was added to the wells and incubated for 1 hour at 37°C. The plate was washed as before and 100 µL of a 1:2,000 dilution of HRP-labelled anti-chicken IgY Fab was added. After an hour incubation at 37°C, the plate was washed as before and HRP was detected as previously described in Section 2.2.5.3.

### **2.2.8 Development of a novel centrifugal microfluidic platform for multiplex biomarker detection**

#### ***2.2.8.1 Centrifugal disc fabrication***

The centrifugal disc consisted of laminated layers made of poly(methyl methacrylate) (PMMA) and double-sized, pressure-sensitive adhesive (PSA). PMMA layers (1.5 mm thick) were cut using a CO<sub>2</sub> laser cutting system (Epilog Zing, USA) to create through-holes, reservoirs and air venting holes. Microchannels were cut in PSA (0.086 mm thick) using a paper cutter (CraftRobo Pro, Graphtec, USA). Dissolvable film (DF) valves were manufactured by cutting through holes in PSA,

sticking the dissolvable film (previous removal of the PSA top layer to expose the adhesive) and performing a final cut to contour the DF tabs.

All layers were carefully aligned and roll-pressed (Hot Roll Laminator, Chemsultant Int., US) following the diagram in Figure 2.1. DF tabs were placed in the voids in DF-support layer and sealed with DF-cover layer.

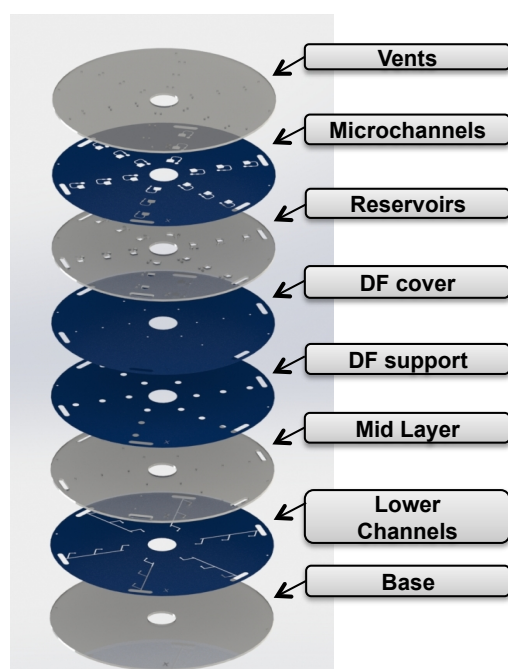


**Figure 2.1.** Exploded assembly drawing of the multi-layered, centrifugal microfluidic disc. The disc is made up of four layers of Poly(methyl methacrylate) (PMMA)—Base, Midlayer, Reservoirs, Vents—and other four layers of Pressure-sensitive adhesive (P-SA)—Microchannels, DF cover, DF support, and Lower channels—. The plastic layers (PMMA) contain the chambers, whereas the adhesive layers (P-SA) contain the fluidic channels. Figure provided by Dr. Rohit Mishra.

### **2.2.8.2 Centrifugal disc testing**

Centrifugal microfluidic discs were tested in an ‘in-house’ built test stand (Figure 2.2) that allowed the spinning of the disc and the observation of reagent release within the fluidic network.

The rotational frequency of the rotor can be set by the user using software in the control PC (Winmotion, Faulhaber, Germany). Images of the spinning disc can be obtained thanks to a stroboscopic light and a camera attached to a 12X zoom lens.

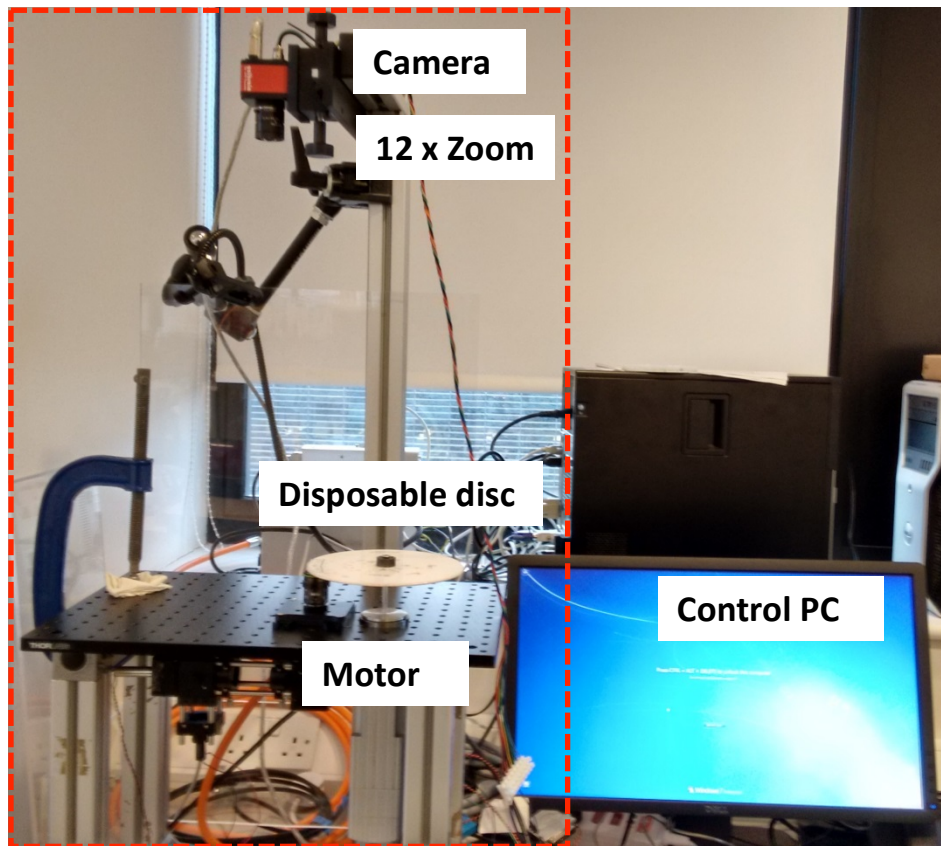


**Figure 2.2.** Centrifugal testing set up for spinning of the disc and observation of the fluids behaviour. The components inside the red dashed-box are inside a protective box.

### **2.2.8.3 Conventional benchtop sandwich ELISA for the detection of fPSA**

The ELISA plate (half-area 4.5 mm well bottom diameter, Corning) was coated with 60  $\mu\text{L}$  of anti-PSA polyclonal antibody (Abcam) at 1.6  $\mu\text{g}/\text{mL}$  in PBS (10 mM, pH 7.4) and stored overnight at 4°C. The immunoplate was blocked with 5 % (w/v) milk Marvel in PBS for 1 hour at 37°C and 40  $\mu\text{L}$  of six different free PSA concentrations (0.1, 1, 4, 10, 100 and 1000 ng/mL) were applied to the wells and incubated for 10 minutes, while shaking, at RT. The plate was washed once with 1 % (w/v) milk Marvel in PBS and 40  $\mu\text{L}$  of anti-PSA scFv B8 were added. The plate was incubated and washed, as above, after the addition of each antibody in the following steps. Bound scFv antibodies were detected using an HRP-labelled anti-HA antibody following the addition of tetramethylbenzidine (TMB) substrate. The reaction was stopped after 10 minutes of incubation by the addition of 10 % (v/v) HCl and the

absorbance was measured at 450 nm. The absorbance values (A) were normalized by dividing by the blank value (A<sub>0</sub>) and plotted as a percentage of relative absorbance (% A/A<sub>0</sub>).

#### ***2.2.8.4 Conventional competitive ELISA for the detection of HER2 extracellular domain (ECD)***

HER2 was added at a concentration of 1 µg/mL in carbonate buffer (50 mM, pH 9.6) onto the wells of an ELISA plate (60 µL per well) and incubated overnight at 4°C. After blocking with 5 % (w/v) milk Marvel for 1h at 37°C, a 1:1 mixture of HER2 concentrations (from 10 to 1000 ng/mL) with anti-HER2 ECD scFv A4 was added to the wells. The plate was incubated for 10 minutes, while shaking, at RT, and washed once with 1 % (w/v) milk Marvel in PBS. An HRP-labelled anti-HA antibody was used to detect bound scFv. This was incubated and washed as above, followed by the addition of TMB substrate. After 10 minutes, the reaction was stopped with 10 % (v/v) HCl and the absorbance was measured and plotted as previously described in Section 2.2.9.5.

#### ***2.2.8.5 Lab-on-a-Disc ELISA protocols***

Prior to assembly of the top two layers of the disc, overnight capture antibody coating followed by blocking of the polystyrene surface of the incubation chamber were carried out in the same manner as in the conventional ELISA (Sections 2.2.8.3 and 2.2.8.4). After blocking, the top two layers were assembled and the assay reagents (40 µL) were added to their corresponding chamber and centrifugally propelled to the incubation chamber. The release sequence was as follows. For the sandwich ELISA: fPSA antibody standards, buffer wash, scFv B8, buffer wash, HRP-labelled anti-HA antibody, buffer wash, TMB and 10 % (v/v) HCl. For the competitive ELISA: HER2 standards-scFv A4 mixture, buffer wash, HRP-labelled anti-HA antibody, buffer wash, TMB and 10 % (v/v) HCl, All washing steps were carried out with 40 µL

of 1 % (w/v) milk Marvel in PBS with an incubation times of 30 seconds. All other incubation times were of 10 minutes, unless stated otherwise.

## **2.2.9 Evaluation of anti-PSA recombinant antibodies by optical and electrochemical magneto-immunoassay**

### ***2.2.9.1 Tosyl-modified magnetic particles bioconjugation***

Surface-activated paramagnetic particles (Dynabeads® M-280 Tosylactivated, Invitrogen) allow covalent binding to primary amino groups in antibodies.

Dynabeads were resuspended in the vial by gently vortexing and approximately 1 mg of beads was washed twice in 1 mL of borate buffer by gently mixing in a 2 mL-tube and discarding the supernatant. To do this, the tube was placed in a magnet separator (DynaMag™-2 magnet) for 2 minutes and the supernatant was carefully pipetted without disrupting the beads that were bound to the magnet. Then, the tube was removed from the magnet and the beads were resuspended in 20 µL of antibody (20 µg anti-fPSA scAb in PBS), followed by adding 130 µL borate buffer and 100 µL of borate/NH<sub>4</sub>SO<sub>4</sub> buffer to a final volume of 250 µL. The addition of ammonium sulfate (borate/NH<sub>4</sub>SO<sub>4</sub> buffer) to a final concentration of 1.2 M increases the amount of antibody coupled to the beads, improving the coupling efficiency. The solution was incubated for 9 hours in a Thermomixer set at 800 rpm and 37°C, and O/N on a roller at RT. After incubation, the bioconjugated beads were gently vortexed and placed in the magnet separator for 2 minutes to separate the beads from the solution. The tube was then removed from the magnet and the beads were blocked by adding 1 mL of 0.5 % (w/v) BSA in phosphate buffer and incubating in the Thermomixer for 2 hours at 800 rpm and 37°C. The blocking solution was discarded and the beads were washed twice with 1 mL of 0.1 % (w/v) BSA in phosphate buffer as described before. After the second wash, the beads were resuspended in 250 µL of 0.1 % (w/v) BSA in phosphate buffer to a final concentration of 4 mg/mL. Sodium azide (0.01 % [w/v]) was added as preservative before storing the beads at 4°C.

### **2.2.9.2 Antibody titration for determination of bioconjugation efficiency**

The coupling efficiency was evaluated by measuring the amount of scAb present in the supernatant after bioconjugation. Once antibody concentration in the supernatant is quantified by magneto-ELISA, bound antibody concentration is estimated.

After bioconjugation, supernatant was collected using a magneto plate separator (see Figure 2.3). ELISA plates (Greiner Bio-One 655061) were coated with 50  $\mu\text{L}$  of supernatant dilutions (1:1–1:500) in triplicate, including also the dilutions for a titration curve for the scAb (in the range of 1–0.015  $\mu\text{g}/\text{mL}$ , prepared in the same buffer used for the bioconjugation step – Borate buffer/Borate ammonium sulphate buffer/ Phosphate buffer in a 100:130:20 ratio). This was incubated O/N at 4°C. After incubation, the coating solution was discarded and the wells were washed with 150  $\mu\text{L}$  of 10 mM phosphate buffer, while shaking, for 5 minutes. The washing solution was removed and the plate was blocked with 150  $\mu\text{L}$  of 3 % (w/v) BSA in 0.05 % (v/v) Tween 20 in PBS (PBS-T), incubating static for 2 hours at RT. The ELISA plate was then washed twice by adding 150  $\mu\text{L}$  of PBS-T to each well and shaking for 5 minutes. After washing, 100  $\mu\text{L}$  of HRP-labeled secondary antibody dilution in 2 % (w/v) BSA in PBS-T were added to the wells and incubated for 30 minutes, while shaking, at RT. The antibody solution was then removed and the plate was washed as before. TMB substrate was diluted tenfold in 0.02 M citrate buffer (pH 6), 100  $\mu\text{L}$  were added to the plate and incubated for 15 minutes, while shaking, in the dark. The reaction was stopped by addition of 100  $\mu\text{L}$  of 2 M  $\text{H}_2\text{SO}_4$  and the absorbance measured at 450 nm. The coupling efficiency, expressed as the % antibody uptake was calculated using the following equation:  $[(\text{Ab concentration in Pre-Coupling Solution} \times D) - (\text{Ab concentration in Post-Coupling Solution} \times D)] \times 100 / (\text{Ab concentration in Pre-Coupling Solution} \times D)$ , where D = dilution factor.

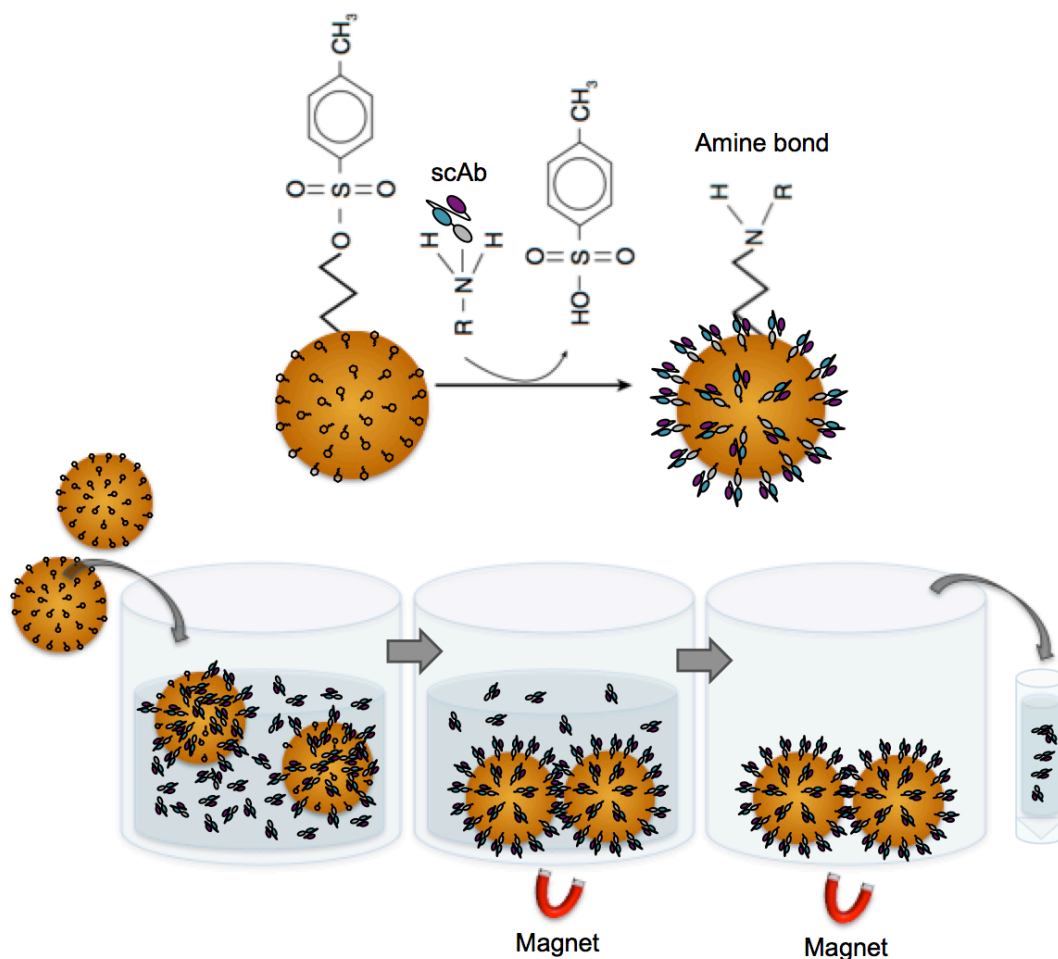


**Figure 2.3.** Schematic display of the steps involved in the bioconjugation of scAb E1 to tosyl-activated magnetic particles (Adapted from Liébana *et al.*, 2013).

### 2.2.9.3 Colorimetric magneto ELISA

Bioconjugated magnetic particles (MPs) were washed twice with 100  $\mu\text{L}$  PBS-T (using the DynaMag<sup>TM</sup>-2 magnet) and resuspended in PBS-T to a final concentration of 2 mg/mL. Once washed, the MPs were added onto each well containing 100  $\mu\text{L}$  PBS-T (final MPs concentration 0.1 mg/mL). The ELISA plate was placed in a magnetic plate separator to remove the supernatant and 100  $\mu\text{L}$  of free PSA dilutions (20, 10, 5, 1, 0.1 ng/mL) or PBS-T (blank) were added to the wells. The plate was incubated for 40 minutes while shaking at room temperature and then washed twice with 100  $\mu\text{L}$  of PBS-T. Secondary antibody, ab24466 (HRP-labelled anti-PSA antibody), was added (100  $\mu\text{L}$  diluted 1:1000 in 2% [w/v] BSA in PBS-T) and incubated for 30 minutes, while shaking, at RT. The ELISA plate was washed twice as before and 100  $\mu\text{L}$  of a

1:10 dilution of TMB in 0.02M citrate buffer, pH 6, was added to the wells and incubated for 20 minutes while shaking at RT. The reaction was stopped with 100  $\mu$ L of 2 M H<sub>2</sub>SO<sub>4</sub> and each sample was transferred to the reading microplate (269620 Thermofisher) to measure the absorbance at 450 nm using a Sunrise™ Tecan Microplate Reader. The results were normalised by subtracting the blank value from the values of the standards prior to plotting the absorbance values.

#### **2.2.9.4 Amperometric magneto-immunoassay**

All the steps involved in the amperometric detection of PSA using a magneto-immunoassay are illustrated in Figure 2.4.

Bioconjugated MPs (130  $\mu$ L) were placed in the DynaMag™-2 magnet and washed twice with 130  $\mu$ L of PBS-T, by changing buffer and gently mixing. Eppendorf tubes containing 100  $\mu$ L of PBS-T (blank) or free PSA standards (0, 0.1, 1, 5, 10, 20 ng/mL) were prepared in PBS (10 mM, pH 7.4) and MPs were added to a final concentration of 0.1 mg/mL and incubated for 40 minutes at 600 rpm and 25°C in a Thermomixer. After incubation, the MPs were washed twice with 100  $\mu$ L of PBS-T. The washing solution was discarded and 100  $\mu$ L of 0.9  $\mu$ g/mL HRP-labelled anti-PSA antibody (ab24466, Abcam) were added to the wells and incubated for 40 minutes at 600 rpm and 25°C in the Thermomixer. The bioconjugated beads were then washed twice as before, the supernatant was removed and the MPs were resuspended in 95  $\mu$ L of 0.1 M phosphate buffer with 0.1 M KCl. Freshly prepared hydroquinone (mediator) and hydrogen peroxide (substrate) were added to a final concentration of 2 mM and 5 mM, respectively. The solution was mixed and transferred to the electrode with a magnet underneath. The solution was incubated on the electrode (BE2150327D2/001, Gwent Group Ltd.) for 2 minutes before applying a -15 V reduction potential during 60 seconds, taking measurements at 30 seconds. Amperometric measurements were taken for each PSA dilution and each electrode design in triplicate. The results were normalised by subtracting the blank value from the values of the standards prior to plotting the amperometric signal values.

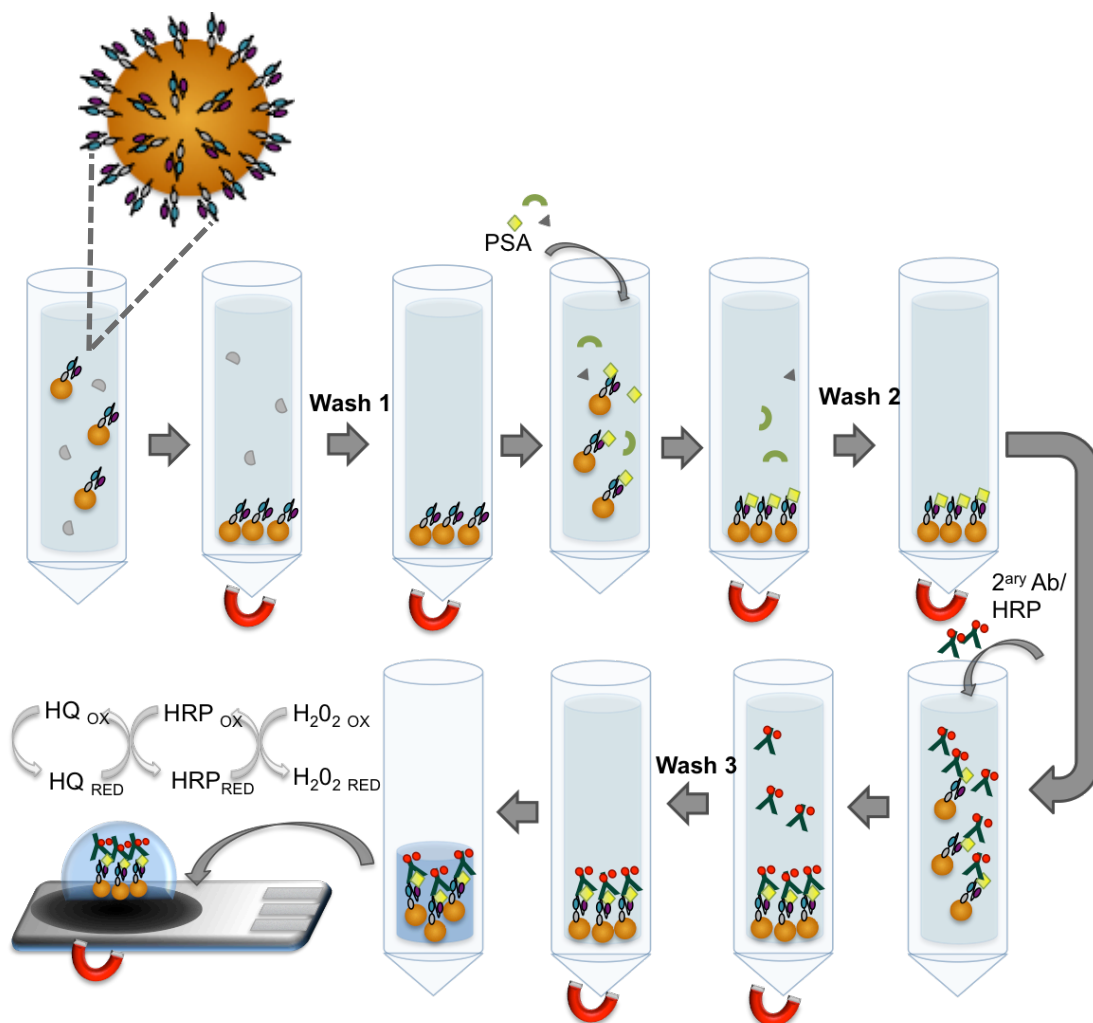


**Figure 2.4.** Schematic representation of the immunomagnetic separation and amperometric detection of free PSA ('two-step' protocol).

## 2.2.10 Immunosensor fabrication and characterization for HER2 detection

### 2.2.10.1 Fabrication of the immunosensor and electrochemical procedure

The colloidal gold was prepared in the Jaypee Institute of Information Technology utilising citrate reduction of chloroauric acid (HAuCl<sub>4</sub>), based on a slightly modified Turkevich method, as reported by (Turkevich *et al.*, 1951; Kimling *et al.*, 2006). The step-by-step fabrication of the nanoparticlebased immunosensor is illustrated in Figure 2.5.

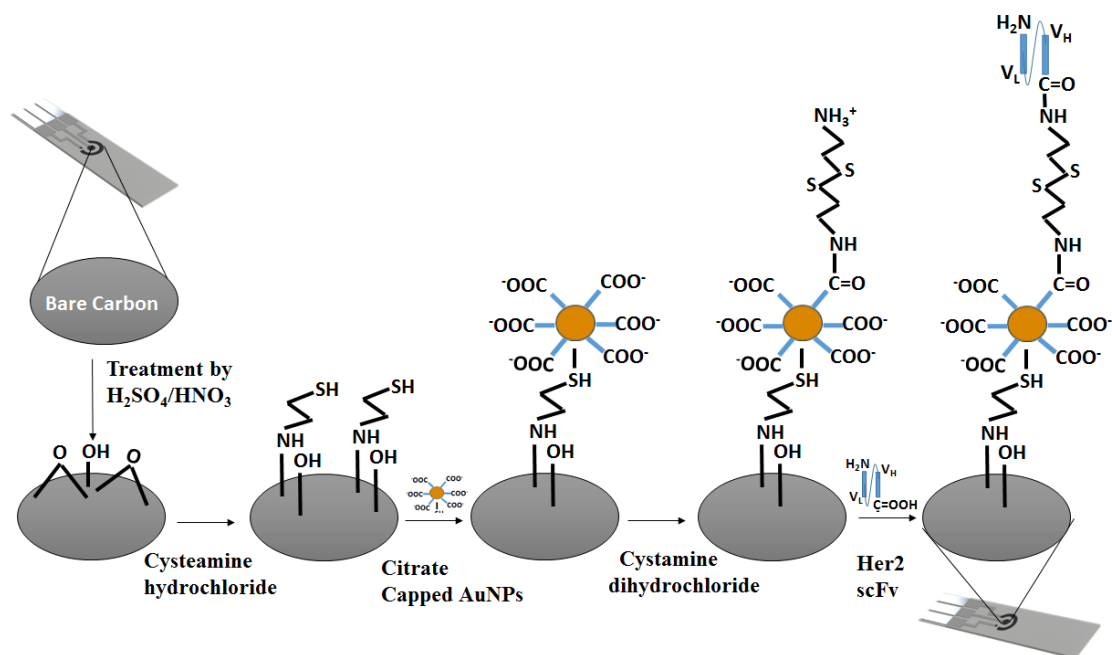


**Figure 2.5.** Schematic representation of the immunosensor fabrication.

Screen printed carbon electrodes (BE2050824D1/015, Gwent Group Ltd.) with carbon as the working and counter electrodes and Ag/AgCl as reference electrode, were used to fabricate the immunosensor. Firstly, the carbon electrode was cleaned by adding 100  $\mu$ L of  $H_2SO_4$  (100 mM) and performing a single cycle of cyclic voltammetry (CV) over the potential range of  $-1$  V to  $+1$  V at a scan rate of 0.1 V/s. The electrode was then washed with 100  $\mu$ L of redistilled water. The cleaning procedure was repeated with a saturated solution of  $Na_2CO_3$  followed by a washing step with 100  $\mu$ L of redistilled water to remove all impurities. The surface of the working electrode was modified using 3  $\mu$ L of 2 mg/mL cysteamine hydrochloride (Cys) and the electrode was kept for a further 2 hours at room temperature in the dark for effective binding of Cys on to the electrode surface. The electrode was washed with 100  $\mu$ L redistilled water followed by addition of 3  $\mu$ L of 0.8 mg/mL citrate-coated gold nanoparticles (AuNPs). The high affinity of thiols groups of Cys towards gold results in stable covalent Au-S bond. Physically adsorbed excess AuNPs were washed away with 100  $\mu$ L PBS (0.1 M, pH 7.4) and then redistilled water.

Subsequently, the AuNP-modified electrode surface was functionalized with amine groups using 3  $\mu\text{L}$  cystamine dihydrochloride (2 mg/mL) to promote the covalent bond formation between the free amine groups on the surface of AuNPs with the carboxylic groups at the tail of the recombinant antibodies to ensure proper orientation of the antibody. Finally, 3  $\mu\text{L}$  of anti-HER2 scFv A4 suspended in carbonate buffer (1  $\mu\text{L}$  of a 1:500 dilution of scFv in 2  $\mu\text{L}$  of carbonate buffer, pH 9.0) was added on the modified working electrode and allowed to incubate overnight at 4°C. The process was followed by casting 3  $\mu\text{L}$  of BSA (1 mg/mL) over the electrode and incubated for 45 min at 37°C to block available active sites to avoid nonspecific binding.

#### ***2.2.10.2 Impedance measurement procedure***

Impedance of the immunosensor was measured by recording electrochemical impedance spectra using the electrochemical workstation CH604E (CH Instruments Ltd.). Initially, a 3  $\mu\text{L}$ -droplet of the desired antigen concentration was added to the immunosensor surface and incubated for 15 minutes. Then, the immunosensor was washed with 100  $\mu\text{L}$  of PBS (0.01 M, pH 7.4) to remove non-specifically bound antigen. Finally, electrochemical impedance (EIS) measurement was performed by dropping 70  $\mu\text{L}$  of the redox couple (5 mM  $\text{K}_4[\text{Fe}(\text{CN})_6]/\text{K}_3[\text{Fe}(\text{CN})_6]$  in 0.01 M PBS (pH 7.4), thus covering the working, counter and reference electrodes of the immunosensor.

Optimum incubation times, pH and temperature for immunocomplex formation was evaluated by recording EIS spectra for 0.1 ng/mL anti-HER2 scFv A4 while varying one of the parameters but keeping the other two parameters constant.  $R_{ct}$  was calculated by fitting Randles equivalent circuit (Randles, 1947) simulation results with experimental data using simulation module of EIS technique, CHI604E.

## **Chapter 3**

# **Anti-HER2 scFv antibody: Production, Characterisation and Use for the Development of an Impedimetric Biosensor**

### 3.1 INTRODUCTION

As previously discussed, there are two major problems with the PSA test for prostate cancer (PCa) diagnosis. Firstly, PSA is not specific for prostate cancer and can also be found elevated in blood during other prostate pathologies. Secondly, this biomarker lacks the capacity to predict aggressive disease at the time of diagnosis. This is the primary reason why it is of utmost importance to develop new biomarkers that can differentiate between indolent and aggressive PCa. A panel of non-invasive biomarkers for PCa represents the best alternative to PSA testing. HER2 is a potential candidate biomarker for this panel.

#### 3.1.1 The *HER2* oncogene

Rodent *neu*, the rodent homologous to *HER2* oncogene, was first discovered in 1981 when Shih *et al.* (1981) described how DNA from a chemically-induced rat neuroglioblastoma was able to induce malignant transformation of mouse fibroblast NIH3T3 cells on transfection (Shih *et al.* 1981). The *neu* gene encodes for a 185 KDa transmembrane protein (p185) with a tyrosine kinase domain and also shows homology to the *v-erbB* (avian erythroblastic leukemia viral oncogene homolog 2) oncogene and the epidermal growth factor receptor (*EGFR*) (Vennstrom and Bishop, 1982; Schechter *et al.*, 1985). In 1985, King *et al.* demonstrated the amplification of this gene in a human breast carcinoma and named it human epidermal growth factor receptor 2 (*HER2*) gene. The two last members of the epidermal growth factor receptor family were subsequently discovered (Kraus *et al.*, 1989; Plowman *et al.*, 1993). The complete family consists of four members: EGFR (*HER1*, *erbB1*), *HER2* (*erbB2*, *HER2/neu*, *p185her2/neu*), *HER3* (*erbB3*), and *HER4* (*erbB4*).

### 3.1.2 HER family signaling pathways

HER family members are type I transmembrane growth factor receptors that achieve activation by forming dimers with other HER receptors, upon ligand binding (Figure 3.1). The exception is HER2, that always exists in a dimerization-prone extended conformation (Figure 3.1) and it is the preferred heterodimerisation partner for all HER receptors (Zhang *et al.*, 2007). Though most receptor dimerisation processes are mediated by ligands, spontaneous formation of HER2 homodimers has been reported in HER2-overexpressing cells (Fichter *et al.*, 2014; Peckys *et al.*, 2015). HER receptors possess a cytoplasmic tyrosine kinase domain and a C-terminal tail with tyrosine autophosphorylation sites that allow downstream trans-activation. The exception is HER3, which has a defective kinase domain and is only activated through heterodimerisation (Zhang *et al.*, 2007).

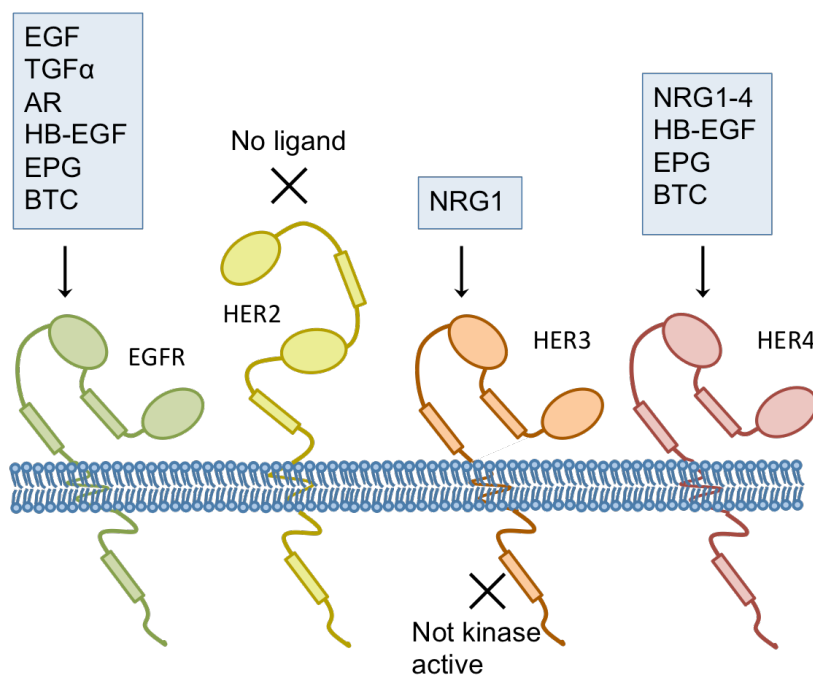


**Figure 3.1.** Representation of HER ligands and receptors. After ligand binding to ErbB receptors, the extracellular domain changes to an open conformation that promotes homo- and heterodimerisation. There are no known ligands that bind to HER2, which is always present in a fixed open conformation. All HER receptors possess tyrosine kinase activity, except HER3, which contains a defective kinase domain. Adapted from Zhang *et al.* (2007). EGF–epidermal growth factor; TGF–transforming growth factor-alpha; AR–amphiregulin; HB-EGF–heparin-binding EGF-like growth factor; EPG–epigen; BTC–betacellulin; NRG1-4–neuregulin 1–4.

Upon dimerization, phosphorylation of the intracellular tyrosine-kinase domain of the receptors occurs. This activates the receptors and initiates downstream signalling pathways (Gollamudi *et al.*, 2016). Phosphorylated tyrosine residues (mainly GRB2 and Shc) activate SOS protein, which catalyses the exchange of GDP with GTP to promote Ras-MAPK pathway activation (Figure 3.2). On the other hand, receptor dimerization leads to the recruitment and activation of phosphoinositide-3-kinase (PI3K), which phosphorylates PIP2 (phosphatidylinositol [3,4]-bisphosphate), activating the Akt pathway (Figure 3.2). These pathways are involved in cell proliferation and survival. Thus, deregulation of HER2 in cancer promotes tumorigenesis by the activation of a number of cellular responses, such as cell proliferation, apoptosis inhibition and angiogenesis (Gollamudi *et al.*, 2016).

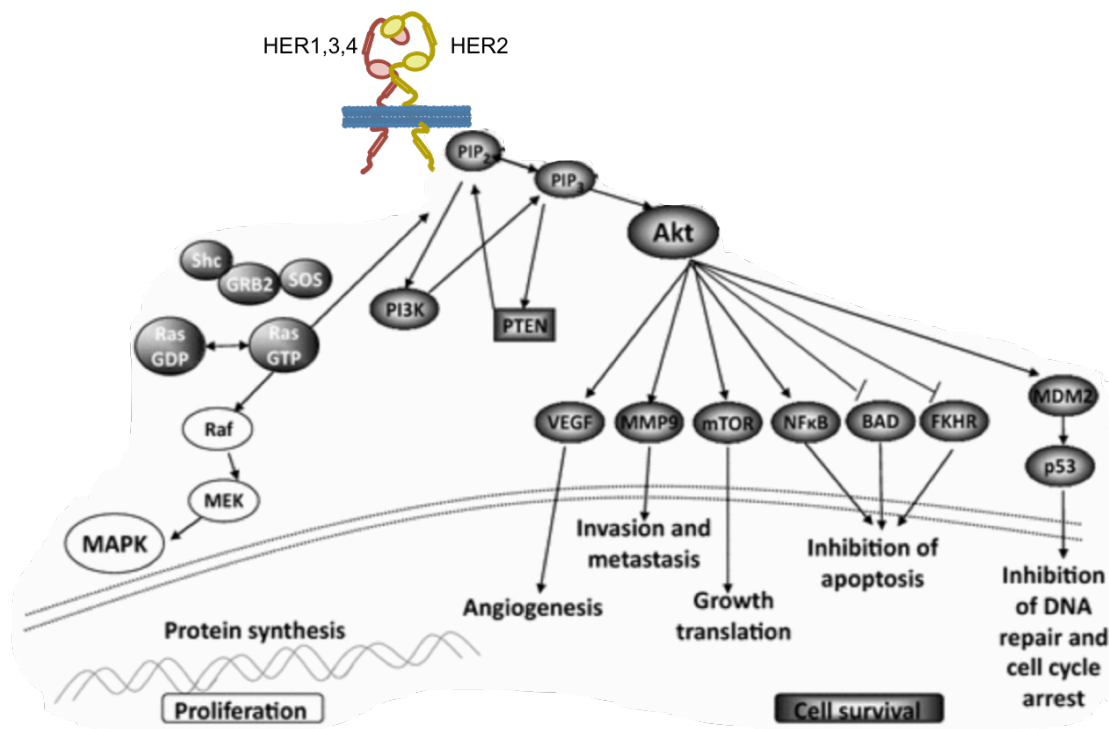


**Figure 3.2** Overview of HER family signalling pathways. Shc–SHC-transforming protein 1; GRB2–Growth factor receptor-bound protein 2; SOS–Son-of-sevenless guanine nucleotide exchange factor; GDP–Guanosine diphosphate; GTP–Guanosine triphosphate; Raf–Rapidly Accelerated Fibrosarcoma protein kinases; MEK–Mitogen-activated protein kinase kinase; MAPK–Mitogen-activated protein kinase; P13K–Phosphoinositide-3-kinase; PIP2–Phosphatidylinositol (3,4)-bisphosphate; PIP3–Phosphatidylinositol (3,4,5)-trisphosphate; PTEN–Phosphatase and tensin homolog; Akt–Protein kinase B; VEGF–Vascular endothelial growth factor; MMP9–Matrix metalloproteinase enzymes; mTOR–Mechanistic target of rapamycin; NFkB–Nuclear factor kappa-light-chain-enhancer of activated B cells; BAD–Bcl-2-associated death promoter; FKHR–Forkhead in rhabdomyosarcoma protein; MDM2–Mouse double minute 2 homolog; p53–Cellular tumor antigen p53. Adapted from Elster *et al.* (2015).

### 3.1.3 HER2 overexpression in cancer

HER2 is commonly expressed in foetal epithelial cells, where it is involved in cell proliferation and differentiation, while lower expression levels are found in adult epithelial cells (Pressl *et al.*, 1990). However, overexpression of HER2 was observed in a variety of cancers, such as lung, breast and prostate and this is usually correlated with a poor prognosis (Papila *et al.*, 2009; Park *et al.*, 2010; Minner *et al.*, 2010; Emi *et al.*, 2011; Takenaka *et al.*, 2011). In PCa this leads to disease progression and hormone-reflective disease for various reasons. Firstly, HER2 promotes androgen-independent prostate cancer through the activation of the MAP kinase and Akt pathways, that result in the phosphorylation and, therefore, ligand-independent activation of the androgen receptor (AR) (Sheikh *et al.*, 2003). Secondly, HER2 signals regulate the activity of the AR for optimal function at low concentrations of androgens through DNA binding and protein stabilisation, protecting the AR from proteasome-mediated degradation (Mellinghoff *et al.*, 2004). This correlation between HER2 and the progression of prostate cancer makes this biomarker a highly attractive target for cancer drugs. However, a phase II trial to assess the utility of anti-HER2 antibody Trastuzumab (which induces antibody-dependent cell-mediated cytotoxicity in HER2-overexpressing breast cancer cells) in the treatment of advanced hormone-refractory prostate cancer (HRPC) showed poor efficacy. These results were attributed to two possible causes: firstly, the low level of protein overexpression (9.5 %) or *HER2* gene amplification by fluorescence *in situ* hybridization (FISH) (17 %) in the biopsy samples used; and secondly, the use of Trastuzumab as a single treatment agent (Ziada *et al.*, 2004). Similarly, the use of Pertuzumab (HER2 dimerization inhibitor) in castrated patients with HRPC showed no clinical efficacy in another II phase study (Bono *et al.*, 2007). More recently, Vaishampayan *et al.* (2015) showed that activated T cells (ATC) armed with anti-CD3 x anti-HER2 bispecific antibody (HER2Bi) have a potential clinical utility for the treatment of patients with castrate-resistant prostate cancer (Vaishampayan *et al.*, 2015). In addition to this, the study of serum HER2 levels may provide novel insights into prostate cancer diagnosis and prognosis, given its role in the progression of the

disease and its correlation with an increased risk of developing metastatic cancer (Minner *et al.*, 2010; Daoud *et al.*, 2016).

### **3.2 AIMS OF THIS CHAPTER**

The extracellular domain (ECD) of HER2 is frequently cleaved from the receptor by proteases and released into serum where it can be measured by ELISA (Leyland-Jones and Smith, 2011). Okegawa *et al.* (2006) reported significantly higher HER2 levels in prostate cancer patients, when compared with healthy patients ( $P=0.006$ ), in a total of 379 patients. Also, they found that the biochemical recurrence-free rate was significantly poorer in metastatic prostate cancer patients with elevated HER2 levels ( $P=0.0078$ ), based on a 'cut-off' value of 12.6 ng/mL (Okegawa *et al.*, 2006). Elevated HER2 levels ( $> 15$  ng/mL) have also been associated with a worse clinical outcome for HRPc patients treated with docetaxel (Domingo- Domenech *et al.*, 2008). The aim of the research described in this chapter is the generation and purification of chicken anti-HER2 ECD polyclonal and recombinant antibodies and their characterisation by competitive ELISA. The application of generated anti-HER2 scFv for the development of a highly-sensitive impedimetric biosensor for the detection of this biomarker in serum is described.

### **3.3 RESULTS**

#### **3.3.1 Immunisation of chicken with HER2 ECD and serum antibody titre determinations**

A Leghorn chicken was selected for immunisation with 30  $\mu$ g HER2 ECD (Creative BioMart) and Freund's complete adjuvant in a 1:1 ratio as described in Section 2.2.2.1. Three boosts with reduced amounts of immunogen (12.5  $\mu$ g, 10  $\mu$ g and 10  $\mu$ g, respectively) were administered 20–35 days apart. Serum antibody titres

(Section 2.2.2.2) were performed after each boost to determine the immune response following immunisation. The chicken developed a strong antibody response after the third boost (day 64) and the antibody titre obtained, calculated as twice the background (control antigen), was 1:78,000 (Figure 3.3). This titre was considered high enough for recombinant antibody library generation. Eggs collected after the third boost were used for IgY purification to obtain polyclonal antibodies to HER2.

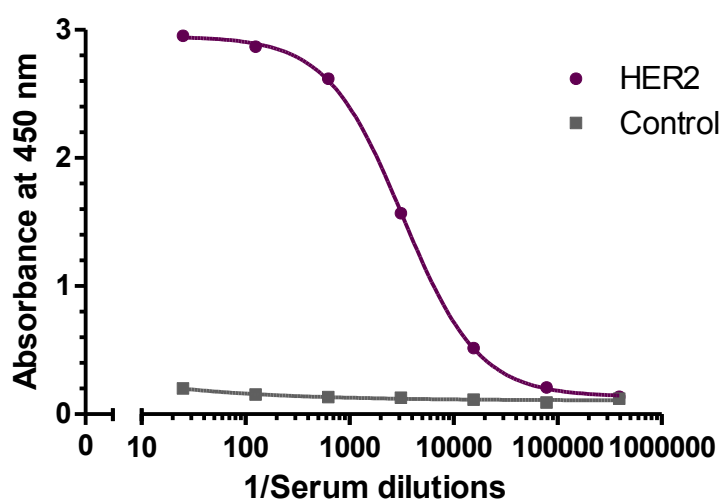


**Figure 3.3.** The antibody titre of an avian antiserum response to HER2 after boost 3. Data was normalised by subtracting the background absorbance value. Serum dilutions (1:25–1:390,625) were added to a HER2-coated ELISA plate and bound antibody was detected following the addition of HRP-labelled anti-chicken IgY antibody. Specific-binding to HER2 is detected above the background (control antigen binding) at a 1:78,000 dilution.

### 3.3.2 Purification of anti-HER2 polyclonal IgY from chicken eggs

Eggs were collected after the 3<sup>rd</sup> boost during the immunisation period. IgY was extracted from the egg yolks using IgY EggsPress Purification Kit (Gallus Immunotech; Section 2.2.1.1) and analysed by SDS-PAGE and Western blotting (Sections 2.2.1.4 and 2.2.1.5), showing distinctive bands at 70 and 28 KDa (Figure 3.4), corresponding with the heavy and light chains, respectively. Two contaminating bands, which have been previously reported in IgY preparations from egg yolks, can also be observed

between 36 and 55 KDa, and may correspond to  $\beta$ -livetin or phosvitin proteins (Hatta *et al.*, 2008; Tong *et al.*, 2014).

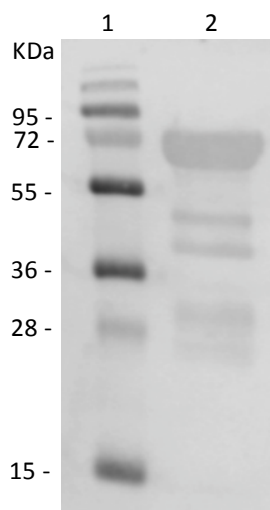


**Figure 3.4.** Western blot analysis of the IgY purified from the eggs. Lane 1–PageRuler Plus prestained protein ladder (Thermo Scientific); Lane 2–purified anti-HER2 polyclonal antibody, with visible bands at 70 and 28 KDa, representing the heavy and light chains of the IgY molecule.

Purified IgY was tested for HER2 binding by competitive ELISA (Section 2.2.7.2). Coating buffers, antigen and antibody concentrations were optimised using checkboard ELISA (data not shown). IgY was incubated with HER2 dilutions from 15 to 600 ng/mL. The assay was performed in quintuplicate and the standard deviations were calculated. Figure 3.5 shows that binding of purified IgY to immobilised HER2 is inhibited in the presence of HER2 free in solution, with a limit of detection (LOD) of 70 ng/mL.

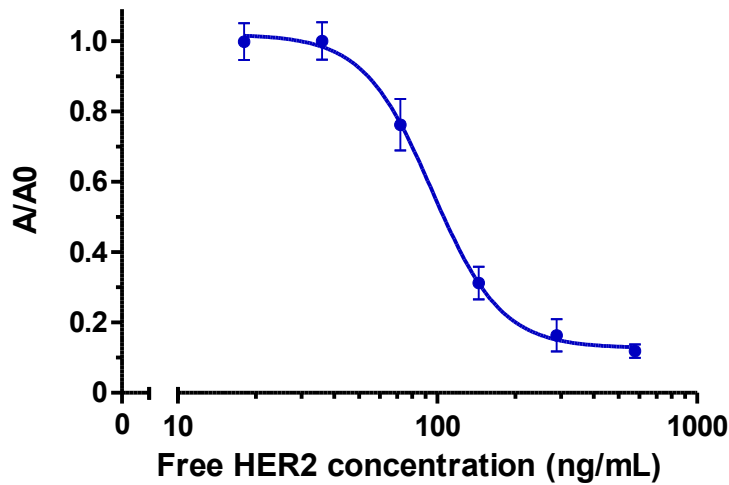


**Figure 3.5.** Competitive analysis for the detection of HER2 using IgY purified from eggs. A 1:1 mixture of HER2 concentrations (for final 15 to 600 ng/mL concentrations) with IgY was added to the HER2-coated wells. The plate was washed to remove unbound antibody and HRP-labelled anti-chicken IgY(Fab')<sub>2</sub> was used to detect bound antibody. The results were normalised by dividing the absorbance values (A) by the absorbance of the blank (A0).

### 3.3.3 Generation of avian anti-HER2 scFv library

#### 3.3.3.1 RNA isolation from immunised chicken spleen lymphocytes and cDNA synthesis

Once RNA extraction from the spleen of the immunised chicken was performed using a RNeasy Mini Kit (Qiagen) as per manufacturer's instructions (Section 2.2.3.1), cDNA was synthesised by reverse transcription using the SuperScript III First-Strand Synthesis kit (Invitrogen), as described in Section 2.2.3.2. RNA and cDNA were run in a 1.5 % (w/v) agarose gel (2.2.1.1) to check integrity (Figure 3.6). Large ribosomal RNA species are visible at 1,500 and 750 base pairs (bp).

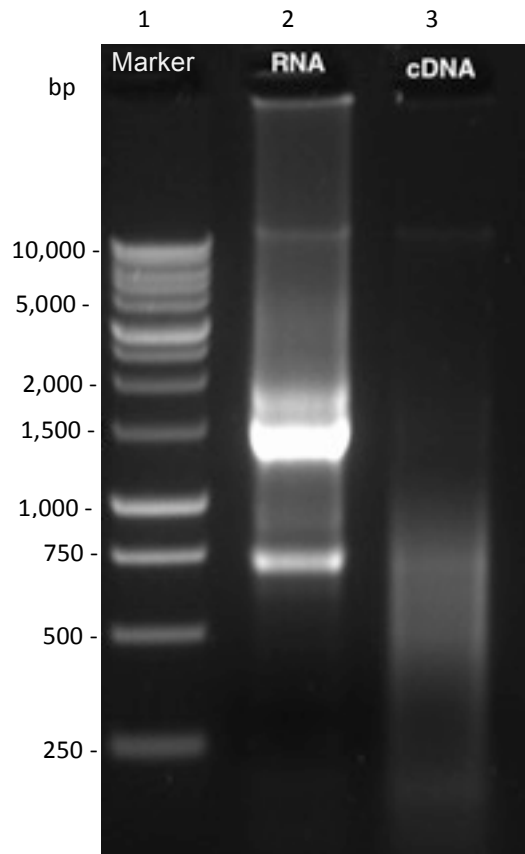


**Figure 3.6.** cDNA synthesis by reverse transcription of mRNA from chicken spleen using the Superscript III first-strand synthesis system for RT-PCR. Lane 1 represents a 1kb DNA ladder. Samples of RNA (lane 2) and cDNA (lane 3) were electrophoretically separated on a 1.5 % agarose gel. First-strand cDNA was synthesised from total RNA.

### **3.3.3.2 PCR amplification of chicken variable heavy ( $V_H$ ) and light ( $V_\lambda$ ) chains**

Both the heavy and the light-chain in chickens are encoded by single  $V_H$  and  $V_\lambda$  genes, which makes the generation of chicken antibody libraries a relative simple process, as only one set of primers is required for each chain (Andris-Widhopf *et al.*, 2000). In the first round of PCR, the  $V_H$  genes were amplified using the CSCVHo-FL and CSCG-B primers, and the  $V_\lambda$  genes using the CSCVK and CKJo-B primers, whose sequences are showed in Section 2.2.3.3.

### 3.3.3.2.1 Optimisation of $MgCl_2$ concentration for PCR amplification

In order to get the highest yield of specific PCR product,  $MgCl_2$  concentrations over the 1 mM–4 mM range were tested in a small-scale (1X) reaction (Section 2.2.3.5). Magnesium is a necessary enzyme co-factor for DNA polymerases—excess magnesium may reduce the specificity of the reaction, while a magnesium deficit may cause a reduced yield (Keer *et al.*, 2008).

The PCR products were resolved in 1.5 % (w/v) agarose gels (Section 2.2.1.1) to allow visualisation using the Gel Doc EZ system and Image Lab software. In the case of  $V_\lambda$  amplification (Figure 3.7A), a slight improvement with increasing  $MgCl_2$  concentration was observed, while  $V_H$  amplification (Figure 3.7B) only took place when 4mM  $MgCl_2$  was used. In both cases, a concentration of 4 mM  $MgCl_2$  was selected for further experiments.

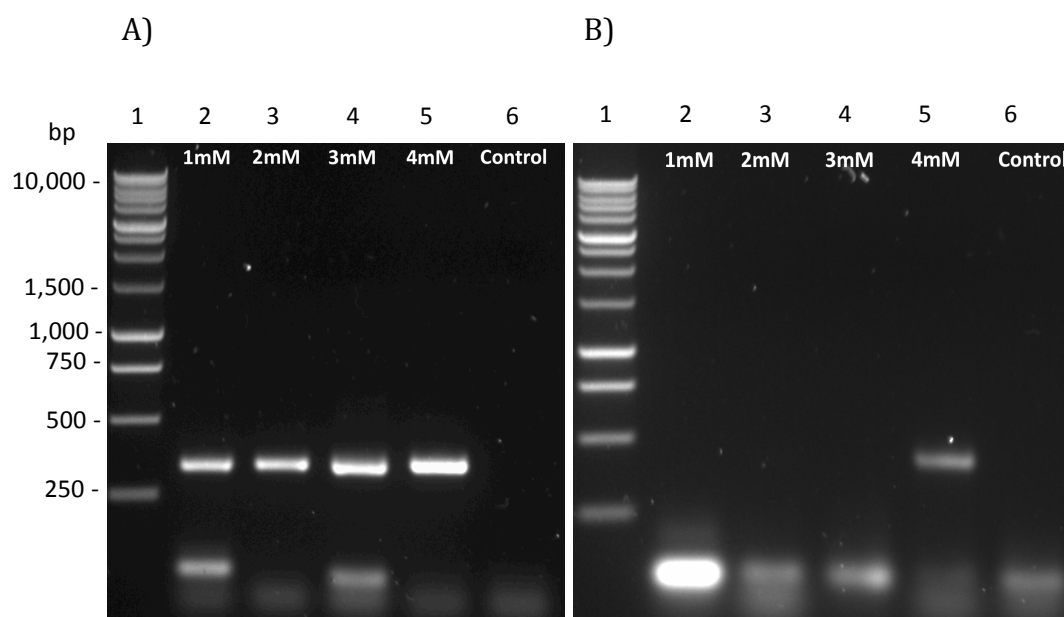


**Figure 3.7.** PCR optimisation for variable light (A) and variable heavy (B) gene amplifications (visible at around 350 and 400 bp, respectively) using  $MgCl_2$  concentrations from 1–4 mM. Lane 1 represents a 1kb DNA ladder. Lanes 2–5 represents different  $MgCl_2$  concentrations. Lane 6 is the control, where the DNA template is missing from the PCR reaction. Primer dimers can be seen at the bottom of the gel.

### 3.3.3.2.2 Optimisation of primer concentration for $V_H$ PCR amplification

To further optimise the  $V_H$  amplification, primer concentrations from 0.4 to 1  $\mu\text{M}$  were tested in a 1X reaction (Section 2.2.3.5). Figure 3.8 shows that a primer concentration of 0.8  $\mu\text{M}$  was optimal, resulting in the higher yield without unspecific amplification products.

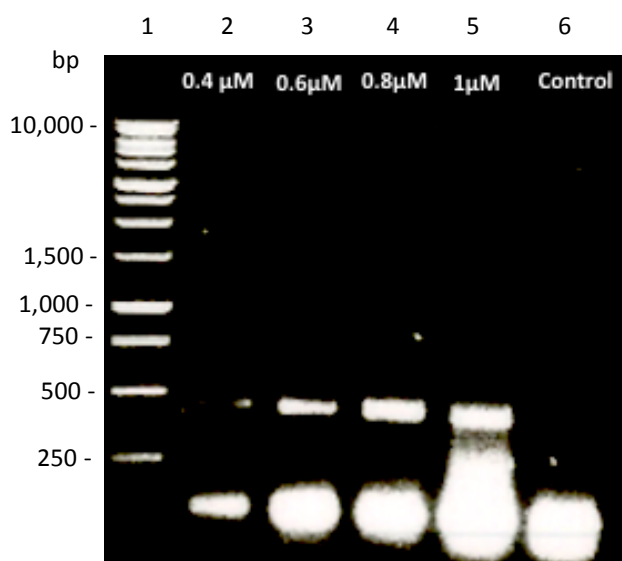


**Figure 3.8.** PCR optimisation of variable heavy gene amplifications using primer concentrations within the range of 0.4–1  $\mu\text{M}$ . Lane 1 represents a 1kb DNA ladder. Lanes 2–5 represent different primer concentrations. Lane 6 is the control, where DNA template is missing from the PCR reaction. Primer dimers can be seen at the bottom of the gel.

### 3.3.3.2.3 Amplification of $V_H$ and $V_\lambda$ with optimised PCR conditions

After successfully optimising the conditions for PCR amplification of the variable regions, a 1X reaction (Section 2.2.3.4) for each chain was carried out and 10  $\mu\text{L}$  of  $V_H$  and  $V_\lambda$  PCR products were evaluated on a 1.5 % (w/v) agarose gel, showing a band at  $\approx 400\text{bp}$  for the  $V_H$  product and 350bp product for the  $V_\lambda$  product (Figure 3.9). Once the reproducibility of the amplification reaction was established, two large-scale reactions (10X) were performed and the PCR products for each chain were run in a

1.5 % agarose gel (Section 2.2.1.1.) and purified using a NucleoSpin® Gel and PCR Clean-Up kit (MN; Section 2.2.1.2).

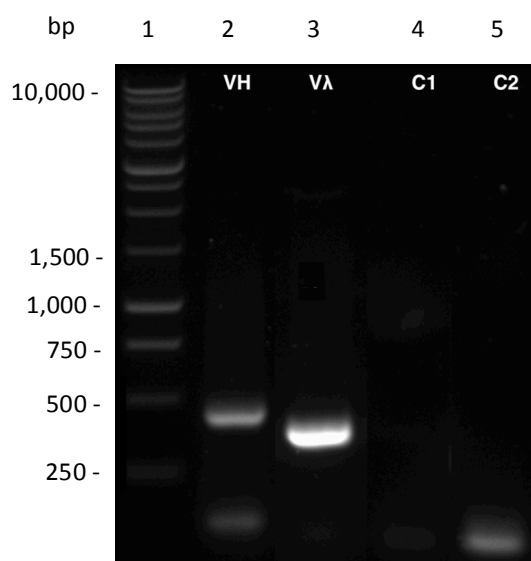


**Figure 3.9.** Optimised PCR amplifications of variable heavy and variable light genes using the cDNA from a HER2 ECD-immunised chicken. Lane 1 represents a 1kB Plus DNA ladder. Lane 2 represents the V<sub>H</sub> chain and lane 3, the V<sub>λ</sub>. Lanes 4 and 5 are controls (no DNA template) for the V<sub>H</sub> and V<sub>λ</sub> chains, respectively.

### ***3.3.3.3 Splice by Overlap Extension (SOE) PCR to anneal variable heavy and variable light chain genes***

The gel-purified V<sub>H</sub> and V<sub>λ</sub> chain gene PCR products were mixed in equal ratios to generate the overlap scFv product. Two 10X reactions were performed as described in Section 2.2.3.6, using the CSC-F and CSC-B primer combination (listed in Section 2.2.3.3), that recognise the sequence tails generated by the primers in the first-round PCR. High Fidelity Platinum Taq DNA Polymerase was used to assure high accuracy, specificity and yield in this crucial step to generate the scFv product. The PCR products were run on a 1.5 % (w/v) agarose gel (Section 2.2.1.1), where bands at 750 bp became visible (see Figure 3.10). The products were purified from the gel using NucleoSpin® Gel and PCR Clean-Up kit (MN; Section 2.2.1.2).

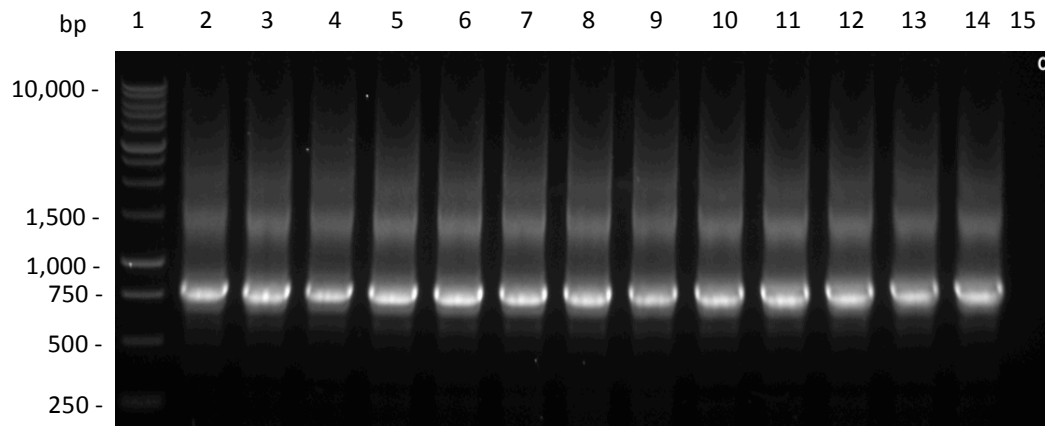


**Figure 3.10.** SOE-PCR of  $V_H$  and  $V_L$  fragments for the construction of a scFv library. Lane 1 represents a 1kb Plus DNA ladder. Lanes 2–14 represent the SOE products. Lane 15 is the control (no DNA template).

#### **3.3.3.4 Restriction-digestion and ligation of the SOE PCR product and the pComb3XSS vector**

The pComb3XSS phagemid vector DNA was purified using a NucleoBond Xtra Midi plasmid purification kit as described in Section 2.2.3.7. The pComb3XSS phagemid vector (Figure 3.11) is designed to contain two *SfiI* restriction enzyme sites that allow directional cloning of antibody fragments for the construction of antibody libraries. The ‘SS’ refers to the double stuffer—a light chain cloning region, bound by *SacI* and *XbaI* restriction sites, and a heavy chain cloning region, bound by *XhoI* and *SpeI* restriction sites. The 1,600-bp double stuffer fragment (both stuffer fragments plus the PelB leader sequence) can be removed by *SfiI* digestion to be replaced by the DNA to be cloned (Levisson *et al.*, 2014).

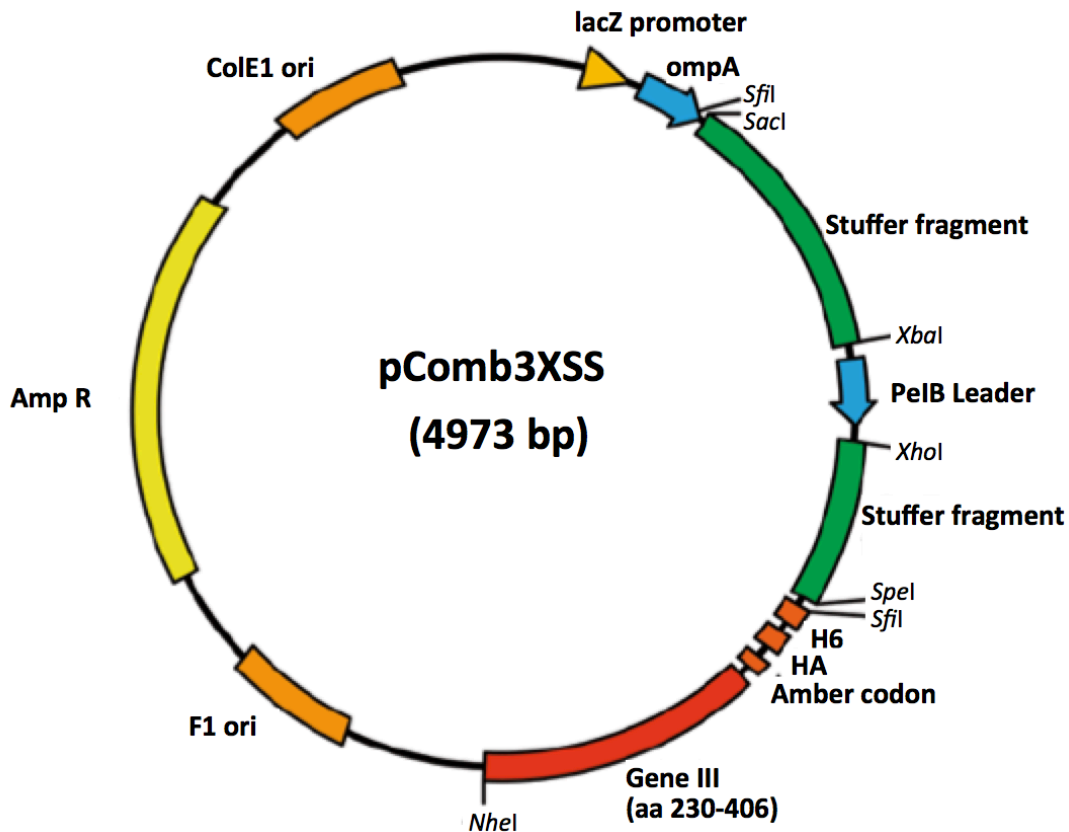


**Figure 3.11.** pComb3XSS vector map. pComb3XSS is a 3<sup>rd</sup> generation phagemid vector for phage display or for soluble expression of antibody fragments or proteins. The ompA leader sequence direct V<sub>H</sub>, V<sub>L</sub> and coat protein III to the periplasm. An asymmetric SfiI cassette allows one-step directional cloning of antibody fragments or other genes. Alternative restriction-digest are present for cloning. An amber stop codon inserted between the 3' SfiI site and the 5' coat protein gene III allows for soluble protein expression in non-suppressor strains of *E. coli*. The hexa-histidine (H6) tag enables purification of the desired protein with immobilised metal affinity chromatography, while the hemagglutinin (HA) decapeptide tag allows detection using commercially available anti-HA antibodies. Adapted from Levisson *et al.*, 2014.

SOE PCR products and the pComb3XSS vector were prepared for cloning by restriction digesting with SfiI, as described in Section 2.2.3.8. Small-scale digestion (1 µg of SOE product and 2 µg of vector) was carried out to assess the suitability of the restriction enzyme for complete removal of the pComb3XSS stuffer fragment and SOE product digestion. Figure 3.12 shows uncut and SfiI-digested pComb3XSS vector ran on a 0.8 % (w/v) agarose gel (Section 2.2.1.1). Complete digestion of double stuffer fragment was demonstrated, with the double-cut vector visible at 3,400 bp and the double stuffer fragment at 1,600 bp.

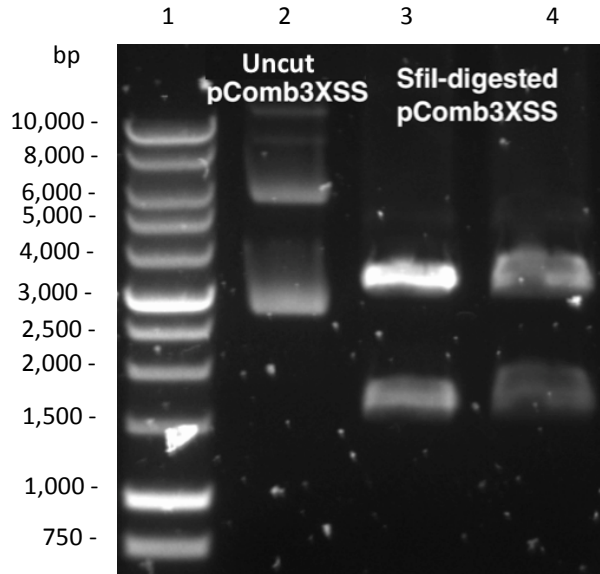


**Figure 3.12.** Digestion of the pComb3XSS vector and SOE product. Lane 1 represents a 1 KB ladder. Lane 2 represents the uncut vector. Lanes 3 and 4 represent the digestion of the pComb3XSS vector and the resulting double-cut vector ( $\approx 3,400$  bp) and stuffer fragment ( $\approx 1,600$  bp).

Large-scale *Sfi*I digestion of SOE scFv product and pComb vector were prepared as described in Section 2.2.3.9 and digested products were resolved in 1 % and 0.8 % (w/v) agarose gels (Section 2.2.1.1), respectively. Purification of desired products from agarose gels was performed using a NucleoSpin® Gel and PCR Clean-Up kit (MN; Section 2.2.1.2).

The purified pComb3XSS vector was treated with Antarctic phosphatase enzyme (Section 2.2.3.8), which removes 5' phosphates from DNA (required by ligases) to prevent self-ligation of the vector. The scFv fragment was ligated into the digested pComb3XSS vector (Section 2.2.3.9). The ligation product was concentrated by ethanol-precipitation (Section 2.2.1.3) and transformed into electrocompetent XL1-Blue cells by electroporation, as described in Section 2.2.4.1. The transformed chicken anti-HER2 scFv library had a size of  $2.5 \times 10^6$  cfu/mL. The desired library size would be in the order of  $5 \times 10^7$  cfu/mL (Barbas *et al.*, 2001), but it has been previously demonstrated that highly specific antibodies can be obtained from relative small ( $7.7 \times 10^5$  and  $5 \times 10^5$  cfu/mL) antibody libraries (Amwersdorfer *et al.*, 2002;

Chassagne *et al.*, 2004, respectively). Therefore, the library size obtained was considered sufficient for the selection of specific antibodies to HER2. The library was rescued with helper phage M13K07 and enriched for HER2-specific clones via panning.

### 3.3.4 Antibody library screening

#### 3.3.4.1 Enrichment of phage library via panning

The scFv library was panned by binding of the scFv-displaying phage to HER2-coated wells on an ELISA plate, washing off non-specific binders and elution of HER2-specific phage by trypsinisation (Section 2.2.4.2). Eluted phage were re-amplified and three further rounds of panning were performed using decreasing concentrations of antigen and increasing the number of washings (Table 3.1). Increasing the stringency of selection at each round enhances the selection of high-affinity scFv fragments.

**Table 3.1.** Panning conditions used for each round of selection for the anti-HER2 scFv library.

	Pan 1	Pan 2	Pan 3	Pan 4
<b>HER2 concentration</b>	50 µg/mL	25 µg/mL	10 µg/mL	5 µg/mL
<b>Number of washes</b>	3X PBS-T 3X PBS	5X PBS-T 5X PBS	10X PBS-T 10X PBS	15X PBS-T 15X PBS

Preliminary analysis of the panned scFv library was performed to assess the success of the panning experiments by polyclonal phage ELISA, as described in Section 2.2.4.3. Phage pools from the unpanned library and those resulting from different rounds of panning were added to a HER2-coated ELISA plate. After washing, bound scFv-displaying phage were detected using a HRP-labelled anti-M13 antibody. The increasing absorbance from round 2 onwards suggested the presence of anti-HER2-

specific scFv-displaying phage within the library (Figure 3.13). Therefore, phage from rounds 3 and 4 were taken forward for further analysis.

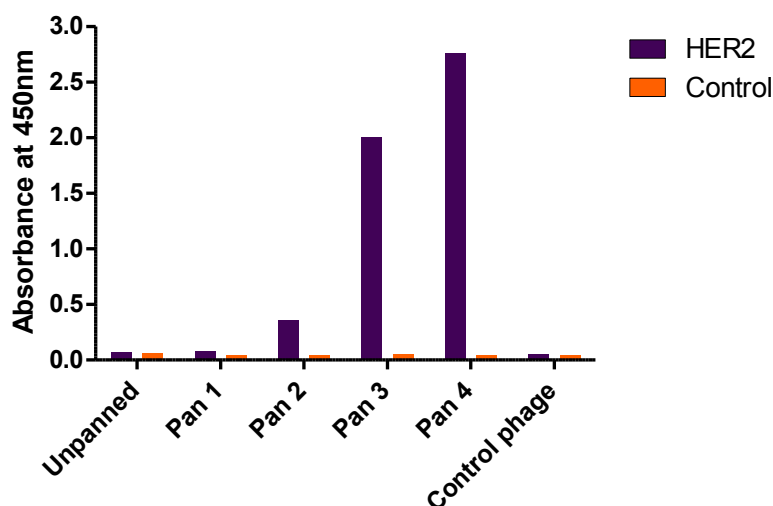


**Figure 3.13.** Polyclonal phage ELISA following four rounds of panning. The scFv-displaying phage were tested for binding to HER2 and control antigen by ELISA. The scFv-displaying phage were detected using a HRP-conjugated anti-M13 antibody and the absorbance was read at 450 nm. M13K07 phage (control) were also tested to identify potential non-specific binding.

### **3.3.4.2 Soluble expression and monoclonal analysis of single clones by ELISA**

Antibody fragments, without the pIII protein, were expressed by transforming the phagemid from rounds 3 and 4 of panning into TOP10F' cells (Section 2.2.5.1). When expressed in XL1-Blue *E.coli* cells, a suppressor transfer RNA (tRNA) binds to TAG ('amber') codons, producing a scFv-pIII fusion protein. However, TOP10F' *E.coli* strain, containing no suppressor tRNA mutation, recognises the stop codon between the pIII protein gene and that for the scFv fragment, allowing the production of soluble scFvs that are fused to hexa-histidine (H6) and hemagglutinin (HA) tags without pIII (Figure 3.11).

Single clones (192) from rounds 3 and 4 of panning were analysed for HER2-specific binding by monoclonal ELISA (Section 2.2.5.2). Figure 3.14 shows that more than

84 % of the clones had ELISA signals higher than the 'cut-off' (defined as three times the background).

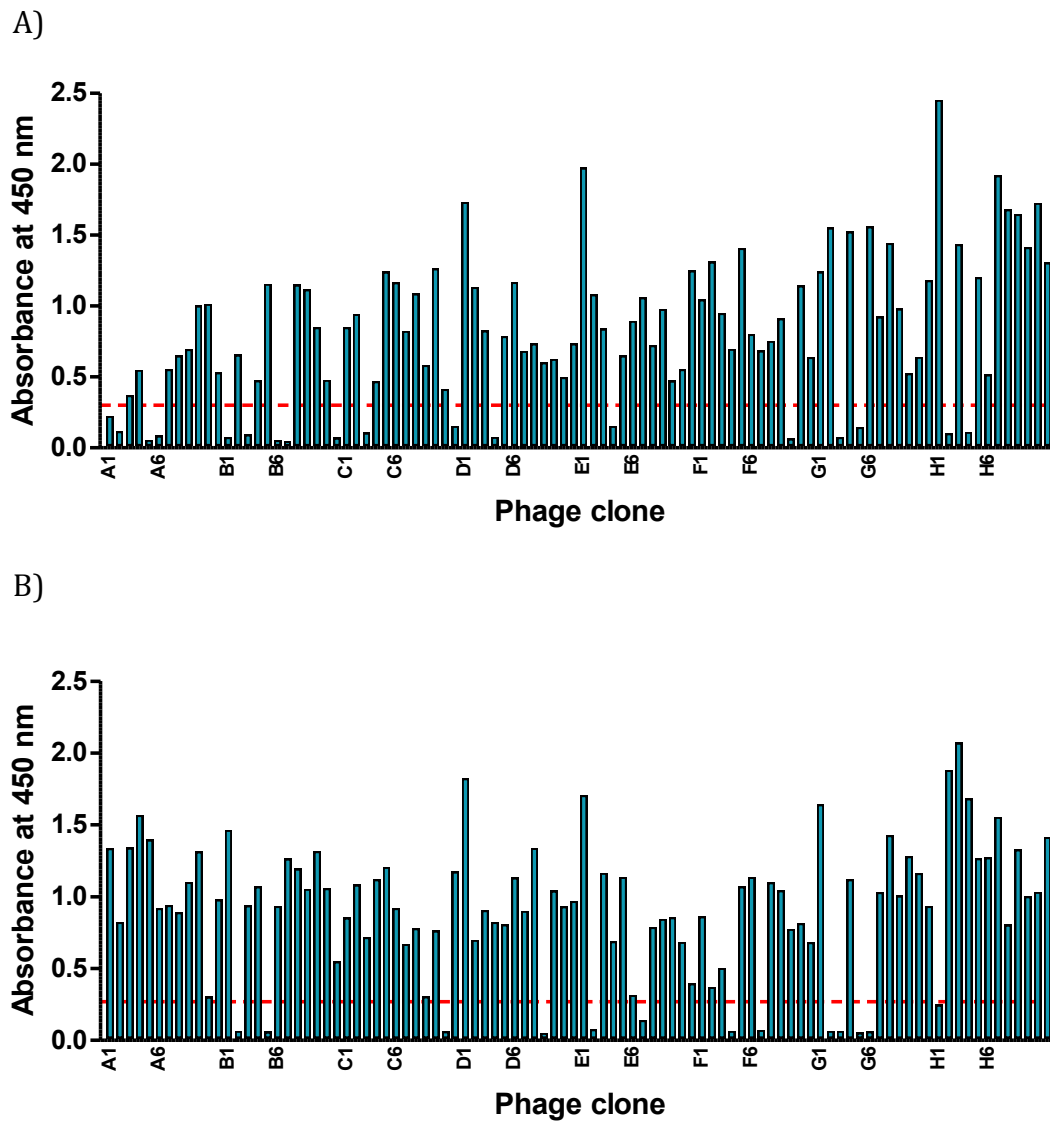


**Figure 3.14.** Soluble monoclonal ELISA screening for anti-HER2-specific scFv from 96 randomly selected clones from round 3 (A) and 4 (B) of panning. The clones were solubly expressed in *Top10F'* cells. Periplasmic fractions were applied to the HER2-coated ELISA plate and specific anti-HER2 scFv were detected using a HRP-labelled anti-HA antibody. The dashed red line represents the 'cut-off' value (three times the background optical density).

### 3.3.4.3 Analysis of putative anti-HER2 clones by competitive ELISA

Six positive HER2-specific clones (A4, D1, G1, H2, H3, H4) selected from the monoclonal ELISA from the 4<sup>th</sup> round of panning were taken forward for further characterisation. Each clone was grown up in 10-mL cultures and induced by IPTG addition. Bacteria cells were lysated by ‘freeze-thaw’ method (Section 2.2.5.1) and scFv-containing lysates were analysed by ELISA. In an attempt to select scFv that recognised HER2 in solution, a ‘single-concentration’ competitive ELISA was performed in parallel to a direct ELISA. Figure 3.15 shows that all clones exhibited competitive inhibition when incubated with a relatively high HER2 concentration of 2 µg/mL. Therefore, all six clones were carried on for further analysis.

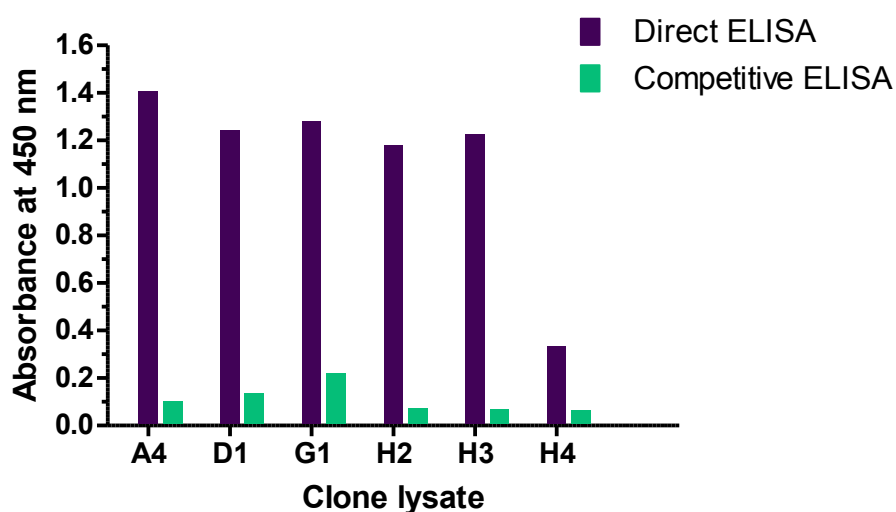


**Figure 3.15.** Competitive analysis of clone lysates. ELISA plates were coated with 2 µg/mL HER2. A direct ELISA was performed by first adding a 1:100 dilution of the scFv-containing lysates on the wells. The competitive analysis was carried out in parallel by adding 2 µg/mL of free HER2 incubated with each of the cell lysates, on the ELISA plate. A HRP-labelled anti-HA antibody was used to detect bound antibodies.

### 3.3.4.4 Sequence analysis of selected clones

Plasmid preparations from clones A4, D1, G1, H2, H3 and H4 were sent to Source BioScience for Sanger sequencing (Sanger and Coulson, 1975), using the primers listed in Section 2.2.5.4. DNA sequence analysis was performed on the selected avian clones (Figure 3.16) using ExPASy translation tool and ClustalW2 sequence alignment software (Section 2.2.5.4). The antibodies CDRs were identified based on Kabat definition (Johnson and Wu, 2004). D1 and H3 scFvs had identical CDR sequences to scFv A4, showing that they were actually the same clone. A4 and H4 show only subtle differences in the light CDR regions. Clones G1 and H2 show differences in both the heavy and light CDR regions. The scFv H2 differs most from those sequenced especially in CDR-L3 and CDR-H3, that are the key regions for antigen recognition.

Interestingly, the CDR-H3 repertory contained cysteine residues at a relatively high frequency. This finding supports Wu *et al.* (2012) study, which reports a higher cysteine content in chicken CDR3 repertory, in comparison to other species (chicken, 9.4 %; human, 1.6 %; and mouse, 0.25 %). Conroy *et al.* (2014) suggested that cysteine residues in chicken CDR-H3 might play an important role in the functional and structural diversity of the IgY repertory, through the establishment of disulphide linkages.

	CDR-L1	CDR-L2	CDR-L3	CDR-H1	CDR-H2	CDR-H3
<b>A4</b>	SGGNN-YYG	W <sup>N</sup> D <sup>K</sup> R <sup>P</sup> S	GSYGSSTN-SGI	G <sup>F</sup> N <sup>F</sup> R <sup>D</sup> Y <sup>A</sup> M <sup>V</sup>	I <sup>S</sup> S <sup>S</sup> I <sup>D</sup> G <sup>E</sup> T <sup>V</sup> Y <sup>G</sup> A <sup>A</sup> V	S <sup>A</sup> V <sup>T</sup> W <sup>C</sup> V <sup>G</sup> G <sup>C</sup> Y <sup>G</sup> -G <sup>L</sup> I <sup>D</sup> T
<b>H4</b>	SGSDSSWYG	Q <sup>N</sup> T <sup>K</sup> R <sup>P</sup> S	GGYDSSAGYTGI	G <sup>F</sup> N <sup>F</sup> R <sup>D</sup> Y <sup>A</sup> M <sup>V</sup>	I <sup>S</sup> S <sup>S</sup> I <sup>D</sup> G <sup>E</sup> T <sup>V</sup> Y <sup>G</sup> A <sup>A</sup> V	S <sup>A</sup> V <sup>T</sup> W <sup>C</sup> V <sup>G</sup> G <sup>C</sup> Y <sup>G</sup> -G <sup>L</sup> I <sup>D</sup> T
<b>G1</b>	SGGSS-YYG	S <sup>N</sup> D <sup>K</sup> R <sup>P</sup> S	G <sup>S</sup> A <sup>D</sup> S <sup>T</sup> A <sup>G</sup> Y <sup>V</sup> G <sup>I</sup>	G <sup>F</sup> T <sup>F</sup> N <sup>G</sup> Y <sup>E</sup> M <sup>Q</sup>	I <sup>N</sup> P--G <sup>S</sup> S <sup>T</sup> Y <sup>Y</sup> G <sup>T</sup> A <sup>V</sup>	S <sup>A</sup> S <sup>G</sup> Y <sup>C</sup> G <sup>W</sup> D <sup>X</sup> S <sup>S</sup> A <sup>G</sup> C <sup>I</sup> D <sup>A</sup>
<b>H2</b>	SGGG--NYG	S <sup>N</sup> N <sup>K</sup> R <sup>P</sup> P	G <sup>S</sup> T <sup>D</sup> S <sup>S</sup> A <sup>G</sup> ---I	G <sup>F</sup> T <sup>F</sup> S <sup>S</sup> Y <sup>D</sup> M <sup>N</sup>	I <sup>N</sup> A <sup>A</sup> -G <sup>S</sup> G <sup>T</sup> N <sup>Y</sup> G <sup>A</sup> A <sup>V</sup>	E <sup>S</sup> S <sup>I</sup> C <sup>I</sup> D <sup>A</sup> S <sup>C</sup> Y <sup>R</sup> T <sup>N</sup> S <sup>I</sup> D <sup>A</sup>

**Figure 3.16.** Sequence alignment of the deduced CDR V<sub>L</sub> and V<sub>H</sub> regions. D1 and H3 scFv (not shown) had identical CDR sequences to scFv A4. Amino acid colour code: Red: small + hydrophobic (including aromatic, with the exception of Y); Blue: acidic; Magenta: basic; Green: hydroxyl + sulfhydryl + amine + G. The dash symbol indicates a gap at that position.

### 3.3.4.5 Dose-response competitive studies of anti-HER2 clones

Previously, the lysates of six clones had been analysed by direct and competitive ELISA (Sections 3.3.4.3 and 3.3.4.4), demonstrating that HER2 binding was inhibited by large amounts of free HER2 in the sample. From the sequence analysis of these positive clones, four different HER2-specific clones were identified and these were then taken forward for a dose-response competitive study. Firstly, scFv-enriched lysates of the clones were prepared (Section 2.2.5.3) and titred against HER2 to select a suitable lysate dilution for the competitive analysis (Figure 3.17). Western blotting analysis (Section 2.2.1.5) of cell lysates was also performed to determine if the higher titres could be explained by a better antibody expression rate. The Western blotting results (Figure 3.18) suggested that H4 and G1 higher titres were the result of higher expression levels. For each clone, the lysate dilution that results in an absorbance value close to 1 (1:300 for H4 and G1, 1:200 for H2 and 1:10 for A4) was selected for competitive analysis (Figure 3.19).

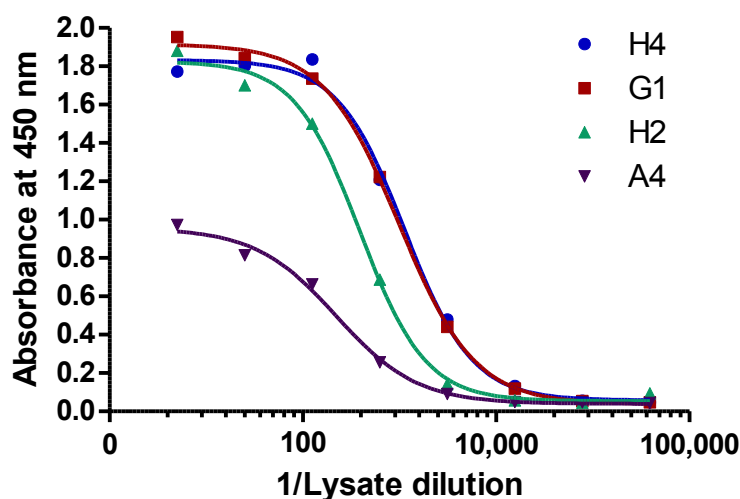


**Figure 3.17.** Antibody titre of HER2-specific clones, screened against HER2. Lysate dilutions (1:5–1:39,000) were tested for binding to HER2. Bound antibody was detected following the addition of a HRP-labelled anti-HA antibody.

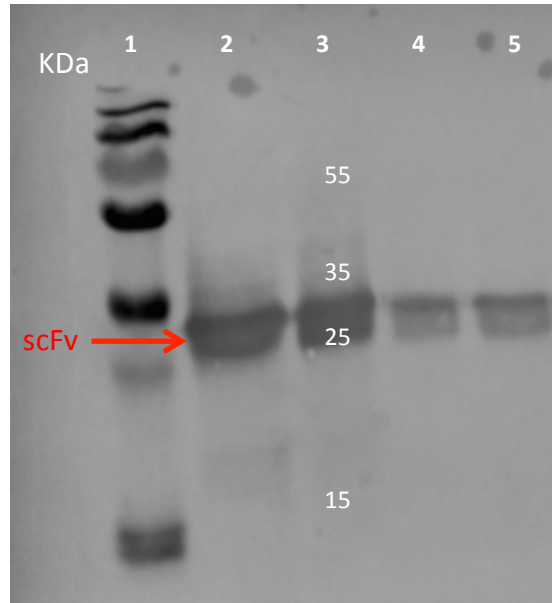


**Figure 3.18.** Western blotting analysis of cell lysates (1:5 dilution). Lane 1– PageRuler Plus prestained protein ladder (Thermo Scientific); lane 2–clone H4; lane 3–clone G1; lane 4–clone H2; lane 5–clone A4. In all cases, a ~27-KDa band, corresponding to the scFv size, is observed.

The dose-response competitive ELISA (Figure 3.19) involved the incubation of the scFv-containing lysates at the appropriate dilution with free HER2 concentrations from 0.2 to 3,125 ng/mL for ten minutes. The mixture was then added to ELISA plates coated with 1 µg/mL HER2 in PBS (10 mM, pH 7.4), and incubated for one hour at 37°C. The remaining steps of the competitive ELISA protocol were performed as described in Section 2.2.6.4. Bound anti-HER2 scFv was detected using a HRP-labelled anti-HA antibody. TMB substrate was then added for five minutes at room temperature. After stopping the reaction with acid, absorbance was read at 450 nm.

The ELISA analysis shows different binding patterns to HER2 (Figure 3.19). Overall, clone A4 showed the best dose-response relationship and a wide HER2 detection range and, therefore, the best potential for immunoassay development. Complete sequencing analysis for scFv clone A4 is available in Appendix 1.

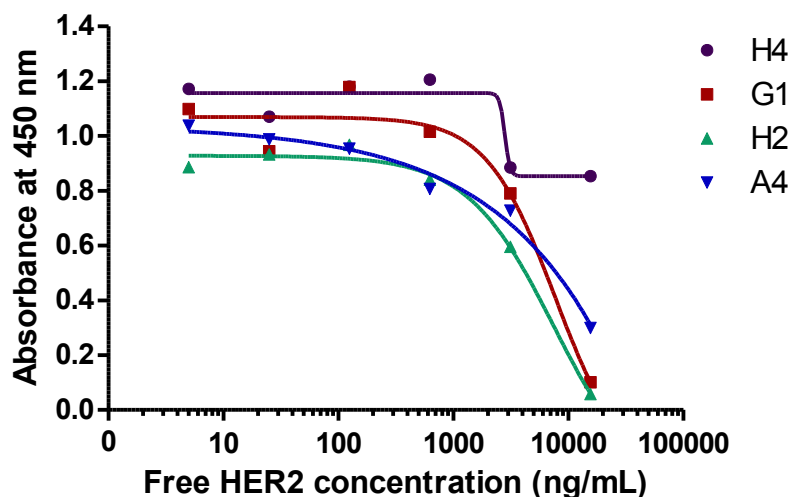


**Figure 3.19.** Competitive analysis of HER2-specific clones H4, G1, H2 and A4. Lysate dilutions from each of the four clones, were incubated with free HER2 concentrations from 0.2–3,125 ng/mL. Bound antibody was detected following the addition of a HRP-labelled anti-HA antibody.

### 3.3.5 Purification and characterisation of anti-HER2 scFv A4

#### 3.3.5.1 Purification of A4 scFv by immobilised metal affinity chromatography (IMAC)

A4 clone expression conditions (IPTG concentration and antibody expression temperature) were optimised as described in Section 2.2.6.2, prior to IMAC purification. It can be observed in Figure 3.20 that the IPTG concentration did not significantly affect to the antibody expression. IPTG concentration does not always affect protein expression (Larentis *et al.*, 2014; Malik *et al.*, 2016). However, induction temperature seemed to have an effect in protein expression, as a higher antibody response could be observed when expressed at 30°C, when compared with expression at 37°C. Since 1 mM IPTG showed a slightly better antibody response when expressing at 30°C, these were the selected conditions for large-scale antibody expression.

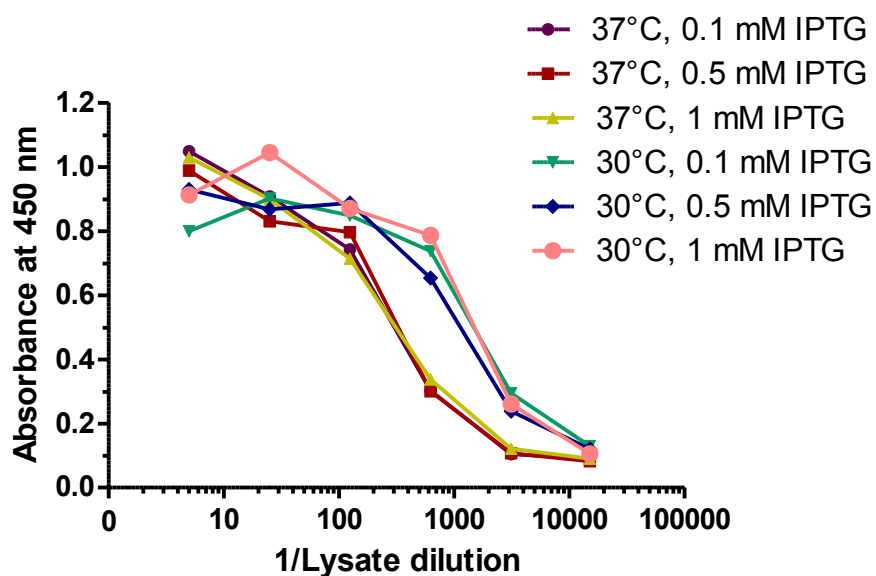


**Figure 3.20.** Antibody titre for the selection of optimal IPTG concentration and expression temperature for scFv A4. Dilutions of lysates (1:5–1:39,000 ) from *E. coli* cultures which scFv expression was induced with different IPTG concentrations (0.1–1 mM) and temperatures (30 and 37°C) were tested and bound antibody was detected following the addition of a HRP-labelled anti-HA antibody.

Large-scale expression and IMAC purification of scFv A4 was performed as described in Section 2.2.6.2. IMAC is commonly used for rapid purification of polyhistidine affinity-tagged proteins. The hexa-histidine (H6) incorporated in the C-terminus of recombinant scFv by the pComb vector allows high-affinity interactions with the nickel-nitrilotriacetic acid ( $\text{Ni}^{2+}$ -NTA) matrix in the purification columns (Bornhorst *et al.*, 2000). Following binding of the tagged scFv, non-specific proteins can be washed away with a buffer containing modest levels of imidazole (10–50 mM). To elute the tagged protein of interest, two methods were used: lowering the pH to 4.4 (elution 1), which protonates the histidines residues, disrupting their bond to the  $\text{Ni}^{2+}$ -NTA resin; and competitive elution (elution 2) using an imidazole-rich buffer (250 mM). Both elution fractions were buffer-exchanged to 10 mM PBS (pH 7.3) and concentrated using Vivaspin 10,000 MW columns. Analysis of IMAC fractions was performed by SDS-polyacrylamide gel electrophoresis and Western blotting. In both elution fractions a distinctive band can be observed at 27 KDa (Figure 3.21), corresponding to the purified scFv. Elution 2 was performed after the first elution

step, and resulted in the elution of many non-specific proteins. Therefore, concentrated elute 1 was selected for assay development.

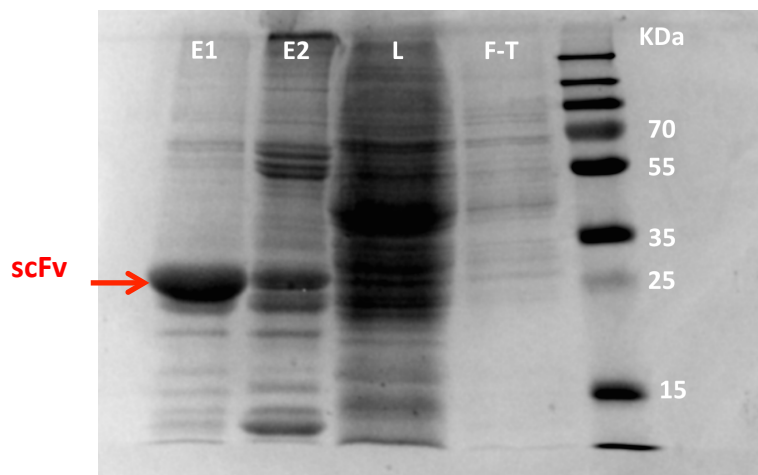


**Figure 3.21.** SDS-PAGE analysis of the fractions obtained during the IMAC purification of A4 scFv. E1–concentrated elute 1 (elution with low pH buffer); E2–concentrated elute 2 (elution buffer with imidazole); L–cell lysate; F-T–‘Flow-Through’.

### ***3.3.5.2 Development of a competitive ELISA assay using scFv A4 for the detection of HER2***

Following purification of anti-HER2 scFv A4, its use for the detection of HER2 in an indirect competitive inhibition ELISA format was investigated (Figure 3.22). The competitive inhibition ELISA is a competitive system in which the HER2-containing sample is incubated with the capture antibody (anti-HER2 scFv A4) for a set time preceding their addition to the HER2-coated wells.

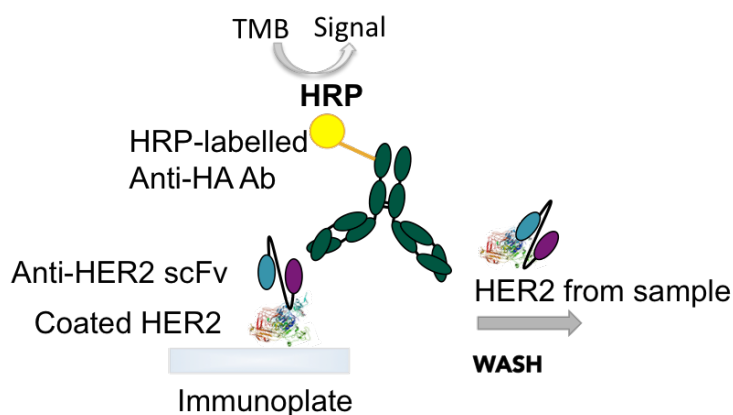


**Figure 3.22.** Indirect competitive inhibition ELISA format. The ELISA plate was coated with HER2. Anti-HER2 scFv was incubated with the sample (containing free HER2) and applied to the wells. The scFv bound to free HER2 from the sample are washed away, while those bound to coated HER2 are detected following the addition of HRP-labelled anti-HA antibody. The amount of signal generated is therefore inversely proportional to the amount of HER2 present in the sample.

### 3.3.5.2.1 Optimisation of assay conditions

The assay conditions were optimised to quantify HER2 as a potential prostate cancer biomarker candidate. To check the optimal pH for HER2 coating into the immunoplates, three different coating buffers with different pH values were investigated by checkerboard titration (Figure 3.23), as described in Section 2.2.6.3. The isoelectric point (IP) of HER2 ECD is 6.06. To effectively bind proteins, the pH of the coating buffer must be greater than the IP of the protein of interest. The buffers tested were PBS, pH 7.3; Tris buffer, pH 8.5; and Carbonate buffer, pH 9.6. The results are illustrated in Figure 3.19, suggesting that the amount of HER2 bound to the plate was optimal using Carbonate buffer, pH 9.6, which was chosen for further experiments.

Once the optimal coating buffer was selected, a checkerboard ELISA was performed for the determination of the optimal HER2 coating concentration and optimal scFv A4 dilution (Figure 3.24). A coating concentration of 1 µg/mL of HER2 was selected as the optimal (in terms of absorbance signal and reagent-saving) antigen coating concentration and a scFv dilution of 1:10,000 was selected for the competitive assay.

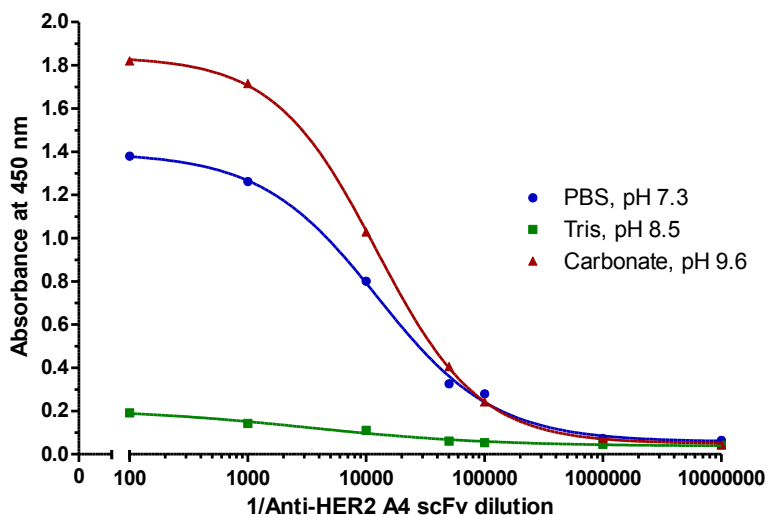


**Figure 3.23.** Selection of optimal coating buffer for use in a competitive ELISA for the detection of HER2. Coating buffers tested were: phosphate buffer, pH 7.3; Tris-buffer, pH 8.5 and carbonate buffer, pH 9.5. The anti-HER2 scFv A4 was serially diluted (1:100–1:10,000,000) and added to the HER2-coated wells. Bound antibody was then detected using HRP-labelled anti-HA secondary antibody.

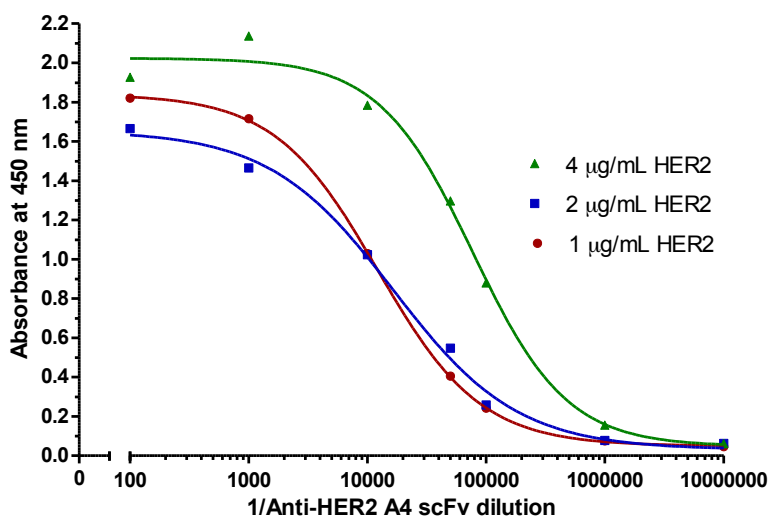


**Figure 3.24.** Selection of optimal HER2 coating concentration (1–4 µg/mL) and scFv dilution for use in a competitive ELISA for the detection of HER2. The anti-HER2 scFv A4 was serially diluted (1:1,000–1:10,000,000) and added to the HER2-coated wells. Bound antibody was then detected using HRP-labelled anti-HA secondary antibody.

Using the optimised conditions, a competitive analysis was carried out (Section 2.2.6.4) to assess the capability of scFv A4 to detect HER2 in solution phase (Figure 3.25). The limit of detection (LOD), calculated as described by Armbruster *et al.* (2008), was 45 ng/mL. Typically, the calculation of the LOD requires at least 20 replicates. However, after analysing six replicates (intra/interday) it became obvious that greater sensitivity was needed to detect HER2 at the clinical ‘cut-off’ for prostate cancer, which is around 15 ng/mL (Okegawa *et al.*, 2006; Domingo-Domenech *et al.*, 2008). Therefore, no further samples were measured.

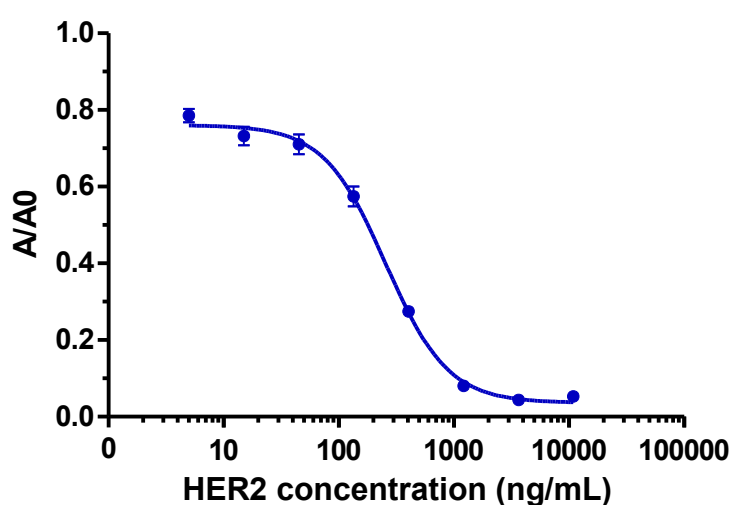


**Figure 3.25.** Competitive analysis of anti-HER2 scFv A4 using optimised conditions. A 1:1 mixture of HER2 (5–10,935 ng/mL) with scFv A4 (1:10,000 dilution) was added to the HER2-coated wells. Bound antibody was then detected using HRP-labelled anti-HA secondary antibody. The results were normalised by dividing the absorbance values (A) by the absorbance of the blank (A0).

#### 3.3.5.2.2 Evaluation of competitive assay in serum

To explore the suitability of generated scFv A4 for the detection of HER2 from clinical samples, human serum samples spiked with HER2 were tested by competitive inhibition ELISA (Section 2.2.6.4) and compared with those results obtained in PBS. HER2 detection in serum can be affected by the presence of rheumatoid factor, autoantibodies or cross-reacting metabolites. Assay interference can also arise from pre-analytical steps, such as from the chemicals used in the sample collection devices (Wild, 2005). As observed in Figure 3.26, no significant matrix effect was

observed when the competitive assay was performed in serum, when compared to the assay performed in HER2-spiked PBS buffer. Once the ability of anti-HER2 A4 scFv to detect HER2 from serum was demonstrated, the assay detection method was modified to investigate if sensitivity could be improved.

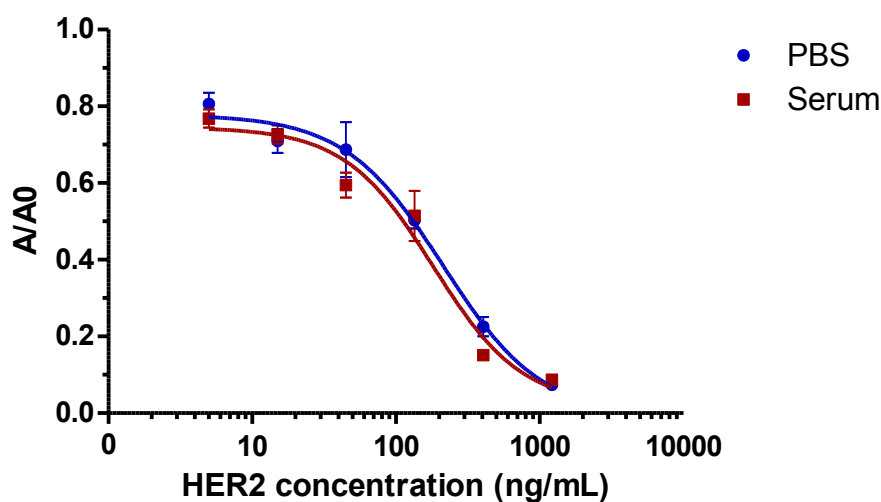


**Figure 3.26.** Competitive analysis of anti-HER2 scFv A4 to detect HER2 in 10 mM PBS buffer and in human serum. The results were normalised by dividing the absorbance values (A) by the absorbance of the blank (A0).

### 3.3.5.3 Fluorescence-based competitive assay

Fluorescence enzyme assays are typically considered more sensitive than colorimetric assays (Bell *et al.*, 2013). It was postulated that the use of fluorescence HER2 detection could improve the sensitivity of the developed competitive assay. To maintain the assay format as similar to the colorimetric-based assay as possible, the only element changed was the peroxidase substrate, substituting TMB for Ampliflu Red. Ampliflu Red (Sigma) is a fluorescence-based enzyme substrate that allows for specific and sensitive detection of HRP-labelled antibodies. Ampliflu Red is enzymatically converted into highly fluorescent Resorufin, by the action of HRP in the presence of H<sub>2</sub>O<sub>2</sub>. Imaging can be done by excitation of the Resorufin ( $\lambda_{ex}$  = 530–560 nm /  $\lambda_{em}$  = 590 nm) and fluorescence imaging. Opaque black Nunc

immunoplates were used for this assay, as these are designed to reduce the light scattering and background fluorescence.

To select the optimal excitation wavelength for Resorufin in our assay, an excitation scan was performed using Tecan Infinite™ 200 microplate reader, and 544 nm was chosen as optimal. Therefore, the competitive assay was performed as described in Section 2.2.6.5 and fluorescence was measured at 544/590 nm excitation/emission wavelengths (Figure 3.27). The results show that the fluorescence-based assay was unable to detect HER2 concentrations below 100 ng/mL and therefore the assay sensitivity was reduced, when compared with the colorimetric assay.

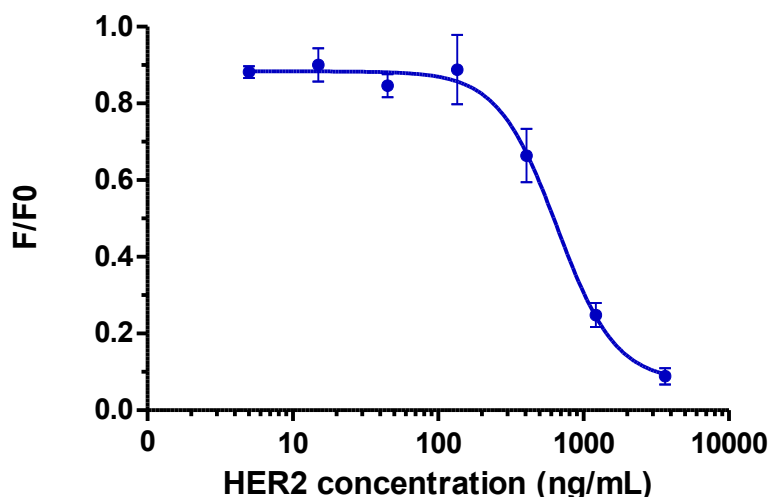


**Figure 3.27.** Fluorescence-based competitive ELISA for HER2 detection (5–3,645 ng/mL). After incubation with the secondary antibody, Ampliflu Red peroxidase substrate was added to the wells in the presence of H<sub>2</sub>O<sub>2</sub> and was incubated for 30 minutes at room temperature. Ampliflu Red is converted into Resorufin (highly fluorescent) by the action of HRP. Fluorescence was measured at 544/590 nm excitation/emission wavelengths. The results were normalised by dividing the fluorescence values (F) by the fluorescence value of the blank (F<sub>0</sub>).

### 3.3.6 Impedimetric biosensor for HER2 detection

In a final attempt to achieve the required sensitivity for HER2 detection from blood using the generated scFv antibodies, a gold nanoparticle-based impedimetric

biosensor was developed by Dr. Shikha Sharma, in collaboration with the Jaypee Institute of Information Technology.

Electrochemical impedance ( $Z$ ) can be measured by applying an alternating current (AC) potential to an electrochemical cell and subsequent measuring the ability of the circuit to resist the current flow (Section 1.6.2). Electrochemical impedance spectroscopy (EIS) measures the variation of the impedance of a medium as a function of the frequency of an applied AC current. One of the most common methods of evaluating EIS data is the Nyquist plot (Figure 3.28), in which the real component ( $Z'$ ) of the impedance, corresponding to Ohmic resistance, is plotted on the X-axis; and the imaginary one ( $Z''$ ), representing the system's reactance, is plotted on the Y-axis (Wang *et al.*, 2012; Santos *et al.*, 2014). In the Nyquist plot (Figure 3.28), the semicircles within the mid-high frequencies imply a charge-transfer limited process (due, for example, to the electrode material), while the linear tail present at lower frequencies implies a mass-transfer limited process, affected by the diffusion within the electrolyte and active electrode materials (Santos *et al.*, 2014).

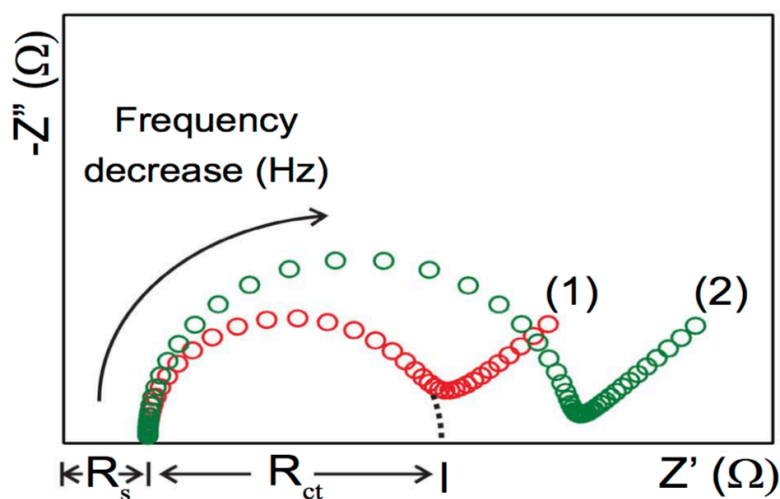


**Figure 3.28.** Example of Nyquist diagram for EIS data representation. When target antigen is captured from the solution (antibody- antigen interaction), an additional layer is formed at the electrode surface, which increases the charge-transfer resistance ( $R_{ct}$ ) (situation 2). Changes in  $R_{ct}$  can, therefore, report the presence of the specific target in the solution. Adapted from Santos *et al.* (2014)

In this work, immunosensor fabrication (Section 2.2.8.1) was performed on screen-printed carbon electrodes modified with gold nanoparticles to which anti-HER2 scFv antibodies were conjugated (Figure 3.29).

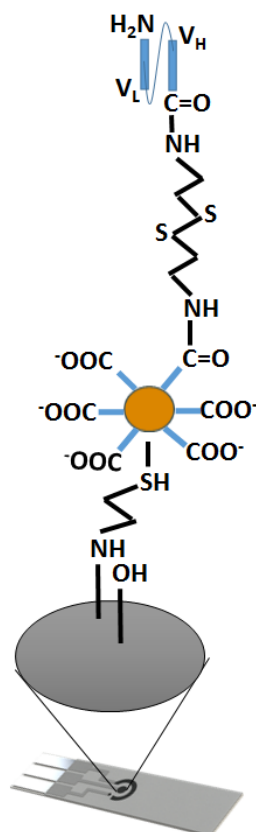


**Figure 3.29.** Representation of the gold nanoparticle-based immunosensor for the detection of HER2. Firstly, epoxy and hydroxyl groups were added on the surface of the electrode by cleaning it with diluted sulphuric acid. Secondly, the working electrode was functionalised with thiol groups (cysteamine hydrochloride) to facilitate the immobilisation of gold nanoparticles. Subsequent addition of cysteamine dihydrochloride onto the gold-modified electrode surface resulted in  $\text{-NH}_2$  groups on the surface. Finally, anti-HER2 scFv A4 was immobilised via amide bonds.

The fabricated immunosensor was then employed for electrochemical immunosensing and quantification of HER2 antigen using electrochemical impedance spectroscopy (EIS) as described in Section 2.2.8.2. Antibody immobilisation techniques based on gold nanoparticles-modified electrodes (Raghav and Srivastava, 2015 and 2016) were selected for immunosensor fabrication.

Immunosensor efficiency was optimized by suitable choice of temperature, pH and time duration that affect immune-complexation between immobilized HER2 scFv A4 and the HER2 antigen present in the sample.

### ***3.3.6.1 Determination of optimum time duration, temperature and pH for immune-complexation***

Optimum time duration for immune-complexation was determined by incubating the immunosensor with 0.1 ng/mL HER2 in 0.01 M PBS (pH 7.4) at ambient temperature conditions followed by recording impedimetric response spectra at 5, 10, 15, 20, 25, and 30 minutes (Figure 3.30A). Figure 3.30B shows charge-transfer resistance ( $R_{ct}$ ) of the electrode/electrolyte interface as a function of time.  $R_{ct}$  increases with increasing incubation time up to 15 minutes, beyond which no further change is observed, indicative of saturation.

Similarly, the optimal temperature for immune-complexation was obtained by incubating 0.1 ng/mL HER2 in 0.01 M PBS (pH 7.4) at various temperatures between 25–75°C for 15 minutes (Figure 3.31A). Figure 3.31B shows the variation of calculated  $R_{ct}$  with temperatures. Recorded impedimetric responses indicates maximum binding of the antigen and antibody at 30°C.

Finally, the pH dependence of the interaction was evaluated by incubating 0.1 ng/mL HER2 antibody in different pH conditions i.e. 5.5, 6.5, 7.4, 8.5, 9.5 and 10.5 for 15 minutes at 30°C (Figure 3.32A). Variation of  $R_{ct}$  with pH is shown in Figure 3.32B. Maximum charge transfer resistance at pH 7.4 suggests maximum immune-complexation. A buffer pH beyond  $7.5 \pm 1.0$  results in a decrease in antibody-antigen complex formation. Hence, for all further measurements an optimal of pH 7.4 was used.

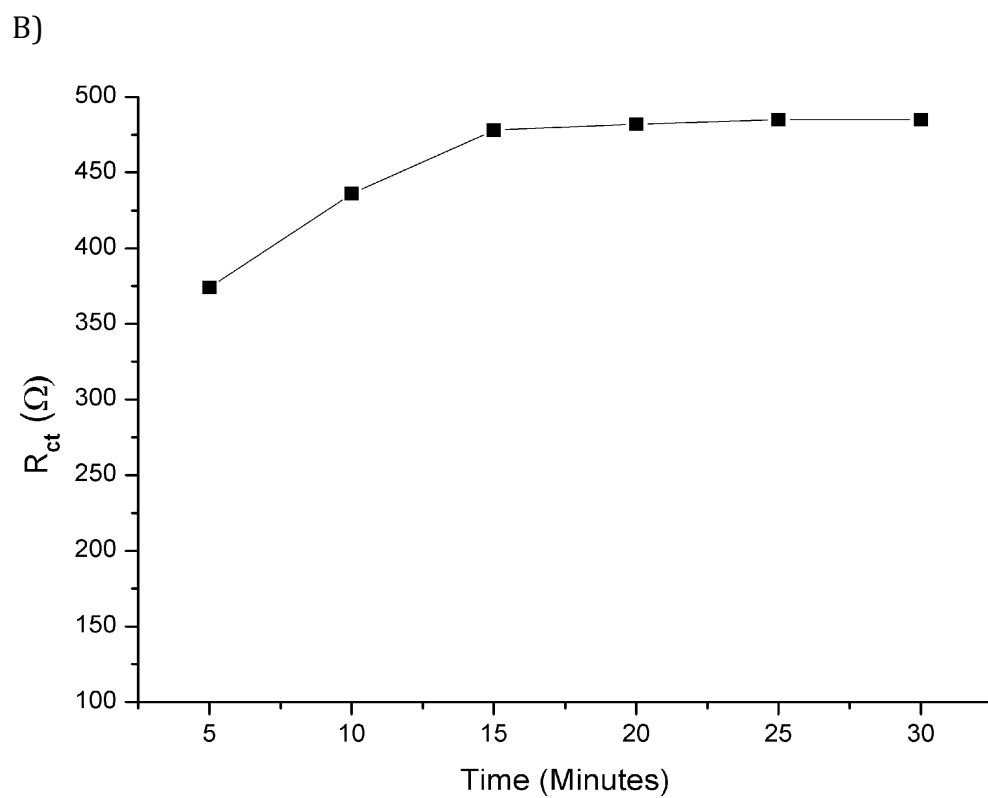
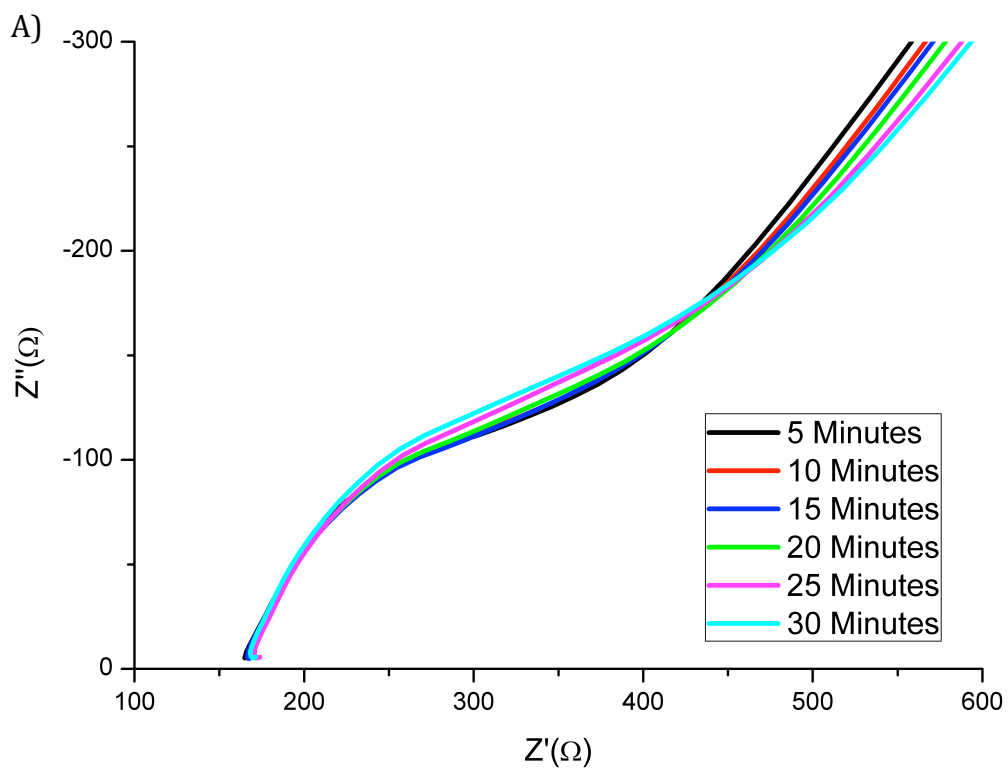


**Figure 3.30.** Optimisation of immune-complexation time. A) EIS of HER2 immunosensor in 5 mM  $[\text{Fe}(\text{CN})_6]^{3-/4-}$  redox probe at 0.1 ng/mL HER2 as a function of HER2 incubation time (5–30 minutes). B)  $R_{ct}$  as a function of HER2 incubation time.

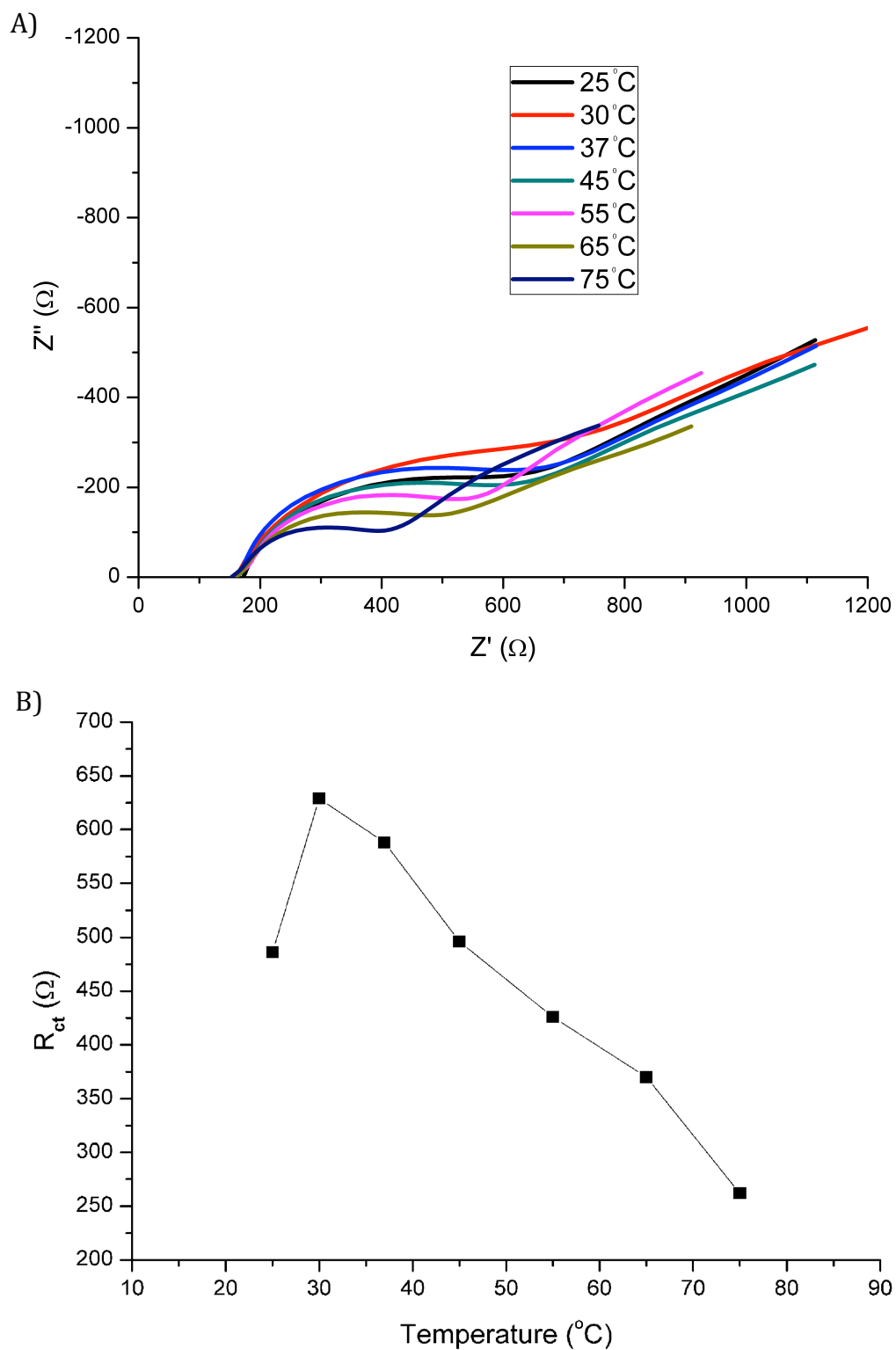


**Figure 3.31.** Optimisation of immune-complexation temperature. A) EIS of HER2 immunosensor in 5 mM  $[\text{Fe}(\text{CN})_6]^{3-/4-}$  redox probe at 0.1 ng/mL HER2 as a function of immune-complexation temperature (25–75°C). B)  $R_{\text{ct}}$  as a function of immune-complexation temperature.

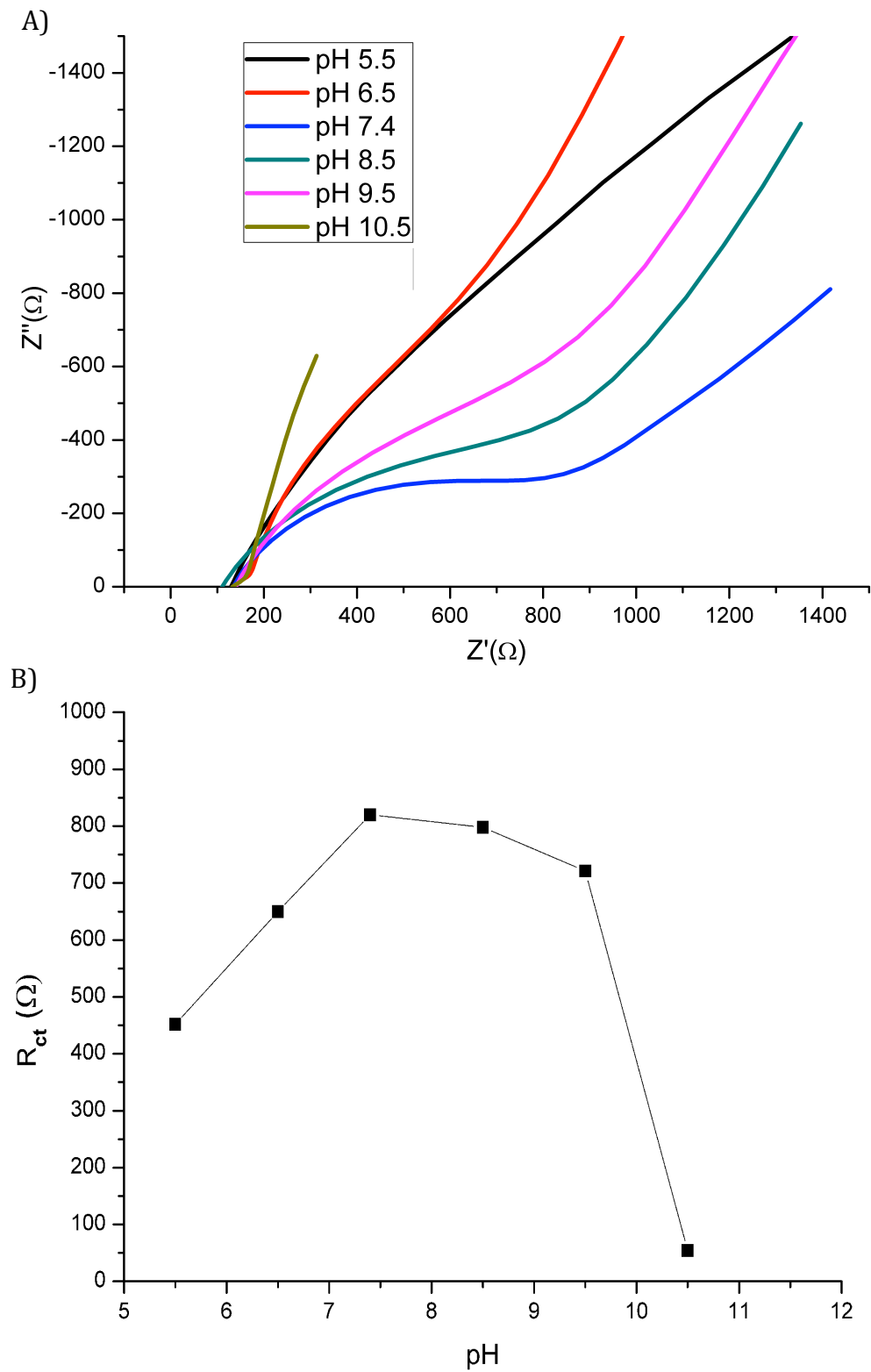


**Figure 3.32.** Optimisation of immune-complexation pH. A) EIS of HER2 immunosensor in 5 mM  $[\text{Fe}(\text{CN})_6]^{3-/4-}$  redox probe at 0.1 ng/mL HER2 as a function of pH (5.5–10.5) for antibody-antigen interaction. B)  $R_{ct}$  as a function of pH.

### **3.3.3.6.2 HER2 measurements using an impedimetric immunosensor**

Figure 3.33 shows the immunosensor response with increasing concentration of antigen spiked in PBS (A) or serum (B). The electrochemical spectra was recorded following the addition of a drop (3  $\mu\text{L}$ ) of each HER2 concentration (0.1–500 ng/mL) to the immunosensor surface. This was incubated for 15 minutes and EIS measurements (Section 2.2.8.2) were performed following the addition of the redox probe (5 mM  $\text{K}_4[\text{Fe}(\text{CN})_6]/\text{K}_3[\text{Fe}(\text{CN})_6]$ ). The immunosensor response in serum was evaluated by addition of known concentration of HER2 in serum (0.001–500 ng/mL) and incubating the immunosensor under optimal conditions. For EIS measurements (Section 2.2.10.2), the redox probe (5 mM  $\text{K}_4[\text{Fe}(\text{CN})_6]/\text{K}_3[\text{Fe}(\text{CN})_6]$ ) was also prepared in serum instead of PBS. The results obtained from serum show that the immunosensor displays a dynamic range of 0.01 ng/mL to 100 ng/mL beyond which saturation is observed. The immunosensor behaviour at lower concentrations (see Figure 3.34) shows the limit of detection of immunosensor as approximately 0.01 ng/mL which is significantly more sensitive than that found with ELISA (LOD= 45 ng/mL).

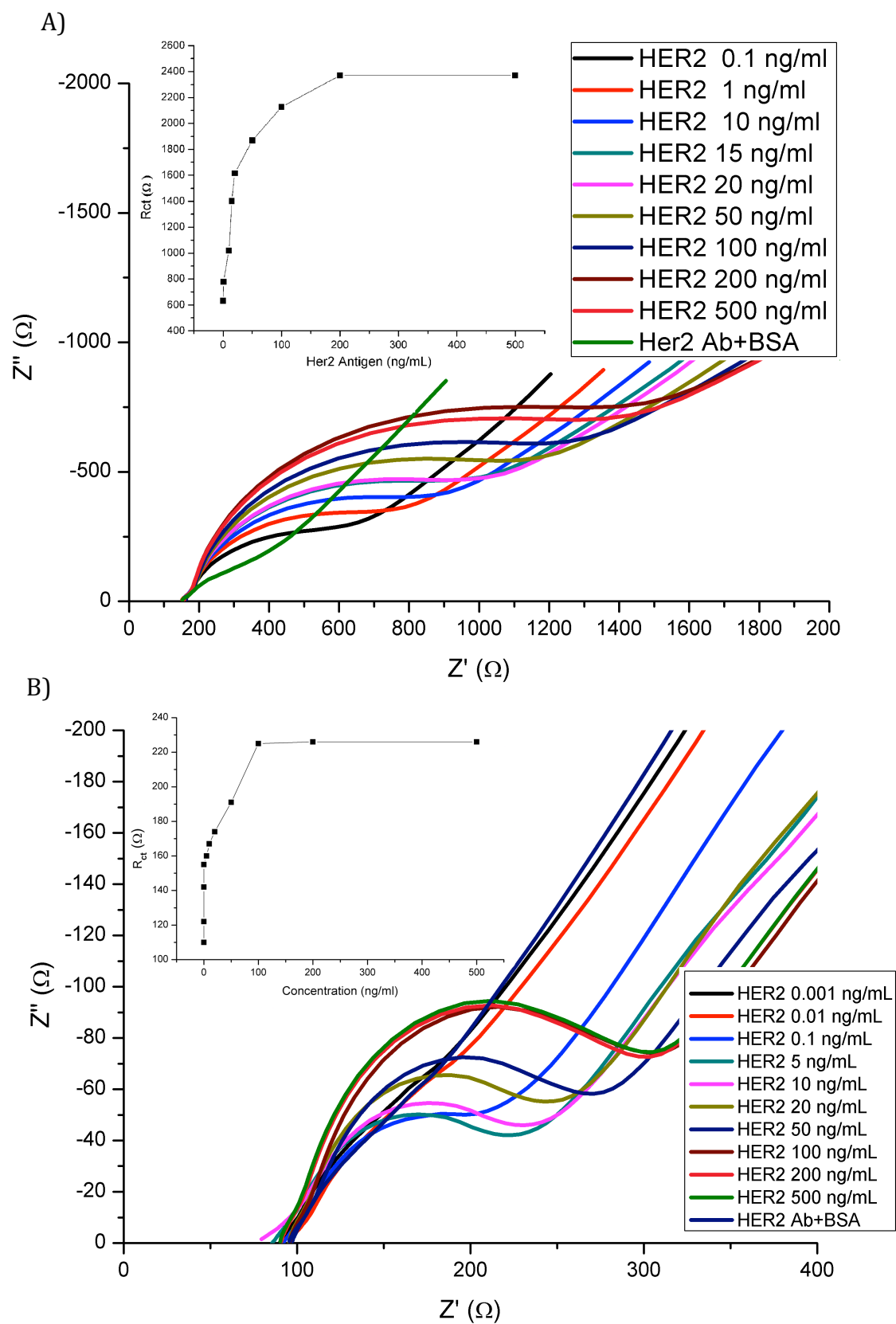


**Figure 3.33.** EIS analysis of immunosensor in 5 mM  $[\text{Fe}(\text{CN})_6]^{3-/4-}$  redox probe with increasing concentrations of HER2 (0.1–500 ng/mL) spiked in PBS buffer (A) or serum (B). Insets show  $R_{ct}$  as a function of HER2 concentration.

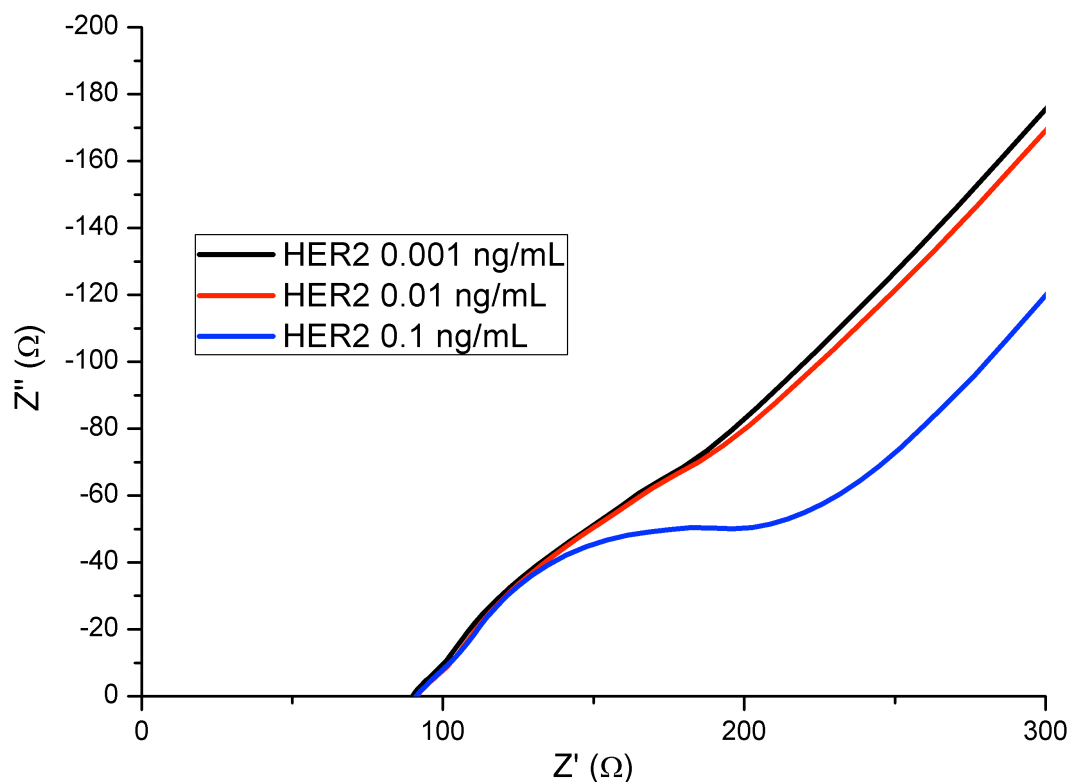


**Figure 3.34.** EIS analysis of immunosensor in 5 mM  $[\text{Fe}(\text{CN})_6]^{3-/4-}$  redox probe at low HER2 concentrations (0.001–0.1 ng/mL). A limit of detection of 0.01 ng/mL of HER2 was obtained.

### 3.4 DISCUSSION

Current HER2 diagnosis focuses on the identification of breast cancer patients that would benefit from HER2-targeted treatments (Table 3.2). Existing HER2 testing technologies rely mainly on immunohistochemical (IHC) techniques, for the determination of HER2 protein expression in cell membranes, or fluorescence in situ hybridization (FISH), for the assessment of *HER2* gene amplification (Perez *et al.*, 2014). Emerging technologies, such as chromogenic in situ hybridization (CISH) or dual in situ hybridization (DISH), rely on chromogenic detection to count how many copies of the *HER2* gene, located on chromosome 17, are present in a tissue sample. All of these methods for HER2 status evaluation are limited by the genetic heterogeneity in the tissue samples used (Barlett *et al.*, 2011; Ohlschlegel *et al.*, 2011) and the ‘real-time’ follow-up difficulties associated with the requirement for biopsy samples. The determination of serum HER2 extracellular domain (ECD) status

**Table 3.2.** List of FDA cleared or approved companion diagnostic (*in vitro* and imaging tools). HER2 tests Adapted from Myers (2015).

Drug trade name	Device name and manufacturer	PMA	Detection probe	Technology
<b>Herceptin (trastuzumab)</b>	PathVysion HER2 DNA probe kit (Abbot Molecular Inc.)	1998	DNA probe	Qualitative FISH
	PATHWAY anti-HER2 neu (Ventana Medical Systems Inc.)	2000	Rabbit mAb (Clone 4B5)	Semiquantitative FISH
	HER2 CISH pharmDx kit (Dako Denmark A/S)	2011	DNA probes with chromogenic dyes attached	Automated, quantitative dual-color CISH
	INFORM HER2 Dual ISH DNA Probe Cocktail (Ventana Medical Systems Inc.)	2011	DNA probe	Automated, quantitative dual-color DISH
	Bond Oracle HER2 IHC System (Leica Biosystems)	2012	Mouse mAb (Clone CB11)	Automated, semiquantitative IHC
<b>Herceptin (trastuzumab); Perjeta (trastuzumab); KADCYLA (trastuzumab)</b>	HercepTest (Dako Denmark A/C) (Dako Denmark A/S)	1998	Rabbit pAb	Semiquantitative IHC
<b>Herceptin (trastuzumab); Perjeta (trastuzumab); KADCYLA (trastuzumab)</b>	HER2 IQFISH pharmDx Kit (Dako Denmark A/S)	2005	DNA probe	Quantitative FISH
<b>(*)</b>	Manual HER-2/neu Microtiter ELISA (Oncogene Science Inc.)	2000	Mouse mAbs (clones NB-3 and TA-1)	Sandwich assay
	Immuno 1 assay for HER-2/neu (Bayer Corp.)	2000	Mouse mAbs (clones NB-3 and TA-1)	MP separation immunoassay
	ADVIA Centaur HER-2/neu Immunoassay (Bayer Corp.)	2003	Mouse mAbs (clones NB-3 and TA-1)	MP separation immunoassay

(\*) These tests are not intended to aid in treatment decisions, but in the monitoring of metastatic breast cancer patients. CISH—chromogenic in situ hybridization; DISH—dual in situ hybridization; FDA—US Food and Drug Administration; FISH—fluorescent *in situ* hybridization; sHER2—serum human epidermal growth factor receptor 2; IHC—immunohistochemistry; MP—magnetic particle; PMA—premarket approval; mAb—monoclonal antibody; pAb—polyclonal antibody.

has the potential to supplement IHC or FISH, reducing the number of false-negative results (Saito *et al.*, 2016). Serum HER2 FDA-approved tests (Table 3.2) are based on sandwich immunoassay techniques and are indicated for the monitoring of metastatic breast cancer patients. However, a number of studies have analysed the clinical significance of serum HER2 levels in other types of cancer, including prostate (Osman *et al.*, 2005; Siampanopoulou *et al.*, 2013), gastric (Saito *et al.*, 2016) and brain (Darlix *et al.*, 2016) cancer. Due to the role of HER2 in tumorigenesis (Section 3.1), this protein is an ideal candidate for the development of non-invasive biomarker panels for cancer detection.

This chapter describes the generation of avian anti-HER2 scFv antibodies for their subsequent incorporation onto a highly sensitive electrochemical biosensor for HER2 detection from serum.

The first step in the antibody library construction involved the immunisation of a host to evoke an immune response to the HER2 extracellular domain (ECD). Chickens are ideal non-mammal hosts when using a human protein for antibody generation as the phylogenetic distance magnifies the immunogenicity of the human HER2 ECD. They also allow rapid and simplified antibody library generation, since chicken immunoglobulin repertory involves a single functional  $V_H$  and  $V_L$  gene that undergo gene conversion (Mc Cormack *et al.*, 1993). Furthermore, chicken antibodies exhibit a broad epitope coverage and high affinity and they express well in *E.coli* as scFv (Wu *et al.*, 2012). Commercially FDA-approved monoclonal anti-HER2 antibodies (Table 3.2) have been selected from murine or rabbit hybridomas, while the generation of immune recombinant antibody libraries to HER2 has not been widely explored. Camelid single-domain antibodies (sdAbs) have been successfully isolated from an immune library generated by immunisation of a llama with the HER2-expressing ovarian cancer cell line SKOv3. After library screening, C7b sdAbs was fused to a human Fc portion (C7b-Fc) and used on a flow cytometry-based assay. C7b-Fc affinity to HER2-overexpressing cells was 7 nM, 11-fold lower than the affinity of the bivalent Herceptin monoclonal antibody analysed in parallel (Even-Desrumeaux *et*

*al.*, 2012). Ayat *et al.* (2013) isolated anti-HER2 and anti-carcinoembryonic antigen (CEA) scFv antibodies from human libraries generated from the lymph nodes of breast cancer patients expressing these biomarkers in their tumors. After panning, they identified two scFv clones that were able to detect the HER2 receptor on the cell membrane and internalized to the cells. Lu *et al.* (2014) selected specific antibodies to HER2 from a human phage scFv library from RNA extracted from lymphatic tissue harvested from breast cancer patients. The specificity of these antibodies for HER2 was confirmed by ELISA and IHC methods. To the best of my knowledge, the work described in this chapter shows, for the first time, the generation of an avian antibody library from an immunised chicken for the selection of specific scFv antibodies to human HER2 extracellular domain. A leghorn chicken was effectively immunised with the human protein, as demonstrated by the serum antibody titres over 1:10,000, indicating that the chicken was producing antibodies against HER2. cDNA was synthesised from the RNA isolated from the spleen of the immunised chicken (which contains antibody-producing B-cells), and the antibody variable heavy and light chains were amplified and annealed by PCR methods for the construction of a scFv library (Barbas *et al.*, 2011). The scFv PCR products were ligated into the pComb3XSS vector for pIII fusion protein display. This allowed the selection of anti-HER2 antibody fragments by phage display (Smith, 1985; Barbas *et al.*, 2001). The scFv genes were cloned in the pComb vector and transformed in *E.coli* XL-1 Blue electrocompetent cells, obtaining a relatively small library size of  $2.5 \times 10^6$  cfu/mL. A larger library size increases the probability of finding antibodies that could potentially bind to HER2, but modest-sized immune libraries can produce excellent antibodies (Amwersdorfer *et al.*, 2002; and Chassagne *et al.*, 2004). Enrichment of the phage antibody library via panning against immobilised HER2 resulted in highly specific anti-HER2 scFv antibodies after rounds 3 and 4 of panning, as revealed by polyclonal phage ELISA. The presence of HER2-specific clones after the 3<sup>rd</sup> and 4<sup>th</sup> round of panning was confirmed by monoclonal soluble-scFv ELISA analysis of 192 clones, from which 84 % exhibit a positive response. Competitive analysis of a selection of six positives clones from round 4 was carried out to determine if they were specific for HER2 in solution. To assess the genetic variability within the selected clones, DNA sequence analysis was performed, revealing that

three of the six clones were identical. From a dose-response analysis, anti-HER2 A4 scFv was selected for IMAC purification (Bornhorst *et al.*, 2000) and assay development. After extensive optimisation, a competitive assay for the detection of HER2, which showed a LOD of 45 ng/mL, was developed. However, to detect HER2 from patients' serum, a greater sensitivity was required, as the 'cut-off' value for HER2 in prostate cancer is around 15 ng/mL (Domingo-Domenech *et al.*, 2008). To overcome this problem, fluorescence-based detection, which is considered more sensitive than colorimetric methods (Bell *et al.*, 2013), was investigated. When comparing the calibration curve of fluorescence-based assay to the original colorimetric-based assay, a loss in sensitivity was observed. This can be attributed to the complexity of the HRP-catalyzed oxidation of the Ampliflu Red substrate (Sigma) by hydrogen peroxide. From a literature review, only a few studies describing Ampliflu Red-based detection of HRP-labelled antibodies by immunoassay were found (Abdelghany *et al.*, 2012; Breault-Turcot *et al.*, 2015), while this substrate has been mainly used as a probe for H<sub>2</sub>O<sub>2</sub> detection (Votyakova *et al.*, 2004; Jomaa *et al.*, 2014; Wulff *et al.*, 2014). However, Breault-Turcot *et al.* (2015) successfully detected PSA as concentrations as low as 10 pM (<1 ng/mL) using Ampliflu Red for HRP-labelled antibodies detection. First, an anti-PSA antibody was immobilised onto a multi-channel microfluidic system to capture PSA complex with HRP-labelled anti-PSA antibody and then this was incubated with Ampliflu Red solution in the presence of H<sub>2</sub>O<sub>2</sub>, leading to a fluorescence signal. Surface plasmon resonance (SPR) and fluorescence ELISA detection were combined on a single microfluidic chip for dual detection of the recognition event and enzymatic conversion.

In a final effort to achieve the required assay sensitivity, the development of an impedimetric immunosensor was also investigated. Electrochemical immunoassays have been gained importance over the last years, emerging as a potential alternative to optical approaches (Lee *et al.*, 2008). Compared with spectrophotometric or fluorescence-based methods, electrochemical methods are not affected by the colour or turbidity of the sample (Lee *et al.*, 2008) or by the volume used during measurements (Ricci *et al.*, 2012). Importantly, it has been shown that electrochemical detection can achieve lower detection limits and therefore higher

sensitivity, when compared with spectrophotometry (Jiao *et al.*, 2000; Tang *et al.*, 2014). Furthermore, signal amplification can be achieved by the incorporation of different nanomaterials into the electrode surface (including gold, graphene, silver and carbon nanoparticles), which act as platforms for an improved immobilisation of biomolecules or for an enhanced electron transfer in modified electrodes (Putzbach *et al.*, 2013; Roberto *et al.*, 2013). Sensitive HER2 detection by electrochemical techniques has previously been reported by other groups. Al-Khafaji *et al.* (2012) described the development of a magnetic bead-based immunosensor for HER2 detection (LOD = 0.6 ng/mL) based on sandwich assay and electrochemical detection by differential pulse voltammetry (DPV). Impedimetric immunosensing of HER2 based on a gold nanoparticles/ multiwall carbon nanotube-ionic liquid electrode (AuNPs/MW-CILE) has also been reported. Gold nanoparticles were used to enhance antibody immobilisation on the electrode, achieving a linear range of 10–110 ng/mL and a limit of detection of 7.4 ng/mL (Arkan *et al.*, 2015). Qureshi *et al.* (2015) developed a capacitance aptamer-based biosensor for HER2 detection in serum. The capacitance change of the gold interdigitated electrode occurred by charge distribution between the ssDNA aptamer and the HER2 protein, allowing the detection of HER2 spiked in serum samples in a linear range of 0.2–2 ng/mL and with a LOD of 0.2 ng/mL. Thus, anti-HER2 A4 scFv was incorporated into a gold nanoparticle-based impedimetric biosensor. Gold (Au) nanoparticles are widely used in biosensing systems for their capacity to enhance transduction signals and their inert nature, which facilitates functionalization with biomolecules without loss of biological activity (Pingarrón *et al.*, 2008). Au nanoparticles also reduce the charge-transfer resistance ( $R_{ct}$ ) of the system, allowing the construction of highly-sensitive impedimetric biosensors at a single low frequency, sensitive to analyte binding (Wang *et al.*, 2006). Capture anti-HER2 A4 scFv antibodies were functionalised onto the surface of gold nanoparticles immobilised on a screen-printed carbon electrode. Following extensive optimisation of immune-complexation conditions, HER2 binding to the capture antibody at concentrations as low as 0.1 ng/mL was demonstrated. Finally, the immunosensor performance in serum was evaluated by spiking different HER2 concentrations in serum samples, obtaining a dynamic range of 0.01 ng/mL to 100 ng/mL, suitable for HER2 detection on patients' serum. The LOD for the

immunosensor was of 0.01 ng/mL, representing a significant sensitivity increase, as compared with the colorimetric competitive ELISA (LOD = 45 ng/mL). These results suggested that A4 scFv antibody sensitivity was not the limiting factor for achieving the required assay sensitivity and that electrochemical detection is a highly sensitive method. Hence, the electrochemical biosensor showed enhanced sensitivity for HER2 detection from serum in the clinically relevant range, outperforming previously described biosensors for the detection of this biomarker (Al-Khafaji *et al.*, 2012; Arkan *et al.*, 2015; Qureshi *et al.* 2015).

Overall, this chapter describes how avian scFv antibodies were generated and used for HER2 immunosensing. When compared with FDA-cleared Bayer Immuno 1 assay for HER-2/*neu* (Payne *et al.*, 2000), our platform shows similar linear range (0.01–100 vs. 0.1–250 ng/mL in Bayer's assay), improved LOD (0.01 vs. 0.1 ng/mL) and reduced assay time (15 minutes for our assay vs. 48 minutes for Bayer Immuno 1 assay). The developed immunosensor needs, however, further characterisation to assess the intra- and inter- assay reproducibility. This platform could then potentially be used for HER2 measurements to monitor disease progression in metastatic breast cancer patients or for the evaluation of serum HER2 status in other types of cancer, such as prostate or lung carcinoma.

## **Chapter 4**

# **'Lab-on-a-Disc' for Multiplexed Detection of PSA and HER2 From Whole Blood**

## 4.1 INTRODUCTION

Over the last two decades, microfluidic technologies have experienced a huge growth in applications in the field of diagnosis. Microfluidics allows the miniaturisation and automation of diagnostic devices and presents several advantages for point-of-care applications. These include the ability to make extensive use of complex multiplexing approaches and formats; the capacity for inclusion of sequential sample pre-conditioning steps of different types; reagent storage; the use of multiple steps involving reagent addition, mixing and washing; the potential for incorporation of centrifugal steps at various speeds; and the application of a range of detection strategies leading to greater sensitivity and resolution of results (Sharma *et al.*, 2015).

The ambiguity associated with PSA test-based prostate cancer diagnosis is the main driving force behind the search of new biomarker panels to distinguish between cancerous and non-cancerous conditions. The use of multiplexed tests based on PSA and additional cancer-specific biomarkers holds great promise for improved diagnosis of prostate cancer. Microfluidic platforms are the ideal tool for the simultaneous analysis of multiple markers in order to obtain precise and reliable diagnostic results without the need of centralised labs.

In the current study, a centrifugal 'lab-on-a-disc' (LoaD) device for the simultaneous detection of free PSA and HER2 from whole blood was developed. The role of HER2 in cancer progression and its association with a bad prognosis was previously discussed in Chapter 3. Free PSA (fPSA) is used in current clinical practice to help select prostate cancer patients in the diagnostic 'gray zone' (4–10 ng/mL total PSA) that should undergo biopsy. Patients with free/total PSA ratio greater than 25 % are considered more likely to have a benign prostatic condition than to have cancer, eliminating the need of biopsy (Catalonga *et al.*, 2000; Harvard Prostate Knowledge website, 2011). This work provides evidence of the value of microfluidic technologies for multi-marker assay-based detection for clinical diagnostics.

### 4.1.1 Centrifugal microfluidics

Microfluidic ‘lab-on-a-disc’ devices use centrifugal forces for fluid propulsion and mixing, by simply controlling the rotational speed. Centrifugal microfluidics exploits mainly two different types of forces: inertia and capillary action. Inertia forces acting on fluids in rotating systems can be divided in three categories—centrifugal force, Euler force and Coriolis force (Figure 4.1) (Tang *et al.*, 2016).

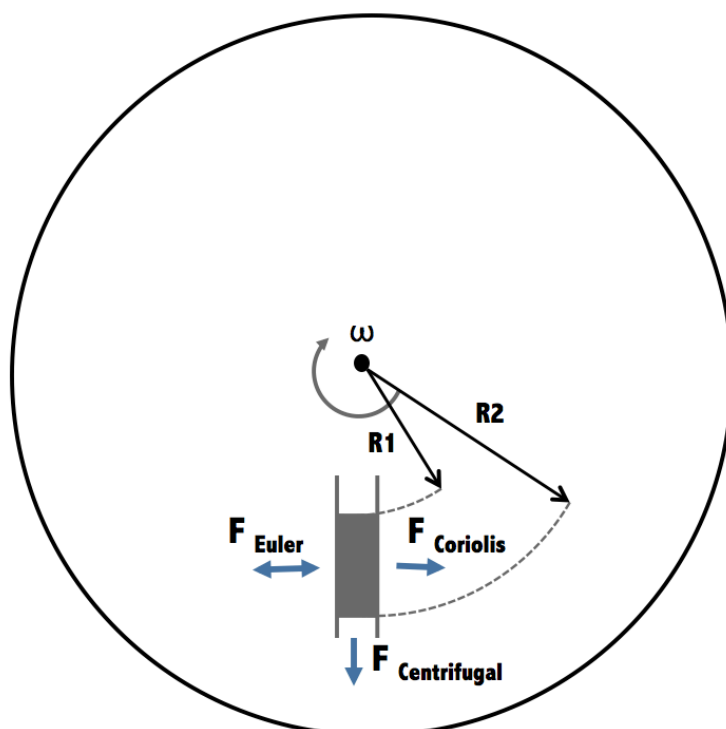


**Figure 4.1.** Inertial forces acting in centrifugal microfluidics. Centrifugal force acts radially outwards, the Coriolis force acts perpendicular to the angular rotational frequency ( $\omega$ ) and the Euler force is related to the angular acceleration. Coriolis and centrifugal forces increase with rotational speed. (Adapted from Strohmeier *et al.*, 2015).

Centrifugal force ( $F_c$ ) acts radially outward on the disc, and can be defined as:

$$F_c = m\omega^2 r$$

where  $m$  is the mass,  $r$  is the position in the disc and  $\omega$  is the angular rotational frequency. According to this equation, the centrifugal force for all fluid samples of the same mass at a given radius is constant. This allows parallel testing of multiple ‘flow-cells’ within the microfluidic disc.

The two other inertial forces affecting centrifugal microfluidic systems are the Coriolis force ( $F_{co}$ ) and the Euler force ( $F_e$ ). The Coriolis force increases with velocity ( $v$ ) and is given by:

$$F_{co} = -2m\omega \times v$$

The Euler force ( $F_e$ ) only exists when the angular acceleration is different than zero, according to the equation:

$$F_e = -m \frac{d\omega}{dt} \times r$$

Capillary action is very important at small-scale, and therefore also plays a role in microfluidics, allowing the fluids to advance in opposition to gravity. Capillary force occurs at the interfaces of liquid, solid and vapour phases and is a well-known mechanism for microfluidic flow propulsion or control by using capillary valves (Cho *et al.*, 2004; Irimia, 2014). Capillary valves use superficial tension at the interface between different fluids to prevent the entrance of fluids in microchannels filled with a second fluid (normally air) until a certain threshold rotational frequency is exceeded and centrifugal forces overcome surface tension forces, causing the liquid to enter the channel (Hugo *et al.*, 2014).

#### 4.1.2 Dissolvable-film tabs

Microvalves allow the control of the liquid flow in the microfluidic channels, and are essential for designs with complex functionality. In centrifugal platforms, the valves can be classified in two main groups, depending on the actuation mechanism: passive valves (solely actuated by centrifugal forces), including capillary (Zeng *et al.*, 2000), hydrophobic (Ducreé *et al.*, 2007), siphoning (Siegrist *et al.*, 2010) and pneumatic (Kinahan *et al.*, 2010) valves; and active (externally actuated) valves (Park *et al.*, 2012; Lee *et al.* 2015).

The main drawback of rotationally actuated valves (such as capillary burst valves) is that their burst frequency depends on the centrifugal force. Because there is a maximum spin rate that can be practically used and a limited radial space in the

microfluidic disc, only a limited number of sequential assay steps can be incorporated into the centrifugal platform (Kinahan *et al.*, 2014). To solve this problem, different designs of centrifugal-pneumatic valving systems based on sacrificial dissolvable film (DF) valves have been proposed, which allow the incorporation of liquid handling steps that are independent of the rotational speed (Gorkin *et al.* 2012, Kinahan *et al.*, 2014, Kinahan *et al.*, 2015). These are event-triggered valves, in which the movement of liquid on-disc actuates the valves. In the microfluidic platform described in this chapter (Figure 4.5), a DF tab design based on those described by Kinahan *et al.* (2013) and Dimov *et al.* (2014) was used. Figure 4.2 shows a representation of the DF valve mechanism, optimised by Dr. Rohit Mishra (from the School of Physical Sciences in DCU), which employs a pneumatic chamber and a DF-sealed chamber, both connected to a bypass-style expansion chamber. They are based on the balance between the centrifugal induced hydrostatic pressure and the pressure of the pocket of trapped air within the pneumatic chamber (Figure 4.2) (Kinahan *et al.*, 2014). These kinds of DF tabs provide liquid and vapour barriers when at rest and burst beyond a critical rotational frequency ( $\omega$ ), above which a small volume of liquid crosses the trigger lip, wetting the DF-tabs and thus opening a new channel, releasing the air pressure and allowing the liquid flow into the incubation chamber (Figures 4.2 and 4.5). The critical release frequency ( $\omega_c$ ) for the current system can be defined as:

$$\omega_c = \sqrt{\left[ \frac{V_t}{V_t - V_d} - 1 \right] \frac{P_o}{\rho \Delta r \bar{r}}}$$

where  $P_o$  is the atmospheric pressure,  $\rho$  is the density of the incoming liquid,  $V_t$  is the total volume of the pneumatic chamber (Figure 4.2A),  $V_d$  is the volume of gas displaced by the proceeding liquid in the valve until the lip (Figure 4.2B), and  $\Delta r$  and  $\bar{r}$  are defined as  $R_2 - R_1$  and  $(R_1 + R_2)/2$ , respectively. Hence, the critical release frequency is directly related to the radial position of the valve (Figure 4.4).

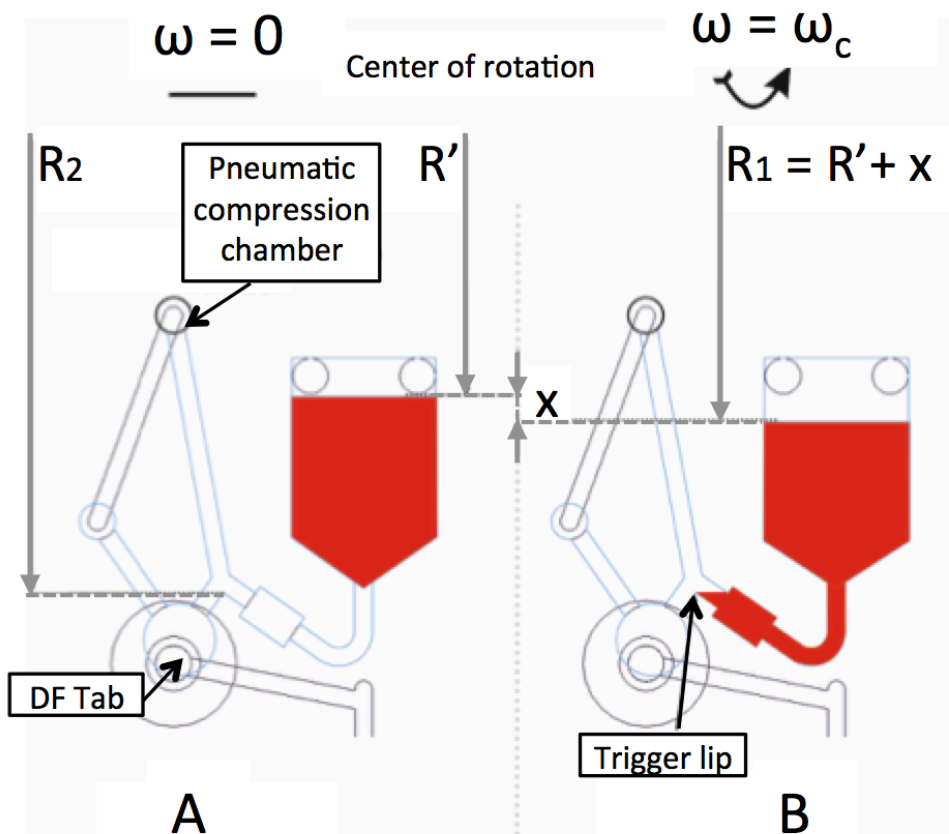


**Figure 4.2.** Actuation of centrifugo-pneumatic dissolvable film (DF) valves using a combination of an expansion chamber opening into the dissolvable film void via an overflow trigger lip at a radial distance  $R_2$  (which in turn is connected to a pneumatic compression chamber). A) Initially, the liquid (red) in the reservoir is held back due to the trapped air in the pneumatic connections between the liquid and the dissolvable film tab. B) At the critical frequency ( $\omega_c$ ), the centrifugally-induced hydrostatic pressure compresses the enclosed gas so that the liquid front reaches the trigger lip. Thereafter, a slight increase in the frequency to reach the so-called release frequency allows a small amount of liquid to leap to the DF tab thus wetting the dissolvable film and hence allowing the release of the liquid in the reservoir. Figure provided by Dr. Rohit Mishra.

Figures 4.3 and 4.4 illustrate how the release frequency ( $\omega_c$ ) of chambers with DF-tabs increases as the pneumatic chamber radius (and therefore, volume) and its distance from the center of the disc (radial position, 'R') decreases. Given a fixed radial position, different  $\omega_c$  of the DF-valves can be achieved by changing the volume of the pneumatic chamber, enabling positional multiplexing (Figure 4.3). Figure 4.4 shows the experimentally characterised release frequencies of the valves with variable pneumatic chamber radii at three different radial positions ( $R_1 < R_2 < R_3$ ) in agreement with the theoretical model. This enables a complex on-disc liquid handling.

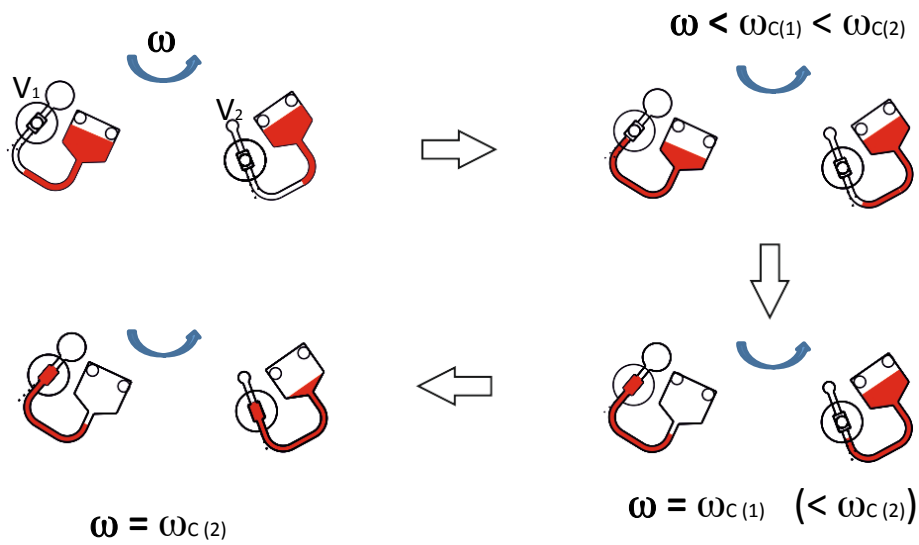


**Figure 4.3.** Radially and circularly patterned release chambers with DF tabs (positional multiplexing). Given a fixed radius from the spin centre the critical release frequency  $\omega_c$  of valve depends on the difference in pneumatic chamber volume ( $V_1 > V_2$ ). Diagram provided by Dr. Rohit Mishra.

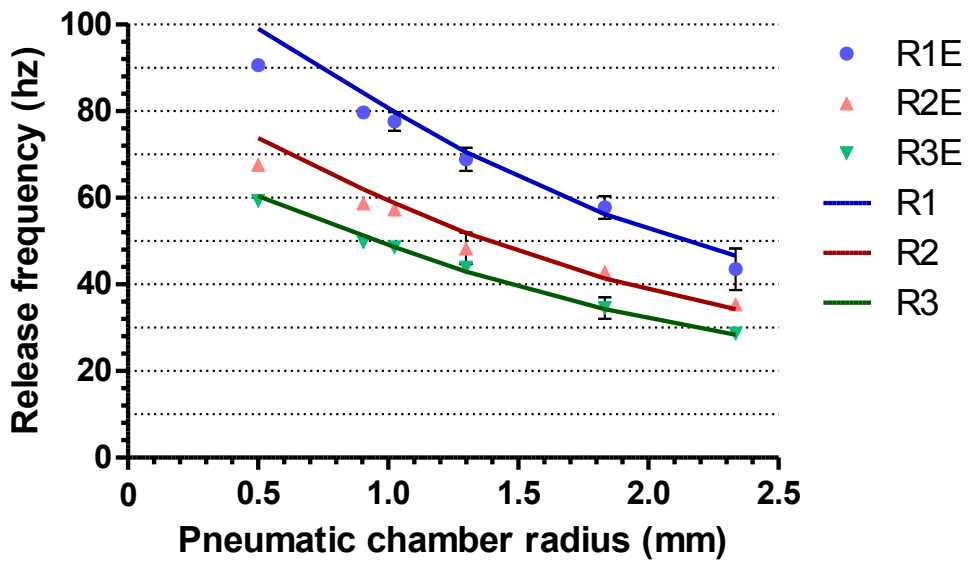


**Figure 4.4.** Dependence of release frequency on the radial position (R) of the trigger lip and the radius of the pneumatic compression chamber. Plot shows theoretical and experimental data (denoted by E) for three radii ( $R1 < R2 < R3$ ). Error bars indicate standard deviation from a minimum of three measurements on multiple discs.

#### **4.1.3 Design of the microfluidic 'flow cell'**

The disc 'flow cells' were designed by Dr. Rohit Mishra for a multiplexed multi-step sample handling protocol on a LoD for the detection of prostate cancer biomarkers from whole blood (Figure 4.5). All steps from the separation, metering and aliquoting of plasma, sequential release and incubation of various reagents and buffer washes including the stop reagent are carried out on the disc using purely rotational flow control.

The liquid handling protocol for the detection of anti-fPSA antibodies using a sandwich ELISA consists of a) plasma extraction from whole blood, b) plasma metering and aliquoting, c) incubation of plasma in the incubation chamber in which the capture antibodies are pre-immobilised, d) buffer wash#1, e) primary antibody release and incubation, f) buffer wash#2, g) secondary antibody release and incubation, h) enzymatic substrate release and incubation, i) and acid release for stop reagent followed by absorbance reading. Detection of the HER2 biomarker is based on a competitive ELISA comprising of a) primary antibody (anti-HER2 scFv) incubation with the whole blood before aliquoting the serum to the incubation chambers, b) plasma separation, metering and aliquoting, c) incubation of plasma in the incubation chamber where HER2 ECD is pre-immobilized, d) buffer wash, e) secondary antibody release and incubation, f) enzymatic substrate release and incubation, g) acid release for termination of the reaction followed by absorbance reading.

The competitive ELISA protocol can be implemented on the same disc as the sandwich ELISA (which requires a higher number of assay steps) by simply leaving the first two reagent chambers in the release series empty (buffer wash #1 and primary antibody as in Figure 4.5). This can be achieved because the incubation times of the secondary antibody and the enzymatic substrate are the same for both protocols.

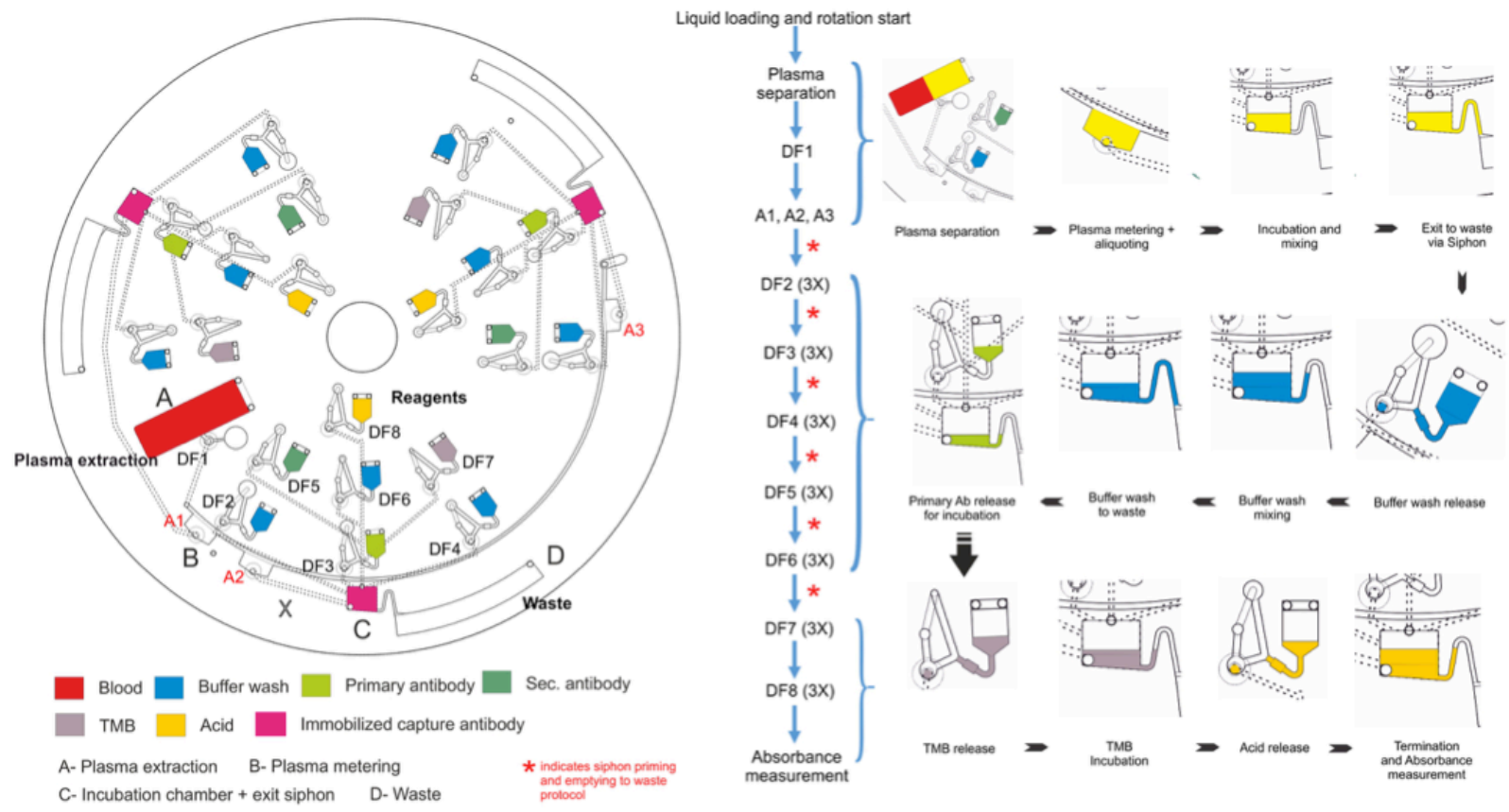


**Figure 4.5.** Lab-on-a-Disc for multiplexed detection of prostate cancer biomarkers from whole blood. The plasma is extracted from the blood in chamber A (for competitive ELISA, the blood is pre-incubated with anti-HER2 scFv A4JZ), metered, aliquoted and then released (using special DF tabs that require around 40 seconds to dissolve as timed release in chambers A1, A2 and A3) into an incubation chamber C immobilized with capture antibodies (in case of the sandwich ELISA; for the competitive ELISA, HER2 ECD is immobilized on the surface). The release frequencies of all the reagents and buffer washes are chosen to exceed those required for plasma extraction, plasma metering and the exit siphon on chamber C. The protocol for an ELISA (depicted here

## **4.2 AIM OF THIS CHAPTER**

In this chapter the use of 'in-house' generated recombinant antibodies to prostate cancer biomarkers (including A4 scFv antibody described in Chapter 3) in a 'lab-on-a-disc' device for the detection of free PSA and HER2 from blood is outlined.

This project focuses on the development of a centrifugal microfluidic-based multi-step immunoassay for the simultaneous detection of up to three prostate cancer biomarkers from whole blood. The final aim is the automation of all assay fluid handling steps, from pre-conditioning of sample to addition of the peroxidase substrate, in this cost-efficient device, suitable for point-of-care applications. The novelty of this platform relies on the ability of multiplexing using a combination of sandwich and competitive immunoassays in a single disc, using recombinant antibodies. Additionally, the flexibility of this disc cartridge design will also allow other ELISA assays to be applied on the same disc, once a suitable panel of prostate cancer biomarkers was validated.

## **4.3 RESULTS**

### **4.3.1 Reduction of assay incubation times**

Fast turn-around times are essential for point-of-care applications. Most conventional ELISA assays use one-hour incubation times for each antibody-antigen recognition step, despite that in an ideal situation the binding occurs within minutes. In order to reduce the total assay time, three different incubation times (5, 10 and 20 minutes) were tested for the antigen binding to the primary antibody and the antigen capture by the secondary antibody incubation times (Section 2.2.8.4). To simulate the lab-on-a-disc conditions (continuous liquid movement in the incubation chamber), the ELISA plate was gently shaken in a rocker during the incubation steps. This allows complete mixing of the reactants and faster interaction kinetics. From the results (Figure 4.6), it was postulated that 10 minutes was the minimum time

required to allow a strong dose-response signal with a good differentiation between the sample results and the negative controls. The same incubation times were applied to the competitive ELISA to allow the parallel running of both assays in the same disc.

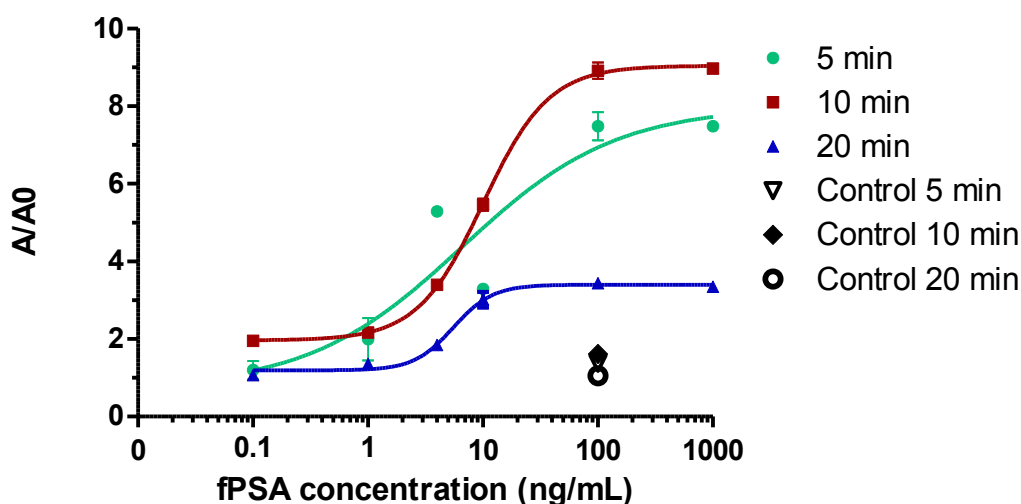


**Figure 4.6.** Optimisation of sandwich ELISA incubation times for the detection of fPSA. Three different incubation times (5, 10 and 20 minutes) for each incubation step (antigen binding to primary and secondary antibody) were tested. The results were normalised by dividing the absorbance values (A) by the absorbance of the blank (A0).

### 4.3.2 Protein immobilisation on the incubation chamber

The microfluidic discs were manufactured using multi-laminae (Figure 2.2) xurography (rapid prototyping techniques) as described by Bartholomeusz *et al.* (2005). Different materials such as silicon, glass or plastic substrates such as PMMA [Poly(methyl methacrylate)], polystyrene (PS) and COC (cyclic olefin copolymer) have been traditionally used for the immobilization of proteins in microfluidic systems (Kim and Herr, 2013). Typically, PMMA is chosen due to the low cost of fabrication (Dimov *et al.*, 2014; Kinahan *et al.*, 2014). Thus, the initial disc design (used for optimization of the fluid handling protocol) was composed of four layers of poly-methyl methacrylate (PMMA) along with four layers of pressure sensitive adhesive (Adhesives Research, Limerick, Ireland), as seen in Figure 2.1. However, PMMA inert

surface proved to be not suitable for protein immobilization in initial microfluidic assay experiments. To prepare the disc base surface for immobilisation of proteins, three different strategies were investigated (Figure 4.7): oxygen plasma treatment, polystyrene coating and surface raster. Oxygen plasma treatment aims to activate PMMA surface, introducing polar groups, improve PMMA surface wettability with changing surface chemistry and topography (Vesel *et al.*, 2012), and facilitate protein immobilisation (via amine groups) by the introduction of aldehyde groups (Zhao *et al.*, 2016). Polystyrene coating intended to simulate the hydrophobic conditions found in the ELISA plates, made of this material. Finally, it was postulated that etching a raster pattern on the wells surface would increase the protein binding area. Immobilisation experiments were performed on the wells of microfluidic chips consisting of the same layers as the microfluidic disc (simulating disc conditions), with the aim of simplifying the device fabrication process during the optimisation testing. Coating with polystyrene resulted in a significant signal increase, as well as in a much higher signal-to-noise ratio (Figure 4.7). This was an expected result, given that polystyrene coating simulated the conditions found in ELISA plates (also made of polystyrene), in which the assays were optimised. To avoid the source of protein immobilisation variability associated to an uneven polystyrene coating within disc manufacturing batches, the bases of the microfluidic discs used for the generation of the dose-response curves were made of polystyrene.

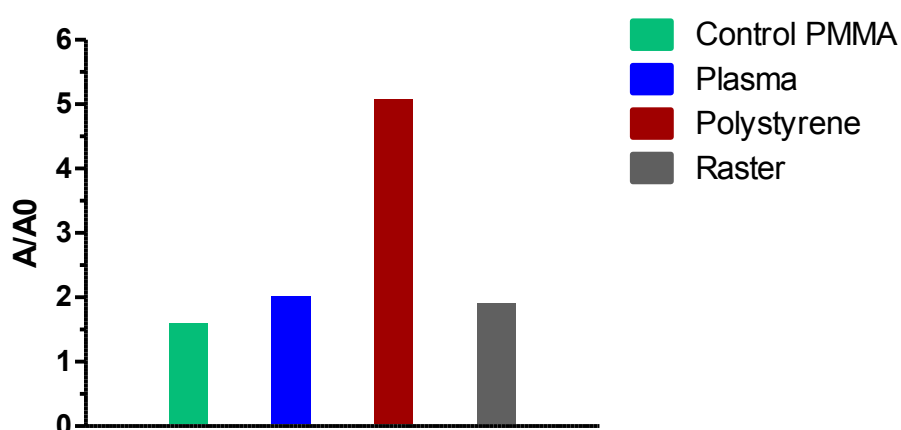


**Figure 4.7.** Functionalisation of disc PMMA surface. Three techniques were used: oxygen plasma treatment, polystyrene-coating and surface raster. Sandwich assay was performed as usual, using 10 ng/mL of PSA and blank wells (0 ng/mL PSA). The results were normalised by dividing the absorbance values (A) by the absorbance of the blank (A0).

### 4.3.3 Liquid handling protocol

Once the disc is loaded with all the reagents and mounted on the centrifugal testing set up (Figure 2.2), the spindle is rotated at a defined frequency curve (Table 4.1). Plasma separation from blood occurs at occurs at 20 Hz over typically 8 minutes, as previously described in other LoaD systems (Haeberle *et al.*, 2006; Nwankire *et al.*, 2014). Thereafter the frequency is increased to 25 Hz to open the DF1 (Figure 4.5) and aliquot the plasma into chambers A1, A2 and A3 (Figure 4.5). The DF valves used in these chambers take 40 seconds to dissolve, providing sufficient time for plasma metering in chambers A1–A3 and overflow of the remaining plasma into waste.

Once the plasma is released into the incubation chamber, 'shake-mode' mixing (Lutz *et al.*, 2008) is induced by rapidly alternating the spin rate between 15 Hz and 30 Hz. After plasma incubation, the incubation chamber is emptied by siphon priming (Siegrist *et al.*, 2010) upon reduction of the spin rate and then lifting to 25 Hz. The mixing and emptying protocols are applied between each step until the TMB substrate is released (Table 4.1) to allow incubation and washing steps, discarding the liquid after each step into the waste chamber (Figure 4.5). After the third wash, bound HRP-labelled antibodies are detected by the release of TMB substrate into the incubation chamber. The TMB is incubated for 10 minutes while applying the 'shake-mode' mixing and finally the reaction is stopped by the addition of acid.

**Table 4.1.** Spin frequency protocol for each laboratory unit operation (LUO) in the Load ELISA.  
\* Steps 5–10 absent in competitive ELISA. (Taken from Mishra *et al.*, 2016).

Step #	Description	Frequency (Hz)	Time (s)
1	Plasma separation	20	480
2	DF1 valve release (plasma aliquoting and release)	25	40
3	Plasma incubation	15–30 (shake mode mixing)	600
4	Incubation chamber empties to waste	Siphon primes at 5Hz, empties at 25Hz	15
5*	Buffer wash 1 release	38	10
6*	Buffer1 washing	15–30 (shake mode mixing)	30
7*	Incubation chamber empties to waste	Siphon primes at 5, empties at 25	15
8*	Primary antibody release	43	10
9*	Primary antibody incubation	15–30 (shake mode mixing)	600
10*	Incubation chamber empties to waste	Siphon primes at 5, empties at 25	15
11	Buffer wash 2 release	48	10
12	Buffer2 washing	15–30 (shake mode mixing)	30
13	Incubation chamber empties to waste	Siphon primes at 5, empties at 25	15
14	Secondary antibody release	53	10
15	Secondary antibody incubation	15–30 (shake mode mixing)	600
16	Incubation chamber empties to waste	Siphon primes at 5, empties at 25	15
17	Buffer wash 3 release	57	10
18	Buffer3 washing	15–30 (shake mode mixing)	30
19	Incubation chamber empties to waste	Siphon primes at 5, empties at 25	15
20	TMB (enzyme substrate) release	62	10
21	TMB incubation	15–30 (shake mode mixing)	600
22	Acid release (stops enzymatic activity)	68	10
23	Termination	15–30 (shake mode mixing)	10
	<b>Total time</b>		<b>3180</b>

TMB–Tetramethyl benzidine; Buffer 1/2/3–1 % (w/v) Marvel semi-skimmed milk in 10 mM PBS.

#### 4.3.4 Detection of prostate cancer markers: Benchtop vs. Lab-on-a-disc

The ability of the sandwich and competitive assay to detect the fPSA and HER2 biomarkers was demonstrated using a standard benchtop ELISA (see Section 2.2.6.4) for competitive ELISA; the sandwich ELISA was developed by Dr. Sarah Gilgunn (Gilgunn 2016) with 100  $\mu$ L reagent volumes (in standard 96 well plates with a 6.35 mm well bottom diameter), one-hour incubation times for the primary and secondary antibodies and six washes (3 times with 0.5 % (v/v) Tween 20 in PBS and 3 times with PBS) after each incubation step.

For point-of-care deployment, the reduction of the assay times and reagent volumes without compromising sensitivity of detection is important. The assay was therefore adapted for incorporation into the microfluidic disc with significant reduction of reagent volumes (to 40  $\mu\text{L}$ ), incubation times (down to 10 min) and washing steps (to only one wash with 1% [w/v] Marvel semi-skimmed milk in PBS after each incubation step).

The biomarker standards (0.1–1000 ng/mL of fPSA and 10–1000 ng/mL of HER2) spiked in PBS buffer and a blank sample were measured in triplicate and the ability of the generated scFv antibodies to detect their target antigens under such adapted conditions were assessed on a half-area 96-well ELISA plate (4.5 mm well bottom diameter, Corning), as described in Sections 2.2.8.3. and 2.2.8.4. The results (Figure 4.8) provide clear evidence for characteristic dose-response curves after the optimisation process.

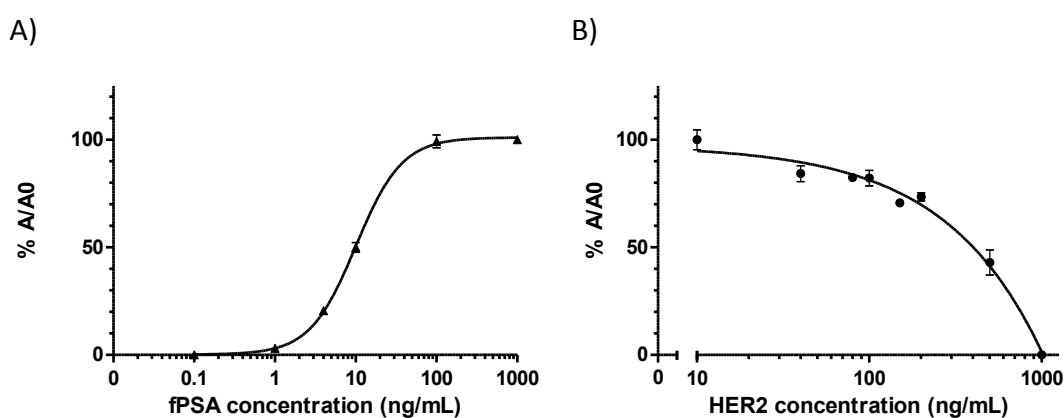


**Figure 4.8.** fPSA and HER2 calibration curves using conventional ELISA. A) Calibration curve for the detection of fPSA using conventional sandwich ELISA. fPSA standards (0.1–1,000 ng/mL) were captured on a goat anti-PSA polyclonal antibody-coated immunoplate. Anti-fPSA scFv B8 was then added and detected following the addition of HRP-labelled anti-HA antibody. B) Calibration curve for the detection of HER2 using conventional competitive ELISA. A 1:1 mixture of HER2 standards (10–1,000 ng/mL) with anti-HER2 scFv A4JZ was added to the HER2-coated wells and bound antibodies were detected using HRP-labelled anti-hemagglutinin (HA) antibody. The results were normalised by dividing the absorbance values (A) by the absorbance of the blank (A0), and expressed as a percentage (% A/A0), where 0% and a 100% are defined as the smallest and biggest value in each data set, respectively. Error bars indicate standard deviation from at least three measurements.

The results from the LoAD measurements, performed as described in Section 2.2.8.5, for the two markers are shown in Figure 4.9. The signal-to-noise ratio ( $A/A_0$ ) was calculated using absorbance values detected on the same disc for the controls ( $A_0$ ) and plotted as a percentage of relative absorbance (%  $A/A_0$ ).

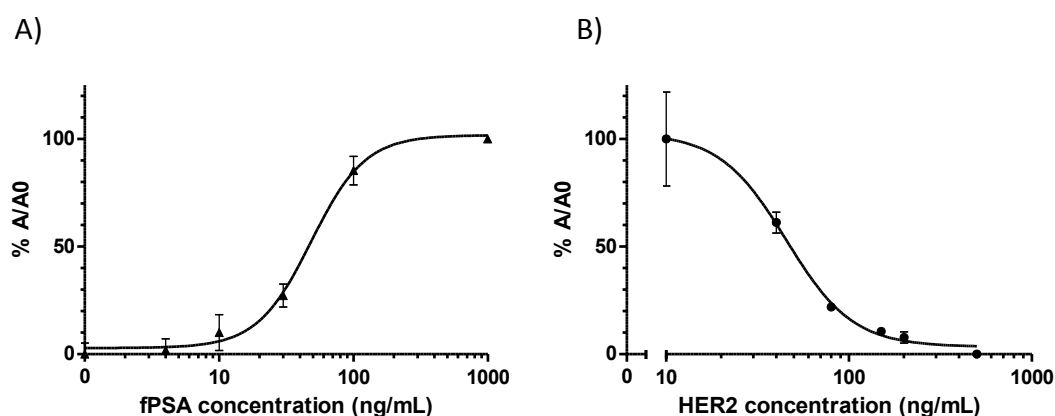


**Figure 4.9.** fPSA and HER2 calibration curves using LoAD platform. Percentage of relative absorbance results for LoAD immunoassays to detect A) fPSA marker in buffer (1–1000 ng/mL) and B) HER2 marker in buffer (10–500 ng/mL). The results were normalised by dividing the absorbance values ( $A$ ) by the absorbance of the blank ( $A_0$ ), and expressed as a percentage (%  $A/A_0$ ), where 0 % and a 100 % are defined as the smallest and biggest value in each data set, respectively. Error bars indicate standard deviation from at least three measurements.

For the sandwich ELISA for fPSA detection, the dose-response curve is similar to that obtained in the benchtop experiment, but the sensitivity of the assay was reduced. The competitive ELISA for the detection of HER2 from buffer also exhibits a characteristic inverse dose-response curve, but with greater variations from the benchtop version than the sandwich assay.

### 4.3.3 Interference studies for the parallel running of competitive and sandwich ELISA on a microfluidic disc

The final aim of this project is to parallel run the sandwich assay for PSA detection and the competitive assay for HER2 detection in the same disc. To do this, the blood sample would have to be pre-incubated with anti-HER2 scFv antibodies (Figure 4.5) to allow the formation of HER2-scFv complexes prior to aliquoting of the serum to the incubation chamber for the competitive assay. Since the same blood sample would be used for the detection of PSA, it is crucial to prove that the anti-HER2 scFv do not interfere with the sandwich assay. In order to check any potential interference, anti-HER2 scFv (1:10,000 dilution, as per the competitive ELISA) was spiked in the PSA standards (0, 10 and 100 ng/mL) and a sandwich ELISA for PSA detection was performed, as described in Section 2.2.8.4, running a positive control (buffer with PSA only) in parallel. No significant interference was observed when anti-HER2 scFv were present in the fPSA standard solutions (Figure 4.10), which suggests that the addition of this antibody to the blood sample would not result in unwanted cross-reactivity or interference with the detection of fPSA.

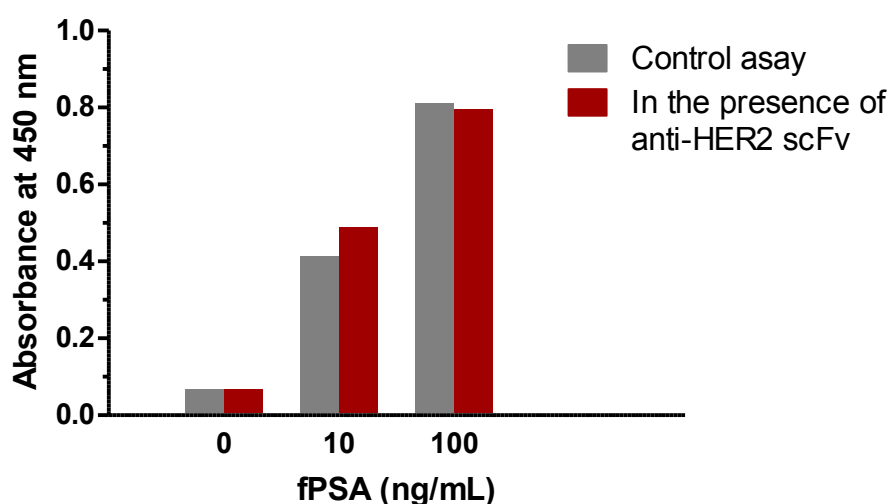


**Figure 4.10.** Investigation of interference of anti-HER2 scFv in the serum sample with PSA detection. fPSA standards (0, 10 and 100 ng/mL) were spiked with anti-HER2 scFv and added to the ELISA plate coated with anti-PSA polyclonal antibody. Control PSA standards (no anti-HER2 scFv) were added in parallel. Bound fPSA was detected following the addition of the primary and secondary antibodies and the response for each spiked sample (red) was compared with the response of the control samples (grey).

#### 4.4. DISCUSSION

Recent advances in microfluidic technology and device fabrication have led to new diagnostic platforms with the potential to be implemented in low-resource laboratory settings (Hugo *et al.*, 2014; Jing *et al.*, 2014; Sharma *et al.*, 2015). On-disc miniaturisation and integration of common laboratory unit operations (LUOs) in easy-to-use low-cost cartridges allows sample analysis outside of traditional labs.

This work underpins the ability of a novel recombinant antibody-based microfluidic 'lab-on-a-disc' device to automate a multi-step ELISA, using a single spindle rotor to implement plasma separation and fluid control. The system also permits multiplexing, suggesting potential for the simultaneous detection of multiple biomarkers of clinical value in disease detection. In this project, the use of generated scFv antibodies for prostate cancer biomarkers detection from whole blood using a 'lab-on-a-disc' platform was investigated. The inherent advantages of utilising 'in-house' produced antibodies (low-cost, easy production and high specificity and sensitivity), in conjunction with those associated with the developed microfluidic platform (cheap to manufacture, easily modifiable and low sample-size requirements), give an ideal combination for point-of-care applications. The actuation of the DF-valves for sequential reagent release was shown, in agreement with theoretical predictions, revealing the feasibility of microfluidic actuation by simple changes on the disc spinning speed. A variety of DF valving systems has already been developed by the Ducrée group in the School of Physical Sciences in DCU. Gorkin *et al.* (2012) described a centrifugal-pneumatic valving technology in which the burst frequency of the DF tabs could be tuned over a wide range of rotational speeds, having potential for the integration of multi-step biochemical assay protocols. However, a major limitation of this system was the dependence of the valve actuation of DF tabs dissolution time and transfer time of the liquid, leaving insufficient time for the long mixing or incubation steps required for more complex immunoassays. To solve this, they presented a new system in which paper imbibition was used to increase the scope of temporal process control (Kilahan *et al.*, 2012). Kinahan *et al.* (2014) also described a centrifugal DF-based 'lab-on-a-disc' in

which liquid handling sequence for RNA extraction from mammalian cell homogenate was controlled through event-triggered mechanisms, independent of the disc rotational frequency. However, the research described in this chapter is the first time in which the integration of a complex sandwich ELISA (with four incubation steps and three washing steps) in the DF-based LoAD platform was achieved. The slight error in experimental values, mainly associated with smaller pneumatic chambers, can be attributed to issues with manufacturing tolerances. The implementation of sequential LUOs, such as liquid transport and metering, as well as plasma separation and fluid mixing in the disc cartridge is demonstrated, allowing the integration of all the steps required for immunoassays in a single disc. Other CD-based multiplexed assays have been reported by a number of academic groups (Lee *et al.*, 2009; Chen *et al.*, 2010; Park *et al.*, 2012; Czugała *et al.*, 2013; Nwankire *et al.*, 2014; Lee *et al.*, 2015), but many of them differ from the system described here in that they are based on methods other than immunoassay. For example, Nwankire *et al.* (2014) developed a 5-parameter liver assay panel (albumin, alkaline phosphatase, gamma glutamyl transferase, total and direct bilirubin) from a finger-prick blood sample (Nwankire *et al.*, 2014). The test, which took about 20 minutes to run, utilized enzyme-based and dye-binding assays, such as Jendrassik and Grof's bilirubin test (Jendrassik *et al.*, 1938) or the Bromocresol Green albumin assay (Doumas *et al.*, 2009), respectively. On the other hand, most of the systems integrating immunoassay protocols relied on external actuators other than the spindle rotor, such as lasers, for the actuation of microvalves (Lee *et al.*, 2009, Park *et al.*, 2012; Lee *et al.* 2015).

Following the demonstration of controlled sequential reagent release in the disc, a sandwich assay for PSA detection and a competitive assay for HER2 detection were optimised for implementation in the LoAD platform. This led to a reduced number of washing steps (from 9 in the conventional ELISA to 3 on-disc), smaller reagent volumes (from 100  $\mu$ L to 40  $\mu$ L) and shorter incubation times (from 60 minutes each to just 10 minutes). The on-disc assays resulted in a slightly lower sensitivity and higher inter-assay variability, when compared with the conventional assays on immunoplates. These variations between the conventional ELISA and the LoAD

assays can be attributed to various factors. A major aspect is the surface-binding capacity of the polystyrene disc surface, compared with that of commercial ELISA plates used for the benchtop assays, which are manufactured from special medical-grade polystyrene for uniform binding and low background absorption. Also, the top vents that seal the incubation chamber are not made of polystyrene due to manufacturing issues, reducing the surface area available for protein coating. Factors such as reagent losses in the channels and valves can lead to variance in the recorded signals. This is especially evident in the competitive ELISA, which is more sensitive to changes in antibody concentration. This method is based on the formation of HER2-scFv complexes that are washed away, while only free antibodies are able to react with the coated antigen. Thus, scFv losses in the microfluidic structure may result in a reduction of free scFv antibodies and therefore a reduction in the absorbance signal, as seen in Figure 4.9B.

Recombinant antibodies produced by the Applied Biochemistry Group in DCU have recently started to be exploited for centrifugal microfluidics-based analytical platforms, leading to a commercial collaboration with Biosurfit SpinIt® startup, and to the development of promising toxin detection systems, such as the Atlanta platform for algal microcystin detection (Maguire *et al.*, 2015; Maguire *et al.*, 2016). The Biosurfit SpinIt® diagnostic solution is a clear example of how microfluidic technology is capable of delivering multi-parameter blood analysis information in minutes. From a finger-prick blood sample, and with no need for sample preparation or extra reagents, the SpinIt® microfluidic discs can provide real-time and accurate results for *in-vitro* diagnostic testing. Currently, there are two commercially-available SpinIt® discs: the CRP test, a quantitative immunoassay for the measurement of C-reactive protein (CRP); and the BC (blood cell counting) test, for the quantitative measurement of total leucocytes, 5-part differential white blood cells and haematocrit. Immunoassays are performed in the SpinIt® analyser (with an integrated spin rotor) using Surface Plasmon Resonance (SPR) detection, while cytology is possible thanks to an integrated microscopy module and standard haematological dyes. Multi-analyte panels, such as the SpinIt® lipid panel, are currently under development (Biosurfit | Solution website). Samsung LABGEO IB10

(Samsung healthcare) and Gyrolab Explore (Gyros) are also commercial centrifugal microfluidic devices for immunoassay applications. The Samsung platform has overcome the difficulties associated with multiplexing, and it allows the testing of up to three analytes in a single run, as in the CD described in this chapter. For example, Samsung's Cardiac 3-in-1 Panel Test measures the amount of Troponin I (cTnI), CK-MB and Myoglobin in human whole blood (500- $\mu$ L sample), providing results in only 20 minutes (Samsung LABGEO IB10 | Samsung Business website). Gyros technology is able to process up to 112 data points per CD run within one hour. Each Gyrolab<sup>TM</sup> Bioaffy CD contains 112 channels with a 15-nL volume affinity column each, in which reagents bind to streptavidin-coated particles. Then, a laser-induced fluorescence detector records fluorescence on each column. The main drawbacks associated with this device are the requirements for a delicate robotic liquid handler system for liquid transfer from a microtiter plate to the CD and the inability to perform plasma separation (Gyrolab Xplore website).

Overall, a proof of concept diagnostic platform that possesses the ability to perform multiplexed assays from whole blood in a total time of less than one hour was demonstrated. Compared with similar commercially available microfluidic systems, our disc demonstrated similar features: lack of need for sample pretreatment (on-disc plasma separation), multiplexing ability (up to three tests per disc), minimal sample and reagents volume requirements (185  $\mu$ L of blood and 40  $\mu$ L of each reagent per test) and automated fluid handling. Significant optimisation and further testing will, however, be required prior to biomarker measurement from blood. In order to increase the analytical sensitivity and reproducibility, the disc base surface could be chemically modified to introduce functional groups for efficient protein immobilization (Bai *et al.*, 2006; Henares *et al.*, 2008; Wen *et al.*, 2009\*). Another approach would be the use of microbeads for antibody (or antigen, in the case of the competitive ELISA) immobilisation (Lee *et al.*, 2006; Lacharme *et al.*, 2009; Park *et al.*, 2012; Glynn *et al.*, 2013). For example, Park *et al.* (2012) used polystyrene beads modified with antibodies for the detection of high sensitive C-reactive protein (hsCRP), cardiac troponin I (cTnI), and N-terminal pro-B type natriuretic peptide (NT-proBNP) by a sandwich ELISA-based LoaD. This system was able to detect the panel

of three cardiovascular disease (CVD) biomarkers with a LOD < 1 ng/mL in 20 minutes. A drawback of this system is the requirement of three types of HRP-labelled detection antibodies (anti-hsCRP, anti-cTnl and anti- NT-proBNP), in contrast to ours, which only requires a universal anti-HA for both assays, as a result of the use of recombinant capture antibodies containing a HA tag. Moreover, Cho's group employed laser irradiated ferrowax microvalves (LIFM) for sequential fluid control, requiring an external laser for the melting and opening of the valves, while our DF-tabs are fully rotationally-controlled. In addition to this, our system is more flexible, in that it allows the incorporation of different assay formats (sandwich and competitive) in the same disc, and requires smaller sample and reagent volumes.

In summary, the benefits of the described LoAD device include the automation of sequential steps, reducing pipetting steps, as well as the reduction of conventional assay times, reagent volumes and number of washes. All immunoassay steps for the detection of fPSA and HER2 markers are performed on the LoAD, by simple variations in the rotational speed. This kind of microfluidic low-cost device holds great promise for revolutionising the way in which diagnostics tests are delivered, allowing fast, multi-marker ELISA-based disease detection.

## **Chapter 5**

# **Development of a Single-Chain Antibody-Based Magneto-Immunosensor for the Detection of Free PSA**

## 5.1 INTRODUCTION

In recent years, magnetic particles (MPs) have been being applied to various fields, including cell separation (Bai *et al.*, 2014; Plouffe *et al.*, 2014), immunoassays (Ranzoni *et al.*, 2012; Wang *et al.*, 2014), drug targeting and delivery (Mody *et al.*, 2013, Mou *et al.*, 2015), and magnetic resonance imaging (Zhu *et al.*, 2014; Estelrich *et al.*, 2015). Advances on synthesis and characterisation of magnetic nanoparticles have allowed the development of a wide range of commercial magnetic biomaterials attractive for clinical applications, such as those produced by BioMag<sup>®</sup>, Dynabeads<sup>®</sup>, Adembeads<sup>®</sup> and SiMAG<sup>®</sup>

Among MPs, superparamagnetic particles, which can be magnetised under an external magnetic field and demagnetise when removed from the magnet, are especially attractive (Ramanujan, 2009). They precipitate under a magnetic field, enabling efficient separation from the sample, yet lose the attraction for each other when the magnetic field is removed, allowing complete resuspension. This is especially useful when the paramagnetic particles are conjugated to antibodies, allowing the separation and concentration of proteins (or microorganisms) from the sample.

### 5.1.1 The history of Dynabeads

In 1976, the Norwegian professor John Ugelstad discovered a process to manufacture monodisperse, uniformly sized spherical polystyrene beads (currently known as Dynabeads). Previously, this had only been achievable by NASA in the weightless conditions of space. The method involves a two-step swelling process: first, a water-insoluble, low-molecular weight compound is introduced in polystyrene seed particles in water, and then, a slightly soluble compound diffuses through water and is absorbed into these particles, which can absorb more than 100 times their own volume (Ugelstad *et al.*, 1979). Soon after this discovery, another breakthrough followed, when these beads were made paramagnetic by mixing

porous beads with oxidative groups with  $\text{Fe}^{2+}$  salt solutions to form magnetic oxides for immunomagnetic cell separation (Nustad *et al.*, 1982; Ugestad *et al.*, 1988).

A wide range of magnetic Dynabeads of various sizes and surface functionalities has since been developed for different purposes, from cell, protein or nucleic acid isolation to assay development, and are commercially available from the Invitrogen corporation.

### **5.1.2 Dynabeads for immunoassay**

For assay development, Dynabeads can be coupled with a ligand (such as an antibody or a DNA/RNA probe) with an affinity for the desired target. When added to the sample, the pre-coupled beads bind to the target biomolecule, which can then be easily separated from the rest of the sample by the use of a magnet to immobilise the beads and their trapped analyte, while the unbound material is removed by aspiration. The ligand can be coupled directly onto tosyl-activated Dynabeads or indirectly onto streptavidin-coated Dynabeads, though biotinylation (He *et al.*, 2004).

Magnetic particles provide several advantages for the development of immunoassays. They allow efficient and reproducible ligand immobilisation and increase the surface area for the immunological reaction, as they are spherical in shape. They facilitate fast assay kinetics because the beads are in suspension. In addition efficient washing and minimising of matrix effects due to the magnetic separation of the target is possible. Their use also shortens assay development time, while increasing sensitivity (Centi *et al.*, 2008; Bruls *et al.*, 2009; Castilho *et al.*, 2011).

The incorporation of MPs in ELISA was shown to be beneficial in multiple studies. Zhang and co-workers evaluated a chemiluminescence enzyme immunoassay based on magnetic microparticles (MPs-CLEIA) to detect serum  $\alpha$ -fetoprotein (AFP) in parallel with traditional colorimetric ELISA. They found that the MPs-CLEIA was

advantageous over the ELISA in terms of the need for less reagent volumes, reduced assay time and wider linear ranges (Zhang *et al.*, 2012). Another study reported the application of a competitive colorimetric immunoassay for the detection of aflatoxin B1 (AFB). They used AFB-BSA-modified MPs as a detection probe and anti-AFB antibody-coated gold nanoparticles as a signal probe. The assay was able to detect AFB from maize sample extract in a timesaving and cost-effective manner, within the low nanogram per liter range (Wang *et al.*, 2014). Other researchers investigated the use of MPs in biosensors. Bruls *et al.* (2009) developed an optomagnetic immunosensor that enables high-sensitive one-step multiplex assays for the detection of drugs of abuse (morphine, amphetamine, methamphetamine, tetrahydro-cannabinol, and cocaine) from saliva, in a disposable cartridge. The detection of sub-nanogram per milliliter concentrations of drugs was achieved in a total assay time of one minute (Bruls *et al.*, 2009). In addition, electrochemical-based magneto-immunosensing for highly sensitive detection of microorganisms, such as *Plasmodium falciparum* (related to malaria) or *Salmonella* has also been reported (Castilho *et al.*, 2011; Liébana *et al.*, 2009).

## 5.2 AIMS OF THIS CHAPTER

PSA exists in serum in at least two forms: uncomplexed/free (fPSA) and complexed to  $\alpha$ 1-anti-chymotrypsin (PSA-ACT) or  $\alpha$ 2-macroglobulin (PSA-A2M). As discussed in Section 1.4, despite wide use, total PSA test (that measures the sum of fPSA and PSA-ACT [PSA-A2M is not detectable by conventional immunoassays, as the PSA is encapsulated by the A2M]) lacks specificity for prostate cancer (Zhang *et al.*, 1998; Wang *et al.*, 1999). Free forms of PSA are less abundant in prostate cancer patients, compared with those with BHP. In current clinical practice, the free PSA (fPSA) to total PSA ratio (% fPSA) is used to avoid unnecessary biopsies. In men with total PSA levels between 4 and 10 ng/mL, a cut-off of <25 % of fPSA is used for biopsy recommendations (Catalona *et al.*, 1998).

In this project, a magneto-immunosensor for the detection of fPSA using 'in-house' generated scAb antibodies was developed. Superparamagnetic Dynabeads M-280

Tosylactivated (Life Technologies) were conjugated with anti-fPSA scAbs for fPSA capture before optical or electrochemical detection. The final aim was to develop an assay that can be run in the Gwent Group Handi-Lab instrument, for point-of-care chronoamperometric measurements of fPSA from clinical samples (Figure 5.1).

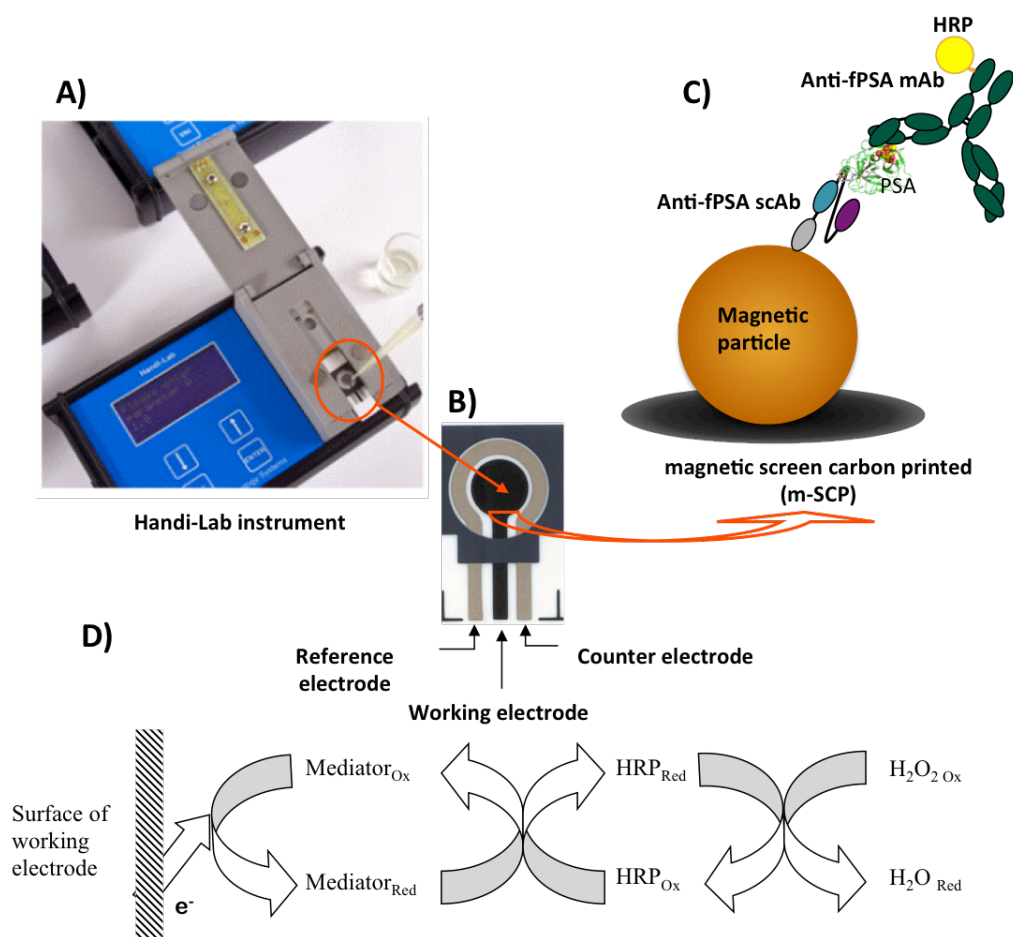


**Figure 5.1.** Selected strategy for the detection of free PSA: A) Handi-Lab instrument (Gwent Group); B) Screen-printed electrode (Gwent Electronic Materials. Ltd.); C) Assay format for the electrochemical detection of fPSA; D) Electron transfer at the electrode/solution interface. Adapted from Liébana *et al.* (2014\*).

## 5.3 RESULTS

### 5.3.1 ScAb E1 conjugation to paramagnetic particles

Dynabeads M-280 Tosylactivated are paramagnetic polystyrene beads (4.5- $\mu\text{m}$  diameter) possessing a hydrophobic surface with p-toluene-sulfonyl (Tosyl) groups to allow covalent binding by primary amine (-NH<sub>2</sub>) or sulphhydryl (-SH) groups.

According to manufacturer instructions, 1 mg of beads can be coupled to 5-20  $\mu\text{g}$  of antibody.

The single-chain antibody fragments were covalently coupled to the tosyl-activated MPs by amine bonds (Section 2.2.9.1). In order to determine the amount of scAb immobilised on the MPs, an antibody titre in the post-conjugation supernatant (Section 2.2.9.2) was carried out. The amount of scAb present in the supernatant after immobilisation was calculated using a calibration curve obtained with known concentrations of the scAb, and compared with the scAb concentration before the conjugation step. The coupling efficiency was found to be greater than 94 %.

### ***5.3.2 Optimisation of assay conditions by magneto-ELISA***

In this procedure, the scAb-conjugated MPs were first incubated with the fPSA solution in the immunoplate wells for 40 minutes. After fPSA capture, immunomagnetic separation of fPSA was performed, following detection by an HRP-labelled anti-PSA secondary antibody. TMB peroxidase substrate was then added and resulting absorbance was read at 450 nm.

The concentration of anti-PSA scAb E1 was optimised using three different antibody concentrations (0.25, 0.5 and 1 mg/mL in 10 mM PBS, pH 7.4) for bioconjugation with MPs. A magneto-ELISA (Section 2.2.9.3) was performed using the MPs conjugated with different antibody concentrations and varying concentrations of fPSA (0.1–20 ng/mL), along with a blank sample. From the dose-response curves (Figure 5.2A), 1 mg/mL of scAb was selected as optimal antibody concentration for coating of MPs.

Similarly, optimal concentration of bioconjugated MPs for magneto-immunoassay was evaluated by incubating fPSA standards with 0.1 mg/mL or 0.2 mg/mL of antibody-MPs conjugate per well (Figure 5.2B). The amount of magnetic particles added to the ELISA wells was shown to have an influence in the dose-response

curve, and a slightly higher response was obtained using 0.2 mg/mL of MPs. However, to reduce the cost of the test, saving expensive antibodies and MPs, 0.1 mg/mL was selected for further experimental work.

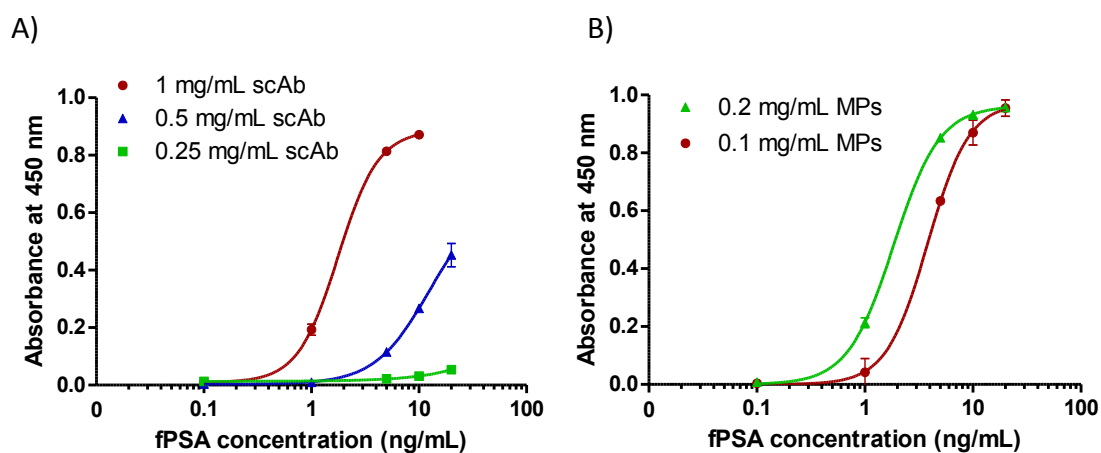


**Figure 5.2.** Optimisation of assay conditions by magneto-ELISA. A) Optimisation of scAb concentration (0.25, 0.5 and 1 mg/mL) for bioconjugation to magnetic beads. B) Optimisation of bioconjugated magnetic beads (MPs) concentration (0.1 or 0.2 mg/mL per well) for magneto-ELISA. The absorbance was read at 450 nm. The error bars represent the mean +/- the standard deviation (n=3).

The magneto-ELISA standard curve for fPSA was performed in PBS buffer (Section 2.2.9.3) on three independent days (n=9) in a three-month period. Figure 5.3A shows the sigmoidal dose-response obtained for the concentrations ranging from 0.1 to 100 ng/mL ( $R^2=0.9936$ ). The signal corresponding to the LOD was estimated by processing the negative control samples and performing three different single inter-day assays, obtaining a mean value of 0.053 AU with a standard deviation of 0.008 AU. The signal corresponding to the LOD value was then extracted with a one-tailed t-test at a 99 % confidence level, giving a value of 0.076 AU (shown in Figure 5.3B as the dashed horizontal line). This method to calculate the detection limit is based on Glaser *et al.* (1981) approach and can be described as “the minimum concentration of a substance that can be identified, measured and reported with 99 % confidence that the analyte concentration is greater than zero”. The limit of detection was found to be 0.3 ng/mL with a dynamic range up to 5 ng/mL of fPSA ( $R^2=0.9961$ ). Coefficients of variability were found to range from 3.5 to 8 %.

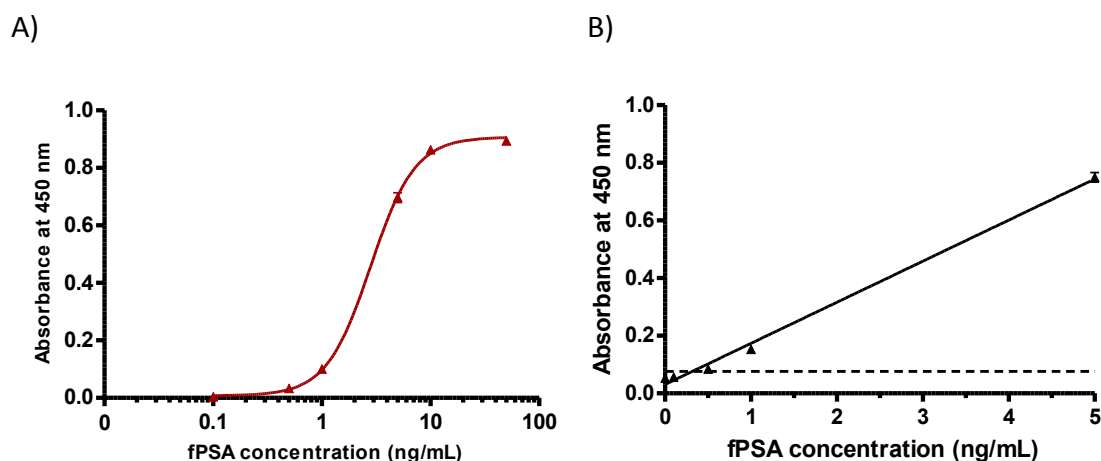


**Figure 5.3.** Magneto-ELISA immunosensing of fPSA. A) Magneto-ELISA standard curve was established using the optimised conditions whilst combining the results from three different days (n=9). B) Magneto-ELISA linear range and limit of detection (represented by dashed line).

### 5.3.3 Development of an amperometric magneto-immunoassay

Following optimisation of assay conditions, electrochemical magneto-immunosensing was performed in order to increase the assay sensitivity and reduce the turn-around time. The amperometric detection of fPSA was performed as illustrated in Figure 5.1, but using an Uniscan Instrument Potentiostat, instead of the Handi-Lab instrument.

#### 5.3.3.1 Cyclic voltammetry

The characterisation of the magnetic screen carbon printed (m-SCP) by cyclic voltammetry (CV) (Bard *et al.*, 1980) was performed by Dr. Susana Liébana (Figure 5.4), using a three-electrode cell composed of a carbon working electrode, and Ag/AgCl reference and counter electrodes (Figure 5.1B). The amperometric detection was based on the action of the HRP enzyme (conjugated to the secondary antibody), by using hydroquinone as a mediator and  $H_2O_2$  as the peroxidase substrate, as previously reported (Ahammad, 2013). A working potential of -0.15 V

vs. Ag/AgCl reference electrode was chosen according to the cyclic voltammogram, shown in Figure 5.4.

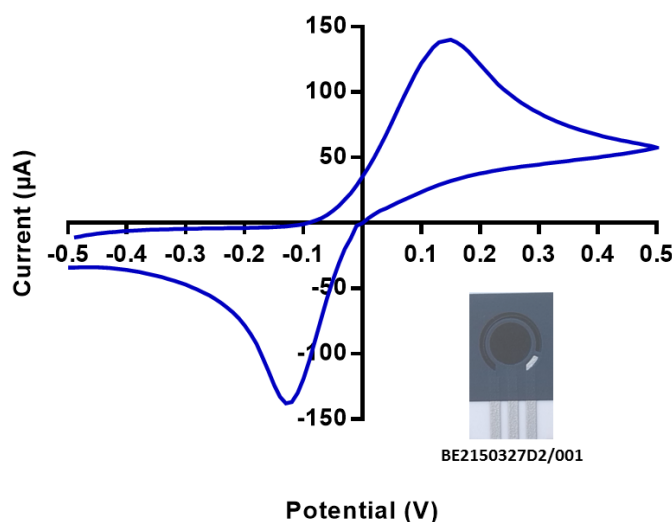


**Figure 5.4.** Cyclic voltammogram derived using a 6-mm working electrode carbon screen-printed electrode. A volume of 100 µL of phosphate buffer with 2 mM/L hydroquinone was used. The scan rate was 10 mV/s.

### 5.3.3.2 Selection of optimal bioconjugated magnetic particles concentration for immunosensor

The concentration of MPs is a critical step for the development of the electrochemical magneto-immunosensor. Low concentrations of MPs may affect the sensitivity of the test, while high deposition of MPs in the screen-printed electrode may compromise electrode transfer. Optimal bioconjugated MPs concentration was determined by incubating the MPs with 5 and 10 ng/mL of fPSA (prepared in 10 mM PBS, pH 7.4), at two different concentrations (0.2 and 0.1 mg/mL per electrode) for the amperometric immunoassay (Section 2.2.9.3). As shown in the Figure 5.5, a MP concentration of 0.2 mg/mL per electrode resulted in a higher signal-to-background ratio ( $\mu\text{A}/\mu\text{A}_0$ , where  $\mu\text{A}$  is the amperometric response for each fPSA value and  $\mu\text{A}_0$  is the amperometric signal of the blank), but 0.1 mg/mL was also able to discriminate between the different fPSA concentrations, so this was selected to allow low-cost testing.

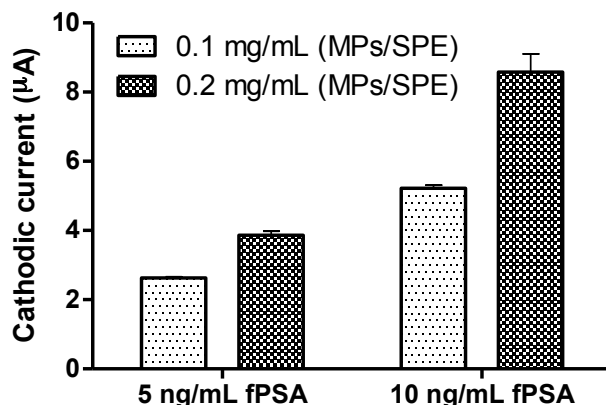


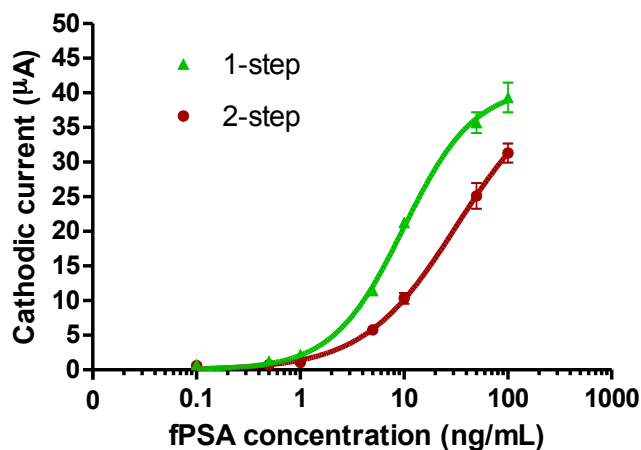
**Figure 5.5.** Amperometric response obtained for 0.1 and 0.2 mg/mL of bioconjugated MPs on the SPE using two different fPSA concentrations (5 and 10 ng/mL). For amperometric measurements, hydroquinone was used as the mediator with H<sub>2</sub>O<sub>2</sub> as the substrate. The potential applied was -0.15V over 30 seconds, with 2 minutes delay. MP–magnetic beads; SPE–screen-printed electrode.

### 5.3.3.3 Amperometric measurements for free PSA detection

Free PSA measurements (0.1-100 ng/mL) were made in 10 mM PBS buffer (Section 2.2.9.4). In order to reduce the assay time, two methodologies were tested:

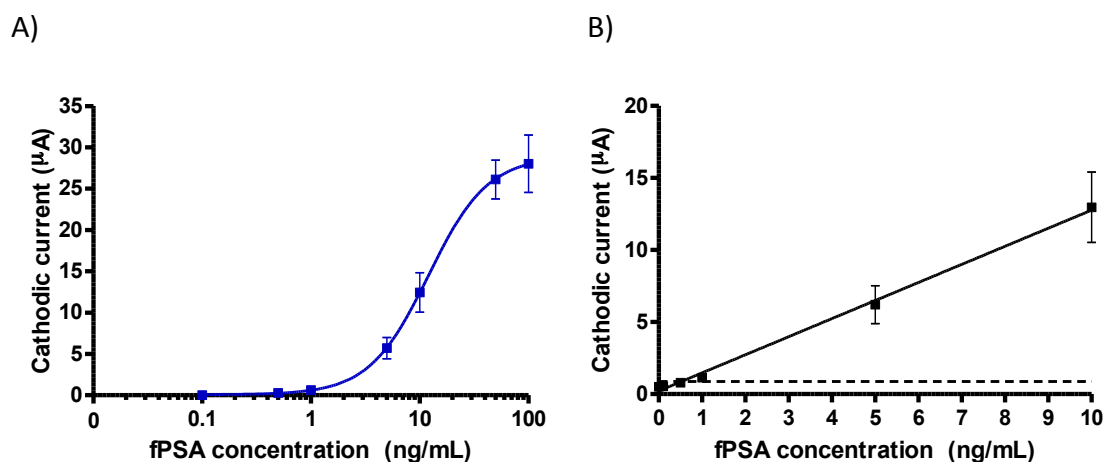
- A ‘two-step’ protocol, consisting of: a) immunomagnetic separation (IMS) of fPSA from the sample using anti-fPSA scAb-MPs conjugates; b) immunorecognition of captured fPSA with an HRP-labelled anti-PSA antibody; and c) amperometric detection based on magnetic screen-printed-electrodes (Figure 2.5); and
- A ‘one-step’ protocol, in which the fPSA and HRP-labelled anti-fPSA antibody were incubated prior to addition of the scAb-conjugated MPs. The ‘one-step’ protocol eliminates one incubation and washing step, reducing the time of assay by approximately one hour.

Figure 5.6 shows that the ‘one-step’ protocol resulted in an improved sensitivity, when compared with the ‘two-step’ assay. Thus, the ‘one-step’ protocol was selected for further studies. These results suggest that the primary and secondary antibody bind to different epitopes in the PSA molecule, as the binding of the HRP-labelled anti-PSA Ab to PSA (epitope 5, as indicated by manufacturer) does not interfere with the PSA capture by the scAb-conjugated MPs.



**Figure 5.6.** Amperometric response obtained using a one-step protocol versus the two-step protocol. A fPSA range from 0.1 to 100 ng/mL was tested. Hydroquinone was used as the mediator and  $\text{H}_2\text{O}_2$  as the substrate. Potential applied was -0.15 V for 30 seconds, with a 2 minute delay.

The standard curve for fPSA detection by the magneto-immunosensor (Section 2.2.9.4) was performed in PBS buffer on three days ( $n=9$ ) in a three-month period. Figure 5.7A shows the sigmoidal dose-response obtained for the concentrations ranging from 0.1 to 100 ng/mL ( $R^2=0.8353$ ). The signal corresponding to the LOD was estimated by processing the negative control samples and performing three different single inter-day assays, using screen-printed electrodes from three different batches, obtaining a mean value of 0.51  $\mu\text{A}$  with a standard deviation of 0.13  $\mu\text{A}$ . The signal corresponding to the LOD value was then extracted with a one-tailed t test at a 99 % confidence level, giving a value of 0.88  $\mu\text{A}$ , (shown in Figure 5.7B as the dashed horizontal line). The limit of detection was found to be 0.5 ng/mL with a dynamic range up to 10 ng/mL of fPSA ( $R^2=0.9979$ ). Coefficients of variability were found to range from 8 to 12%.



**Figure 5.7.** Amperometric magneto-immunosensor standard curve (A) with a linear range from 0 to 10 ng/mL fPSA (B). Hydroquinone was used as the mediator with  $\text{H}_2\text{O}_2$  as the substrate. Potential applied was  $-0.15$  V for 30 seconds, with a 2 minute delay.

### 5.3.4 Interference studies

Potential interferants were evaluated by spiking a PSA standard (50 ng/mL) with 5.5 g/dL human serum albumin (HuSA), 150 ng/mL human kallikrein 2 (hk2) or 50 ng/mL  $\alpha$ 1-antichymotrypsin (ACT)-complexed PSA (cPSA) and checking for interference on the PSA-scAb interaction. The amperometric response for each spiked sample was determined (Section 2.2.9.4) and compared with the response of the PSA-only standard (control). No apparent interference was observed (Figure 5.8).

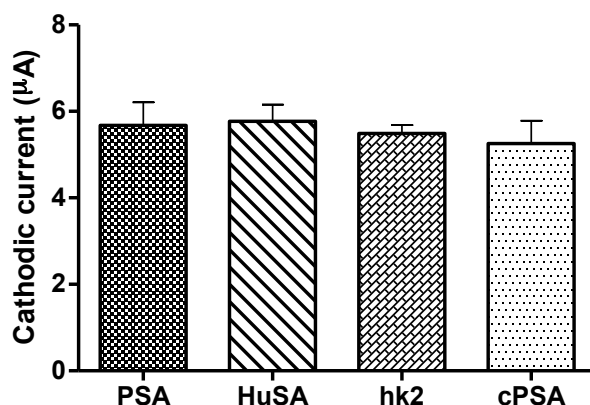


**Figure 5.8.** Interference analysis. Amperometric response obtained for a PSA standard (50 ng/mL) spiked in triplicate with 5.5 g/dL of human serum albumin (HuSA), 140 ng/mL human kallikrein 2 (hk2) or 50 ng/mL of complex PSA (cPSA). Hydroquinone was used as the mediator with  $\text{H}_2\text{O}_2$  as the substrate. The potential applied was  $-0.15$  V for 30 seconds, with a 2 minute delay.

## 5.4 Discussion

The utility of using PSA isoforms for increasing the likelihood of prostate cancer detection was investigated in a recent population screening study, which analysed the free and total PSA levels in a total of 1,277 men aged between 55 and 69 years with total PSA levels of 2-10 ng/mL (Kitagawa *et al.*, 2014). In this study, the probabilities of prostate cancer at three years were 64.5, 41.2, 28.5, and 14.3 % for the men with free/total PSA ratio  $\leq 0.08$ , 0.09–0.13, 0.14–0.22, and  $\geq 0.23$ , respectively. Significant lower free/total ratios were found in patients with unfavorable cancerous features in prostate biopsy. From these results, it was concluded that fPSA measurements are useful for prostate cancer diagnosis and prognosis.

Current and novel analytical technologies used for PSA detection have been recently reviewed (Healy *et al.*, 2007; Sharma *et al.*, 2016), showing the need for development of novel biosensor detection strategies. Most of the methods developed for PSA detection are immunoassay based with different detection approaches. The versatility of antibodies is well demonstrated in a range of clinical applications, ranging from those used as recognition elements in diagnostic assays and bio-sensing devices to therapeutic antibodies and targeted drug delivering systems (Siddiqui *et al.*, 2010). Antibody engineering techniques allowed the production of large amounts of high-quality antibodies in a cost- and time-efficient manner. In order to improve the performance of the traditional immunoassay format, many researchers exploited the possibility of performing the immunoreaction on the surface of magnetic micro and nanoparticles (Mani *et al.*, 2011; Ranzoni *et al.*, 2012; Sharif *et al.*, 2013). Magnetic particles (MPs) have been widely used as a universal separation tool for the separation of biological compounds, such as cells, proteins or DNA, from a sample fluid. The advantages of utilising MPs for immunoassay, along with a number of magneto-immunoassay examples were previously discussed in Section 5.1.2. The use of MPs has proven to be particularly beneficial when combined with electrochemical approaches, as non-specific protein adsorption onto the electrode surface is avoided, thus enhancing

assay sensitivity (Zani *et al.*, 2011; Li *et al.*, 2012; Liébana *et al.*, 2014; Carinelli *et al.*, 2015). In particular, benefits are obtained when screen-printing microfabrication technology is used (Liébana *et al.*, 2016). This technology is nowadays well established for the production of thick-film electrochemical transducers and allows the mass production of reproducible yet inexpensive and mechanically robust strip solid electrodes (Escamilla-Gómez *et al.*, 2009).

The aim of this chapter was to assess the potential of employing an amperometric magneto-immunosensor, based on screen-printed electrodes (SPE) and 'in-house' generated recombinant antibodies, for fPSA detection. The work described here is part of a PROSENSE secondment's collaborative project with Dr. Susana Liébana, from the Gwent Group Ltd.

Initially, scAb antibodies were conjugated to tosyl-activated paramagnetic particles by amine bonds. Antibody-conjugated Dynabeads were used for immunomagnetic separation of free PSA, prior to antigen recognition by a Horseradish peroxidase (HRP)-labelled secondary antibody in a sandwich ELISA format. Immunomagnetic separation is a widely used technique for the capture and separation of pathogenic organisms from body fluids (Intorasoot *et al.*, 2016; Agga *et al.*, 2016), food (Lim *et al.*, 2016; Hohweyer *et al.*, 2016) or environmental matrices (Richard *et al.*, 2016; Brugnera *et al.*, 2016), but also for the purification and enrichment of proteins from complex serum samples (Yao *et al.*, 2008; Neubert *et al.*, 2013; Capangpangan *et al.*, 2014). This last application is especially useful when sandwich assays are used for the capture and/or enrichment of proteins in serum (Sarkar *et al.*, 2008; Osmekhina *et al.*, 2010; Tennico *et al.*, 2010), as they allow highly specific separation and detection of the protein of interest (because two different antibodies are used). The current sandwich assay was optimised by testing the effect of different scAb concentrations (0.25, 0.5 and 1 mg/mL) for bioconjugation to the MPs, and the effect of two scAb-MP conjugate concentrations (0.1 and 0.2 mg/mL) for fPSA immunomagnetic separation, by magneto ELISA (m-ELISA). The optimisation steps were carried out by m-ELISA because this method enables high-throughput simultaneous processing of multiple samples. Use of higher concentrations (>0.5 mg/mL) of scAb

for bioconjugation lead to significantly higher absorbance m-ELISA signals and, therefore, 1 mg/mL of antibody concentration (equivalent to 20 µg of antibody per mg of MPs) was selected as optimal for bioconjugation. The resulting magneto-immunoassay showed a limit of detection of 0.3 ng/mL with a dynamic range up to 5 ng/mL of fPSA. Once the assay conditions were fully characterized by m-ELISA, the development of the electrochemical readout for the implementation of the amperometric magneto immunosensor was addressed. The electrochemical behavior of the screen-printed electrodes was evaluated by Dr. Liébana through the hydroquinone/benzoquinone (HQ/BQ) redox couple. Cyclic voltammetry was used for electrode characterisation. For the electrochemical measurements, an amperometric method was selected, in which a constant potential (-0.15 V) was applied to the working electrode and the current was measured as a function of time (Section 1.6.2.1). The initial amperometric assay format had two incubation steps (one for fPSA binding to the MPs and the other for fPSA recognition by the secondary antibody) of 40 minutes each, with a washing step in between. As a result, the total assay time was more than 90 minutes. In order to further reduce the assay time to make the biosensor suitable for on-site testing, a 'one-step' protocol was implemented, which allowed to eliminate one incubation and washing step, thus reducing the assay time to less than an hour. The limit of detection for the amperometric magneto-immunoassay using the 'one-step' protocol was found to be 0.5 ng/mL with a dynamic range up to 10 ng/mL of fPSA. Although a similar MP-based electrochemical immunoassay for fPSA detection has been previously reported (Sarkar *et al.*, 2008), this new design not only overcomes linearity limitations present in the previous system (with a linear range of 0–1 ng/mL), but also drastically reduces the assay time (from more than 12h to less than 1h). In addition to this, the platform was tested for a number of potential interferants (human serum albumin, human kallikrein 2 and ACT-complexed PSA) and little or no interference was found.

Some high-throughput devices manufactured by big pharmaceutical companies (Siemens, Abbot, Roche) are able to detect fPSA at lower concentrations than the described platform, at levels as low as 0.008 ng/mL (Sharma *et al.*, 2016). However,

they rely on expensive analysers and there is a requirement for centralised laboratories for performance of tests. The magneto-immunosensing strategy described in this chapter could be easily incorporated in the portable Handi-Lab instrument (Gwent Group Ltd.), allowing low-cost on-site testing in medical practitioners' surgeries. Future work will entail the evaluation of the analytical performance of this platform using prostate cancer serum samples to support its clinical utility.

# **Chapter 6**

## **Overall Conclusions**

## 6.1 OVERALL CONCLUSIONS

The research presented in this thesis describes the development and application of recombinant antibody fragments (scFv and scAb) for the detection of prostate cancer biomarkers (fPSA and HER2).

Chapter 3 focuses on generation and characterisation of scFv antibodies to HER2. Firstly, RNA was extracted from avian immune donor spleen and cDNA was synthesised by reverse transcription. This cDNA was used as a template for the amplification of the antibody variable heavy and variable light chains, which were then bound together for the formation of the scFv product. Phage display screening allowed the selection of antibodies against HER2, as confirmed by polyclonal phage ELISA. Individual HER2-specific clones were identified by soluble monoclonal ELISA, and clone A4 was selected for IMAC purification and further characterisation by SDS-PAGE, Western Blotting and ELISA. The purified antibody was utilised for the development of a competitive ELISA, which was not sufficiently sensitive to detect HER2 in the clinically relevant ranges. In an attempt to improve the assay sensitivity, fluorescence-based detection was investigated, but it did not show any comparative advantage over colorimetric methods. In the second part of this chapter, an electrochemical approach for detection of HER2 at the desired levels (<15 ng/mL) was explored. A scFv antibody was incorporated on a gold nanoparticle-based impedimetric biosensor in collaboration with the Jaypee Institute of Information Technology, India. The resulting biosensor was able to detect HER2 from serum at concentrations as low as 0.01 ng/mL, representing a 45-fold improvement, compared with the colorimetric ELISA and, thus, overcoming sensitivity issues. The dynamic range of the biosensor was from 0.01 to 100 ng/mL for HER2. Since HER2 is overexpressed/amplified in a range of tumours (e.g. breast, prostate and lung cancer), the study of serum concentrations of this biomarker could provide a non-invasive method to elucidate the clinical use of serum HER2 detection in a variety of diseases. The developed antibody and biosensor could potentially provide the means to do this.

The incorporation of the generated anti-HER2 scFv antibody and an anti-fPSA scFv in a 'lab-on-a-disc' device was demonstrated in Chapter 4. In a collaboration with the Physics group in DCU, a novel centrifugal microfluidic CD-like platform was designed for the simultaneous detection of a panel of biomarkers from blood. Sandwich and competitive ELISAs for the detection of fPSA and HER2, respectively, were optimised to allow the incorporation in the microfluidic platform. Washing steps and incubation times were reduced. The disc design was then used, as a proof-of-concept strategy for multi-step immunoassay, to detect HER2 and fPSA. Once the blood sample and reagents were loaded in the CD cartridge, all the assays steps were implemented by the use of a spindle rotor with simple variations in rotational speed. The novelty of this platform relies on its capacity to simultaneously run different assay formats (sandwich and competitive ELISA) for the detection of multiple biomarkers (HER2 and fPSA, with the potential to incorporate a third biomarker on the panel). The easy-to-use, low-cost (discs are made of plastic) and rapid result delivery, characteristic of this platform, has potential for point-of-care diagnosis. Future work will focus on the study of new antibody immobilisation techniques for improved assay reproducibility, and the development of a hand-held rotor incorporating an optical reader to record results.

Chapter 5 described the use of an 'in-house' generated recombinant antibody for measurement of free PSA (fPSA). In this case, scAb antibodies were conjugated to paramagnetic particles for the detection of fPSA by magneto-immunoassay. Immunomagnetic separation was combined with optical (magneto-ELISA) and electrochemical (amperometric) approaches, in collaboration with The Gwent Group Ltd., UK. Following optimisation of assay conditions, a screen-printed electrode (SPE)-based electrochemical magneto-immunosensor was developed. Further optimisation resulted in the reduction of the number of assay steps, while maintaining good analytical performance in which fPSA was detectable at a limit of 0.5 ng/mL (with a dynamic range up to 10 ng/mL) in less than one hour. Furthermore, interference from potential serum interfering proteins was evaluated and little or no effect was found on the testing precision. Due to time constraints and company changes, fPSA detection from serum samples could not be evaluated.

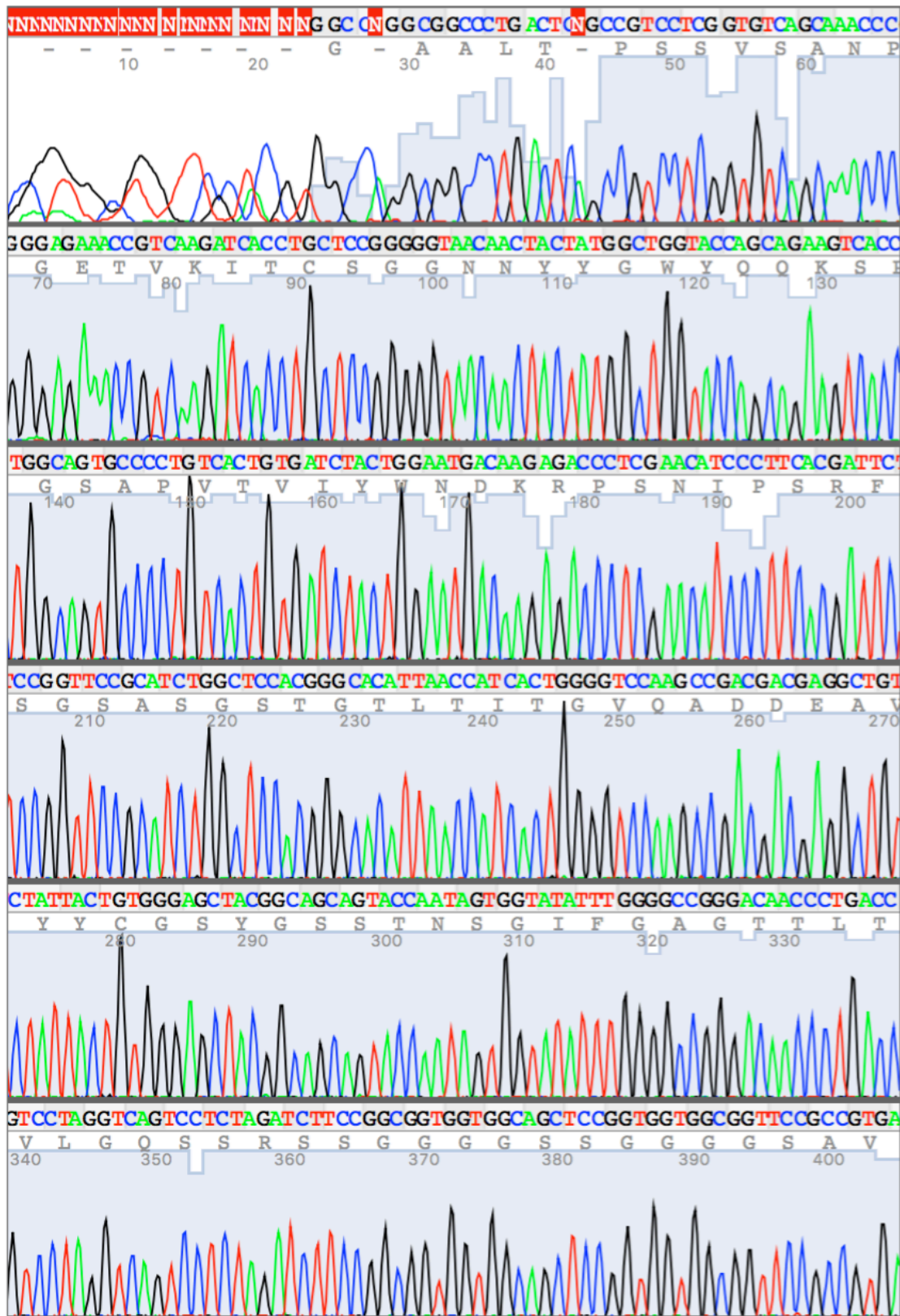
In addition various collaborative projects with other members of the Prosense community are ongoing with reagents developed as part of this Ph.D. The group in Switzerland is investigating the effect of the size of different antibody fragments coated on silicon nanowires, on the memristive signal registered upon ligand binding (Carrara *et al.*, 2012). The Slovak Academy of Sciences is using a scAb antibody for PSA capture prior to glycoprofiling. Because changes in a glycan structure can be indicators not only of disease presence, but also of its stage, glycan analysis may lead to the development of more reliable diagnostic tests (Belicky and Tkac, 2015). Furthermore, INESC and University Lisbon Veterinary School hope to investigate the application of the generated scFv for the detection of HER2 in cats using a microfluidic platform.

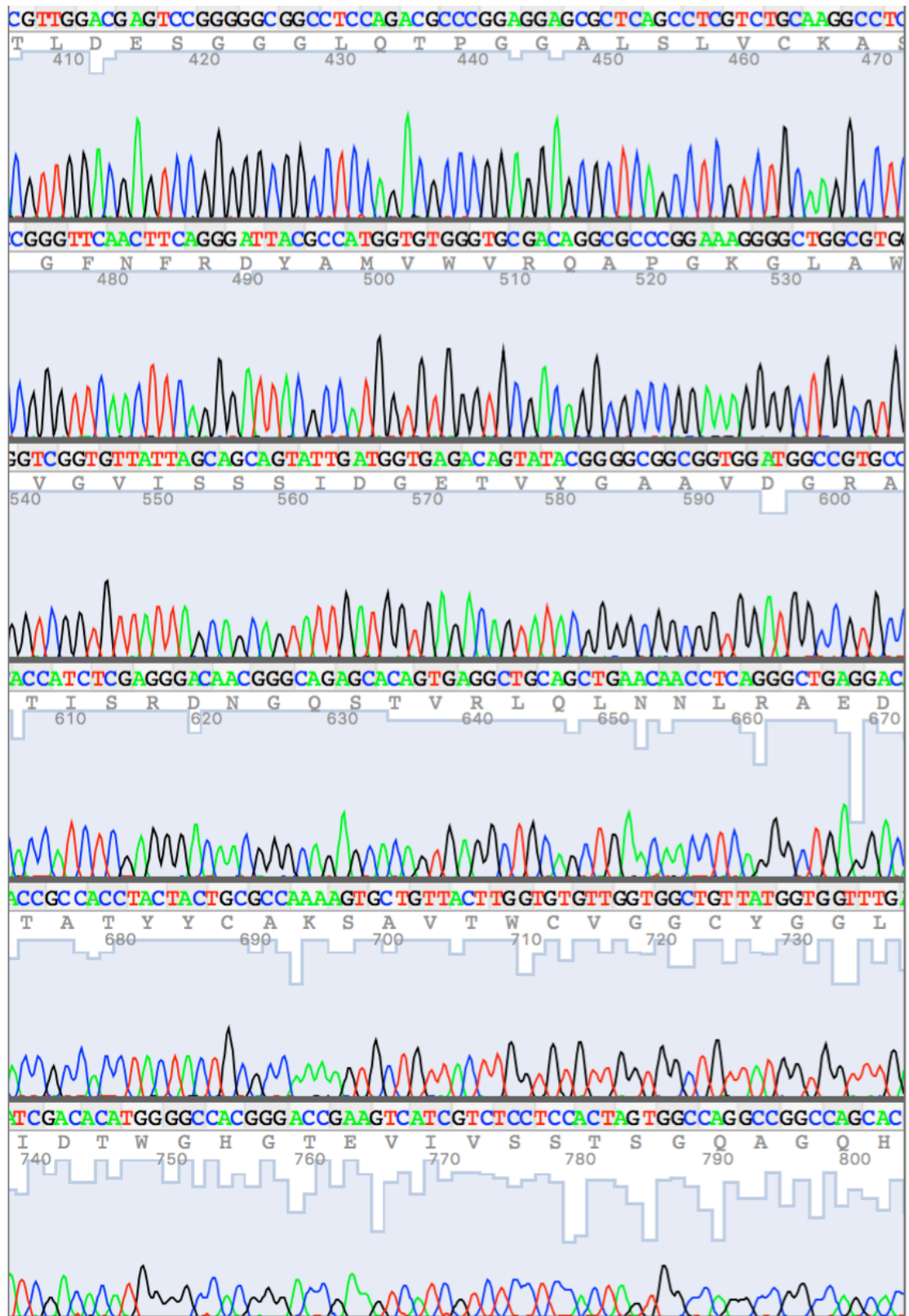
In conclusion, this work describes the production of novel antibody fragments to HER2 (scFv) and PSA (scAb), their use for assay development, and recombinant antibody-based biosensor development. It is expected that the results presented here will be translated into publications that will help to elucidate the utility of HER2 and free PSA, as members of a panel of biomarkers for improved prostate cancer detection.

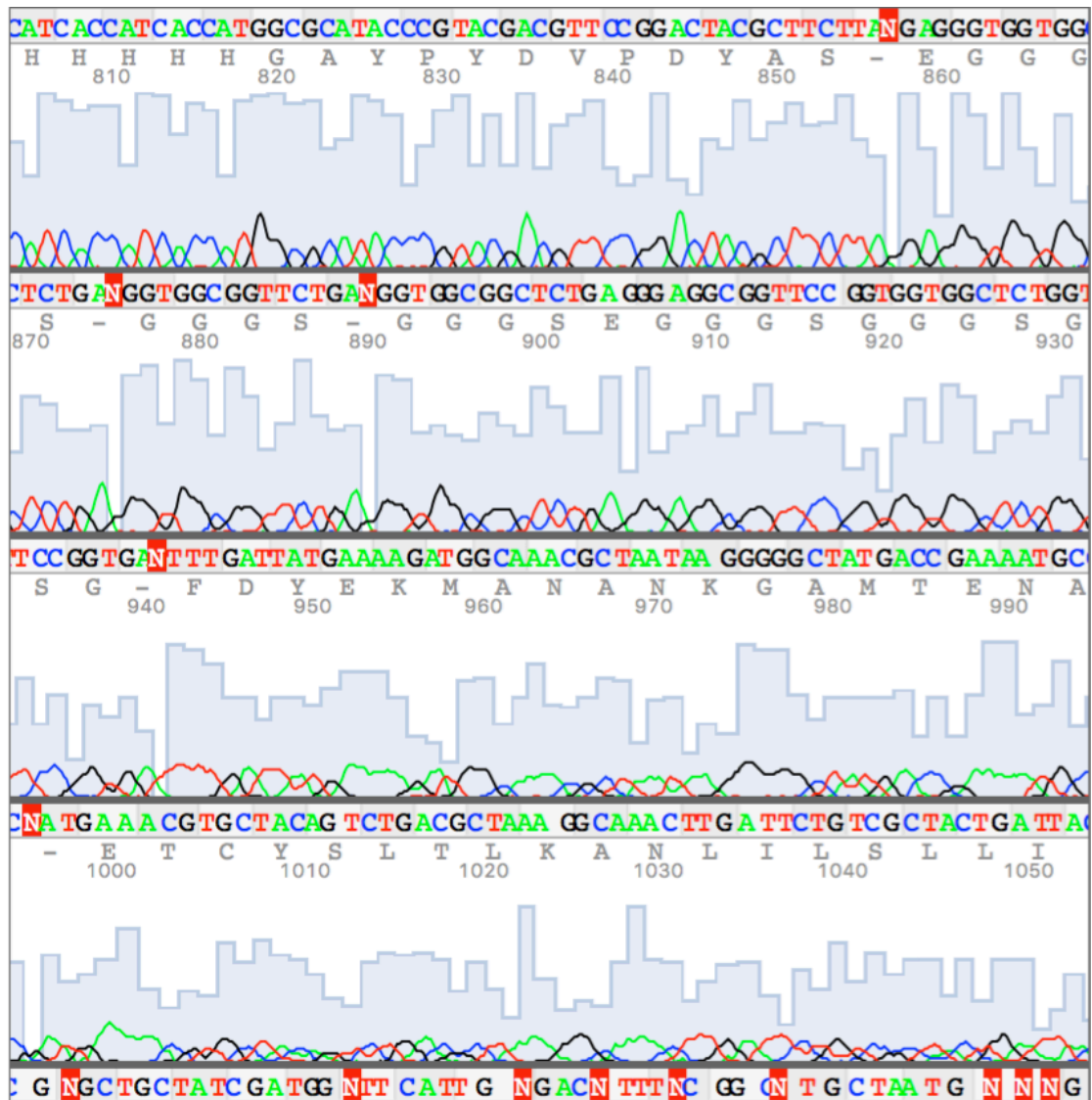
# Appendices

# APPENDIX 1

## Single-chain fragment variable (scFv) antibody A4 sequencing chromatogram:







Clone A4 DNA sequence analysis was performed using ExPASy translation tool and, according to Kabat definition, the following antibody regions were identified:

```

          L1                                L2
AALTQPSSVSANPGETVKITCSGGNNYYGWYQQKSPGSAPVTVIYWNDKRPSNIPSRFSGS
          L3                                Linker
ASGSTGLTITGVQADDEAVYYCGSYGSSTNSGIFGAGTTLTVLQGSSRSSGGGSSGGGSSAV
          H1                                H2
TLDESGGLQTPGGALSLVCKASGFNFRDYAMetVWVRQAPGKGLAWVGVISSIDGETVYGA
          H3
AVDGRATISRDNQSTVRLQLNNLRAEDTATYYCAKSAVTWCVGGCYGGLIDTWGHGTEVIVS
          6X His-tag    HA-tag
STSGQAGQHHHHHGGAYPYDVPDYASX
  
```

# **Bibliography**

Abdelghany, S.M., Quinn, D.J., Ingram, R.J., Gilmore, B.F., Donnelly, R.F., Taggart, C.C. and Scott, C.J. (2012). Gentamicin-loaded nanoparticles show improved antimicrobial effects towards *Pseudomonas aeruginosa* infection. *International Journal of Nanomedicine*, 7, 4053-63.

Abbot Point of Care. *Providing Lab-Quality Results in Minutes: A wide range of cartridges for diagnostic testing at the bedside* [online]. Available from: <https://www.abbottpointofcare.com>.

Agga, G.E., Arthur, T.M., Schmidt, J.W., Wang, R. and Brichta-Harhay, D.M. (2016). Diagnostic Accuracy of Rectoanal Mucosal Swab of Feedlot Cattle for Detection and Enumeration of *Salmonella enterica*. *Journal of Food Protection*, 79(4), 531-537.

Ahammad, A.S. (2013). Hydrogen peroxide biosensors based on horseradish peroxidase and hemoglobin. *Journal of Biosensors and Bioelectronics*, 9, 001.

Al-Khafaji, Q.A.M., Harris, M., Tombelli, S., Laschi, S., Turner, A.P.F., Mascini, M. and Marrazza, G. (2012). An electrochemical immunoassay for HER2 detection. *Electroanalysis*, 24(4), 735-742.

Alberts, B., Johnson, A., Lewis, J., Raff, M., Roberts, K., and Walter, P (2002). The Adaptive Immune System in Alberts B, Johnson A, Lewis J, *et al.* (eds.) *Molecular Biology of the Cell*. 4th ed. New York: Garland Science.

Amersdorfer, P., Wong, C., Smith, T., Chen, S., Deshpande, S., Sheridan, R. and Marks, J.D. (2002). Genetic and immunological comparison of anti-botulinum type A antibodies from immune and non-immune human phage libraries. *Vaccine*, 20(11), 1640-1648.

Amonkar, S.D., Bertenshaw, G.P., Chen, T.H., Bergstrom, K.J., Zhao, J., Seshaiyah, P., Yip, P. and Mansfield, B.C. (2009). Development and preliminary evaluation of a multivariate index assay for ovarian cancer. *PLOS one*, 4(2), e4599.

Arkan, E., Saber, R., Karimi, Z. and Shamsipur, M. (2015). A novel antibody-antigen based impedimetric immunosensor for low level detection of HER2 in serum samples of breast cancer patients via modification of a gold nanoparticles decorated multiwall carbon nanotube-ionic liquid electrode. *Analytica Chimica Acta*, 874, 66-74.

- Arruebo, M., Valladares, M., and González-Fernández, Á. (2009). Antibody-conjugated nanoparticles for biomedical applications. *Journal of Nanomaterials*, 2009 (37), 1-24.
- Arruebo, M., Vilaboa, N., Sáez-Gutierrez, B., Lambea, J., Tres, A., Valladares, M., and González-Fernández, Á. (2011). Assessment of the evolution of cancer treatment therapies. *Cancers*, 3(3), 3279-3330.
- Asav, E. and Sezgintürk, M.K. (2014). A novel impedimetric disposable immunosensor for rapid detection of a potential cancer biomarker. *International Journal of Biological Macromolecules*, 66, 273-280.
- Ayat, H., Burrone, O.R., Sadghizadeh, M., Jahanzad, E., Rastgou, N., Moghadasi, S. and Arbabi, M. (2013). Isolation of scFv antibody fragments against HER2 and CEA tumor antigens from combinatorial antibody libraries derived from cancer patients. *Biologicals*, 41(6), 345-354.
- Bahadır, E.B. and Sezgintürk, M.K. (2016). A review on impedimetric biosensors. *Artificial cells, nanomedicine, and biotechnology*, 44(1), 248-262.
- Bai, L., Du, Y., Peng, J., Liu, Y., Wang, Y., Yang, Y. and Wang, C. (2014). Peptide-based isolation of circulating tumor cells by magnetic nanoparticles. *Journal of Materials Chemistry B*, 2(26), 4080-4088.
- Bai, Y., Koh, C.G., Boreman, M., Juang, Y.J., Tang, I.C., Lee, L.J. and Yang, S.T. (2006). Surface modification for enhancing antibody binding on polymer-based microfluidic device for enzyme-linked immunosorbent assay. *Langmuir*, 22(22), 9458-9467.
- Bailey, C.L., Birch, L. and McDowell, D.G. (2008). PCR: factors affecting reliability and validity in Keer, J.T. and Birch, L. (eds.) *Essentials of Nucleic Acid Analysis: A Robust Approach*. Cambridge, UK: RSC Publishing.
- Barbas, C. F., Burton, D.R., Scott, J. K., and Silverman, G. J. (2001). *Phage display: A Laboratory Manual*. Plainview, N.Y: Cold Spring Harbor Laboratory Press.
- Bard, A.J., Faulkner, L.R., Leddy, J. and Zoski, C.G. (1980). *Electrochemical methods: fundamentals and applications* (Vol. 2). New York: Wiley.
- Bartlett, J.M.S., Starczynski, J., Atkey, N., Kay, E., O'Grady, A., Gandy, M., Ibrahim, M., Jasani, B., Ellis, I.O., Pinder, S.E. and Walker, R.A. (2011). HER2 testing in the UK:

recommendations for breast and gastric *in-situ* hybridisation methods. *Journal of Clinical Pathology*, 64(8), 649-653.

Bartholomeusz, D.A., Boutté, R.W. and Andrade, J.D. (2005). Xurography: rapid prototyping of microstructures using a cutting plotter. *Journal of Microelectromechanical Systems*, 14(6), 1364-1374.

Belicky, S. and Tkac, J. (2015). Can glycoprofiling be helpful in detecting prostate cancer?. *Chemical Papers*, 69(1), 90-111.

Bell, C.W., Fricks, B.E., Rocca, J.D., Steinweg, J.M., McMahon, S.K. and Wallenstein, M.D. (2013). High-throughput fluorometric measurement of potential soil extracellular enzyme activities. *Journal of Visualized Experiments: JoVE*, (81), e50961.

Biella, G., Franceschi, M., De Rino, F., Davin, A., Giacalone, G., Brambilla, P., Bountris, P., Haritou, M., Magnani, G., Boneschi, F.M. and Forloni, G. (2013). Multiplex assessment of a panel of 16 serum molecules for the differential diagnosis of Alzheimer's disease. *American Journal of Neurodegenerative Disease*, 2(1), 40-45.

Biosurfit solution. *Solution SpinIt<sup>®</sup> instrument* [online]. Available at: <http://biosurfit.com>.

Bjartell, A. S., Al-Ahmadie, H., Serio, A. M., Eastham, J. A., Eggener, S. E., Fine, S. W., Udby, L., Gerald, W. L., Vickers, A. J., Lilja, H., Reuter, V. E., and Scardino, P. T. (2007). Association of cysteine-rich secretory protein 3 and  $\beta$ -microseminoprotein with outcome after radical prostatectomy. *Clinical Cancer Research*, 13(14), 4130-4138.

Bohunicky, B., and Mousa, S. A. (2011). Biosensors: the new wave in cancer diagnosis. *Nanotechnology, Science and Applications*, 4, 1-10.

Bornhorst, J.A. and Falke, J.J. (2000). Purification of proteins using polyhistidine affinity tags. *Methods in Enzymology*, 326, 245-254.

Bostwick Laboratories (2011). *New Personalized Genetic Test- Prostavysion™ - Helps Prostate Cancer Patients Make Best Treatment Decisions* [online]. Available from: <https://www.bostwicklaboratories.com>.

Breault-Turcot, J., Poirier-Richard, H.P., Couture, M., Pelechacz, D. and Masson, J.F. (2015). Single chip SPR and fluorescent ELISA assay of prostate specific antigen. *Lab on a Chip*, 15(23), 4433-4440.

Brosel-Oliu, S., Uria, N., Abramova, N. and Bratov, A. (2015). Impedimetric Sensors for Bacteria Detection in Rincken, T. (ed.) *Biosensors-Micro and Nanoscale Applications*. INTECH Open Access Publisher.

Brugnera, M.F., Bundalian, R., Laube, T., Julián, E., Luquin, M., Zanoni, M.V.B. and Pividori, M.I. (2016). Magneto-actuated immunoassay for the detection of *Mycobacterium fortuitum* in hemodialysis water. *Talanta*, 153, 38-44.

Bruls, D.M., Evers, T.H., Kahlman, J.A.H., Van Lankvelt, P.J.W., Ovsyanko, M., Pelssers, E.G.M., Schleipen, J.J.H.B., De Theije, F.K., Verschuren, C.A., Van Der Wijk, T. and Van Zon, J.B.A. (2009). Rapid integrated biosensor for multiplexed immunoassays based on actuated magnetic nanoparticles. *Lab on a Chip*, 9(24), 3504-3510.

Capangpangan, R.Y., dela Rosa, M.A.C., Chang, C.H., Wang, W.C., Peng, J., Shih, S.J., Chiang, M.H., Tzou, D.L., Lin, C.C. and Chen, Y.J. (2014). Selective enrichment and sensitive detection of candidate disease biomarker using a novel surfactant-coated magnetic nanoparticles. In *IOP Conference Series: Materials Science and Engineering* 64(1), 12022-12028. IOP Publishing.

Capoluongo, E., Zambon, C. F., Basso, D., Boccia, S., Rocchetti, S., Leoncini, E., Palumbo, S., Padoan, A., Albino, G., Todaro, A., Payer-Galetti, T., Zattoni, F., Zuppi, C. and Plebani, M. (2014). PCA3 score of 20 could improve prostate cancer detection: results obtained on 734 Italian individuals. *Clinica Chimica Acta*, 429, 46-50.

Carrara, S., Sacchetto, D., Doucey, M.A., Baj-Rossi, C., De Micheli, G. and Leblebici, Y. (2012). Memristive-biosensors: A new detection method by using nanofabricated memristors. *Sensors and Actuators B: Chemical*, 171, 449-457.

Catalona, W.J., Richie, J.P., Ahmann, F.R., Hudson, M.A., Scardino, P.T., Flanigan, R.C., Dekernion, J.B., Ratliff, T.L., Kavoussi, L.R. and Dalkin, B.L. (1994). Comparison of digital rectal examination and serum prostate specific antigen in the early detection of prostate cancer: results of a multicenter clinical trial of 6,630 men. *The Journal of urology*, 151(5), 1283-1290.

Catalona, W.J., Partin, A.W., Slawin, K.M., Brawer, M.K., Flanigan, R.C., Patel, A., Richie, J.P., Walsh, P.C., Scardino, P.T., Lange, P.H. and Subong, E.N. (1998). Use of the percentage of free prostate-specific antigen to enhance differentiation of prostate cancer from benign prostatic disease: a prospective multicenter clinical trial. *JAMA*, 279(19), 1542-1547.

Catalona, W.J., Southwick, P.C., Slawin, K.M., Partin, A.W., Brawer, M.K., Flanigan, R.C., Patel, A., Richie, J.P., Walsh, P.C., Scardino, P.T. and Lange, P.H. (2000). Comparison of percent free PSA, PSA density, and age-specific PSA cutoffs for prostate cancer detection and staging. *Urology*, 56(2), 255-260.

Centi, S., Messina, G., Tombelli, S., Palchetti, I., and Mascini, M. (2008). Different approaches for the detection of thrombin by an electrochemical aptamer-based assay coupled to magnetic beads. *Biosensors and Bioelectronics*, 23(11), 1602-1609.

Chaubey, A. and Malhotra, B.D. (2002). Mediated biosensors. *Biosensors and Bioelectronics*, 17(6), 441-456.

Chandra, S., Barola, N. and Bahadur, D. (2011). Impedimetric biosensor for early detection of cervical cancer. *Chemical Communications*, 47(40), 11258-11260.

Chames, P., Van Regenmortel, M., Weiss, E., and Baty, D. (2009). Therapeutic antibodies: successes, limitations and hopes for the future. *British Journal of Pharmacology*, 157(2), 220-233.

Chassagne, S., Laffly, E., Drouet, E., Hérodin, F., Lefranc, M.P. and Thullier, P. (2004). A high-affinity macaque antibody Fab with human-like framework regions obtained from a small phage display immune library. *Molecular Immunology*, 41(5), 539-546.

Chen, Q.L., Ho, H.P., Cheung, K.L., Kong, S.K., Suen, Y.K., Kwan, Y.W., Li, W.J. and Wong, C.K. (2010). A fluorescence-based centrifugal microfluidic system for parallel detection of multiple allergens. In *Proceedings SPIE 7565, Biophotonics and Immune Responses V*, San Francisco, California (75650F).

Chin, C.D., Linder, V. and Sia, S.K. (2012). Commercialization of microfluidic point-of-care diagnostic devices. *Lab on a Chip*, 12(12), 2118-2134.

Cho, H., Kim, H.Y., Kang, J.Y. and Kim, T.S. (2004). Capillary passive valve in microfluidic system. In *2004 NSTI-Nanotechnology Conference, Boston, Massachusetts* (263-266).

Cho-Chung, Y.S., (2006). Autoantibody biomarkers in the detection of cancer. *Biochimica et Biophysica Acta (BBA)-Molecular Basis of Disease*, 1762(6), 587-591.

Conroy, P. J., Hearty, S., Leonard, P., and O'Kennedy, R. J. (2009). Antibody production, design and use for biosensor-based applications. *Seminars in Cell & Developmental Biology*, 20 (1), 10-26.

Conroy, P.J., Law, R.H., Gilgunn, S., Hearty, S., Caradoc-Davies, T.T., Lloyd, G., O'Kennedy, R.J. and Whisstock, J.C. (2014). Reconciling the structural attributes of avian antibodies. *Journal of Biological Chemistry*, 289(22), 15384-15392.

Corn, P. G., and Thompson, T. C. (2010). Identification of a novel prostate cancer biomarker, caveolin-1: Implications and potential clinical benefit. *Cancer Management and Research*, 2, 111-122.

Cramer, R., and Walter, G (1999). Selective enrichment and high-throughput screening of phage surface-displayed cDNA libraries from complex allergenic systems. *Combinatorial Chemistry & High-Throughput Screening*, 2, 63-72.

Czugala, M., Maher, D., Collins, F., Burger, R., Hopfgartner, F., Yang, Y., Zhaou, J., Ducrée, J., Smeaton, A., Fraser, K.J. and Benito-Lopez, F. (2013). CMAS: fully integrated portable centrifugal microfluidic analysis system for on-site colorimetric analysis. *RSC Advances*, 3(36), 15928-15938.

Daoud, S.A., Darweesh, M.F. and Sharaf, R. M. HER2/neu Immunohistochemical Overexpression in Prostatic Adenocarcinoma in Relation to Tumor Pathological Behavior (2016). *Middle-East Journal of Scientific Research* 24 (2), 459-464.

Darlix, A., Lamy, P.J., Lopez-Crapez, E., Braccini, A.L., Firmin, N., Romieu, G., Thézenas, S. and Jacot, W. (2016). Serum NSE, MMP-9 and HER2 extracellular domain are associated with brain metastases in metastatic breast cancer patients: predictive biomarkers for brain metastases?. *International Journal of Cancer* 139 (10), 2299-2311.

de Bono, J.S., Bellmunt, J., Attard, G., Droz, J.P., Miller, K., Flechon, A., Sternberg, C., Parker, C., Zugmaier, G., Hersberger-Gimenez, V. and Cockey, L. (2007). Open-label phase II study evaluating the efficacy and safety of two doses of pertuzumab in castrate chemotherapy-naive patients with hormone-refractory prostate cancer. *Journal of Clinical Oncology*, 25(3), 257-262.

de Souza Castilho, M., Laube, T., Yamanaka, H., Alegret, S. and Pividori, M.I. (2011). Magneto immunoassays for *Plasmodium falciparum* histidine-rich protein 2 related to malaria based on magnetic nanoparticles. *Analytical Chemistry*, 83(14), 5570-5577.

Dimov, N., Gaughran, J., Mc Auley, D., Boyle, D., Kinahan, D.J. and Ducrée, J. (2014). Centrifugally automated solid-phase purification of RNA. In *2014 IEEE 27th*

*International Conference on Micro Electro Mechanical Systems (MEMS)* (260-263). IEEE.

Domingo-Domenech, J., Fernandez, P. L., Filella, X., Martinez-Fernandez, A., Molina, R., Fernandez, E., Alcaraz, A., Codony, J., Gascon, P., and Mellado, B. (2008). Serum HER2 extracellular domain predicts an aggressive clinical outcome and biological PSA response in hormone-independent prostate cancer patients treated with docetaxel. *Annals of Oncology*, 19(2), 269-275.

Dos Santos, M.B., Aguil, J.P., Prieto-Simón, B., Sporer, C., Teixeira, V. and Samitier, J. (2013). Highly sensitive detection of pathogen *Escherichia coli* O157: H7 by electrochemical impedance spectroscopy. *Biosensors and Bioelectronics*, 45, 174-180.

Doumas, B.T. and Peters, T. (2009). Origins of dye-binding methods for measuring serum albumin. *Clinical Chemistry*, 55(3), 583-584.

Ducrée, J., Haeberle, S., Lutz, S., Pausch, S., Von Stetten, F., and Zengerle, R. (2007). The centrifugal microfluidic Bio-Disk platform. *Journal of Micromechanics and Microengineering*, 17(7), S103.

Dudderidge, T. J., Kelly, J. D., Wollenschlaeger, A., Okoturo, O., Prevost, T., Robson, W., Leung, H. Y., Williams, G. H., and Stoeber, K. (2010). Diagnosis of prostate cancer by detection of minichromosome maintenance 5 protein in urine sediments. *British Journal of Cancer*, 103(5), 701-707.

El Sheikh, S.S., Domin, J., Abel, P., Stamp, G. and Lalani, E.N. (2003). Androgen-independent prostate cancer: potential role of androgen and ErbB receptor signal transduction crosstalk. *Neoplasia*, 5(2), 99-109.

Eletxigerra, U., Martinez-Perdiguero, J., Merino, S., Barderas, R., Torrente-Rodríguez, R.M., Villalonga, R., Pingarrón, J.M. and Campuzano, S. (2015). Amperometric magnetoimmunosensor for ErbB2 breast cancer biomarker determination in human serum, cell lysates and intact breast cancer cells. *Biosensors and Bioelectronics*, 70, 34-41.

Elster, N., Collins, D.M., Toomey, S., Crown, J., Eustace, A.J. and Hennessy, B.T. (2015). HER2-family signalling mechanisms, clinical implications and targeting in breast cancer. *Breast Cancer Research and Treatment*, 149(1), 5-15.

Ertuğrul, H.D. and Uygun, Z.O. (2013). Impedimetric biosensors for label-free and enzymeless detection in Rinken, T. (ed.) *State of the Art in Biosensors-General Aspects*. INTECH Open Access Publisher.

Escamilla-Gómez, V., Hernández-Santos, D., González-García, M.B., Pingarrón-Carrazón, J.M. and Costa-García, A. (2009). Simultaneous detection of free and total prostate specific antigen on a screen-printed electrochemical dual sensor. *Biosensors and Bioelectronics*, 24(8), 2678-2683.

Estelrich, J., Sánchez-Martín, M.J. and Busquets, M.A. (2015). Nanoparticles in magnetic resonance imaging: from simple to dual contrast agents. *International Journal of Nanomedicine*, 10, 1727.

Etzioni, R., Penson, D. F., Legler, J. M., di Tommaso, D., Boer, R., Gann, P. H., and Feuer, E. J. (2002). Overdiagnosis due to prostate-specific antigen screening: lessons from US prostate cancer incidence trends. *Journal of the National Cancer Institute*, 94(13), 981-990.

Even-Desrumeaux, K., Fourquet, P., Secq, V., Baty, D. and Chames, P. (2012). Single-domain antibodies: a versatile and rich source of binders for breast cancer diagnostic approaches. *Molecular BioSystems*, 8(9), 2385-2394.

Ezenwa, E. V., Tijani, K. H., Jeje, E. A., Soriyan, O. O., Ogunjimi, M. A., Ojewola, R. W., Ojewola, O. I. Ajie, and El-Nahas, A. R. (2012). The value of percentage free prostate specific antigen (PSA) in the detection of prostate cancer among patients with intermediate levels of total PSA (4.0–10.0 ng/mL) in Nigeria. *Arab Journal of Urology*, 10(4), 394-400.

Fan, Y., Murphy, T. B., Byrne, J. C., Brennan, L., Fitzpatrick, J. M., and Watson, R. W. G. (2011). Applying random forests to identify biomarker panels in serum 2D-DIGE data for the detection and staging of prostate cancer. *Journal of Proteome Research*, 10(3), 1361-1373.

Ferlay, J., Steliarova-Foucher, E., Lortet-Tieulent, J., Rosso, S., Coebergh, J.W.W., Comber, H., Forman, D. and Bray, F. (2013). Cancer incidence and mortality patterns in Europe: estimates for 40 countries in 2012. *European Journal of Cancer*, 49(6), 1374-1403.

Fichter, C.D., Timme, S., Braun, J.A., Gudernatsch, V., Schöpflin, A., Bogatyreva, L., Geddert, H., Faller, G., Klimstra, D., Tang, L. and Hauschke, D. (2014). EGFR, HER2

and HER3 dimerization patterns guide targeted inhibition in two histotypes of esophageal cancer. *International Journal of Cancer*, 135(7), 1517-1530.

Filip, J., Kasák, P. and Tkac, J., (2015). Graphene as signal amplifier for preparation of ultrasensitive electrochemical biosensors. *Chemical Papers*, 69(1), 112-133.

Fink, M. Y., and Chipuk, J. E. (2013). Survival of HER2-positive breast cancer cells receptor signaling to apoptotic control centers. *Genes & Cancer*, 4(5-6), 187-195.

FluidicMEMS: perspectives on lab-on-a-chip, microfluidic, and biomems technology (2016). *List of microfluidics companies* [online]. Available from: <http://fluidicmems.com>

Gauch, S., Hermann, R., Feuser, P., Oelmüller, U. and Bastian, H. (1998). Isolation of Total RNA Using Silica-Gel Based Membranes. In Karp, A. *et al.* (eds.) *Molecular Tools for Screening Biodiversity*. London: Chapman & Hall.

Ghafar-Zadeh, E. (2015). Wireless integrated biosensors for point-of-care diagnostic applications. *Sensors*, 15(2), 3236-3261.

Gilgunn, S. (2016). Enhanced antibody and glycomics-based approaches for the detection of prostate cancer. PhD thesis. Dublin City University, 2016.

Gilgunn, S., Conroy, P. J., Saldoval, R., Rudd, P. M., & O'Kennedy, R. J. (2013). Aberrant PSA glycosylation—a sweet predictor of prostate cancer. *Nature Reviews Urology*, 10(2), 99-107.

Glaser, J.A., Foerst, D.L., McKee, G.D., Quave, S.A. and Budde, W.L. (1981). Trace analyses for wastewaters. *Environmental Science & Technology*, 15(12), 1426-1435.

Glynn, M., Kirby, D., Chung, D., Kinahan, D.J., Kijanka, G. and Ducreé, J. (2013). Centrifugo-magnetophoretic purification of CD4+ cells from whole blood toward future HIV/AIDS point-of-care applications. *Journal of Laboratory Automation*, 2211068213504759.

Gollamudi, J., Parvani, J.G., Schiemann, W.P. and Vinayak, S. (2016). Neoadjuvant therapy for early-stage breast cancer: the clinical utility of pertuzumab. *Cancer Management and Research*, 8, 21.

Gorkin III, R., Nwankire, C.E., Gaughran, J., Zhang, X., Donohoe, G.G., Rook, M., O'Kennedy, R. and Ducreé, J. (2012). Centrifugo-pneumatic valving utilizing dissolvable films. *Lab on a Chip*, 12(16), 2894-2902.

Grieshaber, D., MacKenzie, R., Voeroes, J. and Reimhult, E. (2008). Electrochemical biosensors-sensor principles and architectures. *Sensors*, 8(3), 1400-1458.

Grönberg, H., Adolfsson, J., Aly, M., Nordström, T., Wiklund, P., Brandberg, Y., Thompson, J., Wiklund, F., Lindberg, J., Clements, M. and Egevad, L. (2015). Prostate cancer screening in men aged 50–69 years (STHLM3): a prospective population-based diagnostic study. *The Lancet Oncology*, 16(16), 1667-1676.

Gyrolab xPlore. *Gyrolab CDs product information sheet* [online]. Available from: <http://www.gyros.com>

Haeberle, S., Brenner, T., Zengerle, R. and Ducleé, J. (2006). Centrifugal extraction of plasma from whole blood on a rotating disk. *Lab on a Chip*, 6(6), 776-781.

Hammers, C. M., and Stanley, J. R. (2014). Antibody phage display: technique and applications. *The Journal of Investigative Dermatology*, 134(2), e17.

Harisinghani, M. G., Barentsz, J., Hahn, P. F., Deserno, W. M., Tabatabaei, S., van de Kaa, C. H., de la Rosette, J., Weissleder, R. (2003). Noninvasive detection of clinically occult lymph-node metastases in prostate cancer. *New England Journal of Medicine*, 348(25), 2491-2499.

Harrison, D.J., Manz, A., Fan, Z., Luedi, H. and Widmer, H.M. (1992). Capillary electrophoresis and sample injection systems integrated on a planar glass chip. *Analytical Chemistry*, 64(17), 1926-1932.

Harvard Prostate Knowledge (2011). *What is the difference between PSA and free PSA?* [online]. Available from: <http://www.harvardprostateknowledge.org>.

Hatta, H., Kapoor, M.P. and Juneja, L.R., 2008. Bioactive components in egg yolk IN Mine, Y. (ed.) *Egg Bioscience and Biotechnology*. New Jersey: John Wiley & Sons Inc.

He, M., Cooley, N., Jackson, A. and Taussig, M.J (2004). Production of human single-chain antibodies by ribosome display IN Lo, B.K. (ed.) *Antibody Engineering: Methods and Protocols*. New Jersey: Humana Press Inc.

Healy, D. A., Hayes, C. J., Leonard, P., McKenna, L., and O’Kennedy, R. (2007). Biosensor developments: application to prostate-specific antigen detection. *Trends in Biotechnology*, 25(3), 125-131.

Heidenreich, A., Bellmunt, J., Bolla, M., Joniau, S., Mason, M., Matveev, V., Mottet, N., Chmid, H-P., van der Kwast, T., Wiegel, T., and Zattoni, F. (2011). EAU guidelines on prostate cancer. Part 1: screening, diagnosis, and treatment of clinically localised disease. *European Urology*, 59(1), 61-71.

Henares, T.G., Mizutani, F. and Hisamoto, H. (2008). Current development in microfluidic immunosensing chip. *Analytica Chimica Acta*, 611(1), 17-30.

Hof, D., Hoeke, M. O., and Raats, J. M. H. (2008). Multiple-antigen immunization of chickens facilitates the generation of recombinant antibodies to autoantigens. *Clinical & Experimental Immunology*, 151(2), 367-377.

Hohweyer, J., Cazeaux, C., Travaillé, E., Languet, E., Dumètre, A., Aubert, D., Terryn, C., Dubey, J.P., Azas, N., Houssin, M. and Loïc, F. (2016). Simultaneous detection of the protozoan parasites *Toxoplasma*, *Cryptosporidium* and *Giardia* in food matrices and their persistence on basil leaves. *Food Microbiology*, 57, 36-44.

Howlader, N., Noone, A.M., Krapcho, M., Garshell, J., Miller, D., Altekruse, S.F., Kosary, C.L., Yu, M., Ruhl, J., Tatalovich, Z., Mariotto, A., Lewis, D.R., Chen, H.S., Feuer, E.J., Cronin, K.A. (2015). *SEER Cancer Statistics Review, 1975-2012*, National Cancer Institute [online]. Bethesda, MD. Available from <http://seer.cancer.gov>.

Hsieh, K., Ferguson, B.S., Eisenstein, M., Plaxco, K.W. and Soh, H.T. (2015). Integrated electrochemical microsystems for genetic detection of pathogens at the point of care. *Accounts of Chemical Research*, 48(4), 911-920.

Hugo, S., Land, K., Madou, M., and Kido, H. (2014). A centrifugal microfluidic platform for point-of-care diagnostic applications. *South African Journal of Science*, 110(1-2), 1-7.

Intorasoot, S., Tharinjaroen, C.S., Phunpae, P., Butr-Indr, B., Anukool, U., Intachai, K., Orrapin, S., Apiratmateekul, N., Arunothong, S., Suthachai, V. and Saengsawang, K. (2016). Novel Potential Diagnostic Test for *Mycobacterium tuberculosis* Complex Using Combined Immunomagnetic Separation (IMS) and PCR-CTPP. *Journal of Applied Microbiology*, 121(2), 528-538.

Irimia, D. (2014). Capillary force vales IN Li, D. (ed.) *Encyclopedia of Microfluidics and Nanofluidics*. New York: Springer US.

Janeway, C. A., Travers, P., Walport, M. J., and Shlomchik, M. J. (2001). The generation of diversity in immunoglobulins in Janeway, C.A., Travers, P., Walport, M.

and Shlomchik, M.J. (eds.) *Immunobiology: the immune system in health and disease*. New York: Garland Science.

Jena, B.K. and Raj, C.R., (2008). Optical sensing of biomedically important polyionic drugs using nano-sized gold particles. *Biosensors and Bioelectronics*, 23(8), 1285-1290.

Jendrassik, L. and Grof, P. (1938). Vereinfachte photometrische methoden zur bestimmung des blutbilirubins. *Biochemische Zeitschrift*, 297(8), 1-9.

Jenrette, E., Pradhan, S.K., Rutherford, G., Flowers, J., Ha, D. and Pradhan, A.K. (2015). Quantum-dot-conjugated graphene oxide as an optical tool for biosensor. *Optics Express*, 23(19), 25017-25027.

Jing, W., Jiang, X., Zhao, W., Liu, S., Cheng, X. and Sui, G. (2014). Microfluidic platform for direct capture and analysis of airborne *Mycobacterium tuberculosis*. *Analytical Chemistry*, 86(12), 5815-5821.

Johari-Ahar, M., Rashidi, M.R., Barar, J., Aghaie, M., Mohammadnejad, D., Ramazani, A., Karami, P., Coukos, G. and Omid, Y. (2015). An ultra-sensitive impedimetric immunosensor for detection of the serum oncomarker CA-125 in ovarian cancer patients. *Nanoscale*, 7(8), 3768-3779.

Johnson, G and We, T.T. (2004). The Kabat database and a bioinformatics example in Lo, B.K (ed.) *Antibody engineering: methods and protocols* (Vol. 248). New Jersey: Humana Press.

Jolly, P., Tamboli, V., Harniman, R.L., Estrela, P., Allender, C.J. and Bowen, J.L. (2016). Aptamer-MIP hybrid receptor for highly sensitive electrochemical detection of prostate specific antigen. *Biosensors and Bioelectronics*, 75, 188-195.

Jomaa, B., de Haan, L.H., Peijnenburg, A.A.C.M., Bovee, T.F., Aarts, J.M. and Rietjens, I.M. (2015). Simple and rapid in vitro assay for detecting human thyroid peroxidase disruption. *Altex*, 32(3), 191-200.

Kai, J., Santiago, N., Puntambekar, A., Lee, S. H., Sehy, D., Schultheis, R., Han, J., Ahn, C. H. (2011). Amplifying Immunoassay Sensitivity with the Optimiser™ Microplate Technology- Repetitive Sample Loading of the Optimiser Microplate allows for Amplification of Assay Sensitivity from Picogram/mL Levels to Femtogram/mL Levels. Application Note. BioTek Instruments, INC., Winooski, Vermont, 05404.

Kaisary, A., V., Ballaro, A. and Piggot, K (2016). Lecture Notes: Urology, 7<sup>th</sup> Ed. Oxford: Wiley-Blackwell.

Karley, D., Gupta, D. and Tiwari, A (2011). Biomarker for cancer: a great promise for future. *World Journal of Oncology*, 2(4), 151-157

Karu, A. E., Bell, C. W., and Chin, T. E. (1995). Recombinant Antibody Technology. *ILAR Journal*, 37(3), 132-141.

Kim, D. and Herr, A.E. (2013). Protein immobilization techniques for microfluidic assays. *Biomicrofluidics*, 7(4), 041501.

Kim, J., Johnson, M., Hill, P. and Gale, B.K. (2009). Microfluidic sample preparation: cell lysis and nucleic acid purification. *Integrative Biology*, 1(10), 574-586.

Kimling, J., Maier, M., Okenve, B., Kotaidis, V., Ballot, H. and Plech, A. (2006). Turkevich method for gold nanoparticle synthesis revisited. *The Journal of Physical Chemistry B*, 110(32), 15700-15707.

Kinahan, D.J., Kearney, S.M. and Ducree, J. (2013). Auto-actuated sequential release valves for Lab-on-a-Disc systems. In *2013 Transducers & Eurosensors XXVII: The 17th International Conference on Solid-State Sensors, Actuators and Microsystems (Transducers & Eurosensors XXVII)* (2189-2192). IEEE.

Kinahan, D.J., Kearney, S.M., Dimov, N., Glynn, M.T. and Ducree, J. (2014). Event-triggered logical flow control for comprehensive process integration of multi-step assays on centrifugal microfluidic platforms. *Lab on a Chip*, 14(13), 2249-2258.

Kinahan, D.J., Kearney, S.M., Faneuil, O.P., Glynn, M.T., Dimov, N. and Ducree, J. (2015). Paper imbibition for timing of multi-step liquid handling protocols on event-triggered centrifugal microfluidic lab-on-a-disc platforms. *RSC Advances*, 5(3), 1818-1826.

King, C.R., Kraus, M.H. and Aaronson, S.A. (1985). Amplification of a novel v-erbB-related gene in a human mammary carcinoma. *Science*, 229(4717), 974-976.

Kitagawa, Y., Ueno, S., Izumi, K., Kadono, Y., Konaka, H., Mizokami, A. and Namiki, M. (2014). Cumulative probability of prostate cancer detection in biopsy according to free/total PSA ratio in men with total PSA levels of 2.1–10.0 ng/ml at population screening. *Journal of Cancer Research and Clinical Oncology*, 140(1), 53-59.

Knezevic, D., Goddard, A.D., Natraj, N., Cherbavaz, D.B., Clark-Langone, K.M., Snable, J., Watson, D., Falzarano, S.M., Magi-Galluzzi, C., Klein, E.A. and Quale, C. (2013). Analytical validation of the Onco type DX prostate cancer assay—a clinical RT-PCR assay optimized for prostate needle biopsies. *BMC genomics*, *14*(1), 1.

Kongsuphol, P., Ng, H.H., Pursey, J.P., Arya, S.K., Wong, C.C., Stulz, E. and Park, M.K. (2014). EIS-based biosensor for ultra-sensitive detection of TNF- $\alpha$  from non-diluted human serum. *Biosensors and Bioelectronics*, *61*, 274-279.

Kowalski, M., Guindon, J., Brazas, L., Moore, C., Entwistle, J., Cizeau, J., Jewett, M.A. and MacDonald, G.C. (2012). A phase II study of oportuzumab monatox: an immunotoxin therapy for patients with noninvasive urothelial carcinoma in situ previously treated with bacillus Calmette-Guerin. *The Journal of urology*, *188*(5), 1712-1718.

Kraus, M.H., Issing, W., Miki, T., Popescu, N.C. and Aaronson, S.A. (1989). Isolation and characterization of ERBB3, a third member of the ERBB/epidermal growth factor receptor family: evidence for overexpression in a subset of human mammary tumors. *Proceedings of the National Academy of Sciences*, *86*(23), 9193-9197.

Laboria, N., Fragoso, A., Kemmner, W., Latta, D., Nilsson, O., Luz Botero, M., Drese, K. and O'Sullivan, C.K. (2010). Amperometric immunosensor for carcinoembryonic antigen in colon cancer samples based on monolayers of dendritic bipodal scaffolds. *Analytical Chemistry*, *82*(5), 1712-1719.

Lacharme, F., Vandevyver, C. and Gijs, M.A.M. (2009). Magnetic beads retention device for sandwich immunoassay: comparison of off-chip and on-chip antibody incubation. *Microfluidics and Nanofluidics*, *7*(4), 479-487.

Larentis, A.L., Nicolau, J.F.M.Q., dos Santos Esteves, G., Vareschini, D.T., de Almeida, F.V.R., dos Reis, M.G., Galler, R. and Medeiros, M.A. (2014). Evaluation of pre-induction temperature, cell growth at induction and IPTG concentration on the expression of a leptospiral protein in *E. coli* using shaking flasks and microbioreactor. *BMC Research Notes*, *7*(1), 1.

Lazerges, M., Tal, V.T., Bigey, P., Scherman, D. and Bedioui, F. (2013). Electrochemical DNA-biosensors: Two-electrode setup well adapted for miniaturized devices. *Sensors and Actuators B: Chemical*, *182*, 510-513.

Lee, B.S., Lee, J.N., Park, J.M., Lee, J.G., Kim, S., Cho, Y.K. and Ko, C. (2009). A fully automated immunoassay from whole blood on a disc. *Lab on a Chip*, 9(11), 1548-1555.

Lee, C.Y., Chang, C.L., Wang, Y.N. and Fu, L.M. (2011). Microfluidic mixing: a review. *International Journal of Molecular Sciences*, 12(5), 3263-3287.

Lee, J.U., Nguyen, A.H. and Sim, S.J. (2015). A nanoplasmonic biosensor for label-free multiplex detection of cancer biomarkers. *Biosensors and Bioelectronics*, 74, 341-346.

Lee, N.Y., Yang, Y.S., Kim, Y.S. and Park, S.S. (2006). Microfluidic immunoassay platform using antibody-immobilized glass beads and its application for detection of *Escherichia coli* O157: H7. *Bulletin of the Korean Chemical Society*, 27(4), 479-483.

Leong, J.C., Tsai, C.H., Chang, C.L., Lin, C.F. and Fu, L.M. (2007). Rapid microfluidic mixers utilizing dispersion effect and interactively time-pulsed injection. *Japanese Journal of Applied Physics*, 46(8R), 5345-5352.

Levisson, M., Spruijt, R.B., Winkel, I.N., Kengen, S.W. and van der Oost, J. (2014). Phage display of engineered binding proteins in Labrou, N.E (ed.) *Protein Downstream Processing: Design, Development and Application of High and Low-Resolution Methods*. New York: Humana Press.

Leyland-Jones, B. and Smith, B.R. (2011). Serum HER2 testing in patients with HER2-positive breast cancer: the death knell tolls. *The Lancet Oncology*, 12(3), 286-295.

Liébana, S., Brandão, D., Alegret, S. and Pividori, M.I. (2014). Electrochemical immunosensors, genosensors and phagosensors for Salmonella detection. *Analytical Methods*, 6(22), 8858-8873.

Liébana, S., Jones, L.J., Drago, G.A., Pittson, R.W., Liu, D., Perrie, W. and Hart, J.P. (2016). Design and development of novel screen-printed microelectrode and microbiosensor arrays fabricated using ultrafast pulsed laser ablation. *Sensors and Actuators B: Chemical*, 231, 384-392.

Liébana, S., Pittson, R. W. and Drago, G. A (2014\*). Electrochemical magneto-immunosensor for prostate cancer biomarkers. In *Application Of Lectins In Various Format Of Analysis For Glycoprofiling workshop*, Bratislava.

Liébana, S., Spricigo, D.A., Cortés, M.P., Barbé, J., Llagostera, M., Alegret, S. and Pividori, M.I. (2013). Phagomagnetic separation and electrochemical magneto-genosensing of pathogenic bacteria. *Analytical Chemistry*, 85(6), 3079-3086.

Liébana, S., Lermo, A., Campoy, S., Cortés, M.P., Alegret, S. and Pividori, M.I. (2009). Rapid detection of Salmonella in milk by electrochemical magneto-immunosensing. *Biosensors and Bioelectronics*, 25(2), 510-513.

Lilja, H., Abrahamsson, P. A., and Lundwall, A. (1989). Semenogelin, the predominant protein in human semen. Primary structure and identification of closely related proteins in the male accessory sex glands and on the spermatozoa. *Journal of Biological Chemistry*, 264(3), 1894-1900.

Lilja, H., Ulmert, D., and Vickers, A. J. (2008). Prostate-specific antigen and prostate cancer: prediction, detection and monitoring. *Nature Reviews Cancer*, 8(4), 268-278

Lim, M.C., Lee, G.H., Huynh, D.T.N., Hong, C.E., Park, S.Y., Jung, J.Y., Park, C.S., Ko, S. and Kim, Y.R. (2016). Biological preparation of highly effective immunomagnetic beads for the separation, concentration, and detection of pathogenic bacteria in milk. *Colloids and Surfaces B: Biointerfaces*, 145, 854-861.

Loeb, S., and Catalona, W. J. (2013). The Prostate Health Index: a new test for the detection of prostate cancer. *Therapeutic Advances in Urology*, 6(2), 74-77.

Lu, X.H., Wang, Z.W., Cai, Y., Huang, J., Zhu, L.H., Yang, Q.L. and Chen, C.J., 2014. [Construction and identification of anti-HER2 phage display single chain fragment of variable region library in human breast cancer]. *Zhejiang da xue xue bao. Yi xue ban= Journal of Zhejiang University. Medical sciences*, 43(4), 434-440.

Lutz, S., Reitenbach, V., Mark, D., Ducreé, J., Zengerle, R. and von Stetten, F. (2008). Unidirectional Shake-Mode for mixing highly wetting fluids on Centrifugal Platforms. In *Proceedings of the 12th International Conference on Miniaturized Systems for Chemistry and Life Sciences* (748-750).

McCormack, W.T., Tjoelker, L.W. and Thompson, C.B. (1993). Immunoglobulin gene diversification by gene conversion. *Progress in Nucleic Acid Research and Molecular Biology*, 45, 27-45.

Maguire, I., Fitzgerald, J., Heery, B., Murphy, C., Nwankire, C., O'Kennedy, R., Ducree, J. and Regan, F. (2015). The ToxiSense detection system: A novel centrifugal-based

microfluidic (Lab-On-A-Disc) system for detecting cyanobacterial toxin microcystin-LR. In *EuroAnalysis 2015 conference, Bordeaux, France*.

Maguire, I., Fitzgerald, J., Heery, B., Murphy, C., Nwankire, C., O'Kennedy, R., Ducreé, J. and Regan, F., 2016. Atalanta: The autonomous analytical algal toxin platform. In *Proceedings of the SWIG 2016 meeting, Ireland*.

Maleki, T., Fricke, T., Quesenberry, J.T., Todd, P. and Leary, J.F. (2012). Point-of-care, portable microfluidic blood analyzer system. In *SPIE MOEMS-MEMS (82510C-82510C)*. International Society for Optics and Photonics.

Malik, A., Alsenaidy, A.M., Elrobh, M., Khan, W., Alanazi, M.S. and Bazzi, M.D. (2016). Optimization of expression and purification of HSPA6 protein from *Camelus dromedarius* in *E. coli*. *Saudi Journal of Biological Sciences*, 23(3), 410-419.

Mani, V., Chikkaveeraiah, B.V. and Rusling, J.F. (2011). Magnetic particles in ultrasensitive biomarker protein measurements for cancer detection and monitoring. *Expert Opinion on Medical Diagnostics*, 5(5), 381-391.

Manz, A., Graber, N. and Widmer, H.Á. (1990). Miniaturized total chemical analysis systems: a novel concept for chemical sensing. *Sensors and actuators B: Chemical*, 1(1), 244-248.

Massoner, P., Lueking, A., Goehler, H., Höpfner, A., Kowald, A., Kugler, K.G., Amersdorfer, P., Horninger, W., Bartsch, G., Schulz-Knappe, P. and Klocker, H. (2012). Serum-autoantibodies for discovery of prostate cancer specific biomarkers. *The Prostate*, 72(4), 427-436.

Mauk, M.G., Liu, C., Song, J. and Bau, H.H. (2015). Integrated Microfluidic Nucleic Acid Isolation, Isothermal Amplification, and Amplicon Quantification. *Microarrays*, 4(4), 474-489.

McPartlin, D.A. and O'Kennedy, R.J. (2014). Point-of-care diagnostics, a major opportunity for change in traditional diagnostic approaches: potential and limitations. *Expert Review of Molecular Diagnostics*, 14(8), 979-998.

Meany, D.L., Zhang, Z., Sokoll, L.J., Zhang, H. and Chan, D.W. (2008). Glycoproteomics for prostate cancer detection: changes in serum PSA glycosylation patterns. *Journal of Proteome Research*, 8(2), 613-619.

Mellinghoff, I. K., Vivanco, I., Kwon, A., Tran, C., Wongvipat, J., and Sawyers, C. L. (2004). HER2/neu kinase-dependent modulation of androgen receptor function through effects on DNA binding and stability. *Cancer Cell*, 6(5), 517-527.

Mhawech-Fauceglia, P., Zhang, S., Terracciano, L., Sauter, G., Chadhuri, A., Herrmann, F. R., and Penetrante, R. (2007). Prostate-specific membrane antigen (PSMA) protein expression in normal and neoplastic tissues and its sensitivity and specificity in prostate adenocarcinoma: an immunohistochemical study using multiple tumour tissue microarray technique. *Histopathology*, 50(4), 472-483.

Minner, S., Jessen, B., Stiedenroth, L., Burandt, E., Köllermann, J., Mirlacher, M., Erbersdobler, A., Eichelberg, C., Fisch, M., Brümmendorf, T.H. and Bokemeyer, C. (2010). Low level HER2 overexpression is associated with rapid tumor cell proliferation and poor prognosis in prostate cancer. *Clinical Cancer Research*, 16(5), 1553-1560.

Mirza, M., Griebing, T. L., and Kazer, M. W. (2011). Erectile dysfunction and urinary incontinence after prostate cancer treatment. *Seminars in Oncology Nursing*, 27(4), 278-289.

Mody, V.V., Cox, A., Shah, S., Singh, A., Bevins, W. and Parihar, H. (2014). Magnetic nanoparticle drug delivery systems for targeting tumor. *Applied Nanoscience*, 4(4), 385-392.

Monnier, P. P., Vigouroux, R. J., and Tassew, N. G. (2013). *In vivo* applications of single chain Fv (variable domain)(scFv) fragments. *Antibodies*, 2(2), 193-208.

Monošík, R., Stredánský, M. and Šturdík, E. (2012). Biosensors-classification, characterization and new trends. *Acta Chimica Slovaca*, 5(1), 109-120.

Morgan, R., Boxall, A., Bhatt, A., Bailey, M., Hindley, R., Langley, S., Whitaker, H.C., Neal, D.E., Ismail, M., Whitaker, H. and Annels, N. (2011). Engrailed-2 (EN2): a tumor specific urinary biomarker for the early diagnosis of prostate cancer. *Clinical Cancer Research*, 17(5), pp.1090-1098.

Mou, X., Ali, Z., Li, S. and He, N. (2015). Applications of magnetic nanoparticles in targeted drug delivery system. *Journal of Nanoscience and Nanotechnology*, 15(1), 54-62.

Moyer, V. A. (2012). Screening for prostate cancer: US Preventive Services Task Force recommendation statement. *Annals of Internal Medicine*, 157(2), 120-134.

Murphy, L., Prencipe, M., Gallagher, W.M. and Watson, R.W. (2015). Commercialized biomarkers: new horizons in prostate cancer diagnostics. *Expert Review of Molecular Diagnostics*, 15(4), 491-503.

Murphy, C. and O’Kennedy, R. (forthcoming in January 2017). Protocols for Key Steps in the Development of an Immunoassay in Murphy, C. and O’Kennedy, R. (eds.) *Immunoassays: Development, Applications and Future Trends*. India: Pan Stanford Publishing

Myers, M.B. (2016). Targeted therapies with companion diagnostics in the management of breast cancer: current perspectives. *Pharmacogenomics and Personalized Medicine*, 9, 7-16.

Narat, M. (2003). Production of antibodies in chickens. *Food Technology and Biotechnology*, 41(3), 259-267.

Neubert, H., Muirhead, D., Kabir, M., Grace, C., Cleton, A. and Arends, R. (2013). Sequential protein and peptide immunoaffinity capture for mass spectrometry-based quantification of total human  $\beta$ -nerve growth factor. *Analytical Chemistry*, 85(3), 1719-1726.

Nustad, K., Michaelsen, T.E., Kierulf, B., Fjeld, J.G., Kvalheim, G., Pihl, A., Ugelstad, J. and Funderud, S. (1987). Antigen-binding properties of antibodies coated on magnetic polymer beads. *Bone Marrow Transplantation*, 2, 81-83.

Nwankire, C., Gorkin, R., Siegrist, J., Gaughran, J., Chan, D.S. and Ducreé, J. (2011) O. Full integration and automation of immunoassay protocols by rotationally actuated dissolvable film valves. In *Proceedings of the 15th International Conference on Miniaturized Systems for Chemistry and Life Sciences, Seattle, WA, USA* (2-6).

Nwankire, C.E., Czugala, M., Burger, R., Fraser, K.J., Glennon, T., Onwuliri, B.E., Nduaguibe, I.E., Diamond, D. and Ducreé, J. (2014). A portable centrifugal analyser for liver function screening. *Biosensors and Bioelectronics*, 56, 352-358.

Öhlschlegel, C., Zahel, K., Kradolfer, D., Hell, M. and Jochum, W., 2011. HER2 genetic heterogeneity in breast carcinoma (2011). *Journal of Clinical Pathology*, 64(12), 1112-1116.

Okafor, C., Grooms, D., Alocilja, E. and Bolin, S. (2008). Fabrication of a novel conductometric biosensor for detecting *Mycobacterium avium* subsp. paratuberculosis antibodies. *Sensors*, 8(9), 6015-6025.

Okegawa, T., Kinjo, M., Nutahara, K. and Higashihara, E. (2006). Pretreatment serum level of HER2/neu as a prognostic factor in metastatic prostate cancer patients about to undergo endocrine therapy. *International Journal of Urology*, 13(9), 1197-1201.

Opko. *Point-of-Care Diagnostics Platform* [online]. Available from: <http://www.opko.com>.

Osman, I., Mikhail, M., Shuch, B., Clute, M., Cheli, C.D., Ghani, F., Thiel, R.P. and Taneja, S.S. (2005). Serum levels of shed Her2/neu protein in men with prostate cancer correlate with disease progression. *The Journal of Urology*, 174(6), 2174-2177.

Osmekhina, E., Neubauer, A., Klinzing, K., Myllyharju, J. and Neubauer, P. (2010). Sandwich ELISA for quantitative detection of human collagen prolyl 4-hydroxylase. *Microbial Cell Factories*, 9(1), 1.

Ouyang, B., Bracken, B., Burke, B., Chung, E., Liang, J. and Ho, S. M. (2009). A duplex quantitative polymerase chain reaction assay based on quantification of  $\alpha$ -methylacyl-CoA racemase transcripts and prostate cancer antigen 3 in urine sediments improved diagnostic accuracy for prostate cancer. *The Journal of Urology* 181(6) 2508-2514.

Papila, C., Uzun, H., Balci, H., Zerdali, H., Sezgin, C., Can, G., and Yanardag, H. (2009). Clinical significance and prognostic value of serum HER-2/neu levels in patients with solid tumors. *Medical Oncology*, 26(2), 151-156.

Park, J., Sunkara, V., Kim, T. H., Hwang, H., and Cho, Y. K. (2012). Lab-on-a-disc for fully integrated multiplex immunoassays. *Analytical Chemistry*, 84(5), 2133-2140.

Park, Y.H., Kim, S.T., Cho, E.Y., La Choi, Y., Ok, O.N., Baek, H.J., Lee, J.E., Nam, S.J., Yang, J.H., Park, W. and Choi, D.H. (2010). A risk stratification by hormonal receptors (ER, PgR) and HER-2 status in small ( $\leq 1$  cm) invasive breast cancer: who might be possible candidates for adjuvant treatment?. *Breast Cancer Research and Treatment*, 119(3), 653-661.

Payne, R.C., Allard, J.W., Anderson-Mausser, L., Humphreys, J.D., Tenney, D.Y. and Morris, D.L. (2000). Automated assay for HER-2/neu in serum. *Clinical Chemistry*, 46(2), 175-182.

Perez, E.A., Cortés, J., Gonzalez-Angulo, A.M. and Bartlett, J.M. (2014). HER2 testing: current status and future directions. *Cancer Treatment Reviews*, 40(2), 276-284.

Pihíková, D., Belicky, Š., Kasák, P., Bertok, T. and Tkac, J. (2016). Sensitive detection and glycoprofiling of a prostate specific antigen using impedimetric assays. *Analyst*, 141(3), 1044-1051.

Pingarrón, J.M., Yañez-Sedeño, P. and González-Cortés, A. (2008). Gold nanoparticle-based electrochemical biosensors. *Electrochimica Acta*, 53(19), 5848-5866.

Plowman, G.D., Culouscou, J.M., Whitney, G.S., Green, J.M., Carlton, G.W., Foy, L., Neubauer, M.G. and Shoyab, M., (1993). Ligand-specific activation of HER4/p180erbB4, a fourth member of the epidermal growth factor receptor family. *Proceedings of the National Academy of Sciences (USA)*, 90(5), 1746-1750.

Plouffe, B.D., Murthy, S.K. and Lewis, L.H. (2014). Fundamentals and application of magnetic particles in cell isolation and enrichment: a review. *Reports on Progress in Physics*, 78(1), 016601.

Pressl, M.F., Cordon-Cardo, C. and Slamon, D.J. (1990). Expression of the HER-2/neu proto-oncogene in normal human adult and fetal tissues. *Liver*, 7, 7.

Punnen, S., Pavan, N. and Parekh, D.J. (2015). Finding the wolf in sheep's clothing: the 4Kscore is a novel blood test that can accurately identify the risk of aggressive prostate cancer. *Reviews in Urology*, 17(1), 3-13.

Qlark Jr, L.C. (1956). Monitor and control of blood and tissue oxygen tensions. *ASAIO Journal*, 2(1), 41-48.

Qureshi, A., Gurbuz, Y. and Niazi, J.H. (2015). Label-free capacitance based aptasensor platform for the detection of HER2/ErbB2 cancer biomarker in serum. *Sensors and Actuators B: Chemical*, 220, 1145-1151.

Raaijmakers, R., de Vries, S. H., Blijenberg, B. G., Wildhagen, M. F., Postma, R., Bangma, C. H., Darte, C., and Schröder, F. H. (2007). hK2 and free PSA, a prognostic combination in predicting minimal prostate cancer in screen-detected men within the PSA range 4–10 ng/ml. *European Urology*, 52(5), 1358-1364.

Raghav, R. and Srivastava, S. (2015). Core-shell gold-silver nanoparticles based impedimetric immunosensor for cancer antigen CA125. *Sensors and Actuators B: Chemical*, 220, 557-564.

Raghav, R. and Srivastava, S. (2016). Immobilization strategy for enhancing sensitivity of immunosensors: L-Asparagine-AuNPs as a promising alternative of EDC-NHS

activated citrate–AuNPs for antibody immobilization (2016). *Biosensors and Bioelectronics*, 78, 396-403.

Ramanujan, R.V. (2009). Magnetic particles for biomedical applications in Narayan, R. (ed.) *Biomedical Materials*. New York: Springer.

Ranzoni, A., Sabatte, G., van IJzendoorn, L.J. and Prins, M.W. (2012). One-step homogeneous magnetic nanoparticle immunoassay for biomarker detection directly in blood plasma. *ACS nano*, 6(4), 3134-3141.

Ricciardelli, C., Jackson, M. W., Choong, C. S., Stahl, J., Marshall, V. R., Horsfall, D. J., and Tilley, W. D. (2008). Elevated levels of HER-2/neu and androgen receptor in clinically localized prostate cancer identifies metastatic potential. *The Prostate*, 68(8), 830-838.

Richard, R.L., Ithoi, I., Abd Majid, M.A., Wan Sulaiman, W.Y., Tan, T.C., Nissapatorn, V. and Lim, Y.A.L. (2016). Monitoring of Waterborne Parasites in Two Drinking Water Treatment Plants: A Study in Sarawak, Malaysia. *International Journal of Environmental Research and Public Health*, 13(7), 641.

Riquelme, M.V., Zhao, H., Srinivasaraghavan, V., Pruden, A., Vikesland, P. and Agah, M. (2016). Optimizing blocking of nonspecific bacterial attachment to impedimetric biosensors. *Sensing and Bio-Sensing Research*, 8, 47-54.

Rizzo, D.C. (2015). *Fundamentals of anatomy and physiology*. 4<sup>th</sup> ed. Boston, MA: Cengage Learning.

Roussel, T.J., Jackson, D.J., Baldwin, R.P. and Keynton, R.S. (2015). Amperometric Techniques IN Li, D. (ed.) *Encyclopedia of Microfluidics and Nanofluidics* (55-64). NY: Springer Science & Business Media.

Saito, M., Kawakami, Y., Yamashita, K., Nasuno, H., Ishimine, Y., Fukuda, K., Isshiki, H., Suzuki, R., Arimura, Y. and Shinomura, Y. (2016). HER2-positive gastric cancer identified by serum HER2: A case report. *Oncology Letters*, 11(6), 3575-3578.

Samsung. *Samsung LABGEO HC10 | Samsung Business* [online]. Available at: <http://www.samsung.com>.

Sanger, F. and Coulson, A.R. (1975). A rapid method for determining sequences in DNA by primed synthesis with DNA polymerase. *Journal of Molecular Biology*, 94(3), 441-448.

Santos, A., Davis, J.J. and Bueno, P.R. (2014). Fundamentals and Applications of Impedimetric and Redox Capacitive Biosensors. *Journal of Analytical & Bioanalytical Techniques*, 57:016.

Sarkar, P., Ghosh, D., Bhattacharyay, D., Setford, S. E., & Turner, A. E. E. (2008). Electrochemical Immunoassay for Free Prostate Specific Antigen (f-PSA) Using Magnetic Beads. *Electroanalysis*, 20(13), 1414-1420.

Sarkar, P., Pal, P.S., Ghosh, D., Setford, S.J. and Tothill, I.E. (2002). Amperometric biosensors for detection of the prostate cancer marker (PSA). *International Journal of Pharmaceutics*, 238(1), 1-9.

Sartori, D. A., and Chan, D. W. (2014). Biomarkers in prostate cancer: what's new?. *Current Opinion in Oncology*, 26(3), 259.

Seven, B., Bourourou, M., Elouarzaki, K., Constant, J.F., Gondran, C., Holzinger, M., Cosnier, S. and Timur, S. (2013). Impedimetric biosensor for cancer cell detection. *Electrochemistry Communications*, 37, 36-39.

Schipper, M., Wang, G., Giles, N. and Ohrnberger, J. (2015). Novel prostate cancer biomarkers derived from autoantibody signatures. *Translational Oncology*, 8(2), 106-111.

Schechter, A.L., Stern, D.F., Vaidyanathan, L., Decker, S.J., Drebin, J.A., Greene, M.I. and Weinberg, R.A. (1984). The neu oncogene: an erb-B-related gene encoding a 185,000-Mr tumour antigen. *Nature*, 312, 513-516.

Schostak, M., Schwall, G. P., Poznanović, S., Groebe, K., Müller, M., Messinger, D., Miller, K., Krause, H., Pelzer, A., Horninger, W., Klocker, H., Hennenlotter, J., Feyerabend, S., Stenzl, A., and Schratzenholz, A. (2009). Annexin A3 in urine: a highly specific noninvasive marker for prostate cancer early detection. *The Journal of Urology*, 181(1), 343-353.

Siddiqui, M. (2010). Monoclonal antibodies as diagnostics; an appraisal. *Indian Journal of Pharmaceutical Sciences*, 72(1), 12-7.

Sharif, E., Kiely, J. and Luxton, R. (2013). Novel immunoassay technique for rapid measurement of intracellular proteins using paramagnetic particles. *Journal of Immunological Methods*, 388(1), 78-85.

Sharma, S., Zapatero-Rodríguez, J., and O'Kennedy, R. Prostate Cancer Diagnostics: Clinical Challenges and the Ongoing Need for Disruptive and Effective Diagnostic Tools (2016). *Biotechnology Advances*, DOI: 10.1016/j.biotechadv.2016.11.009.

Shih, C., Padhy, L.C., Murray, M. and Weinberg, R.A. (1981). Transforming genes of carcinomas and neuroblastomas introduced into mouse fibroblasts. *Nature*, 290, 261-264.

Shindel, A.W. (2016). Genetics and Genomics: Discovery, Validation, and Utility of Novel Tools for management of Prostate Cancer. *Journal of Men's Health*, 12(1), 6-17.

Siegrist, J., Gorkin, R., Clime, L., Roy, E., Peytavi, R., Kido, H., Bergeron, M., Veres, T. and Madou, M. (2010). Serial siphon valving for centrifugal microfluidic platforms. *Microfluidics and nanofluidics*, 9(1), 55-63.

Siampanopoulou, M., Galaktidou, G., Dimasis, N. and Gotzamani-Psarrakou, A. (2013). Profiling serum HER-2/NEU in prostate cancer. *Hippokratia*, 17(2), 108.

Smith, G. P. (1985). Filamentous fusion phage: novel expression vectors that display cloned antigens on the virion surface. *Science*, 228(4705), 1315-1317.

Sokolov, A.N., Roberts, M.E. and Bao, Z. (2009). Fabrication of low-cost electronic biosensors. *Materials Today*, 12(9), 12-20.

Sommariva, S., Tarricone, R., Lazzeri, M., Ricciardi, W. and Montorsi, F. (2016). Prognostic value of the cell cycle progression score in patients with prostate cancer: a systematic review and meta-analysis. *European Urology*, 69(1), 107-115.

Spain, E., Gilgunn, S., Sharma, S., Adamson, K., Carthy, E., O'Kennedy, R. and Forster, R.J. (2016). Detection of prostate specific antigen based on electrocatalytic platinum nanoparticles conjugated to a recombinant scFv antibody. *Biosensors and Bioelectronics*, 77, 759-766.

Stewart, G.D., Van Neste, L., Delvenne, P., Delrée, P., Delga, A., McNeill, S.A., O'Donnell, M., Clark, J., Van Criekinge, W., Bigley, J. and Harrison, D.J. (2013). Clinical utility of an epigenetic assay to detect occult prostate cancer in histopathologically negative biopsies: results of the MATLOC study. *The Journal of Urology*, 189(3), 1110-1116.

Stingl, K., Bartz-Schmidt, K.U., Besch, D., Braun, A., Bruckmann, A., Gekeler, F., Greppmaier, U., Hipp, S., Hörtdörfer, G., Kernstock, C. and Koitschev, A. (2013). Artificial vision with wirelessly powered subretinal electronic implant alpha-IMS. *Proceedings of the Royal Society*, 280, (1757), 20130077.

Strohmeier, O., Keller, M., Schwemmer, F., Zehnle, S., Mark, D., von Stetten, F., Zengerle, R. and Paust, N. (2015). Centrifugal microfluidic platforms: Advanced unit operations and applications. *Chemical Society Reviews*, 44(17), 6187-6229.

Sun, A., Wambach, T., Venkatesh, A.G. and Hall, D.A. (2014). A low-cost smartphone-based electrochemical biosensor for point-of-care diagnostics. In *2014 IEEE Biomedical Circuits and Systems Conference (BioCAS) Proceedings* (312-315).

Tai, C.H., Tsai, Y.C., Wang, C.H., Ho, T.S., Chang, C.P. and Lee, G.B. (2014). An integrated microfluidic platform for rapid detection and subtyping of influenza viruses from clinical samples. *Microfluidics and nanofluidics*, 16(3), 501-512.

Takenaka, M., Hanagiri, T., Shinohara, S., Kuwata, T., Chikaishi, Y., Oka, S., Shigematsu, Y., Nagata, Y., Shimokawa, H., Nakagawa, M. and Uramoto, H. (2011). The prognostic significance of HER2 overexpression in non-small cell lung cancer. *Anticancer Research*, 31(12), 4631-4636.

Tang, M., Wang, G., Kong, S.K. and Ho, H.P. (2016). A Review of Biomedical Centrifugal Microfluidic Platforms. *Micromachines*, 7(2), 26.

Teixeira, S., Conlan, R.S., Guy, O.J. and Sales, M.G.F. (2014). Novel single-wall carbon nanotube screen-printed electrode as an immunosensor for human chorionic gonadotropin. *Electrochimica Acta*, 136, 323-329.

Tehrani, Z., Burwell, G., Azmi, M.M., Castaing, A., Rickman, R., Almarashi, J., Dunstan, P., Beigi, A.M., Doak, S.H. and Guy, O.J. (2014). Generic epitaxial graphene biosensors for ultrasensitive detection of cancer risk biomarker. *2D Materials*, 1(2), 025004.

Tennico, Y.H., Hutanu, D., Koesdjojo, M.T., Bartel, C.M. and Remcho, V.T. (2010). On-chip aptamer-based sandwich assay for thrombin detection employing magnetic beads and quantum dots. *Analytical Chemistry*, 82(13), 5591-5597.

Tomlins, S. A., Day, J. R., Lonigro, R. J., Hovelson, D. H., Siddiqui, J., Kunju, L. P., Dunn, R. L., Meyer, S., Hodge, P., Groskopf, J., Wei, J. T., and Chinnaiyan, A. M. (2015).

Urine TMPRSS2: ERG Plus PCA3 for Individualized Prostate Cancer Risk Assessment. *European Urology*, S0302-2838 (15) 00397-8.

Tong, C., Geng, F., He, Z., Cai, Z. and Ma, M. (2014). A simple method for isolating chicken egg yolk immunoglobulin using effective delipidation solution and ammonium sulfate. *Poultry Science*, doi: 10.3382/ps/peu005.

Turkevich, J., Stevenson, P.C. and Hillier, J. (1951). A study of the nucleation and growth processes in the synthesis of colloidal gold. *Discussions of the Faraday Society*, 11, 55-75.

Ugelstad, J., Kaggerud, K.H., Hansen, F.K. and Berge, A., (1979). Absorption of low molecular weight compounds in aqueous dispersions of polymer-oligomer particles, 2. A two step swelling process of polymer particles giving an enormous increase in absorption capacity. *Die Makromolekulare Chemie*, 180(3), 737-744.

Ummanni, R., Duscharla, D., Barrett, C., Venz, S., Schlomm, T., Heinzer, H., Walther, R., Bokemeyer, C., Brümmendorf, T.H., Murthy, P.V.L.N. and Balabanov, S. (2015). Prostate cancer-associated autoantibodies in serum against tumor-associated antigens as potential new biomarkers. *Journal of Proteomics*, 119, 218-229.

Urdike, S.J. and Hicks, G.P. (1967). The enzyme electrode. *Nature*, 214, 986-988.

Vaishampayan, U., Thakur, A., Rathore, R., Kouttab, N. and Lum, L.G. (2015). Phase I study of anti-CD3 x Anti-Her2 bispecific antibody in metastatic castrate resistant prostate cancer patients. *Prostate Cancer*, 2015.

Vennström, B. and Bishop, J.M. (1982). Isolation and characterization of chicken DNA homologous to the two putative oncogenes of avian erythroblastosis virus. *Cell*, 28(1), 135-143.

Vesel, A. and Mozetic, M. (2012). Surface modification and ageing of PMMA polymer by oxygen plasma treatment. *Vacuum*, 86(6), 634-637.

Votyakova, T.V. and Reynolds, I.J. (2004). Detection of hydrogen peroxide with Amplex Red: interference by NADH and reduced glutathione auto-oxidation. *Archives of Biochemistry and Biophysics*, 431(1), 138-144.

Wang, J., Profitt, J.A., Pugia, M.J. and Suni, I.I. (2006). Au nanoparticle conjugation for impedance and capacitance signal amplification in biosensors. *Analytical Chemistry*, 78(6), 1769-1773.

Wang, T.J., Linton, H.J., Payne, J., Rittenhouse, H.G., Chan, D.W., Partin, A.W., Wolfert, R.L. And Kuus-Reichel, K. (1999). Generation of PSA-ACT-specific monoclonal antibodies and their application in a sandwich immunoassay. *Hybridoma*, 18(6), 535-541.

Wang, X., Niessner, R. and Knopp, D. (2014). Magnetic bead-based colorimetric immunoassay for aflatoxin B1 using gold nanoparticles. *Sensors*, 14(11), 21535-21548.

Wang, Y., Ye, Z. and Ying, Y. (2012). New trends in impedimetric biosensors for the detection of foodborne pathogenic bacteria. *Sensors*, 12(3), 3449-3471.

Wei, F., Patel, P., Liao, W., Chaudhry, K., Zhang, L., Arellano-Garcia, M., Hu, S., Elashoff, D., Zhou, H., Shukla, S. and Shah, F. (2009). Electrochemical sensor for multiplex biomarkers detection. *Clinical Cancer Research*, 15(13), 4446-4452.

Weng, C.H., Lien, K.Y., Yang, S.Y. and Lee, G.B. (2011). A suction-type, pneumatic microfluidic device for liquid transport and mixing. *Microfluidics and Nanofluidics*, 10(2), 301-310.

Wen, C.Y., Yeh, C.P., Tsai, C.H. and Fu, L.M. (2009). Rapid magnetic microfluidic mixer utilizing AC electromagnetic field. *Electrophoresis*, 30(24), 4179-4186.

Wen, X., He, H. and Lee, L.J. (2009\*). Specific antibody immobilization with biotin-poly (l-lysine)-g-poly (ethylene glycol) and protein A on microfluidic chips. *Journal of Immunological Methods*, 350(1), 97-105.

Whitesides, G. M. (2006). The origins and the future of microfluidics. *Nature*, 442(7101), 368-373.

Wild, D. (2005). Standardization and calibration in Wild, D. (ed.) *The immunoassay handbook*. 3<sup>rd</sup> Ed. Oxford: Elsevier.

Wilkes, A. and Evans, B. (2014). Novel Biosensor for Point of Care Medical Diagnostics. *Biophysical Journal*, 106(2), 417a.

Willman, J. H., and Holden, J. A. (2000). Immunohistochemical staining for DNA topoisomerase II-alpha in benign, premalignant, and malignant lesions of the prostate. *The Prostate*, 42(4), 280-286.

Wojno, K.J., Costa, F.J., Cornell, R.J., Small, J.D., Pasin, E., Van Criekinge, W., Bigley, J.W. and Van Neste, L. (2014). Reduced rate of repeated prostate biopsies observed in ConfirmMDx clinical utility field study. *American Health & Drug Benefits*, 7(3), 129-134.

Wu, L., Oficjalska, K., Lambert, M., Fennell, B.J., Darmanin-Sheehan, A., Shúilleabháin, D.N., Autin, B., Cummins, E., Tchistiakova, L., Bloom, L. and Paulsen, J. (2012). Fundamental characteristics of the immunoglobulin VH repertoire of chickens in comparison with those of humans, mice, and camelids. *The Journal of Immunology*, 188(1), 322-333.

Wu, R., Yeung, W.S. and Fung, Y.S. (2011). 2-D t-ITP/CZE determination of clinical urinary proteins using a microfluidic-chip capillary electrophoresis device. *Electrophoresis*, 32(23), 3406-3414.

Wulff, P., Day, C.C., Sargent, F. and Armstrong, F.A. (2014). How oxygen reacts with oxygen-tolerant respiratory [NiFe]-hydrogenases. *Proceedings of the National Academy of Sciences (USA)*, 111(18), 6606-6611.

Xia, L., Xu, L., Song, J., Xu, R., Liu, D., Dong, B. and Song, H. (2015). CdS quantum dots modified CuO inverse opal electrodes for ultrasensitive electrochemical and photoelectrochemical biosensor. *Scientific Reports*, 5, 10838.

Xu, J. L., and Davis, M. M. (2000). Diversity in the CDR3 region of V H is sufficient for most antibody specificities. *Immunity*, 13(1), 37-45.

Yager, P., Edwards, T., Fu, E., Helton, K., Nelson, K., Tam, M.R. and Weigl, B.H. (2006). Microfluidic diagnostic technologies for global public health. *Nature*, 442(7101), 412-418.

Yao, S., Ireland, S. J., Bee, A., Beesley, C., Forootan, S. S., Dodson, A., Dickinson, T., Gerard, P., Lian, L. Y., Risk, J. M., Smith, P., Malki, M. I., Ke, Y., Cooper, C. S., Gosden, C., and Foster, C. S. (2012). Splice variant PRKC- $\zeta$ -PrC is a novel biomarker of human prostate cancer. *British Journal of Cancer*, 107(2), 388-399.

Yao, N., Chen, H., Lin, H., Deng, C. and Zhang, X. (2008). Enrichment of peptides in serum by C 8-functionalized magnetic nanoparticles for direct matrix-assisted laser desorption/ionization time-of-flight mass spectrometry analysis. *Journal of Chromatography A*, 1185(1), 93-101.

Young, A., Palanisamy, N., Siddiqui, J., Wood, D. P., Wei, J. T., Chinnaiyan, A. M., Kunju, L. P., and Tomlins, S. A. (2012). Correlation of urine TMPRSS2: ERG and PCA3 to ERG+ and total prostate cancer burden. *American Journal of Clinical Pathology*, 138(5), 685-696.

Zani, A., Laschi, S., Mascini, M. and Marrazza, G. (2011). A new electrochemical multiplexed assay for PSA cancer marker detection. *Electroanalysis*, 23(1), 91-99.

Zeng, J., Banerjee, D., Deshpande, M., Gilbert, J.R., Duffy, D.C. and Kellogg, G.J., (2000). Design analyses of capillary burst valves in centrifugal microfluidics. In *Micro Total Analysis Systems 2000* (579-582). Springer Netherlands.

Zhang, H., Berezov, A., Wang, Q., Zhang, G., Drebin, J., Murali, R. and Greene, M.I. (2007). ErbB receptors: from oncogenes to targeted cancer therapies. *The Journal of Clinical Investigation*, 117(8), 2051-2058.

Zhang, Q.Y., Chen, H., Lin, Z. and Lin, J.M. (2012). Comparison of chemiluminescence enzyme immunoassay based on magnetic microparticles with traditional colorimetric ELISA for the detection of serum  $\alpha$ -fetoprotein. *Journal of Pharmaceutical Analysis*, 2(2), 130-135.

Zhang, Y., Opresko, L., Shankaran, H., Chrisler, W.B., Wiley, H.S. and Resat, H. (2009). HER/ErbB receptor interactions and signaling patterns in human mammary epithelial cells. *BMC cell biology*, 10(1), 1.

Zhang, W.M., Finne, P., Leinonen, J., Vesalainen, S., Nordling, S., Rannikko, S. and Stenman, U.H. (1998). Characterization and immunological determination of the complex between prostate-specific antigen and  $\alpha$ 2-macroglobulin. *Clinical Chemistry*, 44(12), 2471-2479.

Zhao, M., Li, H., Liu, W., Guo, Y. and Chu, W. (2016). Plasma treatment of paper for protein immobilization on paper-based chemiluminescence immunodevice. *Biosensors and Bioelectronics*, 79, 581-588.

Zhu, B., Witzel, T., Jiang, S., Huang, S.Y., Rosen, B.R. and Wald, L.L. (2016). Selective magnetic resonance imaging of magnetic nanoparticles by acoustically induced rotary saturation. *Magnetic Resonance in Medicine*, 75(1), 97-106.

Ziada, A., Barqawi, A., Glode, L.M., Varella-Garcia, M., Crighton, F., Majeski, S., Rosenblum, M., Kane, M., Chen, L. and Crawford, E.D. (2004). The use of

trastuzumab in the treatment of hormone refractory prostate cancer; phase II trial.  
*The Prostate*, 60(4), 332-337.